The role of QKI and PRMT1 in microglia during de/remyelination

by

Jeesan Lee

Department of Biochemistry

McGill University, Montréal, Québec, Canada

April 2022

A thesis submitted to McGill University in partial fulfillment of the requirements for the degree of

Doctor of Philosophy.

ABSTRACT

Microglia are innate immune cells that reside in the central nervous system (CNS) and exhibit many properties similar to monocyte-derived macrophages. In response to injury, infection and disease, microglia become activated and the number of amoeboid-like cells increases dramatically, thereby promoting migration to the site of injury and engagement in responses that can be both neuroinflammatory and neuroprotective. In multiple sclerosis (MS), or a mouse model mimicking MS, accumulating evidence demonstrates that microglia play a key role in MS pathogenesis, and acquire changes in their transcriptional profile across disease progression. However little is known about how gene expression in this cell type is regulated during MS progression at the transcriptional and/or post-transcriptional level.

QUAKING (QKI), an RNA binding protein (RBP), is aberrantly expressed in Schizophrenia, Alzheimer's, MS and cancer patients. However, the role of QKI, or any RBP, in regulating alternative RNA splicing networks in microglia is unknown. Here, we show that QKI-deficient microglia have increased proinflammatory cytokine release and defects in processing phagocytosed cargo. Splicing analysis reveals a role for QKI in regulating microexon networks of the Rho GTPase pathway. We show increases in RhoA-GTP activation and proinflammatory cytokine production in QKI-deficient microglia, that are repressed by treating with a Rock kinase inhibitor. When fed with a cuprizone diet, mice with QKI-deficient microglia are inefficient at supporting central nervous system (CNS) remyelination and cause the recruited oligodendrocyte precursor cells to undergo apoptosis. Furthermore, the expression of QKI in microglia is downregulated in preactive, chronic active, and remyelinating white matter lesions of MS patients. Overall, our findings identify QKI as a regulator of alternative splicing that governs a network of Rho GTPase microexons, with implications for CNS remyelination and MS pathogenesis.

2

Protein arginine methyltransferase 1 (PRMT1) is the major type I enzyme generating asymmetrical dimethylarginines on histones and non-histones. Arginine methylation is known to modulate diverse biological processes including transcription, pre-mRNA splicing and signal transduction, thereby impacting immune cell differentiation, cell polarization, and pathogen-sensing abilities. Little is known about the role of PRMT1 in microglia and in macrophages under pathological conditions. Herein, we show that PRMT1 is required for regulating interferon-associated microglia and bone-derived macrophage phenotypes. PRMT1-deficient mice were defective in CNS remyelination compared to control mice following cuprizone diet-induced remyelination. We performed single-cell sequencing of primary microglia isolated from mice following a cuprizone diet and identified 8 clusters. From this, we observed that PRMT1-deficient microglia were unable to produce the cell cluster characterized by CD11c and MHCII expression, which is associated with interferon (IFN) pathway response. Additionally, PRMT1 deficient bone marrow-derived macrophages (BMDMs) challenged with polyinosinic:polycytidylic acid (poly(I:C)), an analog of viral dsRNA, were defective in their ability to polarize towards an M1 phenotype (CD86+). Overall, our findings identify PRMT1 as a regulator of CNS pathology, through its control of the IFN pathway in microglia.

Résumé

Les microglies sont des cellules immunitaires qui résident dans le système nerveux central (SNC) et jouent un rôle clé dans la réponse innée. Ces cellules présentent de nombreuses propriétés similaires aux macrophages dérivés des monocytes sanguins (MDMS). En réponse à une blessure, une infection ou une maladie, la microglie s'active et le nombre de cellules de type amiboïde augmente considérablement lorsqu'elles migrent vers le site de la blessure et s'engagent dans des réponses qui peuvent être à la fois neuroinflammatoires et neuroprotectrices. Chez les patients atteints de la sclérose en plaques (SEP) ou dans les modèles de souris imitant la SEP, de nombreuses preuves montrent que la microglie acquiert un profil transcriptionnel distinct et joue un rôle clé dans la pathogenèse de la SEP. Cependant, la régulation transcriptionnelle et/ou post-transcriptionnelle de ces ARNs n'est pas assez étudiée.

QUAKING (QKI) est une des protéines de liaison à l'ARN (RBP), exprimée de manière aberrante chez les patients atteints de schizophrénie, d'Alzheimer, de SEP et de cancer. Cependant, le rôle de QKI, ou de toute autre RBP, régulant les réseaux alternatifs d'épissage d'ARN dans la microglie est inconnu. Ici, nous montrons que la microglie déficiente en QKI augmente la production des cytokines pro-inflammatoires et des défauts dans le traitement de la cargaison phagocytée. L'analyse d'épissage révèle un rôle de QKI dans la régulation des réseaux de microexons de la voie Rho GTPase. Nous montrons une augmentation de l'activation de RhoA et des cytokines pro-inflammatoires dans la microglie déficiente en QKI qui sont réprimées en traitant avec un inhibiteur de la kinase Rock. Les souris avec une microglie déficiente en QKI et suivant un régime de Cuprizone sont incapables de soutenir la remyélinisation du SNC et induisent l'apoptose des cellules précurseurs d'oligodendrocytes. De plus, l'expression de QKI dans la microglie est diminuée dans les lésions préactives et chroniques actives de la substance blanche des patients atteints de SEP. Dans l'ensemble, nos résultats identifient QKI comme un régulateur de l'épissage

alternatif régissant un réseau de microexons Rho GTPase avec des implications dans la remyélinisation du SNC chez les patients atteints de SEP.

La protéine arginine méthyltransférase 1 (PRMT1) est la principale enzyme de type I générant des arginines méthylées d'une façon asymétrique sur les histones et d'autres protéines (non-histones). La méthylation de l'arginine est connue pour moduler divers processus biologiques, notamment la transcription, l'épissage des ARN pré-messagers et les voies de transduction du signal ayant un impact sur la différenciation des cellules immunitaires, la polarisation cellulaire et les capacités de détection des agents pathogènes. Peu de choses sont connues sur le rôle de PRMT1 dans la microglie et dans les macrophages dans des situations pathologiques. Ici, nous montrons que PRMT1 est nécessaire pour réguler la microglie associée à l'interféron et les phénotypes de macrophages dérivés de la moelle osseuse (BMDM). Lors du processus de la démyélinisation induite par un régime Cuprizone, les souris déficientes en PRMT1 présentent un défaut dans la remyélinisation du SNC comparativement aux souris contrôles. Nous avons effectué un séquençage de cellule unique de la microglie triée durant le régime Cuprizone et nous avons identifié 8 différents groupes. Cependant le groupe associé à la voie de l'interféron (IFN) (CD11c+, MHCII+) était absent dans la microglie déficiente en PRMT1. De plus, les BMDM déficientes en PRMT1 traitées avec de l'acide polyinosinique:polycytidylique (poly(I:C)), un analogue synthétique de l'ARN viral double brin, étaient défectueuses dans la polarisation M1 (CD86+, MHCII+). Dans l'ensemble, nos résultats identifient PRMT1 comme un régulateur de la voie IFN dans la microglie ayant un impact sur la pathologie du SNC.

TABLE OF CONTENTS

Contents

LIST OF FIGURES

LIST OF ABBREVIATIONS

A3SS	Alternative 3'-splice site
A5SS	Alternative 5'-splice site
AD	Alzheimer's disease
ADMA	Asymmetric dimethylarginine
AFE	Alternative first exon
ALE	Alternative last exon
APCs	Antigen-presenting cells
AS	Alternative splicing
ASD	Autism spectrum disorders
AS-microexons	Alternative splicing -microexon
ASO	Antisense oligonucleotide
Aβ	Beta-amyloid
BBB	Blood-brain barrier
BMDMs	Bone marrow-derived macrophages
CAMs	CNS-associated macrophages
CC	Corpus callosum
cGAS	GMP–AMP synthase
cKO	conditional knockout
CLRs	Ctype lectin receptors
CNS	Central nervous system
CNV	Copy number analysis
CPZ	Cuprizone
CR3	Complement receptor 3
CS-microexons	Constitutively spliced-microexon
CYTOF	Single-cell mass spectrometry
DAM	Disease-associated microglia
DAMPs	Damage-associated molecular patterns
DAPI	4′,6-diamidino-2-phenylindole
DMD	Duchenne muscular dystrophy
DMT	Disease-modifying treatment
DN	Double-negative
DP	Double-positive
EAE	Experimental autoimmune encephalomyelitis
EBV	Epstein–Barr virus
EMPs	Erythromyeloid precursors
FOXOP3	Forkhead box protein P3
GAPs	GTPase-activating proteins
GC	Germinal center
GDIs	Guanine nucleotide dissociation inhibitors
GEFs	Guanine nucleotide exchange factors
GVHD	Graft-versus-host disease
HIV	Human immunodeficiency virus
hnRNP F	Heterogeneous nuclear ribonucleoprotein F
HSC	Hematopoietic stem cells
hPSCs	human pluripotent stem cells

HSPCs	Hematopoietic stem and progenitor cells
Iba-1	Ionized calcium-binding adapter molecule 1
IFG1	Insulin-like growth factor 1
IFN	Interferon
ISE	Intronic splice enhancer
KSRP	KH-type splicing regulatory protein
LGN	Lateral geniculate nucleus
LNP	Lipid nanoparticle
LPC	Lysophosphatidylcholine
MAVS	Mitochondrial Antiviral Signaling Protein
MBP	Myelin-basic protein
MMA	ω-NG-monomethyl arginine
MS	Multiple Sclerosis
MTA	Methylthioadenosine
NLRs	Nod-like receptors
NOVA	Neuro-oncological ventral antigen
NPCs	Neuronal progenitor cells
OPC	Oligoprogenitor cells
PAMPs	Pathogen-associated molecular patterns
PH	Pleckstrin homology
poly(I:C)	Polyinosinic:polycytidylic acid
PPARγ	Peroxisome Proliferator Activated Receptor Gamma
PPMS	Primary progressive MS
PRMT1	Protein arginine methyltransferase 1
PRR	pattern recognition receptors
PSI	Percent spliced in
PTBP1	Polypyrimidine tract-binding protein
PTM	Post-translation modifications
QKI	Quaking
QRE	QKI response element
RBFOX	RNA Binding Fox-1 Homolog
RBP	RNA binding protein
RI	Retained intron
RLRs	RIG-like receptors
RNA-seq	RNA-sequencing
ROS	Reactive oxygen species
RRM	RNA recognition motif
RRMS	Relapsing-remitting MS
SAH	S-adenosyl-l-homocysteine
SAHH	SAH hydrolase
SAM	S-adenosyl-L-methionine
scRNA-seq	Single-cell RNA sequencing
SDMA	ω-NG, N'G-symmetric dimethylarginine
SDMA	Symmetric dimethylarginine
SE	Skipped exon
SF1	Splicing factor 1
SFARI	Simons Foundation Autism Research Initiative
SH3	Src homology 3
SLE	Systemic lupus erythematosus

SMA	Spinal muscular atrophy
SNPs	Single nucleotide polymorphisms
SP	Single-positive
SPMS	Secondary progressive MS
sQTL	Splicing as a quantitative trait
SRRM4	Serine/Arginine Repetitive Matrix 4
TAM	Tamoxifen
TEM	Transmission electron microscope
TLRs	Toll-like receptors
YS	Yolk Sac

awards. Finally, I want to thank my parents and my boyfriend who always trusted, supported and loved me throughout my career.

PREFACE

This thesis is a manuscript-based thesis which contains Chapters **1**-**4**. **Chapter 1** is a general introduction of microglia, PRMTs and QKI with the literature review that have been published with Dr. Stéphane Richard. **Chapter 2** and **3** are original research manuscripts that have been published (**Chapter 2**) and in preparation for the submission (**Chapter 3**). **Chapter 2** and **3** contains its own summary, introduction, materials and methods, results, discussion, and references sections. **Chapter 4** include final discussion and conclusion.

Papers included in this Thesis

Chapter 1   **Jeesan Lee*,** Nathalie Lamarche-Vane, Stéphane Richard "Microexon alternative splicing of small GTPase regulators: Implication in neurodegenerative diseases"
WIREs RNA, 2021 June 21; e1678. doi: 10.1002/wrna.1678.

Chapter 2   **Jeesan Lee*,** Oscar David Villarreal, Xiaoru Chen, Stéphanie Zandee, Yoon Kow Young, Cynthia Torok, Nathalie Lamarche-Vane, Alexandre Prat, Serge Rivest, David Gosselin and Stéphane Richard "QUAKING regulates microexon alternative splicing of the Rho GTPase pathway and controls microglia homeostasis"
Cell reports, 2020 Dec;33(13): 108560. doi: 10.1016/j.celrep.2020.108560.

Chapter 3   **Jeesan Lee*,** Oscar David Villarreal, Joey Heath, Yu Chang Wang, Jiannis Ragoussis, Alexandre Orthwein, David Gosselin and Stéphane Richard "PRMT1 promotes IFN-associated microglia and affects the remyelination of the central nervous system"
Manuscript in preparation

CONTRIBUTION TO ORIGINAL KNOWLEDGE

The contributions to original knowledge are listed below:

Chapter 2:

• Generation of QKI-deficient microglia mouse model using cx3cr1-creert2 and LoxP system

• The first study to characterize QKI-deficient microglia phenotype

• Identification of QKI as an RNA-binding protein responsible for regulating microexon alternative splicing

• Discovered that QKI regulates RhoA-GTPase pathway in microglia

• Discovered that QKI is required for microglia to promote remyelination of the central nervous system (CNS)

• QKI-5 expression in microglia is down-regulated in multiple sclerosis patient samples

Chapter 3:

• Generation of PRMT1-deficient microglia mouse model using cx3cr1-creert2 and LoxP system

• The first study to characterize PRMT1-deficient microglia phenotype

• Discovered that the PRMT1 is required for the remyelination of the CNS

• Characterization of microglial populations during the de/remyelination condition using scRNAseq in WT and PRMT1-KO mice

• Identification of the IFN-associated microglia cluster controlled by PRMT1

• PRMT1 controls the type I IFN response in bone-marrow-derived macrophages

CONTRIBUTION OF AUTHORS

Chapter 1:

Jeesan Lee wrote the review paper in collaboration with Dr. Stéphane Richard.

Chapter 2-3:

Dr. Stéphane Richard supervised the project and wrote the manuscript with Jeesan Lee. Jeesan Lee designed and performed the experiments and generated, analyzed and performed statistical analysis for the figures. Dr. Xiaoru Chen prepared the brain tissue sections. Yoon Kow Young performed FACS sorting for the microglia.

For Chapter 2, Dr. Oscar Villarreal, a postdoctoral fellow and bioinformatician in our laboratory, generated Figure 4A-B and Supplementary Figure A-B and E. The rest of the figures was produced by JL. Dr. Stephanie Zandee, Cynthia Torok, and Dr. Alexandre Prat provided multiple sclerosis human patient samples for the immunofluorescent analysis of QKI in microglia. Dr. Serge Rivest and David Gosselin provided advice on microglia and the procedure of the cuprizone diet mice model and . Dr. Nathalie Lamarche-Vane provided guidance for the Rho-GTPase assays. Dr. Marie-Eve tremblay provided advice on cuprizone diet mice model.

For Chapter 3, Dr. Oscar Villarreal, a postdoctoral fellow and bioinformatician in our laboratory, generated Figure 4A-B and Supplementary Figure4 A-B and E. The rest of the figures was produced by Jeesan Lee. Dr. David Gosselin provided general advice about microglia, genome-wide analysis and BMDMs. Joey Heath and Dr. Alexandre Orthwein assisted in the generation of the FACs data for BMDMs and its analysis. Dr. Rongtuan Lin and Dr. Zhenlong Liu aided in all the virus infection in BMDMs and in mice cohorts.

CHAPTER 1: INTRODUCTION

PART I : Microglia and CNS pathophysiology
1.1 Microglia

In 1919, the term "microglia" was first coined by the Spanish neuroscientist Pio del Rio Hortega (Ginhoux et al., 2013). After 100 years of research, we now know that microglia are the archetypical tissue-resident innate immune cells of the central nervous system (CNS) (Li and Barres, 2018). Microglia constitute 5–12% of the CNS population and they are integral components to diverse physiological processes. They are highly motile and continuously communicates with other cells of the CNS by surveying around the brain by retracting and protracting their highly ramified processes. Microglia are therefore implicated in CNS development, homeostasis, and immune response (Aguzzi et al., 2013) (Figure 1.1). Furthermore, in response to new 'omic' approach, microglia have become a primary focus in neuroimmunology research, and are considered to be causative of various CNS pathologies (Prinz et al., 2019). In this literature review, I will give a general introduction to the extraordinary research that defined microglia ontogeny and development, as well as their physiological function in pathology. Specifically, I will focus on multiple sclerosis (MS) and the function of microglia during the pathogenesis of MS.
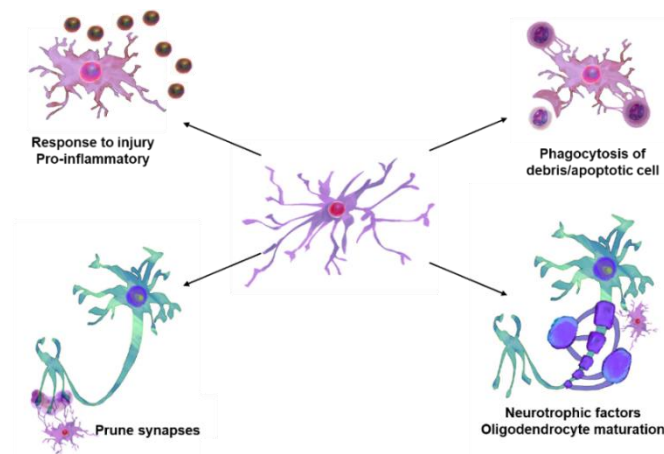
Figure 1.1 Microglia function in the CNS

1.1.1 Microglia Ontogeny and Development

Microglia arise early in embryogenesis and enter the brain parenchyma, where they respond to neural niches and aid in brain development. Unlike neurons, astrocytes and oligodendrocytes, which originate from the neuroectoderm, microglia have a unique origin (Ginhoux and Guilliams, 2016). Different technical procedures, including bone-marrow transplantation (Ginhoux et al., 2010), lineage-tracing (Ginhoux et al., 2010; Hashimoto et al., 2013) and parabiosis experiments (Ajami et al., 2007), have shown that microglia originate from yolk sac (YS) erythromyeloid precursors (EMPs) (Ginhoux et al., 2010; Ginhoux et al., 2013; Hashimoto et al., 2013). Moreover, further research also identified that microglia can originate from Ccr2 and Hoxb8 lineages and infiltrate the CNS around E12.5.(Chen et al., 2020; De et al., 2018).

The master transcription factor PU.1 drives the YS-EMPs towards microglia precursor EMPs (Kierdorf et al., 2013). Then, in an IRF8-dependent manner, microglia develop from CD45+c-Kit+Cx3cr1- EMPs (E7.25) to produce CD45+c-Kit− CX3CR1+ macrophages that move from the vasculature to occupy the brain parenchyma at E9.5 (Kierdorf et al., 2013). Therefore, unlike other tissue-resident macrophages where c-Myb-dependent EMPs migrate to the fetal liver and give rise to a monocyte intermediate, microglia have a distinct origin (Hoeffel et al., 2015; Schulz et al., 2012). After microglia colonize the brain, the blood-brain barrier (BBB) forms and thus limits the infiltration of immune cells.

Besides microglia, CNS-associated macrophages (CAMs), which encompass macrophages located in the meninges, perivascular space, and choroid plexus, also originate from YS EMPs but are c-Myb-dependent (Mrdjen et al., 2018; Van Hove et al., 2019) Microglia and CAMs are therefore distinct populations of cells that acquire heterogeneity even before colonization of the CNS.

Once microglia colonize the CNS, they display a morphology and transcriptional signature that is distinct from postnatal adult microglia (Matcovitch-Natan et al., 2016). During embryonic development and early postnatal stages, microglia have amoeboid morphology with short dendrites and enhanced phagocytosis functionality, which resembles more of macrophage morphology and phenotype (Masuda et al., 2019). Around postnatal 14, microglia acquire a full adult-microglia phenotype by expressing their *bona fide* marker gene Tmem119 and other markers such as Sall1, and P2ry12 (Hammond et al., 2019; Masuda et al., 2019).

Since microglia and neurons differentiate and colonize the brain parenchyma at a similar point in development, the survival, proliferation, and differentiation of microglia are highly dependent on extrinsic factors secreted by neurons or neural cell types, such as cytokines (IL-34, CSF1 and TGF-β), as well as cell-intrinsic programs (Greter et al., 2012; Wang et al., 2012). For instance, neurons and other glial cells secrete IL-34 and colony stimulating factor 1 (CSF-1), that are recognized by microglia CSF-1R receptor which then helps to maintain stable microglia population throughout the development and adulthood (Butovsky et al., 2014; Greter et al., 2012; Wang et al., 2012). Accordingly, CSF-1R-deficient mice, or mice treated with a CSF-1R inhibitor (PLX3397), lack microglia populations in the brain parenchyma (Elmore et al., 2014). Interestingly, depending on the brain region, microglial dependence on IL-34 and CSF-1 can differ. For instance, in the forebrain microglia depend on both IL-34 and CSF-1, whereas in the cerebellum microglia only require CSF-1 (Kana et al., 2019). In addition, transforming growth factor-beta 1 (TGFβ1) plays instrumental roles in postnatal maturation of microglia. Therefore, mice deficient in TGF-β have normal YS-EMPs but lack an endogenous mature microglia population expressing P2ry12, Sall1 (Butovsky et al., 2014).

Since the characteristics of microglia are highly dependent on external factors, primary microglia that are cultured *ex-vivo* completely lose their identity at the levels of gene expression and epigenetic markers (Gosselin et al., 2014; Gosselin et al., 2017). To compensate for this loss, microglia are often cultured in the presence of TGF-β and CSF-1 to maintain the homeostatic microglia feature, however this does not entirely recapitulate the microglia profile found *in vivo*. The identity of microglia is also driven by the intrinsic factors that differ from other innate immune cells. Many studies have soundly supported this notion by engrafting HSC-derived macrophages to the brain parenchyma and compared the transcriptomes to that of resident microglia (Bennett et al., 2018; Shemer et al., 2018). Even after a prolonged period of residence for the HSC-macrophages, engrafted cells remained a distinct population both epigenetically and transcriptionally (Shemer et al., 2018).

Besides environmental and intrinsic factors, microglia heterogeneity also arises from the gut-microbiome, biological sex, and environmental factors (Erny et al., 2015; Guneykaya et al., 2018; Thion et al., 2018b). These findings are interesting as autoimmune diseases are more prevalent in females while neurodevelopment diseases are more common in males (Halladay et al., 2015). However, how sexual dimorphism contributes to the pathogenesis of these diseases is still unclear.

Therefore, microglia communicate with almost all cells of the CNS and sculpt the brain architecture. Hence, it is not surprising that microglia are a critical cell type in CNS disease progression such as multiple sclerosis. In the following sections, I will briefly introduce multiple sclerosis (MS) and how microglia participate in its pathogenesis.

1.1.2 Microglia function during development

Neurons start to develop around the time microglia enter the brain parenchyma, and microglia are involved in rewiring of synapses, pruning synapses and guiding neurogenesis to build neuronal architecture (Li and Barres, 2018; Peri and Nusslein-Volhard, 2008). For instance, during the first two weeks of postnatal development, activation of the neuronal N-methyl-D-aspartate receptor (NMDAR) causes release of ATP. Microglia can sense the secreted ATP using P2RY12 receptor and rewire synapse circuitry (Dissing-Olesen et al., 2014; Sipe et al., 2016). Microglia not only rewire synaptic circuitry, but they also prune (trogocytosis) synapses by using the complement system. Microglia express complement receptor 3 (CR3), composed of the CD11b and CD18 integrin chain, which recognizes C3 and C1q opsonin (Stephan et al., 2012). During neuron development, activation of the complement system induces opsonization of neurons, thereby promoting trogocytosis function of the microglia (Schafer et al., 2012). At the first postnatal week, C1q and C3 tag weak synapse. Microglia then sense these tags via CR3 and prune unnecessary synapses (Schafer et al., 2012). Likewise, genetic deletion of C3 affects synaptic circuitry and causes defects in eye segregation of the lateral geniculate nucleus (LGN). Moreover, C1q-deficient mice experience seizures and contain excessive excitatory neurons (Chu et al., 2010).

  Microglia actively engage in neurogenesis by performing phagocytosis to eliminate unnecessary cells, and by secreting neurotrophic factors to aid in the differentiation process (Marin-Teva et al., 2004; Sedel et al., 2004). For instance, microglia produce reactive oxygen species (ROS) to induce apoptosis of the Purkinje neuron and actively phagocytose dead cells during cerebellar development (Marin-Teva et al., 2004). Moreover, around E20, microglia control the number of neuronal progenitor cells (NPCs) by removing excess or dying NPCs (Sedel et al., 2004). This activity is also observed in adult neurogenesis, in which microglia phagocytose neurons in the

murine hippocampus area. The phagocytosis is performed by TYRO3, AXL and MER (TAM) receptor tyrosine kinases or CD11b and DNAX-activation protein 12 (DAP12) (Fourgeaud et al., 2016).

Following the postnatal time point, microglia start to crosstalk with other cells in their microenvironment to support their differentiation and development. At postnatal 3-5, CD11c+ amoeboid microglia represent 20% of the total microglia population and are mainly observed in the white matter and corpus callosum regions of the brain (Wlodarczyk et al., 2017). These microglia secrete IGF1 and interact with oligoprogenitor cells (OPCs) to promote their differentiation to myelinating oligodendrocytes (Wlodarczyk et al., 2017). In parallel, microglia communicate with other glial cells, including astrocytes. During the CNS development, astrocytes secrete IL-33 in the spinal cord or in the thalamus, which triggers the microglial phagocytic function to engulf unnecessary synapses (Vainchtein et al., 2018). Moreover, microglia control astrocyte number and activity by phagocytosing precursor or mature astrocytes (Fantin et al., 2010).

1.2 Multiple sclerosis

MS is an autoimmune, neurodegenerative disease of the CNS which is characterized by inflammation, demyelination, and axonal transection (Filippi et al., 2018). The clinical course of MS takes on two paths: relapsing or progressive. The relapsing form of MS (RMS) is the most common, accounting for 85% of MS cases, and features discrete episodes of neurological disabilities followed by partial or complete recovery of neurological dysfunction (Hartung et al., 2019). During disease progression, typically 10-20 years, relapses become less frequent and 50-70% of RMS cases develop into secondary progressive MS (SPMS), which is irreversible and eventually leads to loss of cognition and motor function in patients. The remaining 15% of cases

develop primary progressive MS (PPMS), in which patients experience slow and repetitive neurological dysfunction without any relapses or remission. The onset of the disease is 20-40 years of age for RRMS and 40 years of age for PPMS, with 10% of the patients experiencing the first episode in their adolescent years (Hartung et al., 2019). The prevalence of MS is three times higher in women, but the exact mechanism contributing to this female preponderance is not precisely understood (Greer and McCombe, 2011). MS has a tremendous impact on patient quality of life by affecting their cognition, motor movement and financial stability. Globally, 2.3 million people have been diagnosed with MS, with a prevalence of 50–300 per 100 000 people (Filippi et al., 2018). The prevalence of MS differs by the region with North America and eastern Europe having the highest rates (>100 cases per 100,000) and regions closest to the equator having the lowest rates (<30 cases per 100,000) (Alonso and Hernan, 2008; Rosati, 2001). Interestingly, there is a significant correlation between latitude increase with the higher risk of MS in North America and Europe.

The causes of MS are multifactorial and heterogenous, which can be underlined by genetic, environmental, and lifestyle factors (Figure1.2). Research has shown that monozygotic twins have a higher incidence of MS than dizygotic twins and siblings, indicating that genetic factors play a significant role in MS pathogenesis (Harirchian et al., 2018). The genetic cause of MS is polygenic, implicating multiple polymorphisms across several genes. The most common polymorphism is human leukocyte antigen (HLA)- beta chain (DRB)1*15:01, which accounts for 20-30% of the genetic susceptibility of MS. HLA-DRB1 is HLA class II beta chain paralog which play a critical role in immune surveillance by presenting antigen in the surface of the immune cells. Strikingly, carriers with the HLA- DRB1*15:01 polymorphism are three times more likely to develop MS than non-carriers. Moreover, Genome-wide association studies (GWAS) and meta-analyses have

identified more than 200 genes as risk factors for MS (Baranzini and Oksenberg, 2017). These genes include T cell activation and proliferation-associated genes (IL2 and IL7R) and genes involved in the adaptive immune response (STAT3, IRF8 and TNFRSF1A) (Baranzini and Oksenberg, 2017; De Jager et al., 2009; International Multiple Sclerosis Genetics et al., 2013). In addition, environmental and lifestyle factors, such as vitamin D deficiency, cigarette smoking, obesity in adolescent years, and Epstein–Barr virus (EBV) infection during adolescent age, are well-established risk factors for MS (Bjornevik et al., 2022; Filippi et al., 2018).

Currently, no treatments are available on the market that can entirely stall or reverse MS-induced progressive neurological dysfunction (Granqvist et al., 2018). However, several classes of disease-modifying treatments (DMT) have been approved for relapsing and remitting MS to ameliorate the symptoms or reduce the attacks by suppressing immune cell function (Figure1.2).
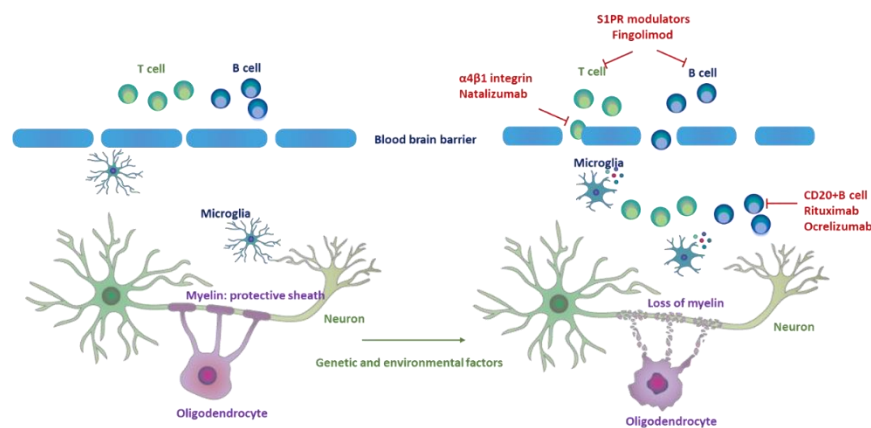
Figure 1.2 Pathogenesis of MS and therapeutic drugs

One of the first drugs approved by the FDA in 1993 was injectable interferon-beta-1b (IFNβ). This IFNβ treatment is cost-effective and has a low risk of severe drug response compared to other MS DMTs, but the effectiveness is moderate. In 2003, subcutaneous injection of Glatiramer acetate, a synthetic polypeptide analogous to the myelin-basic protein (MBP), was clinically proven to decrease the relapses and disability of the disease. In subsequent years, immunotherapies that inhibit lymphocyte infiltration to the CNS, or eliminate a subset of B cells,

have been developed and clinically approved. Natalizumab, an α4 integrin antagonist, inhibits T cells from binding to the endothelial cells of blood vessels, which therefore blocks T cell infiltration to the brain. The use of natalizumab has shown significant success in clinical trials, with a reduction in disability progression, and reduction in relapses (Polman et al., 2006). In addition, the sphingosine-1-phosphate receptor modulator secludes lymphocytes in the primary lymphoid organ and suppresses the infiltration of lymphocytes into the CNS (Kapoor et al., 2018). Lastly, CD20-targeting antibodies Rituximab, Ocrelizumab, and Ofatumumab, which reduce pro-B cell differentiation into plasma cells, have been shown to improve patient outcome (Hawker et al., 2009; Montalban et al., 2017). Importantly, Ocrelizumab has a significant success rate in reducing new episodes, reducing the total volume of brain lesions, reducing the percentage of brain volume loss, and enhancing motor functions (Montalban et al., 2017).

1.2.1 Microglia involvement in MS pathogenesis

The pathological hallmarks of MS are demyelinated inflammatory focal lesions in the white and gray matter of the brain and spinal cord. The demyelination and inflammation are mainly driven by lymphocytes, which cross the BBB and infiltrate to the CNS where they become activated by microglia and myeloid-derived cells (Filippi et al., 2018) (Figure 1.2). I will primarily focus on the involvement of microglia during MS pathogenesis.

When microglia sense pathogens or injury, they become activated and migrate towards the site of damage/infection (Voet et al., 2019)(Figure 1.2). Microglia are, therefore, some of the first cells to encounter and respond to the inflammation and may promote loss of myelin with infiltrating reactive lymphocytes and monocytes/macrophages (Lloyd and Miron, 2019). Likewise, activated microglia are evident in early and chronic lesions, as well as in normal-appearing white

matter of the CNS. These microglia express markers associated with phagocytosis, inflammation, antigen presentation, and T cell activating molecules (Zrzavy et al., 2017).

Different mouse models of MS, including experimental autoimmune encephalomyelitis (EAE) and cuprizone diet-induced demyelination models, have shown that microglia are the central cells that engulf and efficiently remove myelin debris in the CNS, which helps augment the remyelination process (Lloyd and Miron, 2019). Therefore, microglia with an impaired phagocytosis, hinder remyelination process and exacerbate disease progression (Voet et al., 2019). For example, microglia deficient in the innate immune receptor TREM2 failed to induce the expression of genes associated with phagocytosis and lipid degradation, thereby exacerbating the demyelination and disease progression (Poliani et al., 2015). Furthermore, microglia in aged mice are compromised at degrading phagocytosed myelin, leading to aberrant immune cell function and failure to regenerate myelin (Safaiyan et al., 2016).

As an innate immune cell in the CNS, microglia secrete diverse molecules to communicate with multiple cell types. During the pathogenesis of MS, microglia secrete pro-inflammatory chemokines (CCL2, CCL3, and CCL4) to recruit lymphocytes to the CNS (Lewis et al., 2014) (Figure 1.2). Microglia also secrete TNF, IL1α, and complement proteins to activate reactive astrocytes that cause neuronal and oligodendrocyte damage (Pare et al., 2017). Besides pro-inflammatory cytokines and chemokines, microglia also secrete anti-inflammatory molecules. For example, microglial secretion of TGFβ can trigger the differentiation of Th2 helper cells to Treg cells, which can then suppress MS progression (Ponomarev et al., 2007). Likewise, IFNβ secreted from microglia can suppress lymphocyte activation and inflammation (Kocur et al., 2015). In addition to pro- and anti- inflammatory molecules, microglia can also secrete regenerative factors to enhance the remyelination and regeneration of neurons. For instance, microglia-derived IL-4

and activin A can enhance OPCs differentiation and regenerate myelin (Lloyd and Miron, 2019).

In addition, microglia secrete IGF1 and FGF2 to promote neuronal repair and OPCs expansion

(Perez-Martin et al., 2010) (Figure 1.2).

Alongside the phagocytic and secretory functions of microglia, they can also act to present

different surface molecules to activate T cells in the CNS (Almolda et al., 2010). For example, in

the EAE mouse model, microglia use the B7-1 and B7-2 receptors to bind to CD28 expressing T

cells and promote T cell activation and proliferation. Moreover, microglia use the CD40 receptor

to bind to CTLA4 and promote T cell apoptosis or anergy (Dong and Yong, 2019).

Given these data, it is clear that a diverse spectrum of microglia are present within MS

pathogenesis. These conclusions are supported by advances in single-cell sequencing technology,

where microglia heterogeneity is assessed in MS patient samples and MS mouse models (Masuda

et al., 2019). Therefore, I will examine some of the elegant work that identified different microglia

populations during neurodevelopment and disease settings.

1.3 Microglia heterogeneity with single-cell technology

Microglia continuously monitor their surroundings using surface receptors, and quickly adapt their

transcriptional program, morphology, and electrophysical properties to fulfill a wide range of roles

(Masuda et al., 2020b). During CNS development, neurodegeneration and neuroinflammation,

context-specific microglia emerge, promoting the idea that microglia acquire a diverse spectrum

of phenotypes (Fatoba et al., 2020). The advancement of single-cell, single-nucleus, and single-

cell mass spectrometry (CYTOF) technologies conceptualized this idea and enabled us to

comprehensively delineate microglia heterogeneity in an unbiased fashion (Masuda et al., 2020b;

Prinz et al., 2019). We are now just beginning to understand the transcriptional signatures that

define context-specific microglia and their possible functions in normal CNS physiology or during pathophysiology. This section will review the different types of microglia, their specific gene signatures, and their functions during CNS development, neurogenerative and neuroinflammatory disease, and in COVID-19 infected patients (Hammond et al., 2019; Masuda et al., 2019; Mathys et al., 2017; Olah et al., 2020; Schwabenland et al., 2021; Yang et al., 2021) (Figure 1.3). Understanding microglia subtypes will hopefully allow us to further elucidate the specialized functions of these cells in a specific context. It is our hope that this will allow us to identify inflammatory, phagocytic and regenerative microglia that can be potentially translated into the therapeutic avenue (Masuda et al., 2020b).

	Homeostatic	DAM	Early postnatal	Interferon	Antigen-presenting	Pro-inflammatory	Phagocytic
Markers	TMEM119	APOE	IGF1	IRF1	CD74	IL1B	LAMP1
	P2RY12	AXL	CD11c	IRF7	H2-Aa	CCL3	CD68
	CX3CR1	TREM2	SPP1	IFITM3	H2-Ab1	CCL4	CLEC7a
	CSF1R	Clec7a	LAMP1	ISG15	H2-D1	TNF	LPL
	HEXB	CD11c	CD68	OASL2	H2-Q5	JUN	CTSB
	FCRLS	CTSD	APOE	CXCL10	CD11c	NFKB	RAB7
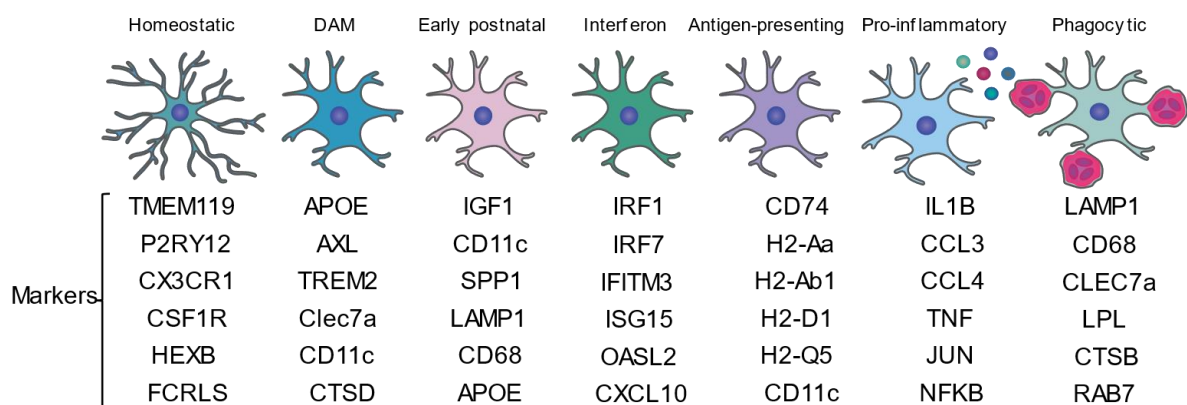
Figure 1.3 Subtypes of microglia and respective marker genes

1.3.1 Disease-associated microglia (DAM)

Keren-Shaul et al., 2017, were pioneers of the concept of microglia heterogeneity in different types of neurodegenerative disease (Keren-Shaul et al., 2017). By utilizing an Alzheimer's disease (AD) mouse model (5XFAD), an ALS mouse model (mSOD1) and aged mice (6 month old), the authors identified a specific sub-cluster of microglia that was found across all conditions, despite each model having disparate pathophysiology (Keren-Shaul et al., 2017). This subcluster was termed disease-associated microglia (DAM) and it expressed phagocytosis- and lipid metabolism-

associated transcripts (Trem2, Apoe, Clec7a, Axl, and Cd11c), with a concomitant decrease in homeostatic markers (P2ry12, Teme119, and Cx3cr1) (Figure 1.4) (Keren-Shaul et al., 2017). Further analysis revealed that DAM microglia take on two transition processes; one TREM2-independent and the other TREM2-dependent (Keren-Shaul et al., 2017). First, stage 1 DAMs appear independently from TREM2 signaling and express the following markers: Tyrobp, Apoe, B2m, and Ctsd (Keren-Shaul et al., 2017). Then, in a TREM2-dependent manner, stage 1 DAMs progressively acquire a unique transcriptional signature and express markers that define stage 2 (Figure 1.4)(Keren-Shaul et al., 2017). Interestingly, TREM2 is only expressed by microglia in the CNS, and genome-wide association studies (GWAS) in AD patients found several loss-of-function single nucleotide polymorphisms (SNPs) in the *TREM2* gene. In line with this, TREM2 KO or TREM2 R47H variant AD mouse models facilitated Aβ accumulation and exacerbated AD pathogenesis, indicating that TREM2 is required for microglia to execute specific functions (Ulland and Colonna, 2018). This evidence suggests that TREM2-mediated stage 2 DAM might be required to ameliorate neurodegenerative disease progression. In addition, different single-cell sequencing analysis identified the DAM phenotype during early post-natal development and across various CNS diseases, including multiple sclerosis, cancer and viral infection (Hammond et al., 2019; Masuda et al., 2019; Ochocka et al., 2021; Olah et al., 2020; Schwabenland et al., 2021; Yang et al., 2021; Zheng et al., 2021). Therefore, the DAM phenotype is not restricted to specific disease contexts, but could perhaps be a phenotype that arises due to changes in the CNS environment, such as increased abundance of apoptotic or necrotic cells as well as the presence of pathogens.

1.3.2 Embryonic and postnatal microglia

According to two independent studies, specific subclusters of microglia are present at embryonic and early postnatal development stages (Hammond et al., 2019; Masuda et al., 2019). For instance, microglia expressing Ms4a7 are only present during the embryonic stage (Hammond et al., 2019) (Figure 1.4). In another study, however, authors did not observe an Ms4a7+ cluster during the embryonic stage but instead used lysosomal-associated genes to define the embryonic microglia cluster (Masuda et al., 2019). Even with these discrepancies, both studies observed remarkable heterogeneity of microglia in the early postnatal period (Hammond et al., 2019; Masuda et al., 2019). For example during the early postnatal period, a specific subcluster of microglia was found to be localized at pre-myelinated axon tracts in the CNS. This cluster contained the DAM phenotype alongside transcripts associated with immune cell activation, lysosomal activity, and phagocytosis (Figure 1.4). This is in line with previous studies in which microglia at the early postnatal stage express one of the DAM markers, CD11c, with distinct amoeboid morphology, while also secreting IGF1 factors that may promote the differentiation of OPCs to myelinating oligodendrocytes (Wlodarczyk et al., 2017) (Thion et al., 2018a). Microglia therefore acquire distinct transcriptional signatures and morphology across CNS development that may contribute to CNS architecture.

1.3.3 Interferon (IFN) microglia

The IFN microglia cluster has been observed across a diverse spectrum of diseases, including AD and MS, and during viral infection (Hammond et al., 2019; Li et al., 2019; Lloyd et al., 2019; Masuda et al., 2019; Mathys et al., 2017; Ochocka et al., 2021; Olah et al., 2020). One study analyzed the trajectory of microglia from the CK-p25 mouse model, which triggers

neurodegeneration by activating p25. These mice progressively accumulate amyloid-β, which causes neuronal loss with astrogliosis and microgliosis (Mathys et al., 2017). Interestingly, during neurodegeneration, microglia first express DNA repair-, replication-, and cell-cycle-associated genes, before gradually transitioning to type I/II IFN- and MHC I/II-expressing microglia (Mathys et al., 2017) (Figure 1.4). Furthermore, IFN-microglia clusters also carried DAM signatures, suggesting similarities between these populations (Keren-Shaul et al., 2017; Mathys et al., 2017). In contrast to this *in vivo* study, the IFN-microglia cluster was one of the clusters absent in AD patient samples compared to controls (Olah et al., 2020) (Figure 1.4). We can therefore infer that IFN-microglia emerge in response to neurodegeneration, and may play a protective role in removing amyloid-β or secreted factors to promote regeneration of the CNS.

IFN-microglia are also prevalent in different MS mouse models and are considered to be regenerative microglia that assist remyelination in the CNS (Hammond et al., 2019; Lloyd et al., 2019; Masuda et al., 2019). According to research by Lloyd *et al*, during de/remyelination processes, microglia transition to a pro-inflammatory phenotype and undergo necroptosis to give rise to IFN-microglia (Lloyd et al., 2019). These microglia appear mostly during the remyelination phase, alluding to their regenerative role. This is supported by studies using an antibody against IFNAR2, which blocks IFN signaling in microglia, which demonstrated further hindering of the remyelination process in the CNS (Lloyd et al., 2019).

1.3.4 Antigen-presenting microglia

The antigen-presenting microglia cluster is apparent in AD, MS, and virus-infected CNS (Ajami et al., 2018; Benedek et al., 2017; Hammond et al., 2019; Li et al., 2019; Mathys et al., 2017; Olah et al., 2020; Schwabenland et al., 2021; Wolf et al., 2018; Yang et al., 2021). In the AD mouse

model, when neurodegeneration is apparent, microglia express MHCI- and MHCII-associated transcripts (Mathys et al., 2017)(Figure 1.4). However, in AD patient samples, the antigen-presenting cluster is lost, indicating that the antigen-presenting cluster might be required for preventing further AD progression (Olah et al., 2020).

In the context of MS, the role of the antigen-presenting cluster is still debated. In MS mouse models, and in MS patient samples, the antigen-presenting cluster (MHCI- and MHCII-expressing) is expressed which indicates a possible role in disease pathogenesis (Ajami et al., 2018; Hammond et al., 2019; Masuda et al., 2019). However, genetic KO of MHCII in microglia does not impact their de/remyelination capabilities, in both EAE and cuprizone diet mouse models. Additionally, in EAE, where CD4+ and CD17+ T cells infiltrate to the CNS, the loss of MHCII in microglia did not alter T cell populations (Wolf et al., 2018). This is a surprising finding as microglia are known to interact with T cells through MHCII to alter T cell activation states. Conversely, in another study, MHCII recombinant protein treatment in male EAE mice stymied the infiltration of T cells and severity of CNS damage, whereas in female EAE mice MHCII recombinant protein led to only a minor change (Benedek et al., 2017). Further studies are still needed to address why responses to MHCII recombinant treatment differ by sex, and whether or not MHCII microglia impact MS pathogenesis.

The antigen-presenting cluster is also seen in COVID-19 infected patients (Schwabenland et al., 2021; Yang et al., 2021)(Figure 1.4). According to recent multiplexed high-dimensional imaging sequencing data, antigen-presenting microglia (HLA-DR) formed microglial nodules and interacted with activated CD8+ T cells. Another study used single-nuclear sequencing and found that the antigen-presenting cluster (CD74) express DAM and neuroinflammatory markers (Schwabenland et al., 2021; Yang et al., 2021). MHCII-expressing microglia may therefore

interact with T cells during COVID-19 infection and modulate T cell function to affect pathophysiology.

1.3.5 Pro-inflammatory microglia

The transcriptional signature of pro-inflammatory microglia overlaps with DAM, IFN, and antigen-presenting microglia clusters (Hammond et al., 2019; Lloyd et al., 2019; Masuda et al., 2019; Mathys et al., 2017; Ochocka et al., 2021; Zheng et al., 2021). However, pro-inflammatory microglia also express cluster-specific markers (Hammond et al., 2019; Lloyd et al., 2019; Masuda et al., 2019; Mathys et al., 2017). For instance, during aging, microglia acquire two distinct populations that are either pro-inflammatory or IFN-microglia. The pro-inflammatory microglia express the inflammatory cytokine Il1b, and chemokines Ccl3 and Ccl4 (Hammond et al., 2019)(Figure 1.4). During Lysophosphatidylcholine (LPC)-induced de/remyelination model, microglia first acquire a pro-inflammatory phenotype (Tnfrsf1b, Jak2, Nfkbid, Cryba1, Gpmnb, Socs1, and Cd40), before undergoing necroptosis to give rise to IFN-associated microglia (Lloyd et al., 2019).

These pro-inflammatory microglia are also evident when a virus or cancer causes damage to the CNS. In a human immunodeficiency virus (HIV)-mouse model, microglia acquire two distinct populations: pro-inflammatory and IFN microglia (Zheng et al., 2021). Similarly, in GL261 glioma-bearing mice, pro-inflammatory microglia were apparent and expressed Ccl3, Ccl4, and Ccl12 (Ochocka et al., 2021). Pro-inflammatory microglia have therefore been identified in multiple disease contexts, but their role remains to be investigated.

1.3.6 Phagocytic microglia

As the primary phagocytes of the CNS, microglia sense and engulf apoptotic or necrotic cells, misfolded proteins, and pathogens to maintain CNS homeostasis (Masuda et al., 2020b; Prinz et al., 2019; Thion et al., 2018a). Moreover, microglia phagocytose unnecessary synapses as well as a pool of OPCs to maintain tissue architecture during CNS development (Masuda et al., 2020b; Prinz et al., 2019; Thion et al., 2018a). Unsurprisingly, phagocytic microglia are found during early postnatal stages, where they express lysosomal- (Lamp1, Lpl, and Apoe) and phagocytic-associated transcripts (CD68, and Clec7a), indicative of phagocytic functionality (Li et al., 2019). Furthermore, phagocytic microglia have amoeboid morphology and are mainly localized at the axon tract of the white matter region. A subsequent study found that phagocytic microglia (Clec7a) engulf apoptotic oligodendrocytes, which further permits new myelin formation during the early postnatal period (Li et al., 2019).

The 5XFAD AD mouse model accumulates amyloid plaque, which is removed by microglia to protect the CNS from further neuronal damage (Grubman et al., 2021). To identify the transcriptional landscape of amyloid plaque engulfing-microglia, the amyloid plaque was labeled with XO4, and microglia were sorted by XO4 expression (Grubman et al., 2021). Single-cell analysis then revealed that XO4+ microglia were enriched in genes encoding the microglial sensosome, including c-lectins (Clec4a2, and Clec4a3), CD markers (Cd33, and Cd68) and phagolysosome markers (Cd68, Ctsa, Ctsb, Ctsd, Ctsz, and Rab7) (Grubman et al., 2021). This cluster also expressed Trem2- and Apoe-interacting partners such as Tyrobp10, Lpl, Ldlr and Lrpap1 (Grubman et al., 2021). These results suggest that amyloid plaque engulfing-microglia express distinct gene signatures, with an enhanced expression of sensosome, phagolysosome, and Trem2 and Apoe-interacting partners (Grubman et al., 2021). A recent study also revealed

phagocytic-exhausted microglia in aged mice. These microglia expressed CD22 and, by blocking this receptor using an anti-CD22 antibody, the microglia were better able to remove myelin debris, amyloid-β oligomers and α-synuclein fibrils *in vivo* (Pluvinage et al., 2019). This indicates that phagocytic microglia are crucial during the early postnatal period, and in pathological settings, to promote appropriate CNS development and protect the CNS from damage. In the following sections, I will briefly introduce two of the proteins I identified as crucial regulators of microglia function during de/remyelination of the CNS.

Method	Cluster and markers	Significance of the cluster
sc-RNA-seq 6mnth WT, 5XFAD Trem2+/+ and Trem2−/−5XFAD mSOD1 80days and 135days 7week, 20mnth, Keren-Shaul et al (2017)	Stage 1 DAM: Tyrobp, Apoe, B2m, Ctsd, Stage 2 DAM: Tyrobp, Apoe, B2m, and Ctsd, Lpl, Cst7, CD11c, Clec7a, and CD63, Apoe, Lpl, CD9, Cst7, Trem2	Stage 1 DAM: Abundant in ALS, AD and aging mice model. Intermediate stage of DAM. Stage 2 DAM: abundant in ALS, AD and aging mice model. With high levels of phagocytic and lipid metabolism pathways
sc-RNA-seq CK-p25 0 week 1 week 2 week 6 week Mathyset al (2017)	Early response 1 (Cluster3): Top2a, Uhrf1, Rrm2, Rad51, Pole Early response 2 (Cluster7): Top2a, Spc25, Plk1, Nusap1, Sdc80 Late response (Cluster6): Ifitm3, Irf7, Oas1a, Rsad2, Zbp1, H2-Aa, H2-Ab1, Cd74, H2-D1, H2-Q5	Early response 1 (Cluster3): appear early in AD-mice, increased expression of DNA repair and replication Early response 2 (cluster7): Cell cycle-related genes Late response (Cluster6): Appears in 6weeks. IFN genes, and MHC I and II associated genes
sc-RNA-seq aging dorsolateral prefrontal cortex (DLPFC): 14 patients Temporal cortex with intractable epilepsy: 3 patients Olah et al (2020)	IFN-cluster (Cluster 4): IRF1, 7 and 8, ISG15, IFITM3, IFIT3 Anti-inflammatory (Cluster 5 and 6): IL-10, IL-4, and IL-13, CREB, ATF, CD83, CCL4, CCL3, CCL2, ID2, CD83, NFKBID Antigen presentation cluster(Cluster 7): CD74, HLA-DRB1, HLA-DM1, HLA-DMB, CD68 Cell cycle cluster(Cluster9): E2F1, CBFB, and NF1, PCNA, MKI67	IFN-cluster (Cluster 4): high expression of MS susceptibility gene (IFITM3), lost in AD patient sample Antigen presentation cluster(Cluster 7): most enriched for DAM Cluster 4 and 7: Higher expression of AD susceptibility genes (APOE and TREM2) and lost in AD patient sample
sc-RNA-seq E14.5, P4/5, P30, P100, _450, LPC-Injury Hammond et al (2019)	Embryonic microglia: Ms4a7, Ms4a6c, Ms4a6b, Ms4a6d, Tmem176a, Tmem176b, Ccr1, Mrc1 Axon Tract-Associated Microglia (ATM): Spp1, Igf1, Gpnmb, Lgals1, Lgals3, Lamp1, Cd68, Lpl, Apoe Aging cluster (OA2): Cst7, Lgals3, CCl4, CCl3, Id2, Atf3 Aging cluster (OA3): Ifitm3, Rtp4, Oasl2, Ifi2712a, Ifi204 Injury-responsive cluster (IR): Cxl10, CCl4, Apoe, Spp1, Lpl, and Apoe, Spp1, Lpl, Apoe, Ifi204	Embryonic microglia: expresses transmembrane chemosensors ATM: early postnatal microglia with DAM signature OA1-OA2: aging microglia with inflammatory signature OA3: aging microglia with IFN-responsive signature IR: IFN-responsive and DAM signature
sc-RNA-seq E16.5, 3weeks 16 weeks Facial-nerve axotomy Cuprizone Multiple sclerosis patient: 5 Control patient: 5 Masuda et al (2019)	Lysosomal associated microglia: Ctsb, Ctsd, Lamp1, Apoe, Demyelinatio/Remyelination 1:Apoe, Axl, Igf1, Lyz2, Itgax, Gpnmb, Apoc1,Fam20c, Cst7, Ccl6, Fn1, Ank, Psat1, Spp1 Demyelinatio/Remyelination 2: Apoe, Axl, Igf1, Lyz2, Itgax, Gpnmb Apoc1,Cybb MHC class II genes Cd74, H2-Aa, H2-Ab1 Neurodegeneration microglia: Ctsc, Apoe, Axl, Igf1, Lyz2, Itgax, Gpnmb MS humnan1: CTSD, APOC1, GPNMB, ANXA2 MS humnan2: CD74, HLA-DRA, HLA-DRB1, HLA-DPB1 MS humnan3:SPP1, PADI2, LPL	Lysosomal microglia: observed only in embryonic stage Demyelination/Remyelination and neurodegenerative microglia: All expressed DAM Human MS microglia: High MHC class II-related molecules and similar signature as cuprzone microglia

Method	Cluster and markers	Significance of the cluster
Single-cell mass cytometry EAEmodel R6/2 model mSOD1 model 255 antibodies Ajami (2018)	Population B: HC-II and CD86, D80, Axl, TIM4, PD-L1, CCR5,CCR4, GM-CSF and TNF-α Population C: CD11c, MHC-II, CD86, CD80, Axl, TIM4, PD-L1, CCR5, CCR4, GM-CSF and TNF-α	Population C: CD11c exclusive. Increase during EAE and decrease after recovery or EAE chronic stage. Low in HD mice Population A-C: HD and ALS express less of GM-CSF and TNF-α compared to EAE. And express more of IL-10.
sn-RNA-seq COVID19 patients: 8 Control patients: 14 Yang(2021)	COVID19 specific microglia population: APOE, TREM2, CD9, CD14, C1QC, FTH1, RIPK1, LRP1b, PTPN1	COVID19 associated microglia expressed some of DAM transcripts and genes associated with neuroinflammation and AD associated genes
Highly multiplexed high-dimensional imaging CoVID19 patient:25 Control: 5 Extracorporeal membrane oxygenation (ECMO) therapy Multiple sclerosis patient: 6 Schwabenland (2021)	Microglia nodule found in the COVID19 patient:PDL-1 and HLA-DR high microglia	Micronodule microglia interacting with activated cD8+ cells

Figure 1.4 Overview of single cell technologies which profiled microglia heterogeneity

Part II : Arginine methylation in immune cells

1.4 Arginine methylation

Post-translation modifications (PTM) of proteins are instrumental in modifying protein stability, interaction, and localization, which can subsequently impact diverse signaling processes (Xu and Richard, 2021). As one example of a PTM, arginine methylation is catalyzed by protein arginine methyltransferases (PRMTs), which utilize the co-substrate S-adenosyl-L-methionine (AdoMet, SAM) to transfer a methyl group to the guanidino nitrogen atoms of arginine residues, giving rise to the formation of methylarginine and S-adenosyl-l-homocysteine (AdoHcy, SAH)(Xu and Richard, 2021). PRMTs are categorized according to the types of methylation they can catalyze. Type I PRMTs (PRMT1, 2, 3, 4, 6, and 8) are the most common type of PRMTs and generate ω-NG-monomethyl arginine (MMA) and ω-NG, NG-asymmetric dimethylarginine (ADMA) (Bedford and Clarke, 2009). Of the type I PRMTs, PRMT1 is the primary enzyme that catalyzes 80% of ADMA in our total proteome, including histone 4 at arginine 3 (H4R3me2a). Type II PRMTs (PRMT5 and 9) generate ω-NG, N'G-symmetric dimethylarginine (SDMA) and type III PRMT (PRMT7) only catalyzes MMA. All PRMTs contain two main domains: the SAM binding Rossman fold domain and the β-barrel domain. The side chain of arginine contains the guanidinium moiety, which is positively charged at physiological pH and can form five hydrogen bonds as well as π-stacking interactions (Bedford and Clarke, 2009). The methylation of arginine enhances its hydrophobicity without changing the positive charge but causes the loss of hydrogen bond donors, thereby possibly affecting specific protein interactions. The methylation *per se* can also enhance π-stacking interactions with aromatic rings, thereby promoting new interaction interfaces. The methylation of arginine can therefore positively or negatively influence protein-protein interactions. The Tudor domains, or WD40 domains, can recognize methylated arginine

(Bedford and Clarke, 2009). There are 36 Tudor-containing proteins; however, only eight bind methyl arginine (Bedford and Clarke, 2009).

1.5 The role of PRMTs in innate and adaptive immune cells

Arginine methylation can provide multiple stimuli to cause immune cells to undergo differentiation, activation, and proliferation, thereby impacting innate and adaptive immune responses (Sengupta et al., 2020; Xu and Richard, 2021). Early studies, in particular, employed mouse models of autoimmune disease to develop our understanding of the function of PRMT1 and PRMT5 in lymphopoieses and lymphocyte activation (Infantino et al., 2017; Litzler et al., 2019; Sengupta et al., 2020; Xu and Richard, 2021).

1.5.1 T cells

The use of pan-methyltransferase inhibitors, PRMT inhibitors, and the generation of conditional knockout (cKO) mice has demonstrated that PRMT1 and 5 are essential regulators of T cell biology, including thymic T cell development, peripheral naive T cell development, effector T cell differentiation, and T cell activation. Initial studies focused on using pan methyltranferase inhibitors (MTA and SAH inhibitor) to observe how these inhibitors impact autoimmune disease progression (Fu et al., 2006; Moreno et al., 2006; Yang et al., 2013). For instance, using the EAE experimental MS mouse model, methylthioadenosine (MTA) treatment reduced the number of chronic relapses by diminishing activation of pro-inflammatory T cells and macrophages (Moreno et al., 2006). In addition, administration of the *SAH hydrolase (SAHH)* inhibitor, DZ2002, reduced the severity and number of relapses in EAE model, which was found to be directly associated with a reduction in type 1 helper T cell (Th1) activity. Similarly, MTA treatment in the systemic lupus

erythematosus (SLE) mouse model reduced pathological symptoms such as inflammation, enlargement of the kidneys and lymph nodes, and decreased production of autoantibodies and IgG. Furthermore, MTA treatment suppressed T and B cell proliferation by inhibiting TCR- and BCR-mediated clonal expansion (Yang et al., 2013). These data highlight the pivotal role of methyltransferase activity on lymphocyte function, and raise further questions regarding the role of PRMTs in autoimmune disease.

HLCL65, a PRMT5 inhibitor, was used in the EAE mouse model and was shown to phenocopy the use of a pan-methyltransferase inhibitors, leading to better clinical outcome, fewer Th1 memory cells, and reduced inflammation compared to the control (Webb et al., 2017). The same group chose to further utilize the CD4-Cre-ERT2 mouse model (PRMT5-cKO) to delete PRMT5 specifically in peripheral CD4+ T cells (Webb et al., 2020). In agreement with the use of a PRMT5 inhibitor treatment, PRMT5-cKO mice showed a dramatic reduction in the clinical symptoms of EAE. Phenotypically, PRMT5-cKO mice had fewer total T cell in the CNS, and these T cells were less activated. Mechanistically, PRMT5 methylates SREBP1 at arginine 321 (R321), which in turn blocks the phosphorylation-mediated proteasomal degradation of SREBP1 protein (Webb et al., 2020). This stabilized SREBP1 then activates cholesterol synthesis and RORγt transcriptional activity to induce Th17 cell differentiation. Expectedly, PRMT5-cKO mice produced fewer Th17 cells, and showed improved clinical outcome compared to control mice in the EAE model.

Like PRMT5 inhibition, pharmacological inhibition of PRMT1, using TC–E5003, was protective against EAE progression through suppression of the Th1 and Th17 cells (Sen et al., 2018). In addition, the inhibition of PRMT1 promoted the generation of immune-suppressive Foxp3+ regulatory T cells. Mechanistically, PRMT1 was shown to asymmetrically dimethylate

41

H4R3 at the gene locus of IL17 (Sen et al., 2018). This methylation event then caused the release of STAT5 and recruitment of STAT3 to activate the transcription of IL17, thereby promoting Th17 cell differentiation (Sen et al., 2018).

One of the lineage master regulators of T cells is Forkhead box protein P3 (FOXP3). A screening of multiple epigenetic modifiers identified PRMT1 as a crucial PTM for FOXP3 activity, and are required to promote Treg development. PRMT1 binds to FOXP3 and methylates arginines (R)48 and (R)51. T cells expressing the methylation-defective mutant of FOXP3 were hyper-sensitive in a xenogeneic graft-versus-host disease (GVHD) mouse model (Kagoya et al., 2019). In addition, an isomethionine methyl-SILAC screening found 2,502 arginine methylation sites across multiple genes in T cells. Some of these arginine-methylated genes were involved in TCR signaling and were transcription factors for T cell differentiation, including FOXP3, RUNX1, RUNX3, IRF4, NFAT1, cRel, RelB, Notch1, and PAX5 (Geoghegan et al., 2015). This accumulating evidence indicates the critical role of arginine methylation in T cell differentiation and activation.

PRMT5 is a critical regulator of hematopoiesis (Liu et al., 2015). The loss of PRMT5 in hematopoietic stem and progenitor cells (HSPCs) using the MX1cre-PRMT5 mouse model resulted in severe pancytopenia, with a reduction in total numbers of white blood cells, platelets, and red blood cells, and were moribund after 1-2days (Love et al., 2015). These mice also had a severe impairment in thymic development, with an increased number of CD4+CD8+ double-positive (DP) cells and a decreased number of CD4/CD8 double-negative (DN) and CD8 single-positive (SP) cells (Liu et al., 2015). In addition to this work, CD4-cre-ERT2 mice were utilized to delete PRMT5 in T cells (Webb et al., 2020). Like the MX1-cre model, the loss of PMRT5 inhibited thymic development and affected populations of DN, SP and DP T cells (Webb et al.,

2020). In addition, PRMT5 regulated the abundance of peripheral CD4+ and CD9+ Th cell, as well as the development of invariant NK (iNK) T cells (Inoue et al., 2018; Webb et al., 2020).

1.5.2 B cells

PRMT1 and 5 also act as critical players in B cell proliferation and differentiation (Infantino et al., 2010; Infantino et al., 2017; Litzler et al., 2019). The PRMT1-mediated methylation of BCR subunit immunoglobulin A (Iga) suppressed Phosphoinositide 3-kinase (PI3K) signaling and promoted the differentiation of pre-B cells to immature B cells (Infantino et al., 2010). A subsequent study further utilized the CD23-cre mouse model to delete PRMT1 specifically in mature B cells (Infantino et al., 2017). The PRMT1-depleted mature B cells were unable to proliferate or differentiate towards activated B cells in the presence of CD40L, IL4, and IL5 *in vitro*. In addition, CD23-cre PRMT1 KO mice immunized with different antigens or influenza virus were unable to promote the formation of antibody-secreting B cells and thus exhibited a reduction in IgG and IgM antibodies. (Infantino et al., 2017).

In the case of PRMT5, Mb1-cre was employed to delete PRMT5 in early immature B cells in the bone marrow (BM) (Litzler et al., 2019). This loss of PRMT5 reduced the total number of pro-B cells in the spleen by activating the p53 pathway and promoting apoptosis of the immature B cells. Furthermore, by using Cd19-cre and Cγ1-cre, PRMT5 was abrogated in a large pre-B cell. This abrogation reduced germinal center (GC) expansion by enhancing apoptosis and reducing the proliferation of large pre-B cells (Lloyd et al., 2019). In addition, pre-B cells could not differentiate to antibody-secreting plasma cells, as evidenced by reduced IgG production *in vivo*. Thus, both PRMT1 and PRMT5 are critical modifiers of B cell development and humoral immune activation.

1.5.3 Myeloid cells

The role of PRMT1 has been documented in macrophages, but to a lesser extent than our knowledge of their functions in lymphocytes (Tikhanovich et al., 2017). The conditional abrogation of PRMT1 in macrophages, using LysM-Cre, inhibited the switch of M0 macrophages to an M2 state. PRMT1-KO mice were therefore more susceptible to cecal ligation punctured infection and exhibited severe weight loss and lower survival rates (Tikhanovich et al., 2017). Mechanistically, PRMT1 methylates H4R3 at the promoter of the Peroxisome Proliferator Activated Receptor Gamma (PPARγ), which increases the transcriptional activity at the PPARγ locus, leading to differentiation towards an M2 macrophage.

1.5.4 The role of PRMTs in innate immune sensing

Innate immune cells can recognize noxious pathogens via pattern recognition receptors (PRR) to elicit an array of immune responses, including the production of type I interferons and proinflammatory cytokines. There are several subfamilies of PRR, including Toll-like receptors (TLRs), Nod-like receptors (NLRs), Ctype lectin receptors (CLRs), and RIG-like receptors (RLRs). Individual PRRs can recognize pathogen-associated molecular patterns (PAMPs) or damage-associated molecular patterns (DAMPs). Amongst the DAMPs, cytosolic nucleic acid DNA and RNA can bind to PRRs such as GMP–AMP synthase (cGAS) and RLR, respectively, to activate antiviral responses. PRMTs modulate the antiviral activity by directly methylating protein associated with PRR to induce type I IFN responses. For example, PRMT5 can symmetrically dimethylate cGAS (R:124), leading to the impaired DNA binding of cGAS, and suppressing the type I IFN signaling cascade. Therefore, the loss of PRMT5 in bone-marrow-derived-macrophages (BMDMs) enhance cGAS binding to DNA and augment type I IFN responses. Likewise, in HSV-

infected mice, treatment with a PRMT5 inhibitor enhanced the type I IFN response and protected the mice from severe infection (Ma et al., 2021). Conversely, another study showed that PRMT5 interacts with cGAS in the nucleus and regulates the transcription of IFN-associated genes (Cui et al., 2020). The nuclear cGAS/PRMT5 complex catalyzes the symmetric dimethylation of H4R3 at the promoters of Ifnb and Ifna4, leading to an activation of the transcription of these genes (Kim et al., 2020).

PRMT7 mediates dsRNA-induced type I IFN responses by methylating Mitochondrial Antiviral Signaling Protein (MAVS) protein (Zhu et al., 2021). PRMT7 forms aggregates and monomethylates MAVS (R52) to suppress RIGI and TRIM31 binding. Upon viral infection, PRMT7 auto-methylates and undergoes proteasomal degradation, which then allows for the formation of the RIGI, TRIM31 and MAVS complex to activate type I IFN responses (Zhu et al., 2021). PRMT1 regulates both cGAS and RLR-mediated antiviral pathways by directly methylating TBK1 protein; a kinase that can bind and phosphorylate IRF3, the master transcription factor for mediating type I IFN responses (Yan et al., 2021). During viral infection, PRMT1 catalyzes asymmetric dimethylation of R54, R134, and R228 residues on TBK1, enhancing the oligomerization and activation of type I IFN production. Myeloid lineage specific PRMT1 KO mice were therefore more susceptible to viral infection (Yan et al., 2021).

Part III: Microexon Alternative Splicing of Small GTPase Regulators: Implication in Central Nervous System Diseases

Jee-San Lee[1, 2] ,Nathalie Lamarche-Vane[3,4] ,Stéphane Richard[1,2,5]

[1]Segal Cancer Center, Lady Davis Institute for Medical Research, Montreal, Quebec, Canada.

[2]Department of Biochemistry, McGill University, Montreal, Quebec, Canada.

[3]Research Institute of the McGill University Health Centre, Cancer Research Program, Montreal, Quebec, Canada.

[4]Department of Anatomy and Cell Biology, McGill University, Montreal, Quebec, Canada.

[5]Gerald Bronfman Department of Oncology, McGill University, Montreal, Quebec, Canada.

1.6 Abstract

Microexons are small sized ($\leqslant 51\,$bp) exons which undergo extensive alternative splicing in neurons, microglia, embryonic stem cells, and cancer cells, giving rise to cell type specific protein isoforms. Due to their small sizes, microexons provide a unique challenge for the splicing machinery. They frequently lack exon splicer enhancers/repressors and require specialized neighboring trans-regulatory and cis-regulatory elements bound by RNA binding proteins (RBPs) for their inclusion. The functional consequences of including microexons within mRNAs have been extensively documented in the central nervous system (CNS) and aberrations in their inclusion have been observed to lead to abnormal processes. Despite the increasing evidence for microexons impacting cellular physiology within CNS, mechanistic details illustrating their functional importance in diseases of the CNS is still limited. In this review, we discuss the unique characteristics of microexons, and how RBPs participate in regulating their inclusion and exclusion during splicing. We consider recent findings of microexon alternative splicing and their implication for regulating the function of small GTPases in the context of the microglia, and we extrapolate these findings to what is known in neurons. We further discuss the emerging evidence

for dysregulation of the Rho GTPase pathway in CNS diseases and the consequences contributed by the mis-splicing of microexons.

1.7 Introduction

Alternative splicing (AS) results in multiple transcripts being synthesized from a single gene and this process is especially pronounced in the nervous system (Gomez et al., 2021; Naro et al., 2021; Zheng, 2020; Zheng and Black, 2013). AS is tightly controlled by the spliceosome complex and associated RBPs with implications in various human diseases and tissue-specific developmental processes (Baralle and Giudice, 2017; Lukong et al., 2008; Paronetto et al., 2016; Scotti and Swanson, 2016). Advances in our understanding of pre-mRNA splicing, coupled with high-throughput sequencing technology, have led to the identification of many AS events, and the RBPs and their binding RNA elements influencing AS selection (Pan et al., 2008). With these achievements, small sized exons (≤51bp) termed 'microexons' were discovered to be present in human tissues, and their alternative splicing to have a role in neuronal differentiation, embryonic differentiation, cellular physiology, and disease progression (Head et al., 2021; Irimia et al., 2014; Lee et al., 2020; Parada et al., 2021; Vecellio Reane et al., 2016). In the human genome, approximately 13,095 microexons are highly conserved across species and are differentially expressed between tissue types (Li et al., 2015). Over the past decades, significant research unveiled the features of microexons, and we now have a better understanding of microexons AS and know that their mis-splicing is implicated in CNS diseases. Emerging evidence indicates a major network of microexons influencing the activity of small GTPases, proteins known to play crucial roles in cytoskeletal organization, vesicular transport, and cell migration (Figure 1) (Cherfils and Zeghouf, 2013; Gonatopoulos-Pournatzis et al., 2018; Johnson et al., 2019; Lee et

al., 2020; Ratcliffe et al., 2019; Reiner and Lundquist, 2018). The involvement of small GTPases has been appreciated during development (Duquette and Lamarche-Vane, 2014) and their deregulation observed in many CNS diseases (DeGeer and Lamarche-Vane, 2013). Thus, the modulation of microexon AS could represent an important mechanism to regulate the activity of these enzymes and contribute to CNS diseases. In this review, we discuss microexon networks of small GTPase pathway, their regulation, and functional implications in diseases of the CNS.
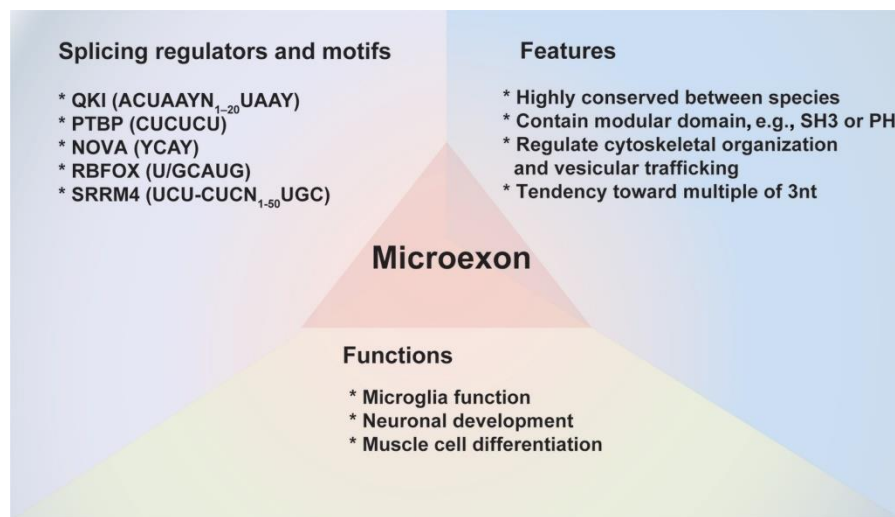
Figure 1. Characteristics of microexon

In 1985, Hogness and coworkers discovered two internal microexons from the *Ubx* transcript in *Drosophila melanogaster* (Beachy et al., 1985). Soon after, the *Troponin T* gene from chicken cardiac muscle led to the identification of a microexon with 6 nucleotides, considered at the time to be a pseudoexon (Cooper and Ordahl, 1985). In 1987, the discovery of *the c-src* microexon termed as N1 exon, which is expressed explicitly in the neurons, paved the way to investigate the microexon splicing network (Levy et al., 1987). Black and coworkers were intrigued as to how N1 exon was selectively included in the mRNA within neurons and not in non-neuronal cell lines. With extensive *in vivo* and *in vitro* experiments they uncovered the *cis-* and *trans*-regulatory elements that provide this microexon selectivity (Black, 1992; Chan and Black, 1995). They discovered that the N1 3' splice site and downstream of the intron contained a CU-rich region

bound by polypyrimidine tract-binding protein (PTBP1). The binding of the PTBP1 in CU-rich regions suppressed the inclusion of the N1 exon in the non-neuronal cell lines by inhibiting the formation of the spliceosome complex (Black, 1992; Chan and Black, 1995, 1997; Sharma et al., 2008). In the context of neurons, downstream of the N1 microexon contains an intronic splice enhancer (ISE) sequence that is bound by heterogeneous nuclear ribonucleoprotein F (hnRNP F), hnRNP H and KH-type splicing regulatory protein (KSRP) to promote N1 inclusion (Chan and Black, 1995, 1997; Markovtsov et al., 2000; Min et al., 1995). Additionally, during the neuronal differentiation, PTBP1 expression is down-regulated and it is compromised by the PTBP2, which does not repress splicing of N1 (Boutz et al., 2007; Markovtsov et al., 2000).

Additional pioneering work contributed to the microexon splicing network and this consisted of the work of Sterner & Berget (1993) who initially utilized microexon (7nt) from *Troponin I* gene and identified that the upstream exon was required for inclusion of microexon (Sterner and Berget, 1993). In subsequent studies, they used the microexon (6nt) from chicken cardiac troponin gene and showed that an intron splicing enhancer element (ISE) containing G-rich sequence was essential for microexon inclusion. Splicing factor 1 (SF1) is a major factor that binds to the ISE motif (GGGGCUG), exerting a bridging effect during the initial phase of spliceosome assembly (Carlo et al., 2000; Carlo et al., 1996). Therefore, early work highlighted that microexons require ISE sequences and different RBPs to enhance their proper splicing.

The identification of microexons expanded to yeast, plants, insects, nematodes, and vertebrates, with a spatiotemporal expression of microexons controlling tissue-specific developmental processes (Kostrub et al., 1997; McAllister et al., 1992; Small et al., 1988; Volfovsky et al., 2003). For instance, microexons are included in the *NCAM* mRNA in cerebellar and hippocampal neurons, and their presence reduce neurite growth (Lahrtz et al., 1997; Small and

Akeson, 1990). Similarly, *Micu1.1*, a skeletal mitochondria transcript, contains a microexon of 12nt, which confers higher calcium uptake and an increase in ATP production (Vecellio Reane et al., 2016). Therefore, tissue- and cell-specific AS of microexons is functionally pertinent for coordinating physiological functions.

A convincing body of RNA-sequencing (RNA-seq) data and bioinformatic analysis from diverse biological contexts indicates that microexons exhibit distinct characteristics, such that microexons conserve reading frame, lie within or proximal to protein-interaction domains, and display high conservation across species (Irimia et al., 2014; Lee et al., 2020; Love et al., 2015). In 2003, a new alignment correction tool computationally identified microexons (≤ 25bp) in four different species: human, *C. elegans*, *D. melanogaster* and *A. thaliana* (Volfovsky et al., 2003). A total of 610 microexons showed high conservation between species. It was noted that microexons were preferentially in multiple of 3 nucleotides in length and only 5% of the cases contained an exon enhancer sequences ([A/G]AAGAA, TGAAGA, CAACAA). Since then, different alignment tools were develop to increase the sensitivity and specificity for identifying microexons (Schulze et al., 2007; Wu et al., 2013). Using genome-wide analysis, Blencowe and coworkers identified neuron-specific spliced events by comparing RNA-seq datasets from >50 different tissues and cell types (Irimia et al., 2014). A total of 308 microexons were identified, explicitly included in neurons. For the most part, these microexons preserve the open reading frame of the transcript and contain highly conserved flanking intronic and exonic sequences. They show sequence conservation between species, possess weak 3′ splice sites and strong 5′ splice sites. The amino acids encoded by the microexon often encode sequences that can engage in protein-protein interactions such as pleckstrin homology (PH) and src homology 3 (SH3) domains (Dergai et al., 2010; Irimia et al.,

50

2014). Gene ontology analysis showed enrichment of microexons in genes encoding regulators of small GTPases (Irimia et al., 2014), but this remained uncharacterized.

High-throughput transcriptomic profiling illustrates the features of microexons and their regulatory elements (Irimia et al., 2014; Li et al., 2015). To scrutinize these regulatory elements and genomic features of microexons, Li and coworkers further divided microexons (<51nt) into two groups: microexon undergoing AS (AS-microexons) and microexons being constitutively spliced (CS-microexons) (Li et al., 2015). Using 901 human and mouse RNA-seq libraries, they discovered 7,949 microexons in the brain, of which 6,269 were CS-microexons and 1,480 were AS-microexons. Interestingly, both AS- and CS-microexons carried shorter flanking intronic sequences than regular exons and displayed higher conservation across species. However, AS- and CS-microexons also showed disparate genomic features, with CS-microexons displaying stronger splice sites and harboring exon splicing enhancer sequences. For the AS-microexons, a high density of RNA Binding Fox-1 Homolog (RBFOX) and PTBP1 binding motifs located in the intronic sequences upstream of the 3' splice site was apparent. Notably, although previous research reported exon splicing enhancers to be frequently absent, Li et al. (2003) found exon enhancer sequences in CS-microexons, which could be due to the screening of the longer length of the microexon (<51nt) (Irimia et al., 2014; Li et al., 2015; Volfovsky et al., 2003). Overall, this analysis comprehensively delineates the splicing mechanisms exerted by AS- and CS-microexons and provides a new compensatory mechanism to overcome the short sequence of the microexons.

1.8 RBPs controlling microexon alternative splicing

The small size of the microexons presents obvious challenges to the splicing machinery (Li et al., 2015; Ule and Blencowe, 2019). Investigations using various CLIP and RNA-seq experiments are beginning to probe the required RBPs to coordinate the inclusion or exclusion of these microexons (Irimia et al., 2014; Lee et al., 2020; Li et al., 2015; Weyn-Vanhentenryck et al., 2014). In the following section, we discuss the characteristics and specific regulatory elements of five RBPs known to regulate alternative splicing namely QKI, PTBP, NOVA, RBFOX and SRRM4 that also regulate the AS of certain microexons (Figure 3).
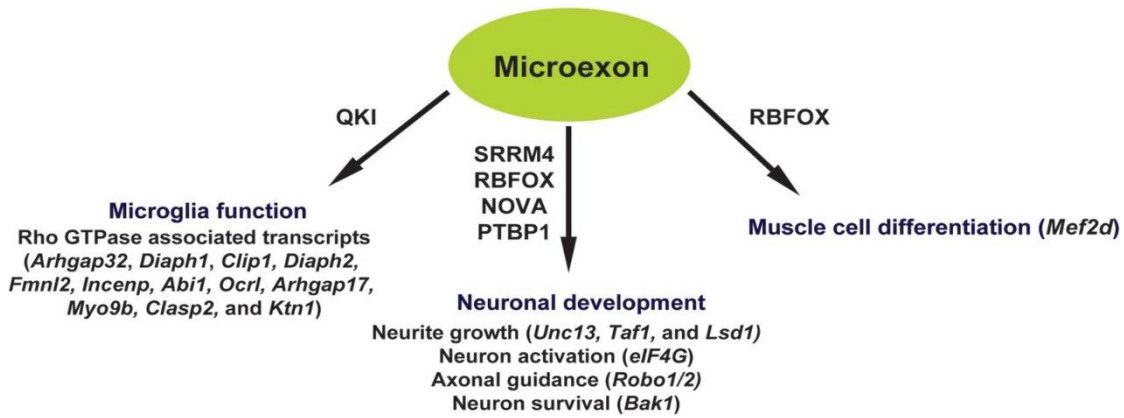
Figure 2 Microexon splicing during development and functional consequences

1.8.1 QKI

The QKI (QUAKING) RBP belongs to the heteronuclear ribonucleoprotein particle K (hnRNP K) homology (KH) domain family (Lukong et al., 2008). The *qkI* gene encodes three major isoforms that differ in their C-termini (Ebersole et al., 1996) and are termed QKI-5, QKI-6, and QKI-7 for the size of their respective mRNAs (for review (Darbelli and Richard, 2016)). The QKI proteins bind RNA as dimers (Beuck et al., 2012; Chen and Richard, 1998; Ryder et al., 2004; Teplova et al., 2013) using a bipartite sequence ACUAAY (N_{1-20}) UAAY (Y represents C or U) (Galarneau

and Richard, 2005b). This binding site, termed the QKI response element (QRE), is frequently located in introns, as observed by various CLIP strategies (Hafner et al., 2010; Van Nostrand et al., 2020). QKI has been extensively studied in the context of oligodendrocyte maturation, cancer progression, immune cell function, and muscle cell differentiation as regulating pre-mRNA splicing, mRNA export, mRNA stability, miRNA maturation and circular RNA biogenesis (Conn et al., 2015; Darbelli and Richard, 2016; de Bruin et al., 2016; de Bruin et al., 2020; Fagg et al., 2020; Ren et al., 2021).

New evidence shows that QKI is a specialized regulator of microexon AS in microglia, and embryonic stem cells requiring a neighboring QRE (Fagg et al., 2020; Lee et al., 2020). In QKI-deficient microglia, 206 significant alternative exon events were identified. Among these events, 36% (<51nt) and 18% (<27nt) were microexons (Lee et al., 2020). QKI regulated microexons exhibit similar features to previously identified microexons, (Dergai et al., 2010; Gonatopoulos-Pournatzis et al., 2018; Irimia et al., 2014) such that most of these microexons were of multiples of 3 nucleotides in length and displayed a high enrichment of protein-protein interaction domains such as SH3 and PH domains. Notably, these transcripts were enriched in vesicle-mediated transport and cytoskeleton organization. Despite such similarities, QKI equally promotes and represses microexon inclusion, unlike SRRM4, which mainly promotes microexon inclusion (see below). In general, if a QRE is located upstream of a given microexon, it is excluded, while if the QRE is downstream, the microexon is included (Figure 2). Microglia RNA-seq data reveals low expression of *NOVA*, *RBFOX*, and *SRRM4* mRNAs (Lee et al., 2020), suggesting that the abundant QKI might be the main RBP driving microexon AS in these cells. However, in neurons a CRISPR/Cas9 screen did not implicate QKI as a general microexon regulator (Gonatopoulos-Pournatzis et al., 2018). These findings were not surprising, as QKI is not expressed in neurons,

and the reporter did not harbor a QRE near the interrogated microexon. Therefore, understanding the tissue-specific expression of RBPs with the combinatorial splicing regulation by RBPs is crucial for unveiling the complexity of the tissue-specific microexon splicing events.
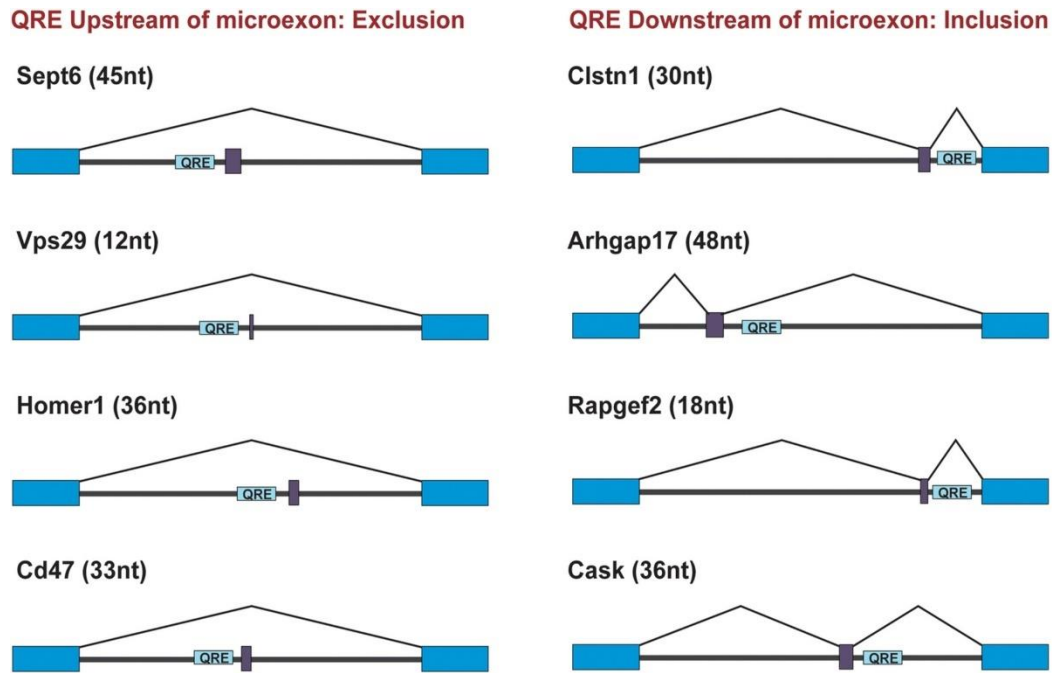
Figure 3 Microexon inclusion or exclusion according to the QRE location

1.8.2 PTBP

PTBP, known as hnRNPI, binds the polypyrimidine-rich region (U/CUCUCU) within introns and affects neuronal AS (Gil et al., 1991; Patton et al., 1991; Zheng, 2020). PTBPs has been extensively shown to be involved in AS of microexons in neurons during different contexts (Black, 1992; Chan and Black, 1995; Markovtsov et al., 2000). Neural progenitor cells abundantly express PTBP1 and during neurogenesis the expression of PTBP1 decreases, while the expression of its paralog PTBP2 increases (Chan and Black, 1997; Makeyev et al., 2007; Spellman et al., 2007). As a result, the synchronization of PTBP paralogs is critical for neuronal development and the switching of neuronal programs. The CLIP and RNA-seq data reveal that PTBP1 regulates microexon AS by

binding upstream of the microexon (Li et al., 2015). In the Neuro2A mouse neuroblastoma cell line, PTBP1-depletion caused microexon inclusion (~94%), whereas only 8% showed exclusion, inferring that PTBP1 is a repressor of microexon inclusion (Li et al., 2015). This is in line with previous work from Black's lab, where PTBP1 represses the N1 microexon inclusion of *c-src* mRNA in non-neuronal cells (Black, 1992; Chan and Black, 1997; Min et al., 1995). Likewise, PTBP1-depletion caused microexon skipping within the *eIF4G* transcript in neurons (Gonatopoulos-Pournatzis et al., 2020). Another study demonstrated that in the neural progenitor cell, microexon 5 of *BAK1* transcript is skipped and this is promoted by the PTBP1 binding to the intronic region proximity to the 3'splice site of the microexon. However as neural progenitor cells differentiate to neurons, PTBP1 expression decreases, allowing the microexon to be included in the *BAK1* transcript triggering the loss of BAK1 protein and enhancing neuronal survival (Lin et al., 2020). Therefore, PTBP1 is a microexon AS regulator playing crucial roles in neurons.

1.8.3 NOVA

NOVA (Neuro-oncological ventral antigen) is a KH domain-type neuronal specific RBP that binds YCAY-rich elements predominantly within intronic sequences (Buckanovich et al., 1996; Yang et al., 1998). NOVA is composed of two paralogs, NOVA1 and NOVA2, and shows differential expression within brain regions. The cerebellum and spinal cord exhibit high expression of NOVA1, while NOVA2 is the isoform predominantly expressed in the cortex (Buckanovich et al., 1996; Yang et al., 1998). NOVA RBPs regulate neuronal development and processes such as axon pathfinding, organizing the architecture of synapses, and controlling specific surface receptors (Meldolesi, 2020). During the midline crossing, NOVA1/2 protein binds to the YCAY sequences flanking microexon6/6b of *Robo1/2* transcripts and promotes microexon skipping. In NOVA1/2

mutant mice, micoexon6/6b is included causing defects in midline crossing. The inclusion of microexon6/6b induced more pronounced activation of Rac1 and inhibition of Cdc42 (Johnson et al., 2019). Therefore, this study highlights NOVA1/2 mediated temporal splicing of microexons during CNS development.

1.8.4 RBFOX

RBFOX (RNA Binding Fox-1 Homolog) belongs to the Fox-1 family of RBPs, having a critical role in AS in muscles, neurons, and germ cells (Auweter et al., 2006; Conboy, 2017; Hafner et al., 2010). This family of RBPs includes three paralogs, RBFOX1, RBFOX2 and RBFOX3, containing a single RNA recognition motif (RRM) and bind to (U)GCAUG sequence elements (Kuroyanagi, 2009; Nakahata and Kawamoto, 2005). Computational studies for RBP motifs in microexons identified RBFOX binding motifs near the 3′ splice sites of microexons (Li et al., 2015). The binding of RBFOX mainly supports microexon inclusion. For example, RBFOX2 assist the *Mef2d* microexon (21nt) inclusion during the myoblast differentiation by binding to the flanking intron (Singh et al., 2014). Indeed, a CRISPR/Cas9 screen also identified RBFOX2 as a microexon splicing regulator in a neuronal cell line (Gonatopoulos-Pournatzis et al., 2018). Distinctively, RBFOX2 regulate a smaller number of microexons (17%) than SRRM4 (see below)(Gonatopoulos-Pournatzis et al., 2018). Moreover, the RBFOX2 regulated microexons contained the GCAUG sequence in the intronic elements and lacked the SRRM4 cognate binding site. RBFOX is also known to regulate the AS of cassette exons in coordination with QKI (Danan-Gotthold et al., 2015; Li et al., 2018), therefore it is conceivable that the concerted action of more than one RBP, e.g., QKI and RBFOX, could modulate certain microexon AS events.

1.8.5 SRRM4

SRRM4 (Serine/Arginine Repetitive Matrix 4) is an SR-type RBP shown to promote exon inclusion in the brain (Irimia et al., 2014; Ule and Blencowe, 2019). SRRM4 binds to a bipartite sequence (UCU-CUC(N_{1-50})UGC), defined as an intronic splice enhancer (ISE), located upstream of 3' splice site to coordinate microexon inclusion (Gonatopoulos-Pournatzis et al., 2018; Torres-Mendez et al., 2019).

SRRM4 expression increase during neurogenesis to promote microexon inclusion for neurite growth and neuronal activity (Ule and Blencowe, 2019). In the absence of conditional allele of *Srrm4* , SRRM4 haploinsufficient mice were characterized and shown to have aberrant social behavior, hypersensitivity to environmental stimulus, altered synaptic density, and heightened neuronal activity (Quesnel-Vallieres et al., 2016). In separate studies, the deletion of SRRM4 caused microexon skipping of *Unc13b, Taf1,* and *eIF4G* transcripts, which hindered the formation of neuronal processes and caused aberrant neuronal activity (Gonatopoulos-Pournatzis et al., 2020; O'Rawe et al., 2015; Quesnel-Vallieres et al., 2015). Thus SRRM4-mediated microexon inclusion is crucial during neuronal development and for neuronal function.

In summary, RBPs bind specific sequences neighboring the microexon and inclusion is a coordinated effort of several RBPs, as observed for regular-size exons. The presence of microexons within transcripts adds extra amino acids in the protein isoforms that impact protein function in immune cell, muscle cell, and CNS cells.

1.8.6 Microexons controlling small GTPases associated transcripts

Small GTPases from the Ras superfamily are molecular switches that orchestrate the cytoskeletal and cell adhesions dynamics affecting cellular growth, differentiation, migration, and vesicle

trafficking (Niftullayev and Lamarche-Vane, 2019). Ras, Rho, Rab, Arf, and Ran are members of the Ras superfamily (Niftullayev and Lamarche-Vane, 2019). The small GTPases cycle between two states: an active-GTP bound and an inactive-GDP bound state. Two main regulatory factors control this process: guanine nucleotide exchange factors (GEFs), which catalyze GDP exchange for GTP and GTPase-activating proteins (GAPs), promoting GTP hydrolysis. In addition, guanine nucleotide dissociation inhibitors (GDIs) bind to some GTPases, and restrict them to an inactive state in the cytoplasm (Olofsson, 1999). With the advent of RNA-seq, the genes encoding GAPs and GEFs have been found to undergo microexon AS during neurodevelopment, cancer progression and immune reaction, and their mis-splicing culminating in aberrant cellular function (Irimia et al., 2014; Johnson et al., 2019; Lee et al., 2020; Ratcliffe et al., 2019)(Figure 4). During the differentiation of mouse embryonic stem cells to glutamatergic neurons, 151 microexons undergo AS which are enriched in small GTPases pathway, such as Dock7, Dock9, Robo1/2, Git2, and Itsn1 (Irimia et al., 2014). Later studies using *in vivo* and *in vitro* models showed that the splicing of microexons could influence protein-protein interactions and the activity of the small GTPases, impacting CNS development (Gerth et al., 2019; Johnson et al., 2019). For instance, as mentioned previously in the review, during the CNS development, Robo1/2 microexon6/6b is alternatively spliced, which confers differential activities of RAC1 and CDC42 (Johnson et al., 2019). Another example is intersectin1 (ITSN1), a Cdc42 GEF protein implicated in clathrin-mediated endocytosis in the synapse, which undergoes microexon AS within its SH3 domain (Gerth et al., 2019; Tsyba et al., 2008). Specifically, the inclusion of the 15 nucleotide microexon in *ITSN1* changes the protein binding affinity with synaptic interacting partners including SYN1, CYFIP2, and WIPF3. However, how *ITSN1* microexon AS modulates neuronal function has not been investigated thus far.
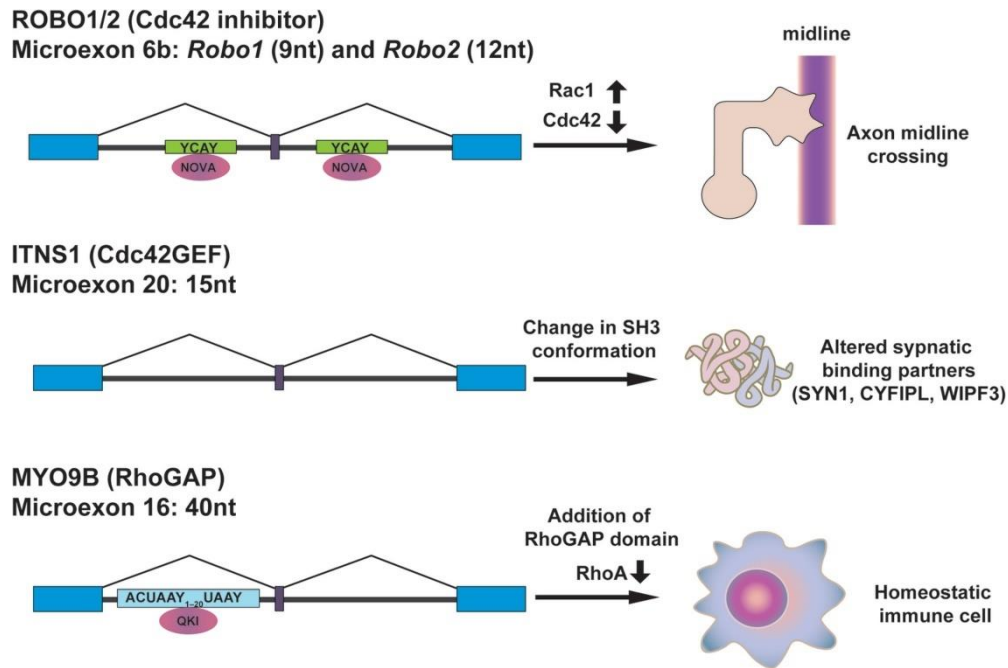
Figure 4 Microexon splicing regulates small GTPase associated transcripts

In the brain, QKI regulates microexon AS of genes encoding positive regulators of the Rho GTPase pathway in microglia (Lee et al., 2020). The transcripts include Rho GAPs, Rho GEFs, and effector proteins such as *Arhgap32, Diaph1, Clip1, Diaph2, Fmnl2, Incenp, Abi1, Ocrl, Arhgap17, Myo9b, Clasp2,* and *Ktn1*. Microexon AS of these transcripts are in-frame insertions generating new protein isoforms. For instance, the depletion of QKI leads to microexon (24nt) inclusion in the *Ocrl* pre-mRNA, thereby creating an isoform that has a higher affinity with clathrin (Choudhury et al., 2009). Moreover, QKI-depletion promotes microexon skipping of *Myo9b* introducing a premature stop codon that leads to the loss of the Rho GAP domain. *Myo9b* loss-of-function results in RhoA activation in macrophage (Hanley et al., 2010). Accordingly, QKI-depletion in microglia activates RhoA GTP and ROCK2 downstream targets and it remains to be shown whether *Myo9b* AS contributes to the change in morphology with defects in processing phagocytosed cargo (Lee et al., 2020).

1.8.7 Alternative splicing of small GTPases transcripts in CNS disease

As a modulator of cytoskeletal organization, Rho GTPases play a pleiotropic role in neuronal differentiation, migration, endocytosis and morphogenesis. The alteration of RhoA, Rac1 and Cdc42 activity and expression using various mouse models (Antoine-Bertrand et al., 2011) revealed severe changes in neuron synapse formation, dendritic elaboration, axonal polarization, and axonal growth (Ahnert-Hilger et al., 2004; Dupraz et al., 2019; Leone et al., 2010; Tahirovic et al., 2010). Given the crucial role of Rho GTPases in neuronal development and homeostasis of the CNS, it is not surprising that Rho GTPases as well as their regulators and effectors are mis-regulated or mis-spliced in CNS disorders such as autism spectrum disorders (ASD), intellectual disability, schizophrenia, and Alzheimer's disease (AD) (DeGeer and Lamarche-Vane, 2013; Huang et al., 2017; Kippert et al., 2007; Lee et al., 2020; Rajasekharan et al., 2010; Socodato et al., 2020; Zeug et al., 2018).

The pathophysiology of patients with ASD include synaptic dysfunction, alteration in neural circuitry and increase in neuroinflammation (de la Torre-Ubieta et al., 2016). Yet, the causal chain of molecular events that results in ASD is still undefined (Woodbury-Smith and Scherer, 2018). RNA-seq of 12 ASD and 12 control patient samples collected from the superior temporal gyrus were analyzed (Irimia et al., 2014). Notably, 30% of microexons displayed alternations in splicing events, whereas only 5% of longer exons exhibited mis-splicing, suggesting alternative microexon splicing as a quantitative trait (sQTL). The mis-spliced microexons were enriched in the Rho GTPase pathway (e.g. *DOCK4, DOCK9, ASAP1, VAV2, CLASP2*, and *ROBO*) (Irimia et al., 2014), further underscoring the importance of Rho proteins in CNS function. Similarly, The Simons Foundation Autism Research Initiative (SFARI) discovered > 20 Rho GTPase regulators and effectors as risk genes for ASD (Guo et al., 2020). Of these, seven genes encoded Rho GAPs

(*MYO9B, OPHN1, ARHGAP5, ARHGAP11B, ARHGAP32, SRGAP3*, and *OCRL*), and seven were

Rho GEFs (*ARHGEF9, TRIO, DOCK8, PREX1, ARHGEF10, DOCK1,* and *DOCK4*) and six

encoded Rho effectors (*NCKAP1, CYFIP1, PAK2, ITPR1, PRKCA,* and *WASF1*)(Guo et al., 2020).

In general, 20% of mutations are localized at splicing regulatory elements, which confer

differential binding of RBPs, and a change in splicing pattern (Anna and Monika, 2018; Lim et al.,

2011; Wang and Cooper, 2007). Therefore, defects in GEF and/or GAP activity might lie in

splicing regulatory elements, consequently causing mis-splicing; however, direct evidence for this

possibility needs further investigation. In addition to these findings, a comparison of the

hippocampal synaptic proteomes of seven types of ASD mouse models unveiled common

alterations in the Rho GTPase signaling pathway (Carbonell et al., 2021). In particular, Rac1

expression was significantly increased in ASD mouse models. Therefore, studies with mouse

models combined with patient-derived genomic sequencing analysis correlate Rho GTPase

signaling pathways to ASD pathogenesis. Additionally, perturbations in RBFOX1/2, PTBP1/2,

and NOVA1/2 expression have been reported in patients with ASD (Parikshak et al., 2016).

Considering that RBFOX1/2 and PTBP1/2 are strong candidates for splicing of transcripts

implicated in Rho GTPases and also microexon AS, this suggests that dysregulation of these

splicing factors will inevitably lead to microexon AS of the regulators of the Rho GTPase pathway

(Begg et al., 2020; Hannigan et al., 2017; Misra et al., 2020; Quesnel-Vallieres et al., 2019).

The impairment of cortical circuitry and disruption of neurotransmitter systems are the

hallmarks of psychotic disorders such as bipolar and schizophrenia. The transcriptomic analysis

of schizophrenia and bipolar disorder patient samples revealed a global mis-regulation of AS

events (Gandal et al., 2018). The mis-regulated transcripts were in fact enriched in small GTPases

pathways and involved RBFOX1 (Gandal et al., 2018). The RBFOX1 isoform found in psychiatric

disorders differed in its RNA regulating function, causing aberrant splicing. Additionally, QKI expression is down-regulated in schizophrenia patients, however, the molecular impact triggered by loss of QKI has not been addressed (Aberg et al., 2006). Several Rho GTPase regulators (ARAP1, ARAP3, ARHGAP10, ARHGAP12, ARHGAP29, ARHGAP33, ARHGAP40, ARHGAP45, ARHGAP18, OPHN1, and MYO9B) have been linked to psychiatric disorders (Niftullayev and Lamarche-Vane, 2019). For instance, genome-wide copy number analysis (CNV) identified the association of the ARHGAP10 gene with schizophrenia. The ARHGAP10 variant caused hyperactivation of RhoA and decreased the mouse prefrontal cortex's spine density, culminating in aberrant emotional behavior (Sekiguchi et al., 2020). Therefore, this evidence suggests an association between the dysregulation of RBPs and the effect on AS of Rho GTPases in psychotic disease progression.

The hallmarks of AD include increased accumulation of beta-amyloid (Aβ) peptide and deterioration of cholinergic pathways. Increasing evidence shows the presence of AS events associated with the pathology of AD (Biamonti et al., 2019). A new transcriptomic study discovered aberrant splicing associated with AD. The RNA-seq from the dorsolateral prefrontal cortex of AD patients identified splicing as a sQTL where single nucleotide polymorphisms in *cis-*acting elements were identified that potentially affects the binding of RBPs and splicing choice. Some of the mis-spliced transcripts identified were linked with GTPases and are involved in the endocytosis-lysosomal pathway (AP2A1, AP2A2, and MAP1B) (Raj et al., 2018). In fact, the endosomal and vesicular trafficking pathways are associated with early AD pathogenesis (Zhang et al., 2019). The Rab family GTPases are the main regulator controlling early and late steps of the endocytic pathway governing vesicle formation, endosome tethering, and endosome fusion. Since endosomal dysfunction is one of AD's pathological phenotypes, the increased expression of Rab

GTPases is apparent in AD patient samples (Cataldo et al., 2000). Likewise, the Rab7 and RIN3 (RAB5 GEF protein) are risk factor genes in AD (Kunkle et al., 2017). The sQTL, however, do not infer causality for the pathogenesis of AD. Additionally, these studies focused on the mis-splicing of classical mRNAs; therefore, further studies are required to understand the involvement of mis-spliced variants and micoroexons in AD pathogenesis.

In microglia, morphological changes, migration, and cytokine secretion are influenced by the ROCK2 pathway (Roser et al., 2017). ROCK1/2 are two serine/threonine protein kinase isoforms and downstream effectors of Rho GTPases, playing crucial roles in migration, proliferation, and apoptosis. For example, once microglia detect neuronal cell death during hypoxic conditions, they show enhanced ROCK2 expression accompanied by pro-inflammatory cytokine secretion (Ding et al., 2010). The ROCK inhibitor, Fasudil, decreases ROCK activation in microglia and alleviates cytokine release resulting in neuronal protection (Ding et al., 2010). Similarly, in the nerve injury mouse model, microglia change their morphology by decreasing the total length of their processes, whereas the ROCK inhibitor reverses this morphological change (Tatsumi et al., 2015).

In a mouse model where RhoA was ablated in microglia, Rho to Src pathway was stimulated and the microglia activated with TNFa and excitotoxic glutamate secretion causing altered long-term potentiation and synapse loss in neurons(Socodato et al., 2020). Moreover, the APP/PS1 mouse model of AD had decreased active RhoA-GTP with increase Src activity in microglia and injection of a Src inhibitor decreased microglia activation and Ab deposition (Socodato et al., 2020). The data show that RhoA ablation in adult microglia in mice reproduce the hallmarks of animal models of AD and in human AD patients

We also found that depletion of QKI in microglia leads to RhoA and ROCK2 activation, as evidenced by the increase in RhoA GTP, phosphorylated-MLC (myosin light chain) and -cofilin with a pro-inflammatory phenotype (Lee et al., 2020). Inhibition of ROCK decreased the secretion of pro-inflammatory cytokines in these QKI-depleted microglia. As mentioned previously, QKI coordinates the microexon AS of Rho GTPase-related transcripts which likely contribute to the activation of the RhoA-ROCK2 axis. Additionally, the microglia QKI-deleted mouse model had aberrant microglia phagocytosis. Phagocytosed particles accumulated in QKI deficient microglia, mimicking the morphology of 'engorged microglia', a phenotype observed in Ragulator-Rag GTPase complex disrupted microglia (Shen et al., 2016). The Ragulator-Rag GTPase complex regulates the lysosomal process by actively binding GTP.

In addition, mice with QKI-deficient microglia have defects in remyelination capabilities in cuprizone-diet induced demyelination model with decreased number of oligoprogenitor cells (OPC) at sites of lesion. As OPCs are influenced by microglia, altered splicing of microexons may contribute to the enhanced inflammatory phenotype and defective phagocytosis (Lee et al., 2020). Nevertheless, further studies are warranted to unveil the role of microexons in microglia.

As microglia are highly mobile and phagocytic cells, the involvement of small GTPase pathway is not surprising (Li and Barres, 2018). Moreover, substantial studies highlight the importance of microglia in preventing CNS disease progression (Priller and Prinz, 2019). Likewise, QKI regulated microexon AS events are risk factors for intellectual disability syndromes, epilepsy (*Med23, Diaph1, Rbfox1, Ralgapa1, Cask*, and *Sptan1*), deafness (*Diaph1*, and *Myo6*), Huntington disease (*Mbnl1*, and *Mbnl2*), and AD (*Cacnb1*, and *Apba1*) (Lee et al., 2020). Collectively, these studies illustrate that small GTPases, in particular the Rho signaling pathway, are intrinsically linked to microglia function and could impact disease progression.

1.9 Conclusion

High-throughput RNA-seq and advanced computation enhanced the discovery of many non-canonical splicing events, including the AS of microexons. The alteration of the small GTPase pathway and mis-splicing of small GTPase regulatory genes is apparent in various CNS diseases. Despite this understanding, most of the microexon splicing events have been elucidated in neurons or by total brain RNA-seq, and we are only beginning to unveil the microexon splicing events in other cell types in the CNS, such as in microglia. Still, much work is needed to comprehensively profile microexon events across different cell types and possible implications in disease progression. Moreover, the physiological consequences or the causality of mis-spliced microexons has not been functionally examined. Possible ways to solve such a conundrum include performing gene editing with e.g., CRISPR/Cas9 to precisely remove individual microexons or flanking RNA elements and examine the functional outcomes (Du et al., 2020; Yuan et al., 2018). This approach will improve our comprehension of different small GTPase protein isoforms in regulating cellular physiology and CNS function. The observation of microexons AS in autism spectrum disorders is the beginning of mining these splicing events, especially of small GTPase regulators in CNS disorders at large, and determining whether microexon AS defects are a common feature of other disorders.

CHAPTER 2: QUAKING REGULATES MICROEXON ALTERNATIVE SPLICING OF THE RHO GTPASE PATHWAY AND CONTROLS MICROGLIA HOMEOSTASIS

Jeesan Lee[1], Oscar David Villarreal[1], Xiaoru Chen[1], Stéphanie Zandee[2], Yoon Kow Young[1], Cynthia Torok[2], Nathalie Lamarche-Vane[3], Alexandre Prat[2], Serge Rivest[4], David Gosselin[4], Stéphane Richard[1]

[1]Segal Cancer Center, Lady Davis Institute for Medical Research and Gerald Bronfman Department of Oncology and Departments of Biochemistry, Human Genetics, and Medicine, McGill University, Montréal, QC H3T1E2, Canada

[2]Neuroimmunology Research Laboratory, Centre du Recherche du Centre Hospitalier de l'Université de Montréal (CRCHUM), QC H2X0A9, Canada

[3]Research Institute of the McGill University Health Centre, Cancer Research Program, and Department of Anatomy and Cell Biology, McGill University, Montréal, QC H4A 3J1, Canada

[4]Neuroscience laboratory, CHU de Québec Research Center and Department of Molecular Medicine, Faculty of Medicine, Laval University, Québec City, QC G1V 4G2, Canada

2.1 Preface

RNA binding proteins (RBPs) are mutated or misregulated in various CNS disorders by mediating the post-transcriptional regulation of genes, which is critical for brain cell physiology. Previously Dr. Richard's lab showed one RBP, QKI, to be a significant protein governing the differentiation process of oligoprogenitor cells to myelinating oligodendrocytes by modulating RNA biogenesis. However, despite the abundant expression of QKI in microglia, how QKI regulate RNA splicing networks in microglia is unknown. Therefore, to investigate the role of QKI in microglia, we, for the first time, generated QKI-deficient microglia mice using the CX3CR1-CreERT and analyzed the microglia phenotypes and transcriptional signatures.

2.2 Abstract

The role of RNA binding proteins in regulating the phagocytic and cytokine-releasing functions of microglia is unknown. Here, we show that microglia deficient for the QUAKING (QKI) RNA binding protein have increased proinflammatory cytokine release and defects in processing phagocytosed cargo. Splicing analysis reveals a role for QKI in regulating microexon networks of the Rho GTPase pathway. We show an increase in RhoA activation and proinflammatory cytokines in QKI-deficient microglia that are repressed by treating with a Rock kinase inhibitor. During the cuprizone diet, mice with QKI-deficient microglia are inefficient at supporting central nervous system (CNS) remyelination and cause the recruited oligodendrocyte precursor cells to undergo apoptosis. Furthermore, the expression of QKI in microglia is downregulated in preactive, chronic active, and remyelinating white matter lesions of multiple sclerosis (MS) patients. Overall, our findings identify QKI as an alternative splicing regulator governing a network of Rho GTPase microexons with implications for CNS remyelination and MS patients.

2.3 Introduction

Microglia are the innate immune cells resident in the central nervous system (CNS). These cells represent 5% to 20% of brain cells and most adopt a highly ramified morphology under healthy conditions (Gomez Perdiguero et al., 2013; Salter and Stevens, 2017). In response to injury, infection, and disease, microglia become amoeboid-like in shape and migrate to the site of injury to engage in proinflammatory immune responses (Butovsky and Weiner, 2018; Fani Maleki and Rivest, 2019; Song and Colonna, 2018). Under neurodegenerative conditions, microglia acquire a chronically proinflammatory phenotype that may contribute to disease progression (Butovsky and Weiner, 2018; Deczkowska et al., 2018). Despite the unique gene expression signatures that define microglia under disease conditions (Hammond et al., 2019; Keren-Shaul et al., 2017; Krasemann et al., 2017), little is known about how RNA transcripts are regulated transcriptionally and/or post-transcriptionally.

RNA binding proteins (RBPs) play a pivotal role in post-transcriptional gene regulation critical for cell physiology and pathology (Corley et al., 2020; Ule and Blencowe, 2019). It is now clear that RBPs are frequently mutated or misregulated in various diseases, thereby augmenting disease susceptibility and progression (Cooper et al., 2009; Lukong et al., 2008; Masaki et al., 2020). One of the RBPs, QUAKING (QKI), is aberrantly expressed in schizophrenia, Alzheimer's disease (AD), multiple sclerosis (MS), and cancer patients (Aberg et al., 2006; Farnsworth et al., 2016; Lavon et al., 2019; Shingu et al., 2017; Zong et al., 2014). QKI belongs to the heteronuclear ribonucleoprotein particle K (hnRNP K) homology (KH) domain family (Darbelli and Richard, 2016). The major isoforms QKI-5, QKI-6, and QKI-7, which differ in their C-terminal 30 amino acids, bind a specific RNA QKI response element (QRE) with the sequence ACUAAY (1–20) UAAY (Y; C/U) (Galarneau and Richard, 2005). Notably, genome-wide RNA sequencing (RNA-

seq) data revealed a significant number of alternative splice defects in QKI-deficient cells (Darbelli et al., 2017; de Bruin et al., 2016; Hall et al., 2013).

QKI RBPs have been shown to play key roles in RNA metabolism in numerous cell types. QKI regulates mRNA translation, mRNA export, mRNA stability, and pre-mRNA splicing in the myelinating oligodendrocyte (for review see Darbelli and Richard, 2016). It also regulates pre-mRNA splicing in skeletal and smooth muscles (Hall et al., 2013; van der Veer et al., 2013) and in the monocyte-to-macrophage differentiation process (de Bruin et al., 2016). Reduced QKI expression in cancerous cells alters the pre-mRNA splicing signatures, influencing endolysosomal and epithelial-mesenchymal transition processes (Pillman et al., 2018; Shingu et al., 2017; Zong et al., 2014). However, the role of QKI, or any RBP, in regulating alternative RNA splicing networks in microglia is unknown.

Here, we generated mice with QKI-deficient microglia to investigate the role of RNA processing in the regulation of these cells in vivo. We show that in the absence of QKI, microglia exhibit an amoeboid-like morphology with increased production of proinflammatory cytokines under basal, healthy conditions and have defects in processing cargo after phagocytosis. These QKI-deficient microglia hindered CNS remyelination by engulfing the recruited oligodendrocyte precursor cells (OPCs). Notably, transcriptional analyses revealed that QKI regulated microexon alternative splicing (AS) events within the Rho GTPase pathway. Indeed the RhoA GTPase pathway was aberrantly activated in QKI-deficient microglia. Furthermore, the inhibition of the Rock kinases with Y-27632 reduced microglia cytoskeleton reorganization and the levels of the proinflammatory cytokines released by the QKI-deficient microglia. Brains from MS patients had reduced QKI expression in their microglia compared to areas of normal white matter controls. Our findings identify the QKI RBPs as key regulators of AS in microglia.

2.4 Results

2.4.1 QKI-deficient microglia exhibit increased proliferation with altered morphology

The role of the QKI RBPs in microglia is undefined. Thus, we first examined whether microglia expressed the QKI RBPs. Immunofluorescence staining using pan-QKI antibodies and ionized calcium-binding adaptor molecule 1 (Iba-1), a marker for microglia in the CNS, revealed QKI staining in Iba-1-positive cells in the mouse brain (Figure S1A). To investigate the role of QKI in microglia, we generated QKI-deficient microglia ($qkI^{Cx3cr1-KO}$) by breeding Cx3cr1CreERT with $qkI^{FL/FL}$ mice. Injection of 4-hydroxytamoxifen (TAM) led to the deletion of expression of qkI exon 2 and completely nullified protein expression of all QKI isoforms in microglia (Figures S1B and 1C) but not in GFAP+ astrocytes nor in Olig2+ oligodendrocytes (Figures S1D and S1E). In line with previous findings (Shingu et al., 2017), QKI was not expressed in the NeuN+ neurons in both genotypes (data not shown). We next assessed whether QKI deficiency affected the number of microglia in the mouse brain. Indeed, brains of $qkI^{Cx3cr1-KO}$ mice had statistically more Iba-1+ microglia (>2-fold) in various areas of the CNS, including the cortex, hippocampus, and corpus callosum than control qkI^{FL} mice (Figures 1A and 1B). In addition, we used fluorescence-activated cell sorting (FACS) analysis to detect proliferating microglia by using the previously published gating strategy (Gosselin et al., 2014; Figure S2A). Corroborating the immunofluorescence observation, FACS analyses of CD11b^{high}CD45^{inter} microglia stained with the cellular marker for proliferation of Ki-67 also revealed a dramatic increase (from ∼1.4% to 28.1%) of Ki67+ microglia in the brain of $qkI^{Cx3cr1-KO}$ mice, suggesting their increased proliferation (Figure 1C). To assess the morphology of microglia, we performed the morphometric analysis by using Imaris software. This analysis revealed that QKI null microglia had enlarged cell bodies along with decreased branch points, terminal points, and reduced total dendritic length (Figures 1D and 1E). Despite the

70

pronounced changes in microglia morphology, we did not observe astrocyte reactivity (anti-GFAP), neuronal loss (anti-NeuN), or apparent defects in the myelination process (anti-MBP) (Figures S2B and S2C). Finally, to exclude the possibility that the phenotype observed in QKI null microglia was due to haploinsuffiency at the Cx3cr1 locus and caused the CreERT allele that inactivates 1 copy of Cx3cr1 (Goldmann et al., 2013), we compared the number and morphology of microglia in qkI^{FL} mice (Cx3cr1+/+) and $qkI^{Cx3cr1-KO}$ (Cx3cr1+/−) without TAM treatment. No difference was observed in the number and the morphology of microglia in qkI^{FL} and $qkI^{Cx3cr1-KO}$ mice (Figures S3A–S3D). Taken together, our findings showed that QKI deficiency in microglia caused their deregulated proliferation with an enlarged cell body morphology with short dendrites.
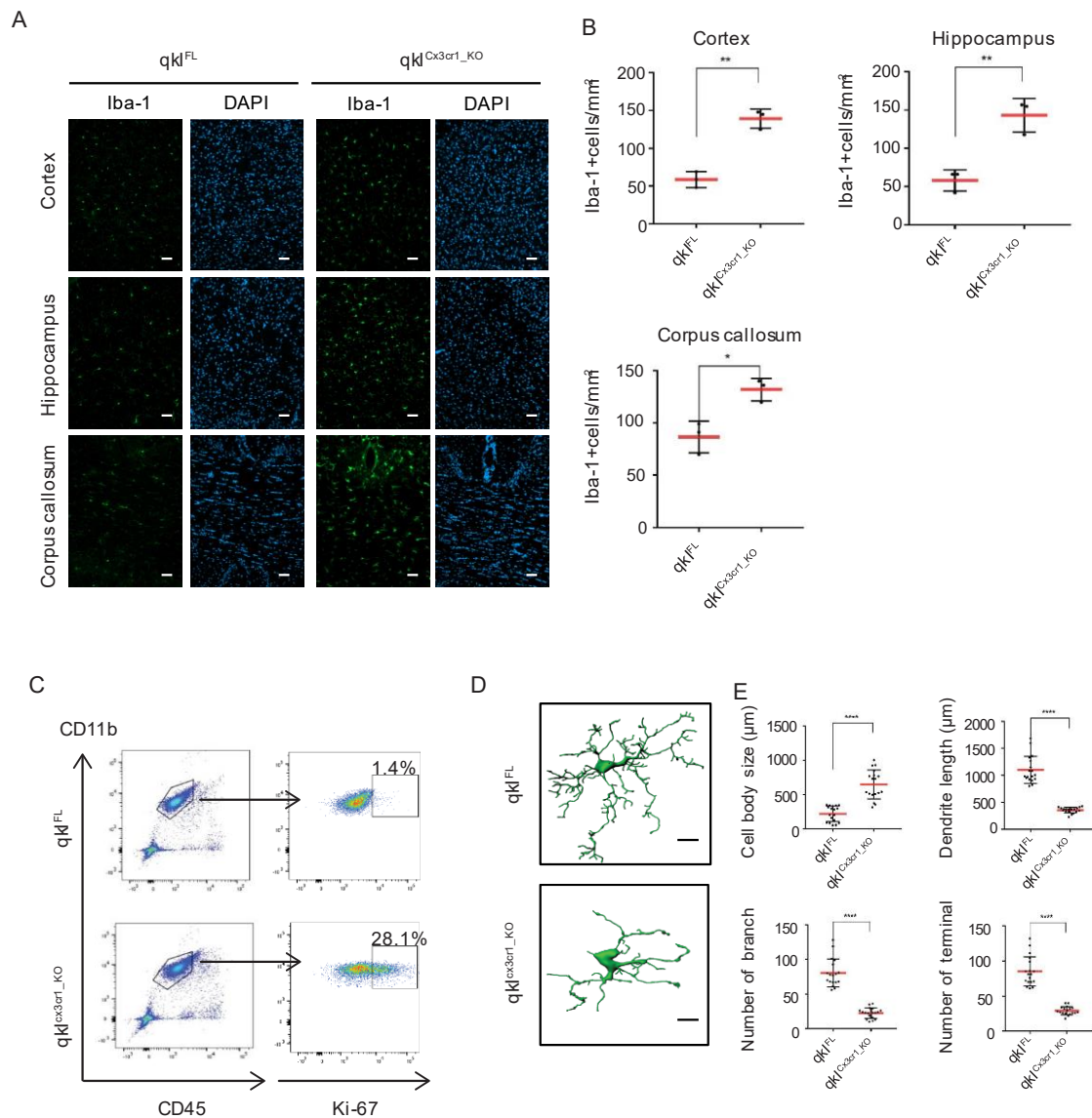
Figure 1 QKI-deficient microglia exhibit increased proliferation with altered morphology.

A, Iba-1 and DAPI staining in cortex, hippocampus, and corpus callosum of *qkI^FL*, and *qkI^Cx3cr1-KO* mice after TAM injection. Representative images are shown. Scale bar represents 50 µm.

B, Iba-1-positive microglial cells counts. Each dot represents one mouse with a total of 3 mice used per genotype. Data presented as mean ± SEM. *P* values were analyzed using the Mann–Whitney U-statistical test (*p < 0.05, ** *p*<0.01).

C, Flow cytometric quantification of Ki-67-positive cells for CD11b+CD45^inter microglia in *qkI^FL*, and *qkI^Cx3cr1-KO* mice after the TAM injection. Data is representative of three independent experiments.

D, IMARIS based 3D reconstruction images of Iba-1+ microglia of *qkI^FL*, and *qkI^Cx3cr1-KO* mice. Scale bar represents 10 µm.

E, IMARIS based morphometric analysis of microglia of *qkI^FL*, and *qkI^Cx3cr1-KO* mice after injection of TAM. Three mice per genotype, and 6 cells per mouse were analyzed. Data presented as mean ± SEM. *P* values were analyzed using the Mann–Whitney U-statistical test (**** *p* < 0.0001)

2.4.2 Alternative splicing of microexons of the Rho GTPase pathway regulated by QKI

QKI functions as an RNA processing protein and is a known regulator of AS (Darbelli and Richard, 2016). To identify whether QKI regulates AS in microglia, we performed bulk paired-end RNA-seq on FACS-sorted purified microglia from TAM-treated qkI^{FL} and $qkI^{Cx3cr1-KO}$ mice. Hierarchical clustering of the heatmaps and principal component analysis (PCA) showed that qkI^{FL} and $qkI^{Cx3cr1-KO}$ microglia had a distinct transcriptional output with 93% variance (Figures S4A and S4B).

Next, we quantified AS events by using rMATs, MAGIQ, and MISO software. These pipelines generated highly overlapping AS events (Figure S4C; Table S1). We further confirmed the individual splicing events using IGV (Integrative Genomics Viewer) (Robinson et al., 2011). The union of all 3 pipelines yielded a total of 344 alternatively spliced events, including 163 skipped exon (SE), 58 alternative last exon (ALE), 50 alternative 3′-splice site (A3SS), 38 alternative 5′-splice site (A5SS), 3 alternative first exon (AFE), and 3 retained intron (RI) events (Figure 2A; Table S1). Given that QKI is a well-known splicing regulator for exon skipping events, we focused our analysis on SEs, alternative first and last exon events. We previously showed that QKI binds RNA at QREs with a sequence of ACUAAY (N1–20) UAAY (Galarneau and Richard, 2005). Therefore, we analyzed microglia transcripts for this motif upstream and downstream of SE events. We found 68.8% of the SE events contained the "core" (ACUAAY) and 34.4% contained the entire QRE (ACUAAY [N1–20] UAAY; N represents any nucleotide in the range of 1 to 20; Figure S4D). QRE sequences were more frequently observed upstream of excluded exons, whereas the presence of a QRE downstream was associated with exon inclusion (Figure S4E). To further assess the pathways involved in QKI-regulated alternative splice events, we performed Enrichr analysis (Chen et al., 2013). The most significant top 10 Reactome pathway

73

database showed enrichment for "signaling by Rho GTPase," "membrane trafficking," "Rho GTPase effectors," and "vesicle-mediated transport" (Figure 2B). Gene Ontology (GO) cellular component analysis identified engagement of alternatively spliced genes in the trans-Golgi network, cytoskeleton, and microtubule (Figure S4F). Moreover, QKI-regulated AS was significantly associated with the Rock2 pathway (Figure S4G).

Intriguingly, QKI-regulated transcripts were composed of smaller exons, and by measuring the length, we found QKI-regulated exons were significantly shorter than the control, non-QKI-regulated exons (mean: 187.9 nucleotides [nt] versus 104.7 nt). The small-sized exons termed microexons are highly conserved in neurons and play a crucial role in protein-protein interaction and protein function (Irimia et al., 2014), but their function in microglia is largely unknown. According to the Irimia et al. (2014) definition of microexons (3–27 nt), 37 of 221 of the QKI-regulated events could be classified as microexons, of which 20 contain a neighboring QRE. The less stringent description by Li et al. (2015) (<51nt) showed 74 of the QKI-regulated transcripts qualified as microexons, of which 49 contain a neighboring QRE (Figures 2C and 2D; Irimia et al., 2014; Li et al., 2015). Thus, QKI is a selective regulator of microexon AS in microglia. We performed ARCHS4 and Reactome pathway analysis by using both of these criteria. Despite involving a small number of events, QKI-regulated microexons were mainly detected in the CNS (prefrontal cortex and midbrain) and were significantly associated with the Rho GTPase pathway (Figure 2E; Table S1). Indeed, we confirmed that QKI profoundly regulated AS of microexons associated with the Rho GTPase pathway by using Sashimi plot analysis and RT-PCR analysis for Myo9b, Diaph1, Ocrl, Arhgap17, Clasp2, and Arhgap32 (Figures 2F and S5A). We further confirmed the specificity of QKI-mediated splicing events by performing RT-PCR analysis on

transcripts in which cassette exons were not regulated by QKI, including Cd81, Bnip2, and Gapdh, and as expected, QKI did not influence their AS (Figure S5B). Therefore, these data disclose the unprecedented role of QKI as an essential regulator of microexon AS in microglia.
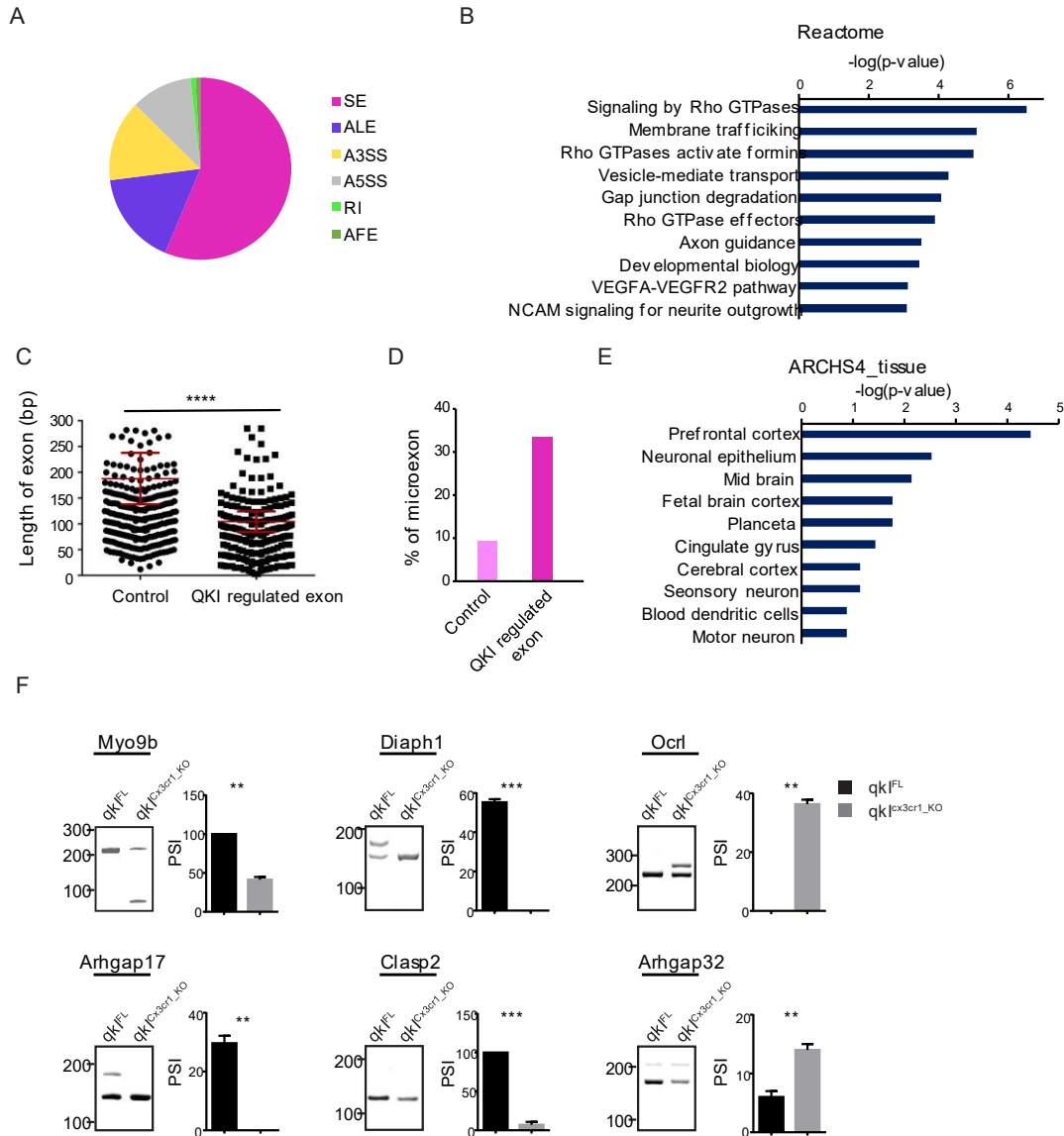
Figure 2 Alternative splicing of microexons of the Rho GTPase pathway regulated by the QKI RNA binding proteins.
A, Differential alternative splicing events were analyzed using rMATS, MAJIQ, and MISO software. Pie chart depicts 6 different alternative splicing events affected by QKI; Skipped exon (SE), alternative last exon (ALE), alternative 3' splice site (A3SS), alternative 5' splice site (A5SS), retained intron (RI), and alternative first exon (AFE). **B,** QKI-mediated SE, ALE, and AFE events were analyzed for the Reactome pathway using Enrichr software. The top 10 pathways are listed according to the most significant p-value. **C,** Dot plots of SE, ALE, and AFE events analyzed for exon length, and compared with that of control exons. Data presented as mean ± SEM. *P* values were analyzed using a parametric unpaired t-test (**** $p<0.0001$). **D,** Bar graph showing the percentage of microexons present in QKI-regulated, and control exons. **E,** QKI-mediated microexons were analyzed for ARCHSS4 tissue pathway using Enrichr software. **F,** Alternatively spliced microexons associated with Rho GTPase pathway were further validated with exon specific primers using RT-PCR. Primers were designed upstream, and downstream of cassette exons. Percent spliced in (PSI) was calculated and depicted in the bar graph. At least 3 independent experiments were performed. Data presented as mean ± SEM. *p* values were analyzed using the Mann–Whitney U-statistical test (*$p < 0.05$, ** $p<0.01$, *** $p<0.001$).

2.4.3 The RhoA GTPase pathway is activated in qkI-deficient microglia.

The genes harboring the alternatively spliced microexons (Diaph1 and Myo9b) or normal exons (Arhgef11) are direct activators of RhoA, balancing its inactive and active states (Hanley et al., 2010; Itoh et al., 2012; Kitzing et al., 2007). We then sought to examine whether the microexon AS events culminated in RhoA GTPase pathway activation. For this, we used the G-LISA assay to measure the active RhoA level in freshly sorted primary microglia with a purity of 93.4% (Figure S2A). G-LISA analysis showed a significant increase in active RhoA in $qkI^{Cx3cr1-KO}$ microglia compared to control qkI^{FL} microglia (Figure 3A). We further validated this finding by performing immunofluorescence analysis by using an active RhoA antibody on primary microglia (Qi et al., 2020). The immunofluorescence results also revealed an increase of active RhoA intensity in $qkI^{Cx3cr1-KO}$ microglia compared to control qkI^{FL} microglia (Figures 3B and 3C). Next, we looked at the Rock2 pathway, one of the critical downstream effectors of RhoA. For this investigation, we performed immunofluorescence staining for Iba-1 along with Rock2 substrates pThr18/Ser19 Mlc2 and pSer3 Cofilin in primary microglia. Immunostaining revealed $qkI^{Cx3cr1-KO}$ microglia exhibited a substantial increase of Phalloidin, p-Mlc, and p-Cofilin in comparison to control qkI^{FL} microglia (Figures 3D and 3E; Figures S5C and S5D). We corroborated evidence for the Rock pathway activation in $qkI^{Cx3cr1-KO}$ microglia by experiments using the Rock1/Rock2 inhibitor Y-27632 (Tönges et al., 2011). We observed that the Y-27632 treatment significantly abolished the expression of Phalloidin, p-Mlc, and p-Cofilin (Figures 3D and 3E; Figures S5C and S5D). Our findings show that the RhoA GTPase pathway is activated in QKI-deficient primary mouse microglia.
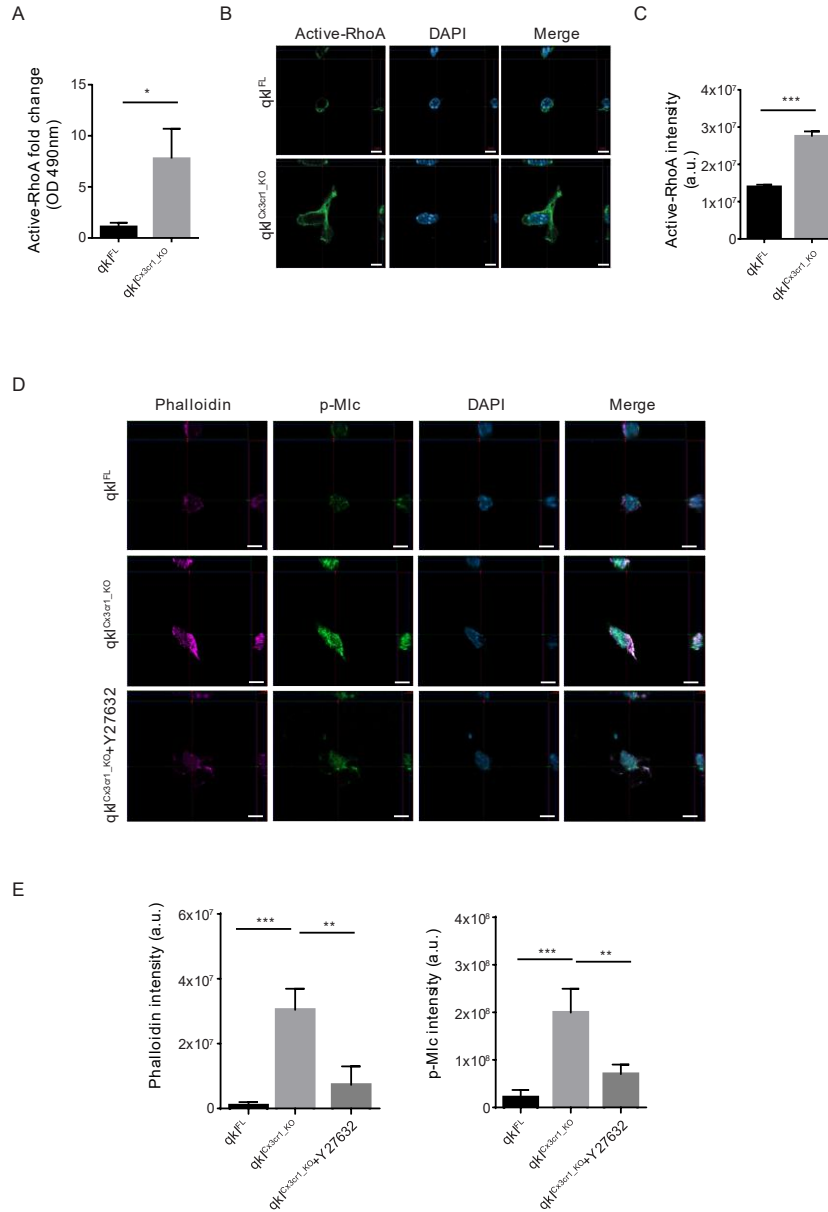
Figure 3 The RhoA GTPase pathway is activated with *qkI*-deficiency.
A, Freshly sorted microglia from *qkI*^{FL,} and *qkI*$^{Cx3cr1-KO}$ mice were analyzed for active RhoA GTPase using G-LISA assay (absorbance at 490nm). At least two independent experiments were performed. Data presented as mean ± SEM. *P* values were analyzed using the Mann–Whitney U-statistical test (*p < 0.05) **B,** Primary microglia from *qkI*^{FL} and *qkI*$^{Cx3cr1-KO}$ mice were FACS sorted, and seeded on poly-D-lysine coated slides. The next day cells were serum starved for 6h and stained with an active RhoA antibody. Images were taken using Zeiss confocal microscope, and projected as an orthogonal view. Scale bars represent 5µm. **C,** Immunofluorescence intensity for active RhoA (green) was measured using IMARIS software. Bar graph shows mean intensity with SEM. *P* values were analyzed using a parametric unpaired t-test (*** *p*<0.001). Data is representative of two independent experiments. **D,** Primary microglia from *qkI*^{FL} and *qkI*$^{Cx3cr1-KO}$ mice were FACS sorted, and seeded on poly-D-lysine coated slides. The next day cells were serum starved for 6h, and treated with either DMSO or Rock kinase inhibitor (Y-27632, 10µM) for

3h. Cells were fixed, and stained for Phalloidin (red), p-Mlc (green), and DAPI (Blue). Images were taken using Zeiss confocal microscope, and projected as an orthogonal view. Scale bars represent 5µm.
E, Immunofluorescence intensity for Phalloidin (violet), and p-Mlc (green) was measured using the IMARIS software. Bar graph shows mean intensity with SEM. *P* values were analyzed using a one-way ANOVA test (** *p*<0.01, *** *p*<0.001). Data is representative of three independent experiments.

2.4.4 QKI-deficient microglia exhibit up-regulation of inflammatory genes dependent on the Rock pathway.

Volcano plot analysis of the differential gene expression of the RNA-seq data revealed the upregulation of 326 genes and downregulation of 294 genes in $qkI^{Cx3cr1-KO}$ microglia compared to qkIFL (2-fold change at false discovery rate [FDR] of 0.05, base mean of >10; Figure 4A; Table S2). In particular $qkI^{Cx3cr1-KO}$ microglia exhibited higher expression of genes known to encode proteins related to inflammation (Il-6, Apoe, Cxcl10, Il-1b, Il-12b, and Tnf-α). In line with this finding, functional annotation by DAVID, Reactome, and GO analysis showed enrichment of cell cycle and inflammation-related pathways in the upregulated transcripts in $qkI^{Cx3cr1-KO}$ mice (Figures 4B and 4C; Figure S6A; Huang et al., 2009; Kuleshov et al., 2016). Notably, we also found "Rho-GTPase activate formins" like in Figure 2B in the upregulated pathway category. However, close inspection of the genes for this category reveals cell cycle or apoptosis pathway genes (Aurkb, Birc5, Bub1, Bub1b, Cdc20, Cenpem, Cenpm, and Kntc1) that are downstream effectors of the Rho GTPase pathway (David et al., 2012). Thus, the alternative spliced category of Figure 2B contains the most upstream regulators of the Rho pathway such as "signaling by Rho GTPases," the "Rho GTPase effectors," and the downstream regulators "Rho-GTPases Activate formins." Thus, the AS events are likely driving the observed differential gene expression. The downregulated transcripts were mainly associated with calcium ions, metal ions, filamin, and tubulin binding, which are involved in nervous system development (Figure S6B). Interestingly, Trrust transcription and ARCHS4 kinase analysis showed enrichment in nuclear factor κB (NF-

κB), Rock1, and Rock2 signaling pathways (Figure 4D). Rock2 is known to activate the transcriptional role of NF-κB (Anwar et al., 2004); therefore, differential gene expression analysis highlights the connection between Rock2 and the inflammatory phenotype of $qkI^{Cx3cr1-KO}$ microglia (Roser et al., 2017). Given these findings, we next explored whether Rock2 activation could underpin the proinflammatory phenotype observed in $qkI^{Cx3cr1-KO}$ microglia. Consistent with RNA-seq-based gene expression analysis, mouse cytokine 44-Plex analysis confirmed $qkI^{Cx3cr1-KO}$ primary microglia secreted more proinflammatory cytokines (interleukin-6 [IL-6], IL-1α, and transforming growth factor α [TNF-α]) and chemokines (CXCL10, CCL5, CCL22, and CCL12) than qkI^{FL} microglia (Figure S6C). We then treated primary microglial cells with Y-27632 and observed a reduction in the inflammatory transcripts (Ccl22, Ccl5, Il-6, and Il-1β) of $qkI^{Cx3cr1-KO}$ microglia (Figure 4E). Additionally, we analyzed the expression of disease-associated microglia (DAM) phenotype transcripts, a subtype of microglia prevalent in neurodegenerative and inflammatory CNS diseases (Deczkowska et al., 2018). RNA-seq and qRT-PCR analysis showed that DAM transcripts such as Apoe, Spp1, Ccl2, Fabp5, Axl, and Cybb were upregulated in $qkI^{Cx3cr1-KO}$ microglia compared to control qkI^{FL} microglia, but not Trem2 (Figure S6D). These data suggest that the loss of QKI in microglia confers a proinflammatory and DAM phenotype that is frequently observed in neurodegenerative and inflammatory diseases of the CNS.
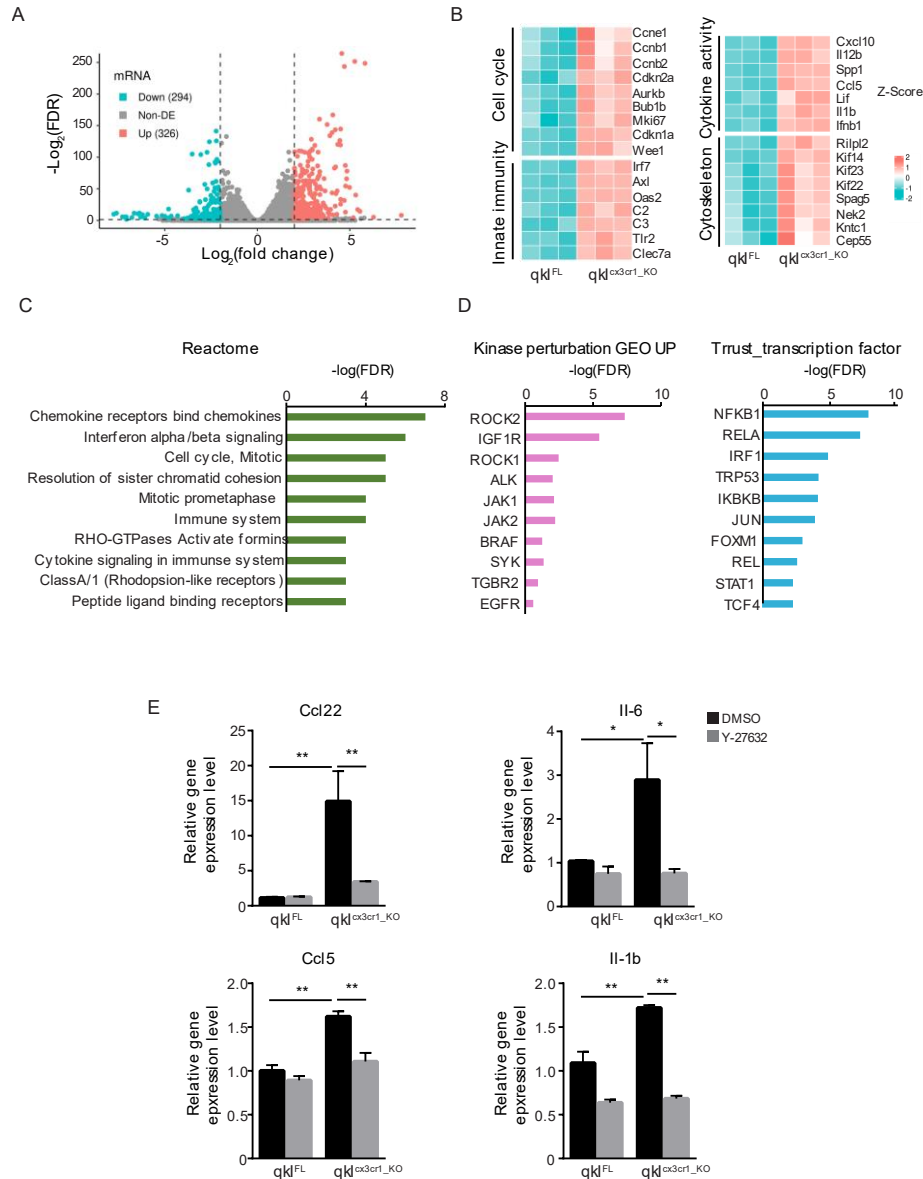
Figure 4 QKI-deficient microglia exhibit up-regulation of inflammatory genes dependent on Rock2 pathway.

A, RNA-seq on FACS sorted microglia cells from qkI^{FL} and $qkI^{Cx3cr1-KO}$ mice injected with TAM. Volcano plot for differentially expressed transcripts of qkI^{FL} and $qkI^{Cx3cr1-KO}$ microglia showing the significantly up-regulated (red) and down-regulated genes (blue) with a fold change higher than 2, FDR < 0.05, and base mean > 10. **B,** Pathways were analyzed using the up-regulated transcripts by DAVID informatic software. Heatmap shows the up-regulation of gene sets related to activated microglia phenotype. Each column represents microglia from one independent sample. Color code represents row Z score.

C, D, Bar graph shows Reactome, Kinase perturbation up, and Trrust transcription factor pathways analyzed using Enrichr software. **E,** FACS sorted primary microglia were seeded on poly-D-lysine coated plates. The next day cells were treated with DMSO or Y-27632 (10μM) for 3h. Inflammatory related transcripts were analyzed using RT-qPCR. Three independent experiments were performed. Data presented as mean ± SEM. p values were analyzed using a one-way ANOVA test (*$p < 0.05$, ** $p<0.01$).

2.4.5 Abnormal phagocytic phenotype and CNS remyelination defects in absence of QKI in microglia.

We examined the ability of the $qkI^{Cx3cr1-KO}$ mice to influence CNS demyelination and remyelination by using the cuprizone mouse model of myelin lesion (Gudi et al., 2009). Of note, at the 5-week endpoint of the cuprizone diet (CPZ), wild-type control mice showed a noticeable increase of fluorescent intensity for QKI expression in Olig2+ oligodendrocytes (2.3-fold), a slight decreased in QKI staining in Iba-1+ microglia (0.86-fold), and glial fibrillary acidic protein (GFAP)+ astrocytes (0.85-fold) (Figure S7A). An increased expression of QKI in Olig2+ oligodendrocytes was expected, as QKI controls the differentiation process of oligoprogenitor cells (OPCs) to mature oligodendrocytes (Darbelli et al., 2016). After 5 weeks of CPZ, both qkI^{FL} and $qkI^{Cx3cr1-KO}$ genotypes exhibited extensive demyelination in their corpus callosum, as visualized by Black Gold II staining (Figure 5A; CPZ 5 weeks; quantified on the right). After 5 weeks of CPZ, both qkI^{FL} and $qkI^{Cx3cr1-KO}$ genotypes exhibited extensive demyelination in their corpus callosum, as visualized by Black Gold II staining (Figure 5A; CPZ 5 weeks; quantified on the right). We confirmed the microexon splicing defects of Myo9b, Diaph1, Ocrl, Arhgap17, Clasp2, and Arhgap32 in the $qkI^{Cx3cr1-KO}$ microglia compared to qkI^{FL} mice were maintained at the 5-week endpoint of CPZ (Figure S7B). Following the 5 weeks of CPZ, the mice were then fed with regular chow diet for 1, 2, and 3 weeks (+1, 2, 3 week(s) off, Figure 5A) and sacrificed to assess the quality of CNS remyelination by Black Gold II staining. The qkI^{FL} control mice showed extensive remyelination during all 3 weeks after CPZ with ~75%, ~85%, and ~100% remyelination, respectively (Figure 5A). In contrast, $qkI^{Cx3cr1-KO}$ mice had a significant delay in remyelination with ~20%, 35%, and 45% of the areas stained with Black Gold II post-CPZ for 1, 2, and 3 weeks, respectively (Figure 5A). The 5-week CPZ induced extensive microgliosis in the corpus callosum

of both qkI^{FL} and $qkI^{Cx3cr1-KO}$ mice, as detected using Iba-1 and the Mac2 stainings, of which the latter labels highly phagocytic microglia (Figures 5B and 5C). The Iba-1 staining dissipated equally between qkI^{FL} and $qkI^{Cx3cr1-KO}$ mice during the remyelination phase; however, the microgliosis observed with Mac2 staining were much slower to dissipate in $qkI^{Cx3cr1-KO}$ mice (Figures 5B and 5C). In contrast, Mac2 + microglia completely returned to basal levels after 2 weeks of regular chow diet in qkI^{FL} mice (Figure 5C). Staining with anti-GFAP antibody showed extensive astrogliosis, and this phenotype remained elevated in $qkI^{Cx3cr1-KO}$ mice compared to qkI^{FL} mice during the later stages of remyelination (Figure 5D). Similar increases in Mac2+ and GFAP+ cell numbers were observed when using 4',6-diamidino-2-phenylindole (DAPI) (Figures S7C and S7D). These findings suggest that the microglia from $qkI^{Cx3cr1-KO}$ mice remain phagocytic (Mac2+ microglia) and cause the activation of astrocytes (GFAP+ astrocytes) during remyelination. To characterize the cause of the continuous activation in $qkI^{Cx3cr1-KO}$ microglia (Mac2+), we performed in vitro phagocytosis assays by using pHrodo red zymosan bioparticles. These particles are pH sensitive and emit red fluorescent light in acidic environments, such as in the phagosome (Kapellos et al., 2016). We isolated primary microglia from qkI^{FL} and $qkI^{Cx3cr1-KO}$ mice and incubated them with pHrodo red zymosan particles for 15 min, and then we visualized the engulfed particles by immunofluorescence microscopy. Notably, we observed an accumulation of large fluorescent zymosan particles in the QKI-deficient microglia, but not in the microglia isolated from qkI^{FL} (Figures S7E and S7F). Similarly, a study by Shen et al. (2016) showed that the deletion of the lysosomal protein Rag-Ragulator complex in microglia caused an accumulation of the phagocytic particles, which resembled "engorged" microglia. Taken together, our findings suggest the QKI-deficient microglia have difficulty processing engulfed particles that may contribute to the prolonged phagocytic phenotype in the remyelination phase.
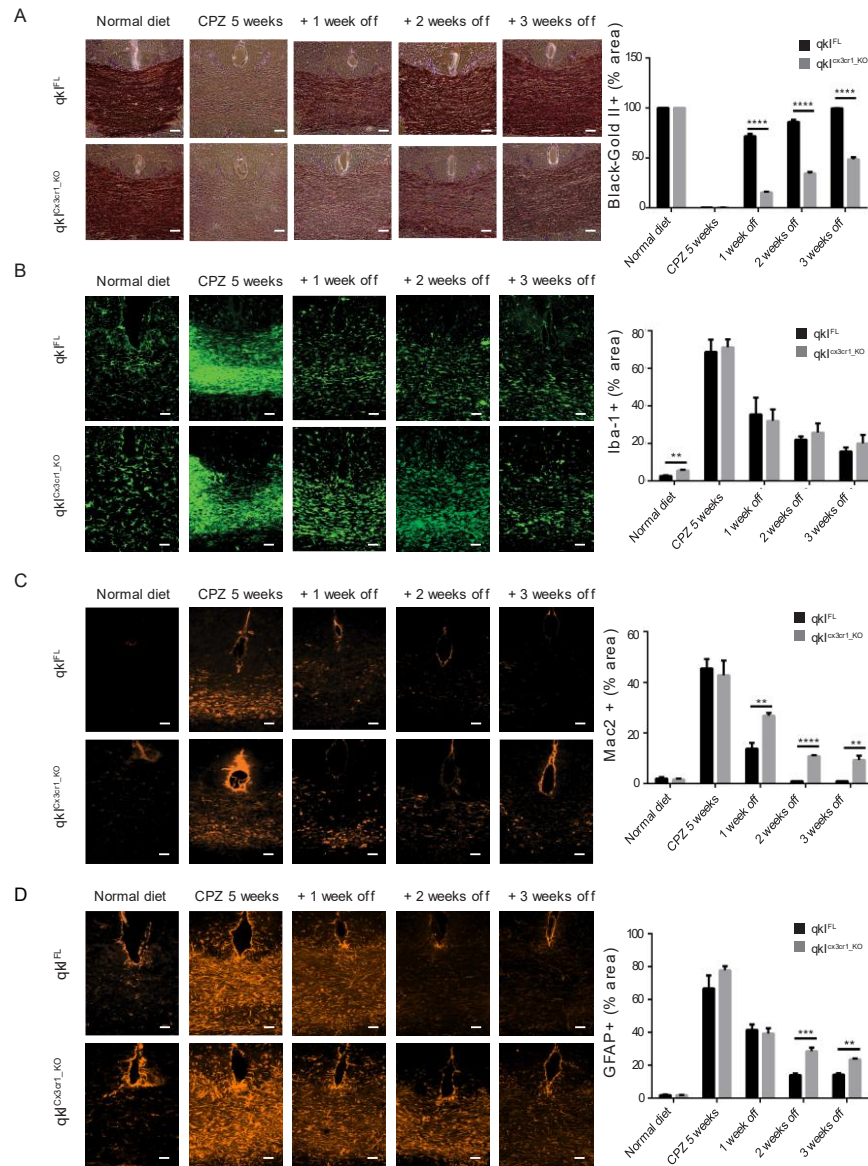
Figure 5 CNS remyelination defects in qkI-deficient mice.

Mice were fed with 0.2% cuprizone diet (CPZ) and 4 mice were sacrificed at each time point; 5 weeks CPZ, 5 weeks CPZ + 1 week off, 5 weeks CPZ + 2 weeks off, and 5 weeks CPZ + 3 weeks off.

A, Images of in vivo corpus callosum stained with Black gold II was analyzed in qkI^{FL} and $qkI^{Cx3cr1-KO}$ mice. The bar graph shows average density of myelin (brown) per mm2. Data presented as mean ± SEM. P values were analyzed using the Mann–Whitney U-statistical test (**** p<0.0001). Scale bars represent 50µm.

B, The anti-Iba-1 (green), and **C**, -Mac2 (red) antibodies were used to stain microglia, and phagocytic microglia cells, respectively. Bar graph depicts the average density of Iba-1 (green), and Mac2 (red) per mm2 in corpus callosum of qkI^{FL} and $qkI^{Cx3cr1-KO}$ mice. Data presented as mean ± SEM. P values were analyzed using the Mann–Whitney U-statistical test (** p<0.01, **** p<0.0001). Scale bars represent 50µm.

D, The anti-GFAP (red) antibody was used to detect astrocytes in corpus callosum of qkI^{FL} and $qkI^{Cx3cr1-KO}$ mice. Bar graph depicts the average density of astrocyte per mm2. Data presented as mean ± SEM. P values were analyzed using the Mann–Whitney U-statistical test (** p<0.01, *** p<0.001). Scale bars represent 50µm.

2.4.6 qkICx3cr1-KO mice exhibit defects in OPC recruitment.

The remyelination process is normally preceded by the proliferation of OPCs, which subsequently differentiate into myelinating oligodendrocytes (Matsushima and Morell, 2001). Therefore, we first analyzed the number of OPCs by staining with anti-Olig2-antibody (Yokoo et al., 2004). We observed that $qkI^{Cx3cr1-KO}$ mice exhibited fewer Olig2+ cells both during the demyelination and remyelination periods (Figure 6A). These findings were further validated by staining with anti-PDGFRα antibodies, a marker of OPCs (Figure 6B). We surmised that the reduced number of OPCs was likely due to cell death and engulfment by the activated microglia remaining at the demyelination sites. Indeed, we observed a prominent ~15% increase of Olig2+ cells being also positive for Cleaved-caspase-3 in the $qkI^{Cx3cr1-KO}$ mice (Figure 6C), indicating increased OPC apoptosis. To examine whether OPCs were being lost by phagocytosis by the microglia, we performed colocalization between the microglia Mac2 marker and the OPC marker PDGFRα. The 3D reconstruction of images using z stack confocal imaging showed complete internalization of PDGFRα+ OPCs in Mac2+ microglia (Figure 6D). Our findings show that $qkI^{Cx3cr1-KO}$ mice have reduced OPC survival at sites of remyelination because these cells die by apoptosis and are engulfed by phagocytic Mac2+ microglia remaining at sites of demyelination.
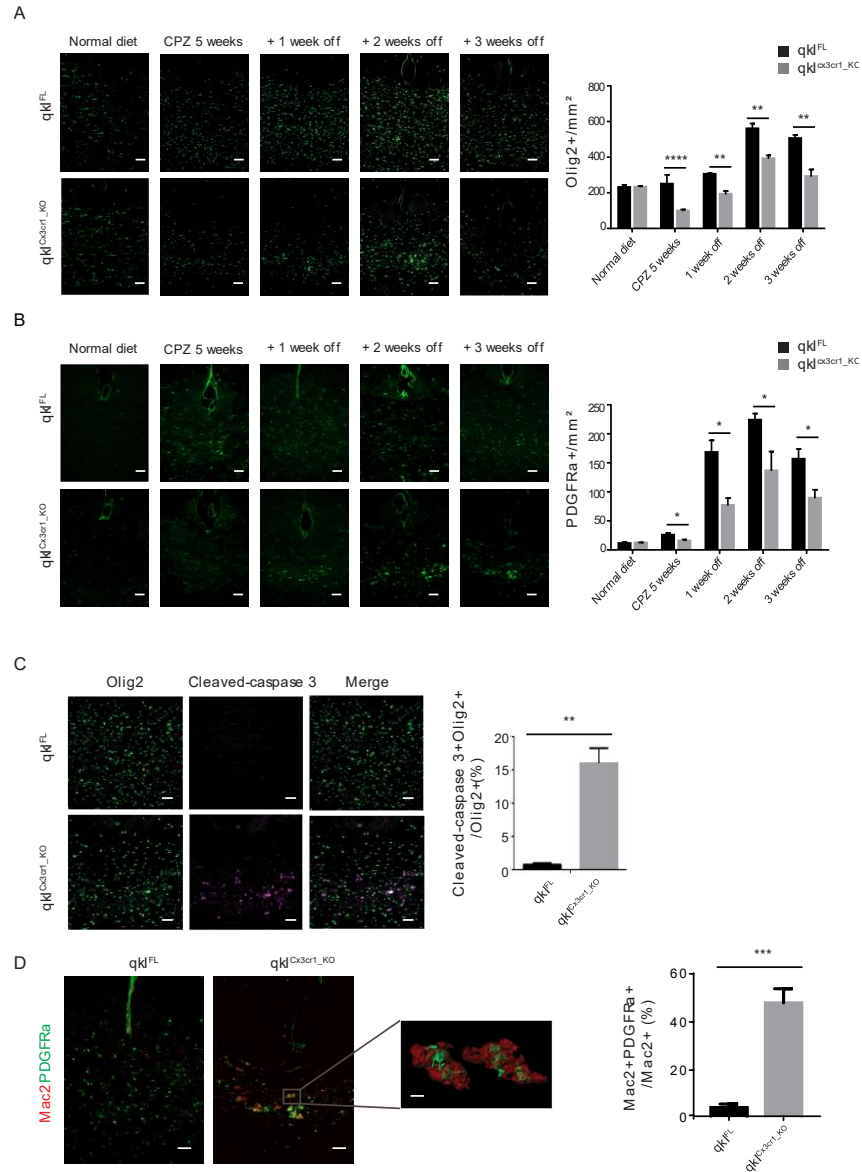
Figure 6 Elevated OPC apoptosis and OPC-engulfing microglia at sites of CNS remyelination in $qkI^{Cx3cr1-KO}$ mice.

A, B, The presence of oligoprogenitor cells was analyzed using anti-Olig2 (A,) and -PDGFRantibodies, respectively and representative images are shown on the left and their quantification shown on the right. Bar graph depicts an average number of Olig2+ (green), and PDGFRgreen) cells per mm2 in corpus callosum of qkI^{FL} and $qkI^{Cx3cr1-KO}$ mice. Data presented as mean ± SEM. P values were analyzed using the Mann–Whitney U-statistical test (*p < 0.05, ** p<0.01, **** p<0.0001). Scale bars represent 50μm. Four mice were sacrificed at each time point per genotype. **C,** Representative image of in vivo corpus callosum stained for Olig2 (green) and Cleaved- caspase3 (violet) at remyelination 3 week. Average percentage of Cleaved-caspase 3 positive, and Olig2 cells in corpus callosum. Data presented as mean ± SEM. P values were analyzed using the Mann–Whitney U-statistical test (** p<0.01). Scale bars represent 50μm. Four mice were sacrificed at each time point per genotype.**D,** Representative 3D-reconstruction images of anti-Mac2 (red) with PDGFR (green) are shown. Data presented as mean ± SEM. P values were analyzed using the Mann–Whitney U-statistical test (*** p<0.001). Scale bars represent 50μm. The scale bar for 3D-reconsruction image is 10μm.

2.4.7 Brains of MS patients have decreased microglia QKI expression.

To translate our findings to human CNS diseases, we analyzed post-mortem brain tissue of MS patients for expression of QKI in microglia. The staining of the major alternative splice regulator QKI-5 showed perfect nuclear localization in IBA-1-positive cells in a control sample of the white matter (Figure 7A). We then examined the expression of QKI in different histopathological types of white matter lesions; preactive, chronic active lesions, and remyelinated lesions (Kuhlmann et al., 2017). Our immunostaining analysis showed a significant reduction of nuclear expression of QKI-5 in preactive, chronic active, and remyelinating white matter lesions of the MS patients compared to that of normal controls (Figure 7B). Our results show that microglial QKI-5 expression is repressed in MS patient samples, and this might lead to the chronic proinflammatory microglia phenotype that could enhance the disease progression.
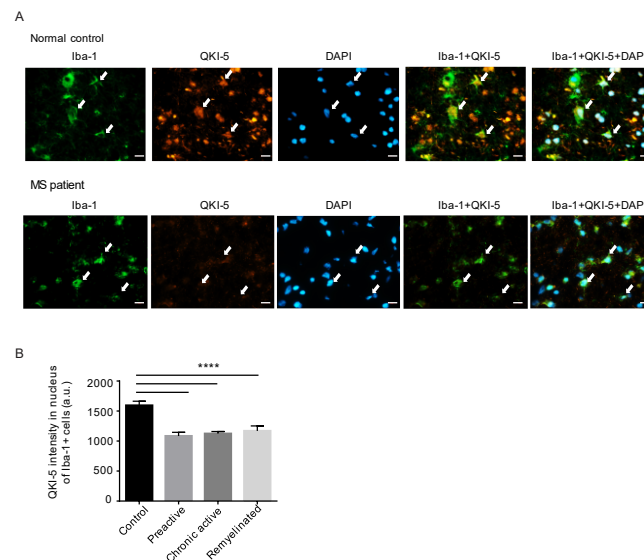
Figure 7 Brains lesions of MS patients have decreased microglia QKI-5 expression.
A, Expression of QKI in microglia was detected using anti-QKI-5, and -Iba-1 antibodies in white matter of normal, preactive, chronic activated and remyelinating brain areas from MS patient tissue samples. Scale bar represents 20 µm. **B,** Immunofluorescence intensity of QKI-5 in Iba-1 positive cells was measured in control and different lesion types of MS patient tissue samples as indicated. Bar graph depicts mean ± SEM. Each box plot represents separate lesions (Control=6, Preactive=3, Chronic active= 6, Remyelinated=4). *P* values were analyzed using a one-way ANOVA with Tukey correction for multiple comparisons (**** $p<0.0001$).

2.5 Discussion

In the present manuscript, we define QKI as a novel regulator of AS in microglia. Moreover, we show that the QKI RBPs regulate microexon AS, culminating in the RhoA GTPase pathway activation. We show that RhoA GTPase was active in QKI-deficient primary mouse microglia, as measured by G-LISA and by using an active RhoA GTPase antibody for immunofluorescence analysis. QKI-deficient microglia exhibited amoeboid-like morphology with short ramifications with proinflammatory transcriptome signatures. The proinflammatory transcription signature was reversed by inhibition of the Rock pathway with the inhibitor Y-27632. Remyelination defects were observed in $qkI^{Cx3cr1-KO}$ mice by using the cuprizone myelin pathology model, as recruited OPCs died by apoptosis and were engulfed by the QKI-deficient microglia. Importantly, we show the downregulation of human QKI-5, the main nuclear isoform regulating pre-mRNA splicing, protein expression in microglia near preactive, chronic active, and remyelinating white matter lesions of MS patient brain samples. Our findings suggest the loss of QKI in microglia activates the RhoA GTPase pathway, altering microglia morphology and function and hindering CNS remyelination at demyelinated lesions.

Early studies by Zhang et al. (2014) defined alternatively spliced events in microglia; however, the splicing factors contributing to these effects have remained uncharacterized. To understand how QKI regulates splicing dynamics in microglia, we performed deep RNA-seq in cell-sorted primary wild-type and QKI-deficient mouse microglia. We now define a role for QKI-regulated microexon selection composed of multiple of 3 nucleotides and a major network QKI modulates is the Rho GTPase pathway (Table S1). A major splicing factor for neural-specific microexons, SRRM4, is misregulated in autism spectrum disorders and promotes aberrant microexon splicing patterns, leading to disease progression (Gonatopoulos-Pournatzis et al., 2020;

Irimia et al., 2014). Interestingly, there was a subset of QKI-regulated microexons in microglia that overlapped with neural-specific microexons (Myo9b, Abi1, Clasp2, Cpeb2, Rapgef2, Myo6, Apba1, and Baz2b), while Macf1, Cacnb1, Ocrl, Atp9b, Mbnl2, Homer1, and Rbfox1 showed the opposite pattern of splicing. These findings suggest that SRRM4 and QKI may function together in cell types that express both proteins for optimal microexon AS regulation. Our findings show that microexons regulating GTPase activity are indeed functional, especially in microglia. A category of the Rho GTPase pathway was also identified in QKI-deficient microglia with altered transcript expression, and thus, we cannot rule out that QKI also regulates the steady-state levels of certain mRNAs of the Rho pathway in microglia.

Genes with misregulated microexons in QKI-deficient microglia are associated with mental retardation and epilepsy (Med23, Diaph1, Rbfox1, Ralgapa1, Cask, and Sptan1), deafness (Diaph1 and Myo6), and Huntington disease (Mbnl1 and Mbnl2). Moreover, alternatively spliced genes that were not microexons were associated with AD (Picalm, Bin1, Cacnb1, and Apba1). Given the multifaceted function of microglia in CNS, QKI-deficient microglia might impact a whole spectrum of CNS diseases by misregulating the microexon and longer exon AS.

Our study also identified targets of QKI that are known to impact the Rho GTPase pathway (Arhgap32, Arhgef11, Diaph1, Clip1, Diaph2, Fmnl2, Incenp, Abi1, Ocrl, Arhgap17, Myo9b, Clasp2, and Ktn1). Most of the splicing events of these transcripts caused the insertion of extra amino acids without disrupting overall protein domains, thereby forming new protein isoforms consistent with spliced isoforms having altered interface domains (Irimia et al., 2014). Of particular interest, exon skipping of Myo9b introduced a premature stop codon. Notably, the deletion of macrophage Myo9b results in amoeboid-like morphology, activating the Rock2 pathway and reducing migration capabilities upon chemoattractant stimuli (Hanley et al., 2010).

QKI-depleted microglia exhibited altered morphology with increased p-Mlc and p-Cofilin, well-known substrates of the Rock2 signaling pathway. Activation of the Rock2 pathway has been shown to enhance microglia cells toward the proinflammatory phenotype (Roser et al., 2017). Similarly, our cytokine array showed an increase in proinflammatory molecules (IL-6, CCL22, and CCL5). The Rock kinase inhibitor treatment Y-27632 reverted part of this phenotype. Additionally, during the CPZ, we treated qkI^{FL} and $qkI^{Cx3cr1-KO}$ mice with the Rock inhibitor Y-27632 or DMSO. Unfortunately, we did not observe significant remyelination changes in $qkI^{Cx3cr1-KO}$ mice treated with Y-27632 (data not shown). However, active RhoA GTP was observed in microglia isolated from wild-type qkI^{FL} mice fed with CPZ (Figure S7G), indicating that the CPZ per se did not affect AS of Myo9b, Diaph1, Ocrl, Arhgap17, Clasp2, and Arhgap32. As QKI is a significant regulator of AS and mRNA expression in microglia, it may not be entirely surprising that inhibiting one effector of RhoA, i.e., Rock kinases, would enhance such a complex process such as remyelination. However, RhoA activation in microglia seems crucial. Previous research reported that the RhoA expression is increased in reactive macrophages and microglia in the experimental autoimmune encephalomyelitis (EAE) model, and it was shown to be associated with MS lesions (Zhang et al., 2008). Furthermore, genetic ablation of RhoA in microglia causes aberrant microglia morphology with increased cytokine production, causing neuronal cell death (Socodato et al., 2020).

Our findings have important implications for understanding the role of Rho GTPases microglia proliferation and phagocytic function. In our differential gene expression analysis, we found an increased expression of proliferation-related transcripts known to be modulated by the Rho GTPase pathway (Aurkb, Birc5, Bub1, Cdc20, and Diaph3). There are a plethora of research papers that delineated how the Rho GTPase pathway coordinates cell cycle progression. For

instance, Rho GTPases influence the cyclin D1 transcription and translation and thus mediates the cell cycle progression (David et al., 2012). Using an in vitro phagocytosis assay, we found that the QKI-deficient microglia were defective in digesting engulfed particles and showed an engorged microglia phenotype, as observed with Rag-Ragulator null microglia (Shen et al., 2016), suggesting that QKI-deficient microglia might impact the phagosome maturation process. The role of Rho GTPase has been linked to phagocytosis (Caron and Hall, 1998), suggesting QKI may regulate phagocytosis functions by Rho GTPase.

In several CNS medical conditions such as schizophrenia, MS, AD, and cancer, the expression of QKI is downregulated (Darbelli and Richard, 2016). However, deregulated expression of QKI in microglia affecting CNS disease progression is unprecedented. Using the CPZ mouse model, we found that inhibition of QKI significantly impacted the remyelination abilities in the CNS. The remyelination process requires an adaptive microglia role: engulfing myelin debris and secreting neurotrophic factors that aid OPCs to differentiate into myelinating oligodendrocytes (Lloyd and Miron, 2019). Based on our immunofluorescence data, we show that OPCs in $qkI^{Cx3cr1-KO}$ mice were subjected to apoptosis. The apoptotic body of OPCs triggered the phagocytic activity of microglia, which were detected by staining with an anti-Mac2 antibody. Likewise, we observed phagocytic microglia (Mac2+) co-localizing with the OPCs in $qkI^{Cx3cr1-KO}$ mice during remyelination. Moreover, we also noticed enhanced astrogliosis (GFAP+) during remyelination in $qkI^{Cx3cr1-KO}$ mice. These findings were consistent with astrocytes being highly sensitive to the microenvironment stimuli that cross-talk with microglia and/or OPCs (Baaklini et al., 2019). It is still unclear, however, what drives the OPCs to undergo apoptosis in $qkI^{Cx3cr1-KO}$ mice. One possible explanation is that the absence of QKI might deplete a specific sub-population

of microglia crucial for growth factor release to permit OPC survival, proliferation, and differentiation (Masuda et al., 2020).

In summary, our work here provides an important understanding of the regulation of microglial activity in the brain. We have identified QKI as a regulator of microexon AS of the Rho GTPase pathway in microglia. Mice with QKI-deficient microglia had morphological changes with proinflammatory properties and phagocytosis processing defects that hinder CNS remyelination when we used the cuprizone model of myelin pathology. Finally, the QKI-5 expression is reduced in microglia of MS patient brain tissue samples.

2.6 Methods

2.6.1 Animals

All mouse procedures were performed following McGill University guidelines, set by the Canadian Council on Animal Care. Mice were acclimated to the laboratory condition following 12-hour light/dark cycle and 22-24˚C temperature and free access to food and water. Conditional *qkI* knockout mice maintained on a C57BL/6 background were generated previously (Darbelli et al., 2016), where two loxP sites flank exon 2 of the *qkI* gene (qkI^{FL}). These mice were crossed with transgenic mice expressing C57BL/6 mice expressing CreERT2 recombinase under *Cx3cr1* promoter (Jackson lab # 021160) to generate $qkI^{Cx3cr1-KO}$ mice. For the induction of Cre recombinase activity, a solution of tamoxifen (TAM, T5648, Millipore-Sigma, Burlington, MA) dissolved in corn oil (C8267, Millipore-Sigma) was injected intraperitoneally in 5-6 week old mice once daily for 5 consecutive days with a concentration of 1mg/ml. For all experiments, sex-and age-matched mixed populations of males and females were used for each genotype.

2.6.2 Patient tissues

Human brain tissue was obtained from patients diagnosed with clinical and neuropathological MS diagnosis according to the revised 2010 McDonald's criteria (Polman et al., 2011). Tissue samples were collected from healthy donors and MS patients with full ethical approval (BH07.001) and informed consent as approved by the local ethics committee (Table S3). Autopsy samples were preserved and lesions were classified using Luxol Fast Blue/Hematoxylin & Eosin staining as previously published (Dhaeze et al., 2019; Kuhlmann et al., 2017). The age and sex of the human samples are described in Table S3.

2.6.3 Microglia isolation

Mice were deeply anesthetized using isoflurane and transcardially perfused with ice-cold phosphate-buffered saline (PBS). The brains were carefully removed from the skulls and placed in 1X HBSS buffer containing 1% BSA and 1mM EDTA. According to the manufacturer's instructions, brains were minced using a scalpel and dissociated using a neural tissue dissociation kit (Miltenyi Biotec Inc). Debris was then removed by resuspending in 10 mL of 30% percoll (Millipore-Sigma) to the cell pellet and spun for 20 min at 600xg at room temperature (RT), Accel 5, Decel 1. The supernatant was discarded, and cells were filtered through 70 μm cell strainer to remove clumps and washed twice with 1X HBSS buffer. Cells were then resuspended in FACS buffer (0.5% BSA, 2 mM EDTA in PBS) for further flow cytometry analysis.

2.6.4 Flow cytometry

Isolated cells were Fc- blocked with anti-CD16/32 (1:200, BD Biosciences) to avoid unspecific antibody binding. Cells were then stained with anti-CD11b APC (1:200, BioLegend), and anti-CD45 BV786 (1:200, BD Biosciences) for 30 min at 4 °C in the dark. Stained cells were washed with PBS, and subsequently stained with pre-titrated LIVE/DEAD™ Fixable Aqua Dead Cell

Stain (1:500, Invitrogen) for 20 min. CDllb$^+$CD45^{inter} microglia were sorted using a FACSAria Fusion (BD Bioscience). To assess the proliferative capacity of CDllb$^+$CD45^{inter} microglia, cells were fixed and permeabilized using Cytofix/Cytoperm TM Plus kit (BD Biosciences) and subsequently stained with anti-Ki-67 PE (1:200, BioLegend). Flow cytometry analysis of Ki-67 was performed on the FACSAria Fusion. Data was analyzed with FlowJo software (Tree Star).

2.6.5 Cuprizone diet

Two weeks after the tamoxifen injection, *qkI^{FL}* and *qkI$^{Cx3cr1-KO}$* mice were fed ad libitum a powdered standard diet (Envigo Teklad) containing 0.2% cuprizone (Millipore-Sigma) for every two days for five weeks (Lampron et al., 2015). For the remyelination experiments, mice were then fed with standard chow for 1, 2 and 3 weeks after the 5 weeks cuprizone diet. The weight of each mouse was monitored every three days.

2.6.6 Immunohistochemical analysis for in vivo brain section

Mice were anesthetized using isoflurane followed by transcardial perfusion with PBS and 4% paraformaldehyde (PFA). Brains were removed to postfix in 4% PFA for 24 h and incubated in graded sucrose in PBS (10%, 20%, 30%) for 24 h each. After the sucrose infiltration, brains were rapidly frozen in a mixture of dry ice and isopentane and embedded in OCT compound (Fisherbrand), and cut into 12 μm sections with a cryostat (Leitz Camera). Sections were mounted onto Superfrost (+) slides (Fisherbrand). For immunofluorescent staining, sections were blocked with PBS containing 5% bovine serum albumin and 0.3% Triton X-100 for 1h. The following primary antibodies were used overnight at 4°C: Iba-1 (1:200, WAKO), anti-GFAP (1:300, Abcam), anti-Olig2 (1:200, Novus Biologicals), anti-PDGFRα (1:100, Cell signaling Technology), anti-NeuN(1:300, Abcam), anti-cleaved caspase3 (1:100, Cell signaling Technology Inc), anti-QKI (1:200, Neuromab), anti-MBP (1:300, Abcam), and anti-Mac2 (1:200, Cedarlane) antibodies.

Secondary antibodies were added as follows: Alexa Fluor 488 (1:200, Invitrogen) and Alexa Fluor 568 (1:200, Invitrogen). Nuclei were counterstained with DAPI for 30 sec and mounted. The presence of myelin was analyzed by mounting the sections with distilled water for 3 min and stained with the Black Gold II staining kit (Millipore, Temecula) according to the manufacture's instruction. Images were taken with an LSM880 confocal microscope or Zeiss Axio Imager M1 microscope (Carl Zeiss, Thornwood, NY). For quantification of Iba-1 positive cells, at least three images were taken (500 mm x500 mm) at cortex, hippocampus, and corpus callosum of each animal. Anti-Iba-1, -GFAP, and -Mac2 antibodies and black-gold II staining intensity during the cuprizone diet experiment were quantified by IMARIS program (Bitplane). Counting the Anti-Olig2, -PDGFRα, -Mac2 and -GFAP positive cells were performed utilizing IMARIS software. Analyzing the QKI immunofluorescent intensity for Olig2+, GFAP+, and Iba-1+ cells was performed using Zen Zeiss software.

2.6.7 3D reconstruction of microglia

Free-floating 30 μm cryosections from qkI^{FL} and $qkI^{Cx3cr1-KO}$ mouse brain tissues were stained with primary antibodies at 4°C overnight. The secondary antibody Alexa Fluor 488 was

incubated at RT for 2h and counterstained with DAPI. Confocal images were taken using LSM880 Zeiss microscope with an x40 oil immersion objective. Z-stacks with 1μm interval images were taken at a depth of 20 μm. Images were further analyzed using IMARIS software as previously described.

2.6.8 RNA-seq

RNA-seq was performed on FACS sorted CDllb$^+$CD45^{inter} microglia cells from qkI^{FL} and $qkI^{Cx3cr1-KO}$ mice. At least 6 mice were pooled together to generate one replicate sample, yielding around 1 million microglia cells/ sample. This procedure was repeated three times to obtain three replicates.

FACS sorted cells were spun and RNA extracted using the PicoPure RNA extraction kit (Applied Biosystems) according to the manufacture's protocol. Total RNA was assessed for quality using an Agilent Tapestation 4200, and RNA sequencing libraries were generated using TruSeq Stranded mRNA Sample Prep Kit with TruSeq Unique Dual Indexes (Illumina). Samples were processed following the manufacturer's instructions, starting with 50 ng of RNA and modifying RNA shear time to 5 min. The resulting libraries were multiplexed and sequenced with 100 base pair (bp) paired-end reads (PE100) to a depth of ~60 million reads per sample on an Illumina HiSeq 4000. Samples were demultiplexed using bcl2fastq v2.20 Conversion Software (Illumina).

2.6.9 RNA isolation, cDNA synthesis, RT-qPCR analysis, and polyacrylamide gel electrophoresis

Total RNA of microglia was extracted using TRIzol (Invitrogen), as previously described. cDNA synthesis was performed using M-MLV reverse transcriptase (Promega). A total of 10 ng of cDNA with targeted primers were used with PowerUp SYBR Mastermix (Life Technologies), and applied on 7500 Fast Real-Time PCR System (Applied biosystem). mRNA expression was determined using ΔΔCT method, and was normalized to *Gapdh* mRNA levels. For splicing assay forward, and reverse primers detecting targeted exons were designed, and RT-PCR reaction was performed with cDNA. The resulting products were separated on a TBE-based polyacrylamide gel electrophoresis (PAGE), and stained with ethidium bromide. All PCR reactions were performed in triplicates. The percentage sliced in (PSI) values was calculated for each condition using Image J software. The primers used in this study are listed in Table S4.

2.7.0 Protein extraction and immunoblotting

FACS-sorted microglia cells were lysed with 2X Laemmli buffer and sonicated. Protein extracts were separated by SDS-PAGE, transferred to nitrocellulose membranes using an immunoblot

TurboTransfer system (Bio-Rad). Membranes were blotted with 5% skim milk for 1h at RT and incubated with primary antibody followed by appropriate horse radish peroxidase (HRP)-conjugated secondary antibodies for 1h each at RT. Chemiluminescence signals were achieved by SuperSignal West-Dura® Extended Duration Substrate (ThermoFisher Scientific) for HRP.

2.7.1 Cell culture, drug treatment, cytokine array, phagocytosis assay and immunofluorescent analysis

Isolated microglia cells from adult qkI^{FL} and $qkI^{Cx3cr1-KO}$ mice were seeded on pre-coated poly-D-lysine (Millipore-Sigma) dishes and maintained in DMEM/F12 (Invitrogen) supplemented with 10% FBS, 100 U/ml penicillin,100 μg/ml streptomycin, mouse recombinant MCSF 10 ng/ml (PeproTech) and 50 ng/ml human recombinant TGFβ1 (Peprotech) to better mimic *in vivo* conditions (IButovsky et al., 2014). After 24h, the media were removed, and cells were treated with 1 μM of Rock inhibitor (Y-27632, Cayman Chemical) or DMSO for 3h. For cytokine array, 5×10^5 cells were seeded on a 96 well plate coated with poly D-lysine. After 72h, the supernatant was collected, and protein array was performed using Mouse Cytokine Array / Chemokine Array 44-Plex (MD44) (Eve technologies). Experiments were repeated at least two independent times. For *in vitro* phagocytosis assays, cells were maintained in 0.1% serum for at least 3hr and treated with pH-rhodo zymosan particle for 15 min. Immunofluorescence analysis for active RhoA, phalloidin, p(Thr18/Ser19)-Mlc, and p(Ser3)-Cofilin, were performed by serum starving microglia for 6 hr and fixing the cells with 4% PFA. Cells were then permeabilized with PBS containing 0.3% Triton X-100 for 15 min. Slides were then subjected to blocking with 5% BSA, and primary antibodies for active RhoA (1:200, NewEast Biosciences), p-Mlc (1:200, Cell signaling) and p-Cofilin (1:200, Cell signaling) were treated overnight at 4°C. The next day, slides were washed and treated with Alexa Fluor™ 594 Phalloidin (1:200, Thermo Fisher) and Alexa Fluor secondary

antibodies for 1h at RT. Slides were washed and stained with DAPI. The images were taken using a Zeiss Axio Imager M1 Microscope and LSM880 Zeiss microscope. Images were analyzed using IMARIS software.

2.7.2 RhoA Activation G-LISA Assay

The RhoA G-LISA kit (Cytoskeleton) was purchased to monitor the activation of RhoA GTPase and the assay was performed following the manufacturer's guidelines. Briefly, microglia were FACs sorted and lysed in ice-cold lysis buffer provided by in the kit. Protein concentration was quantified and additional lysis buffer was added to each sample to achieve equal protein concentration. Lysates were immediately used for colorimetric G-LISA assays according to the manufacturer's protocol.

2.7.3 RNA-seq analysis

Paired-end reads of length 100 nucleotides (nt) were first trimmed through Trimmomatic v0.39 to remove Illumina adapter sequences. STAR v2.7.1a was then used to align the reads to the mouse genome (mm10/GRCm38) using the Gencode vM23 gene annotations. Gene expression was quantified across all samples with HOMER v4.11.1, and the normalization was carried out through the regularized logarithm (rlog) transformation of DESeq2 v1.26.0 (Heinz et al., 2010; Love et al., 2014). Gene expression hierarchical clustering with average linkage was performed using Gene Cluster 3.0 after removing genes where none of the samples has more than 25 normalized reads in the gene or where the samples with highest and lowest expression is less than 2-fold different, as well as subtracting the mean values of the gene from each sample (de Hoon et al., 2004). Clustering results were exported with Java TreeView v1.16r4 (Saldanha, 2004), and the functional enrichment tests were performed through DAVID v6.8 and visualized as a heatmap with the ComplexHeatmap R package (Gu et al., 2016; Huang et al., 2009). Differential expression between the control and

treatment samples was calculated through DESeq2 v1.26.0, and the gene expression was considered significantly different if the absolute value of the log-fold-change (LFC) was higher than 2, the base means larger than 10 and the false discovery rate (FDR) less than 0.05. Pathway enrichment analysis of differentially expressed genes was performed with Enrichr (Chen et al., 2013; Kuleshov et al., 2016).

2.7.4 Splicing analysis

Alternative splicing (AS) events between qkI^{FL} and $qkI^{Cx3cr1-KO}$ microglia were quantified through rMATS v4.0.2 with default settings (Shen et al., 2014) and Gencode vM23 gene annotations (Frankish et al., 2019) using the untrimmed paired-end reads of length 101nt which were further filtered to have a false discovery rate (FDR) smaller than 0.05 as well as an inclusion level difference of 0.4. The relative abundance (PSI) of local splicing variations (LSV) were then quantified with MAJIQ v2.1 (Vaquero-Garcia et al., 2016) with default settings and the gene annotation files provided by the authors in the documentation. The LSVs were filtered to have a relative abundance between the control and treatment samples larger than 0.2, with a probability of 95%. The expression levels of skipped exons, alternative 3' / 5' splice sites, retained introns and alternative first / last exons was also quantified in the form of percent spliced in (Psi) values through the MISO model. Differentially expressed events identified by MISO were filtered to contain at least 1 inclusion read, 1 exclusion read, 10 inclusion + exclusion reads, at least 0.2 difference in Psi values and a Bayes factor larger than 10. The exon skipping events from the three splicing pipelines were used and each splicing event was validated using IGV. For each exon skipping or inclusion event, we searched on the same strand of the genome sequence (mm10/GRCm38) for the QRE half-site or full-site motifs within a window of 200nt located at the introns on the vicinity upstream or downstream of the exon. The QKI response element (QRE)

consists of a core sequence NACUAAY (Y is a pyridine) and a half-site UAAY located between 1- 20 nt apart from each other (Galarneau and Richard, 2005a).

2.7.5 Human MS tissue samples Immunohistochemical analysis

Tissue containing slides were removed from -80°C and thawed for 20-30 min at RT. Subsequently, slides were immersed in 100% acetone for 10 min and 75% ethanol for 5 min at 20°C. Afterward, slides were washed in 1X PBS for 3 min in RT, and sections were marked using PAP-pen (Dako). Blocking was performed using 10% serum and incubated with anti-QKI-5 antibody (1:100, Millipore-Sigma) and -Iba-1 antibodies (1:100, Millipore-Sigma) overnight at 4°C. The next day, sections were washed three times with PBS-T and subjected to Alexa Fluor conjugated antibodies (1:100) for 1h. After the incubation, 1% Triton-X100 was applied for 10 min and rewashed. Slides were stained with DAPI and mounted. Images were taken using Zeiss Axio Imager M1 microscope (Carl Zeiss), and at least 10 images were taken in high power field for individual samples. The mean fluorescence intensity was calculated using IMARIS software.

2.7.6 Quantification and statistical analysis

All data were statistically tested using GraphPad Prism 6. Error-values are expressed as means ± standard error of the mean (SEM). The specific tests used for the analysis are described in the Figure legends. The number of animals and experimental replicates is indicated in the Figure legends. No outliers were excluded in the experiments and the samples were not blinded. Data collection was randomized for all experiments. We used the Mann-Whiteny Test, multiple t-tests, and one-way ANOVA with different corrections depending on the experiments to compare groups.

2.8 References

Aberg, K., Saetre, P., Jareborg, N., and Jazin, E. (2006). Human QKI, a potential regulator of mRNA expression of human oligodendrocyte-related genes involved in schizophrenia. Proc Natl Acad Sci U S A *103*, 7482-7487.

Anwar, K.N., Fazal, F., Malik, A.B., and Rahman, A. (2004). RhoA/Rho-associated kinase pathway selectively regulates thrombin-induced intercellular adhesion molecule-1 expression in endothelial cells via activation of I kappa B kinase beta and phosphorylation of RelA/p65. J Immunol *173*, 6965-6972.

Baaklini, C.S., Rawji, K.S., Duncan, G.J., Ho, M.F.S., and Plemel, J.R. (2019). Central Nervous System Remyelination: Roles of Glia and Innate Immune Cells. Front Mol Neurosci *12*, 225.

Butovsky, O., and Weiner, H.L. (2018). Microglial signatures and their role in health and disease. Nat Rev Neurosci *19*, 622-635.

Caron, E., and Hall, A. (1998). Identification of two distinct mechanisms of phagocytosis controlled by different Rho GTPases. Science *282*, 1717-1721.

Chen, E.Y., Tan, C.M., Kou, Y., Duan, Q., Wang, Z., Meirelles, G.V., Clark, N.R., and Ma'ayan, A. (2013). Enrichr: interactive and collaborative HTML5 gene list enrichment analysis tool. . BMC Bioinformatics *14*, 128.

Cooper, T.A., Wan, L., and Dreyfuss, G. (2009). RNA and disease. Cell *136*, 777-793.

Corley, M., Burns, M.C., and Yeo, G.W. (2020). How RNA-Binding Proteins Interact with RNA: Molecules and Mechanisms. Mol Cell *78*, 9-29.

Darbelli, L., Choquet, K., Richard, S., and Kleinman, C.L. (2017). Transcriptome profiling of mouse brains with qkI-deficient oligodendrocytes reveals major alternative splicing defects including self-splicing. Scientific reports *7*, 7554.

Darbelli, L., and Richard, S. (2016). Emerging functions of the Quaking RNA-binding proteins and link to human diseases. Wiley Interdiscip Rev RNA *14*, doi: 10.1002/wrna.1344.

Darbelli, L., Vogel, G., Almazan, G., and Richard, S. (2016). Quaking Regulates Neurofascin 155 Expression for Myelin and Axoglial Junction Maintenance. J Neurosci *36*, 4106-4120.

David, M., Petit, D., and Bertoglio, J. (2012). Cell cycle regulation of Rho signaling pathways. Cell Cycle *11*, 3003-3010.

de Bruin, R.G., Shiue, L., Prins, J., H.C., d.B., Singh, A., Fagg, W.S., van Gils, J.M., Duijs, J.M., Katzman, S., Kraaijeveld, A.O.*, et al.* (2016). Quaking promotes monocyte differentiation into pro-atherogenic macrophages by controlling pre-mRNA splicing and gene expression. Nat Commun *7*, 10846.

de Hoon, M.J., Imoto, S., Nolan, J., and Miyano, S. (2004). Open Source Clustering Software. . Bioinformatics *20*, 1453-1454.

Deczkowska, A., Keren-Shaul, H., Weiner, A., Colonna, M., Schwartz, M., and Amit, I. (2018). Disease-Associated Microglia: A Universal Immune Sensor of Neurodegeneration. Cell *173*, 1073-1081.

Dhaeze, T., Tremblay, L., Lachance, C., Peelen, E., Zandee, S., Grasmuck, C., Bourbonniere, L., Larouche, S., Ayrignac, X., Rebillard, R.M.*, et al.* (2019). CD70 defines a subset of proinflammatory and CNS-pathogenic TH1/TH17 lymphocytes and is overexpressed in multiple sclerosis. Cell Mol Immunol *16*, 652-665.

Fani Maleki, A., and Rivest, S. (2019). Innate Immune Cells: Monocytes, Monocyte-Derived Macrophages and Microglia as Therapeutic Targets for Alzheimer's Disease and Multiple Sclerosis. Front Cell Neurosci *13*, 355.

Farnsworth, B., Peuckert, C., Zimmermann, B., Jazin, E., Kettunen, P., and Emilsson, L.S. (2016). Gene Expression of Quaking in Sporadic Alzheimer's Disease Patients is Both Upregulated and Related to Expression Levels of Genes Involved in Amyloid Plaque and Neurofibrillary Tangle Formation. J Alzheimers Dis *53*, 209-219.

Frankish, A., Diekhans, M., Ferreira, A.M., Johnson, R., Jungreis, I., and et al. (2019). GENCODE reference annotation for the human and mouse genomes. . Nucleic acids research *47*, D766-773.

Galarneau, A., and Richard, S. (2005). Target RNA motif and target mRNAs of the Quaking STAR protein. Nat Struct Mol Biol *12*, 691-698.

Goldmann, T., Wieghofer, P., Muller, P.F., Wolf, Y., Varol, D., Yona, S., Brendecke, S.M., Kierdorf, K., Staszewski, O., Datta, M.*, et al.* (2013). A new type of microglia gene targeting shows TAK1 to be pivotal in CNS autoimmune inflammation. Nat Neurosci *16*, 1618-1626.

Gomez Perdiguero, E., Schulz, C., and Geissmann, F. (2013). Development and homeostasis of "resident" myeloid cells: the case of the microglia. Glia *61*, 112-120.

Gonatopoulos-Pournatzis, T., Niibori, R., Salter, E.W., Weatheritt, R.J., Tsang, B., and al., e. (2020). Autism-Misregulated eIF4G Microexons Control Synaptic Translation and Higher Order Cognitive Functions. Mol Cell *77*, 1176-1192.

Gosselin, D., Link, V.M., Romanoski, C.E., Fonseca, G.J., Eichenfield, D.Z., Spann, N.J., Stender, J.D., Chun, H.B., Garner, H., Geissmann, F.*, et al.* (2014). Environment drives selection and function of enhancers controlling tissue-specific macrophage identities. Cell *159*, 1327-1340.

Gu, Z., Eils, R., and Schlesner, M. (2016). Complex heatmaps reveal patterns and correlations in multidimensional genomic data. Bioinformatics *18*, 2847-2849.

Gudi, V., Moharregh-Khiabani, D., Skripuletz, T., Koutsoudaki, P.N., Kotsiari, A., Skuljec, J., Trebst, C., and Stangel, M. (2009). Regional differences between grey and white matter in cuprizone induced demyelination. Brain Res *1283*, 127-388.

Hall, M.P., Nagel, R.J., Fagg, W.S., Shiue, L., Cline, M.S., Perriman, R.J., Donohue, J.P., and Ares, M.J. (2013). Quaking and PTB control overlapping splicing regulatory networks during muscle cell differentiation. RNA (New York, NY) *19*, 627-638.

Hammond, T.R., Dufort, C., Dissing-Olesen, L., Giera, S., Young, A., Wysoker, A., and Walker, A.J. (2019). Single-Cell RNA Sequencing of Microglia throughout the Mouse Lifespan and in the Injured Brain Reveals Complex Cell-State Changes. Immunity *50*, 253-271.

Hanley, P.J., Xu, Y., Kronlage, M., Grobe, K., Schon, P., Song, J., Sorokin, L., Schwab, A., and Bahler, M. (2010). Motorized RhoGAP myosin IXb (Myo9b) controls cell shape and motility. Proc Natl Acad Sci U S A *107*, 12145-12150.

Heinz, S., Benner, C., Spann, N., Bertolino, E., and al., e. (2010). Simple Combinations of Lineage-Determining Transcription Factors Prime cis-Regulatory Elements Required for Macrophage and B Cell Identities. . Mol Cell *38*, 576-589.

Huang, D., Sherman, B., and Lempicki, R. (2009). Systematic and integrative analysis of large gene lists using DAVID bioinformatics resources. Nat Protoc *4*, 44-57.

IButovsky, O., Jedrychowski, M.P., Moore, C.S., Cialic, R., Lanser, A.J., and al., e. (2014). Identification of a unique TGF-β-dependent molecular and functional signature in microglia. Nat Neurosci *17*, 131-143.

Irimia, M., Weatheritt, R.J., Ellis, J.D., Parikshak, N.N., Gonatopoulos-Pournatzis, T., Babor, M., and al., e. (2014). A highly conserved program of neuronal microexons is misregulated in autistic brains. Cell *159*, 1511-1523.

Itoh, M., Tsukita, S., Yamazaki, Y., and Sugimoto, H. (2012). Rho GTP exchange factor ARHGEF11 regulates the integrity of epithelial junctions by connecting ZO-1 and RhoA-myosin II signaling. Proc Natl Acad Sci U S A *109*, 9905-9910.

Kapellos, T.S., Taylor, L., Lee, H., Cowley, S.A., James, W.S., Iqbal, A.J., and Greaves, D.R. (2016). A novel real time imaging platform to quantify macrophage phagocytosis. Biochem Pharmacol *116*, 107-119.

Keren-Shaul, H., Spinrad, A., Weiner, A., Matcovitch-Natan, O., Dvir-Szternfeld, R., Ulland, T.K., David, E., and al., e. (2017). A Unique Microglia Type Associated with Restricting Development of Alzheimer's Disease. Cell *169*, 1276-1290.

Kitzing, T.M., Sahadevan, A.S., Brandt, D.T., Knieling, H., Hannemann, S., Fackler, O.T., Grosshans, J., and Grosse, R. (2007). Positive feedback between Dia1, LARG, and RhoA regulates cell morphology and invasion. Genes Dev *21*, 1478-1483.

Krasemann, S., Madore, C., Cialic, R., Baufeld, C., Calcagno, N., El Fatimy, R., and al., e. (2017). The TREM2-APOE Pathway Drives the Transcriptional Phenotype of Dysfunctional Microglia in Neurodegenerative Diseases. Immunity *47*, 566-581.

Kuhlmann, T., Ludwin, S., Prat, A., Antel, J., Bruck, W., and Lassmann, H. (2017). An updated histological classification system for multiple sclerosis lesions. Acta Neuropathol *133*, 13-24.

Kuleshov, M.V., Jones, M.R., Rouillard, A.D., Fernandez, N.F., Duan, Q., and al., e. (2016). Enrichr: a comprehensive gene set enrichment analysis web server 2016 update. Nucleic acids research *44*, W90-97.

Lampron, A., Larochelle, A., Laflamme, N., Préfontaine, P., Plante, M.M., Sánchez, M.G., Yong, V.W., Stys, P.K., Tremblay, M.È., and Rivest, S. (2015). Inefficient clearance of myelin debris by microglia impairs remyelinating processes. J Exp Med *212*, 481-495.

Lavon, I., Leykin, I., Charbit, H., Binyamin, O., Brill, L., Ovadia, H., and Vaknin-Dembinsky, A. (2019). QKI-V5 is downregulated in CNS inflammatory demyelinating diseases. Mult Scler Relat Disord *39*, 101881.

Li, Y.I., Sanchez-Pulido, L., Haerty, W., and Ponting, C.P. (2015). RBFOX and PTBP1 proteins regulate the alternative splicing of micro-exons in human brain transcripts. Genome Res *25*, 1-13.

Lloyd, A.F., and Miron, V.E. (2019). The pro-remyelination properties of microglia in the central nervous system. Nat Rev Neurol *15*, 447-458.

Love, M.I., Huber, W., and Anders, S. (2014). Moderated estimation of fold change and dispersion for RNA-seq data with DESeq2. Genome Biol *15*, 550.

Lukong, K.E., Chang, K.W., Khandjian, E.W., and Richard, S. (2008). RNA-binding proteins in human genetic disease. Trends Genet *24*, 416-425.

Masaki, K., Sonobe, Y., Ghadge, G., Pytel, P., Lépine, P., and al, e. (2020). RNA-binding protein altered expression and mislocalization in MS. Neurol Neuroimmunol Neuroinflamm *7*, e704.

Masuda, T., Sankowski, R., Staszewski, O., and Prinz, M. (2020). Microglia Heterogeneity in the Single-Cell Era. Cell Rep *30*, 1271-1281.

Matsushima, G.K., and Morell, P. (2001). The neurotoxicant, cuprizone, as a model to study demyelination and remyelination in the central nervous system. Brain Pathol *11*, 107-116.

Pillman, K.A., Phillips, C.A., Roslan, S., Toubia, J., Dredge, B.K., Bert, A.G., Lumb, R., Neumann, D.P., Li, X., Conn, S.J.*, et al.* (2018). miR-200/375 control epithelial plasticity-associated alternative splicing by repressing the RNA-binding protein Quaking. EMBO J *37*.

Polman, C.H., Reingold, S.C., Banwell, B., Clanet, M., Cohen, J.A., Filippi, M., Fujihara, K., Havrdova, E., Hutchinson, M., Kappos, L., *et al.* (2011). Diagnostic criteria for multiple sclerosis: 2010 revisions to the McDonald criteria. Ann Neurol *69*, 292-302.

Qi, S., Perrino, S., Miao, X., Lamarche-Vane, N., and Brodt, P. (2020). The chemokine CCL7 regulates invadopodia maturation and MMP-9 mediated collagen degradation in liver-metastatic carcinoma cells. Cancer Lett *483*, 98-113.

Robinson, J.T., Thorvaldsdottir, H., Winckler, W., Guttman, M., Lander, E.S., Getz, G., and Mesirov, J.P. (2011). Integrative genomics viewer. Nat Biotechnol *29*, 24-26.

Roser, A.E., Tonges, L., and Lingor, P. (2017). Modulation of Microglial Activity by Rho-Kinase (ROCK) Inhibition as Therapeutic Strategy in Parkinson's Disease and Amyotrophic Lateral Sclerosis. Front Aging Neurosci *9*, 94.

Saldanha, A.J. (2004). Java Treeview—extensible visualization of microarray data. . Bioinformatics *20*, 3246-3248.

Salter, M.W., and Stevens, B. (2017). Microglia emerge as central players in brain disease. Nat Med *23*, 1018-1027.

Shen, K., Sidik, H., and Talbot, W.S. (2016). The Rag-Ragulator Complex Regulates Lysosome Function and Phagocytic Flux in Microglia. Cell Rep *14*, 547-559.

Shen, S., Park, J.W., Lu, Z.X., Lin, L., Henry, M.D., Wu, Y.N., Zhou, Q., and Xing, Y. (2014). rMATS: robust and flexible detection of differential alternative splicing from replicate RNA-Seq data. Proceedings of the National Academy of Sciences of the United States of America *111*, E5593-5601.

Shingu, T., Ho, A.L., Yuan, L., Zhou, X., Dai, C., Zheng, S., Wang, Q., Zhong, Y., Chang, Q., Horner, J.W., *et al.* (2017). Qki deficiency maintains stemness of glioma stem cells in suboptimal environment by downregulating endolysosomal degradation. Nat Genet *49*, 75-86.

Socodato, R., Portugal, C.C., Canedo, T., Rodrigues, A., Almeida, T.O., Henriques, J.F., Vaz, S.H., Magalhaes, J., Silva, C.M., Baptista, F.I., *et al.* (2020). Microglia Dysfunction Caused by the Loss of Rhoa Disrupts Neuronal Physiology and Leads to Neurodegeneration. Cell Rep *31*, 107796.

Song, W.M., and Colonna, M. (2018). The identity and function of microglia in neurodegeneration. Nat Immunol *19*, 1048-1058.

Tonges, L., Koch, J.C., Bahr, M., and Lingor, P. (2011). ROCKing Regeneration: Rho Kinase Inhibition as Molecular Target for Neurorestoration. Front Mol Neurosci *4*, 39.

Ule, J., and Blencowe, B.J. (2019). Alternative Splicing Regulatory Networks: Functions, Mechanisms, and Evolution. Mol Cell *76*, 329-345.

van der Veer, E.P., de Bruin, R.G., Kraaijeveld, A.O., and al., e. (2013). Quaking, an RNA-binding protein, is a critical regulator of vascular smooth muscle cell phenotype. Circ Res *113*, 1065-1075.

Vaquero-Garcia, J., Barrera, A., Gazzara, M.R., González-Vallinas, J., Lahens, N.F., Hogenesch, J.B., Lynch, K.W., and Barash, Y. (2016). A new view of transcriptome complexity and regulation through the lens of local splicing variations. Elife *5*, e11752.

Yokoo, H., Nobusawa, S., Takebayashi, H., Ikenaka, K., Isoda, K., Kamiya, M., Sasaki, A., Hirato, J., and Nakazato, Y. (2004). Anti-human Olig2 antibody as a useful immunohistochemical marker of normal oligodendrocytes and gliomas. Am J Pathol *164*, 1717-1725.

Zhang, Y., Chen, K., Sloan, S.A., Bennett, M.L., Scholze, A.R., O'Keeffe, S., Phatnani, H.P., Guarnieri, P., Caneda, C., Ruderisch, N., *et al.* (2014). An RNA-sequencing transcriptome

and splicing database of glia, neurons, and vascular cells of the cerebral cortex. J Neurosci *34*, 11929-11947.

Zhang, Z., Schittenhelm, J., Meyermann, R., and Schluesener, H.J. (2008). Lesional accumulation of RhoA(+) cells in brains of experimental autoimmune encephalomyelitis and multiple sclerosis. Neuropathol Appl Neurobiol *34*, 231-240.

Zong, F.Y., Fu, X., Wei, W.J., Luo, Y.G., Heiner, M., Cao, L.J., Fang, Z., Fang, R., Lu, D., Ji, H.*, et al.* (2014). The RNA-binding protein QKI suppresses cancer-associated aberrant splicing. PLoS Genet *10*, e1004289.

2.9 Supplemental information
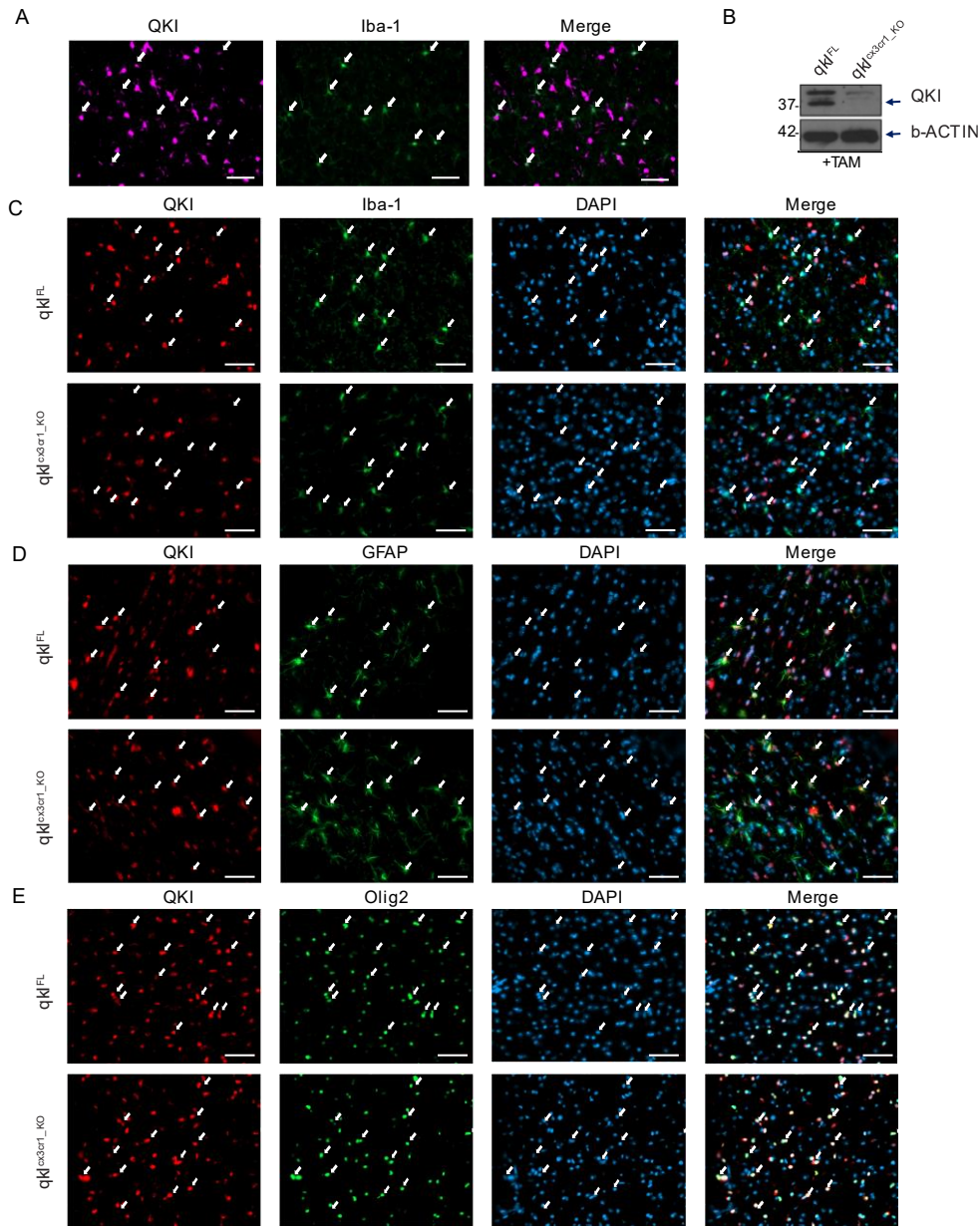
Figure S1 Loss of QKI expression in microglia of TAM-treated qkI^{FL} and $qkI^{Cx3cr1-KO}$ mice. Related to Figure 1. A, Immunofluorescence staining of QKI, and Iba-1 in cortices of control mice brain. The white arrow indicates the Iba-1 positive cells. Scale bar represents 20 μm. **B**, Ten days post-TAM injection, three of qkI^{FL} and $qkI^{Cx3cr1-KO}$ mice were deeply anesthetized then perfused with ice-cold PBS to isolate microglia and pooled together. Protein expression of QKI was examined using western blot analysis in TAM-treated qkI^{FL} and $qkI^{Cx3cr1-KO}$ microglia. **C**, Immunofluorescence staining of QKI, and Iba-1 in TAM injected qkI^{FL} and $qkI^{Cx3cr1-KO}$ cortices. The white arrow indicates the Iba-1 positive cells. Scale bar represents 20 μm. **D**, Immunofluorescence staining of QKI, and GFAP in the cortex of TAM injected mice with the following genotypes qkI^{FL} and $qkI^{Cx3cr1-KO}$. The white arrow indicates the GFAP positive cells. Scale bar represents 20 μm. **E**, Immunofluorescence staining of QKI, and Olig2 in TAM injected $qkI^{Cx3cr1-KO}$ and qkI^{FL} cortices. The white arrow indicates the Olig2 positive cells. Scale bar represents 20 μm.
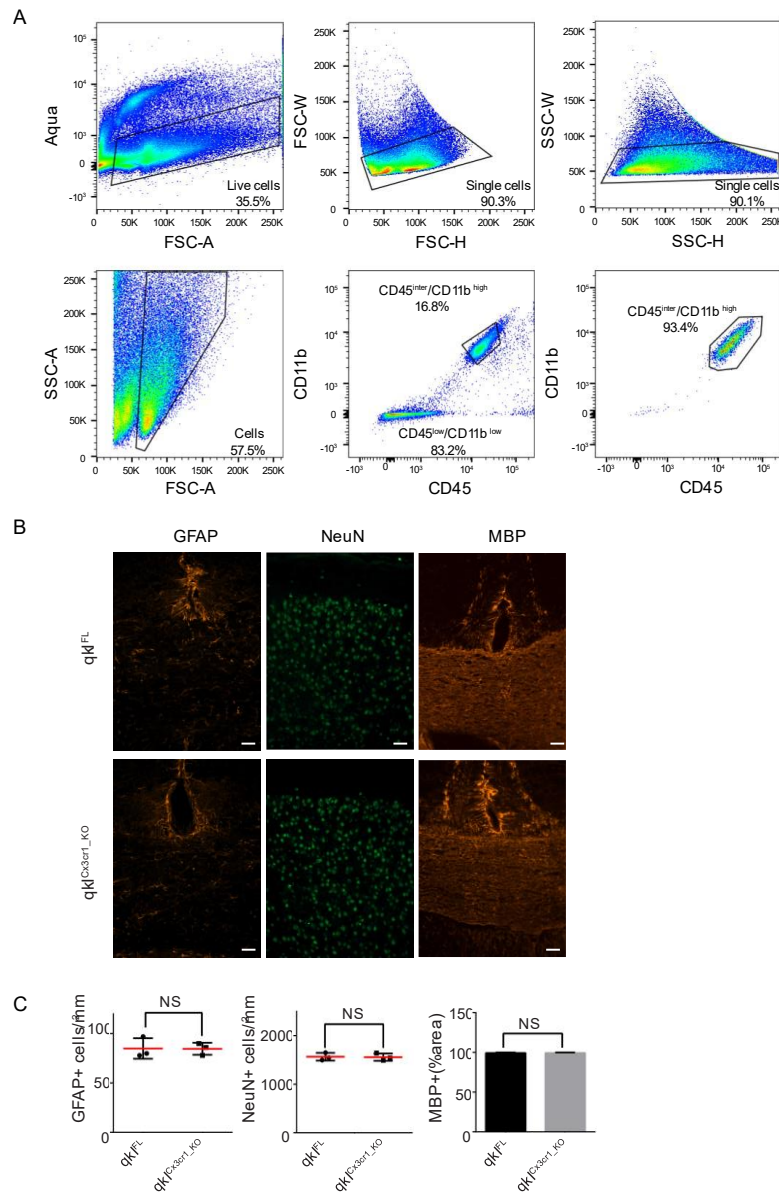
Figure S2 Histological analysis of qkI^{FL} and qkI$^{Cx3cr1-KO}$ mice and FACs gating strategy to isolate microglia.

A, Isolation of primary microglia using CD11b and CD45 antibodies. Dead cells were detected using Aqua and removed. Single cells were sorted with FSC-H with FSC-W followed by SSC-H with SSC-W. FSC-A and SSC-A was gated to remove remaining debris. Microglia were gated for CD45^{inter}/CD11b^{high} and sorted. The sorted CD45^{inter}/CD11b^{high} cells were subsequently re-analyzed by FACS to confirm the purity of cells.

B, Histological analysis of astrocyte (anti-GFAP), neuron (anti-NeuN), and myelin (anti-MBP) was examined in *qkI^{FL}* and *qkI$^{Cx3cr1-KO}$* mice injected with TAM. Scale bar represents 50 μm**.**

C, Boxplot showing the number of GFAP+, NeuN+ and percentage area MBP+ in *qkI^{FL}* and *qkI$^{Cx3cr1-KO}$* mice injected with TAM. Each point represents one mouse with a total of 3 mice used per genotype. GFAP+ cells and percentage MBP+ was analyzed in the corpus callosum region of the brain. NeuN+ cells were counted in the cerebral cortex region of the brain. Data presented as mean ± SEM. *P* values were analyzed using Mann–Whitney U-statistical test.
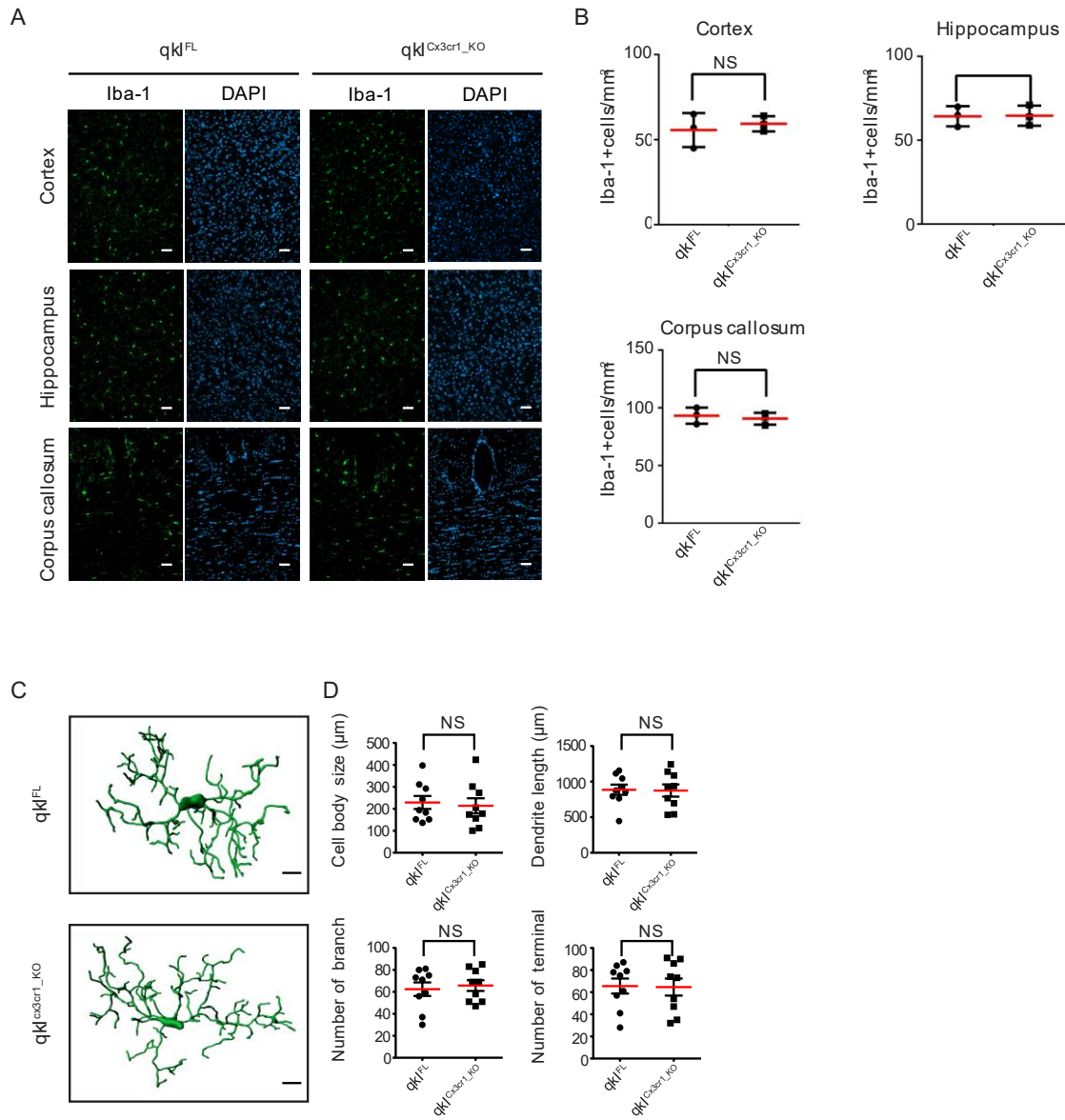
Figure S3 Phenotypic analysis of qkI^{FL} and $qkI^{Cx3cr1-KO}$ mice without TAM treatment.
A, Iba-1 and DAPI staining in the cortex, hippocampus, and corpus callosum of qkI^{FL}, and $qkI^{Cx3cr1-KO}$ mice. Representative images are shown. Scale bar represents 50 µm.
B, Iba-1-positive microglial cells counts. Each dot represents one mouse with a total of 3 mice used per genotype. Data presented as mean ± SEM. *P* values were analyzed using the Mann–Whitney U-statistical test.
C, IMARIS based 3D reconstruction images of Iba-1+ microglia of qkI^{FL}, and $qkI^{Cx3cr1-KO}$ mice. Scale bar represents 10 µm.
D, IMARIS based morphometric analysis of microglia of qkI^{FL}, and $qkI^{Cx3cr1-KO}$ mice. Three mice per genotype, and 6 cells per mouse were analyzed. Data presented as mean ± SEM. *P* values were analyzed using the Mann–Whitney U-statistical test.
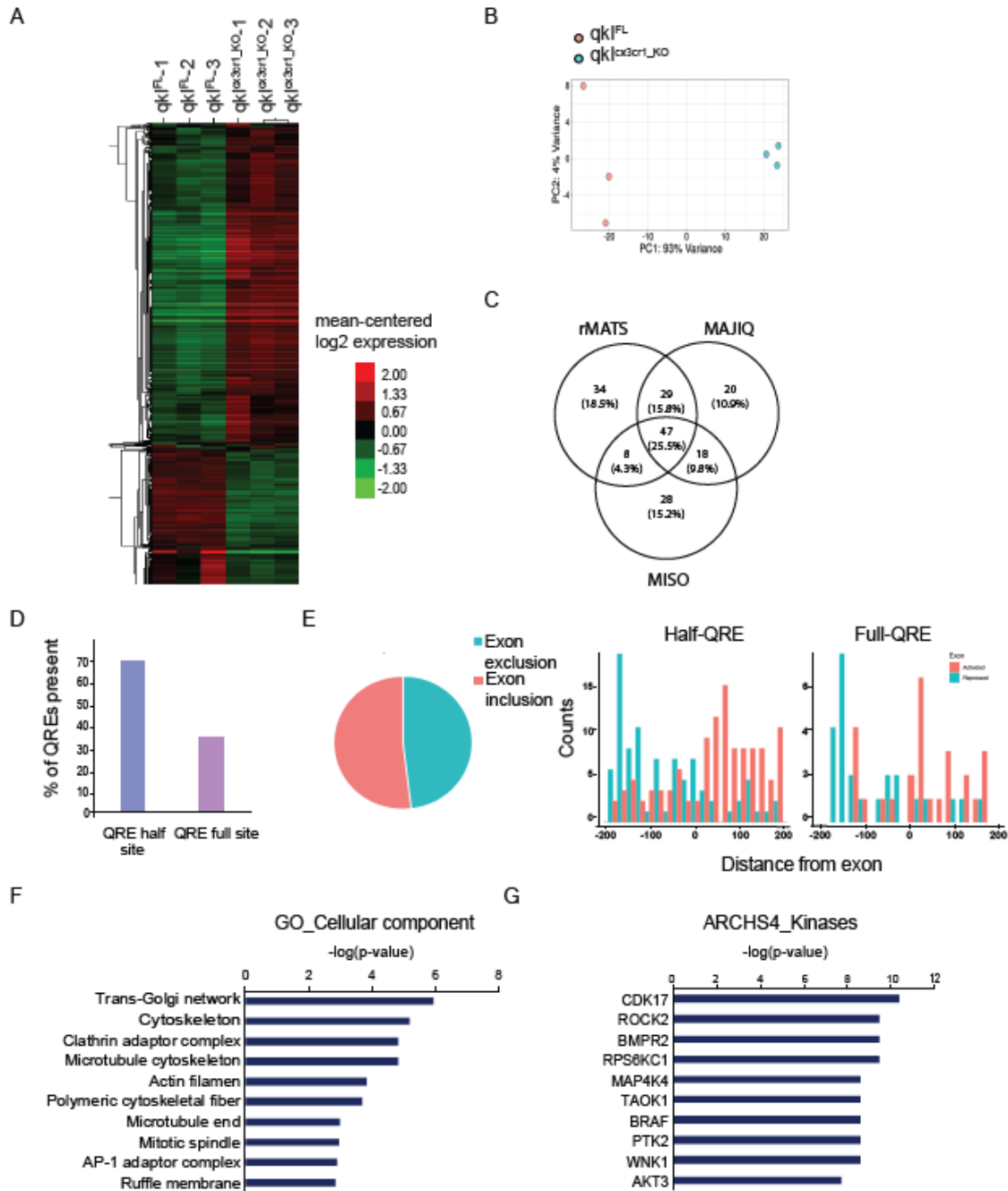
Figure S4 Alternative splicing events regulated by QKI in microglia.
A, Hierarchically clustered heatmap depicts the expression patterns of qkI^{FL} and $qkI^{Cx3cr1-KO}$ samples. The rows represent genes and the column the biological replicate. **B**, PCA of the 3 biological replicates of qkI^{FL} and $qkI^{Cx3cr1-KO}$ microglia. X- and Y-axes represent the percentage of variance. **C**, Venn diagram depicting the overlaps between rMATS, MAJIQ and MISO. **D,** Bar graph showing the percentage of QKI binding motif present in the intronic sequence of spliced genes within a window of 250 nt upstream or downstream of the spliced exon. **E,** SE, AFE, and ALE events were further divided into exon inclusion or exclusion and depicted in the pie chart. The location of QREs frequency was mapped upstream and downstream of the skipped exon event. **F,** Gene ontology of cellular components for differentially regulated splicing events. **G,** ARCHS4_Kinase analysis for QKI regulated splicing events.
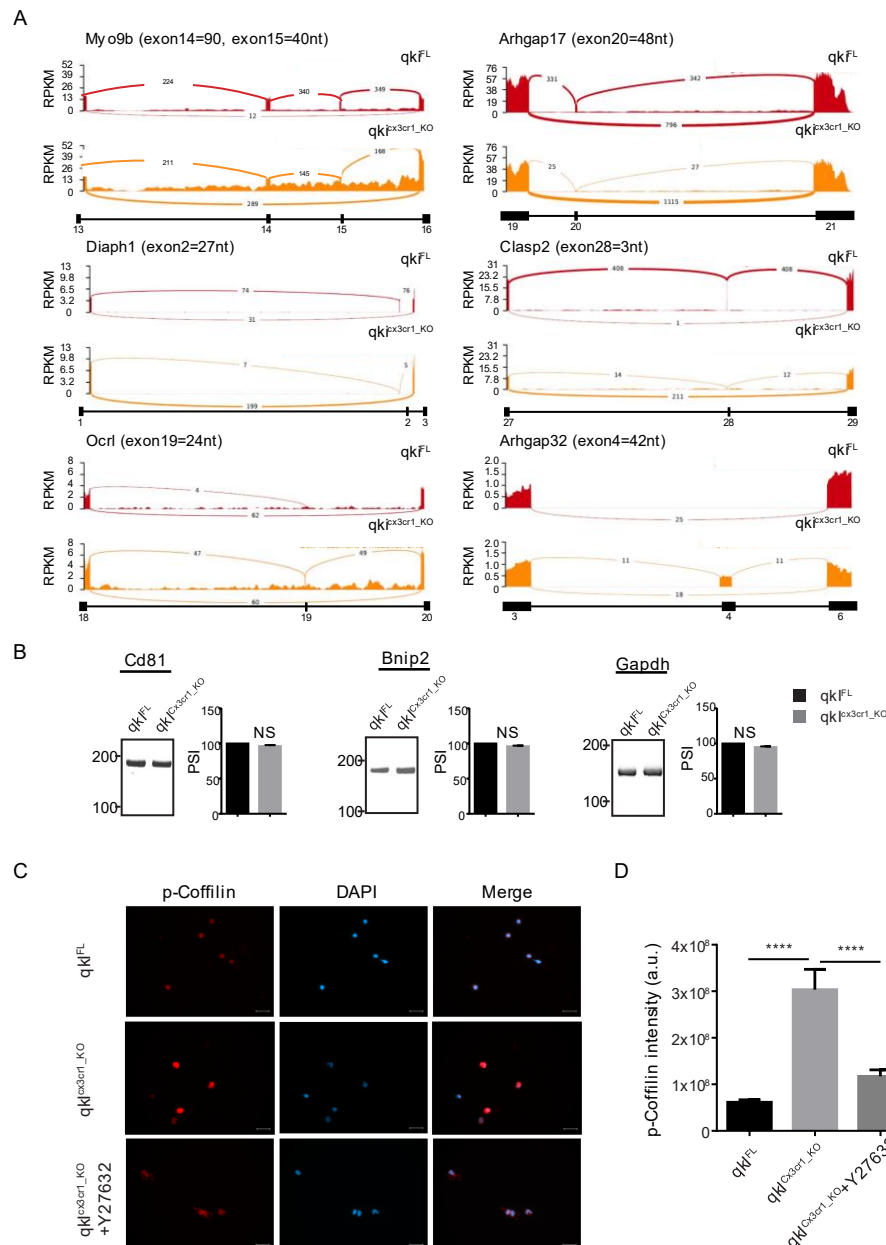
Figure S5 Depletion of QKI induces alternative splicing of Rho GTPase related transcripts and activates the Rock2 pathway.

A, Sashimi plot showing exon skipping events for microexons involved in the regulation of Rho GTPase pathway.

B, Transcripts not affected by QKI. Exon specific primers were generated, and RT-PCR was performed as in panel A. Percent spliced in (PSI) was calculated and depicted in the bar graph. At least 3 independent experiments were performed. Data presented as mean ± SEM. *p* values were analyzed using the Mann–Whitney U-statistical test.

C, Immunofluorescence of p-Cofilin (red) in primary microglia cells from qkI^{FL}, $qkI^{Cx3cr1-KO}$, and $qkI^{Cx3cr1-KO}$ treated with Y-27632. Scale bar represents 20 μm.

D, Immunofluorescence intensity for p-Cofilin (red) were quantified using IMARIS software. Bar graph shows mean intensity with standard deviation. *P* values were analyzed using a one-way ANOVA (**** *p*<0.0001). Data is representative of three independent experiments.

A

GO_UP:Biological Process
-log(p-value)

- cytokine-mediated signaling pathway
- cellular response to type I interferon
- type I interferon signaling pathway
- negative regulation of viral genome replication
- mitotic sister chromatid segregation
- lymphocyte chemotaxis
- regulation of viral genome replication
- cellular response to cytokine stimulus
- response to interferon-gamma
- inflammatory response

GO_UP:Molecular Function
-log(p-value)

- chemokine receptor binding
- cytokine activity
- chemokine activity
- microtubule binding
- CCR chemokine receptor binding
- tubulin binding
- phospholipase activator activity
- cytokine receptor binding
- CXCR chemokine receptor binding
- MAP kinase tyrosine/serine/threonine phosphatase activity

B

GO_DOWN:Biological Process
-log(p-value)

- nervous system development
- myelination
- axonogenesis
- negative regulation of cell communication
- extracellular matrix organization
- central nervous system myelination
- negative regulation of signaling
- glial cell differentiation
- positive regulation of superoxide anion generation
- axon guidance

GO_DOWN:Molecular Function
-log(p-value)

- calcium ion binding
- metal ion binding
- filamin binding
- tubulin binding
- transmembrane receptor protein tyrosin kinase activity
- transmembrane receptor protein kinase activity
- ephrin receptor binding
- mitogen-activated protein kinase kinase binding
- metalloendopeptidase activity
- metallopeptidase activity

C — Concentration (pg/mL): IL-6, CXCL10, IL-1a, TNF-a, CCL-5, CCL-22, CCL-12 (qkI^{FL}, qkI^{cx3cr1_KO})

D — Relative mRNA expression of the targeted genes: Qki, Trem2, Apoe, Spp1, Ccl2, Fabp5, Axl, Cybb (qkI^{FL}, qkI^{cx3cr1_KO})

Figure S6 RNA-Seq analysis of differentially expressed genes and altered pathways in QKI-deficient microglia.

A, Gene ontology of biological process and molecular functions of up-regulated transcripts in $qkI^{Cx3cr1-KO}$ microglia.

B, Gene ontology of biological process and molecular functions of down-regulated transcripts in $qkI^{Cx3cr1-KO}$ microglia.

C, Representative bar graph showing the result of cytokine array from primary microglia isolated from qkI^{FL} and $qkI^{Cx3cr1-KO}$ mice. Serum was collected and cytokine array was performed for two independent replicates per genotype with similar results.

D, DAM associated transcripts were examined using RT-qPCR in freshly isolated qkI^{FL} and $qkI^{Cx3cr1-KO}$ microglia. Three mice were pool together per genotype. Data presented as mean ± SEM. p values were analyzed using the Mann–Whitney U-statistical test (*$p < 0.05$, ** $p<0.01$, *** $p<0.001$).
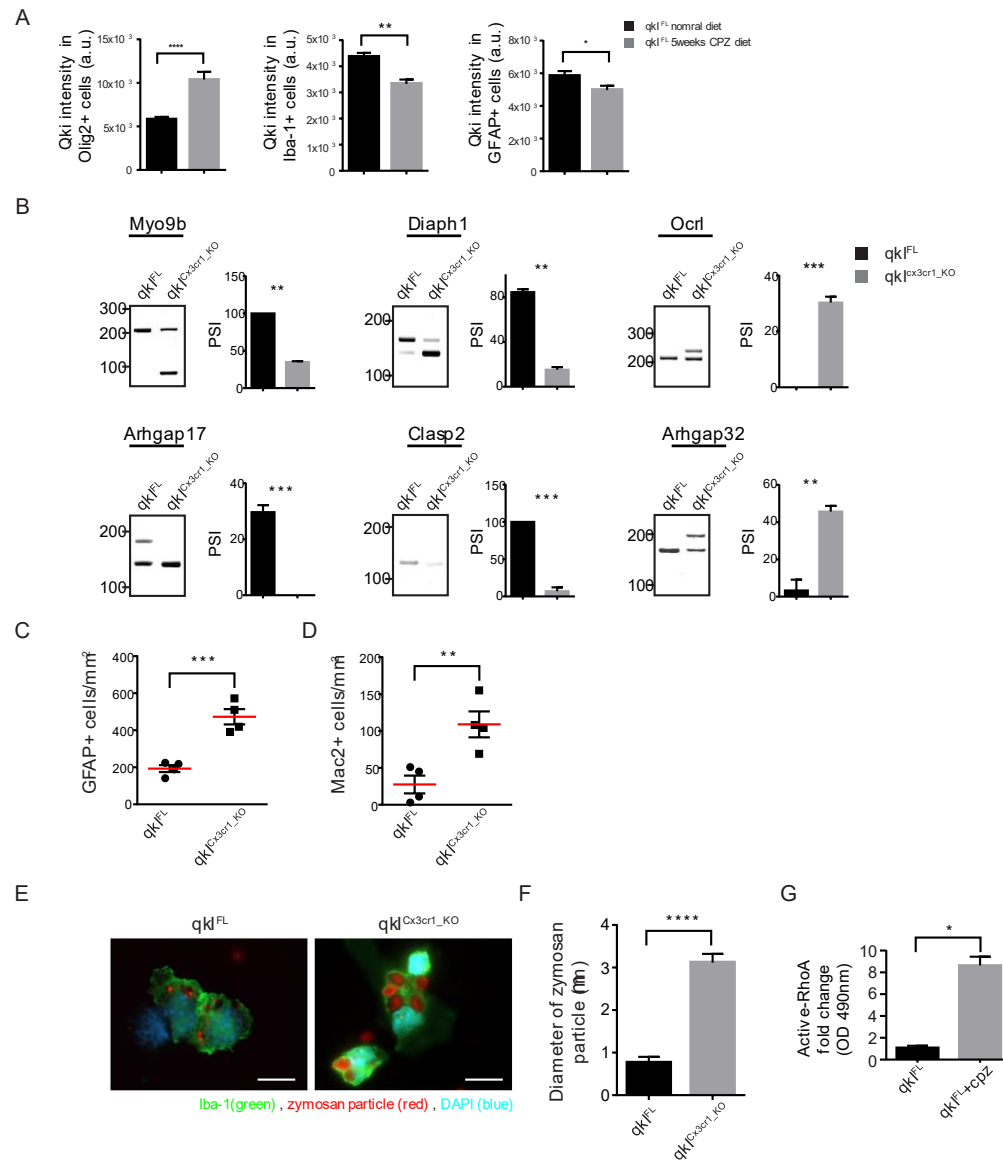
Figure S7 Splicing and immunofluorescent analysis of CPZ treated qkI^{FL} and $qkI^{Cx3cr1-KO}$ mice and phagocytosis assay

A, Anti-QKI immunofluorescence staining in Olig2+, Iba+ and GFAP+ cells in qkI^{FL} mice treated with normal diet and 5weeks of CPZ diet. Bar graph shows mean intensity with SEM. *P* values were analyzed using a parametric unpaired t-test (**** $p<0.0001$, ** $p<0.01$, * $p<0.05$). Two mice per time point were analyzed.

B, Alternatively spliced microexons associated with Rho GTPase pathway were further validated with exon specific primers using RT-PCR. Primers were designed upstream, and downstream of the cassette exons. The percent spliced in (PSI) was calculated and depicted in the bar graph on the right. At least 3 independent experiments were performed. Data is presented as mean ± SEM. *p* values were analyzed using the Mann–Whitney U-statistical test (** $p<0.01$, *** $p<0.001$).

C-D, The number of GFAP+ DAPI+ and Mac2+DAPI+ cells were counted in the corpus callosum region of the brain during 3 weeks of remyelination in qkI^{FL} and $qkI^{Cx3cr1-KO}$ mice. Each point represents one mouse with a total of 4 mice used per genotype. Data presented as mean ± SEM. *P* values were analyzed using the Mann–Whitney U-statistical test (** $p<0.01$, *** $p<0.001$).

E, Immunofluorescence of zymosan particle (red), Iba-1(green) and DAPI (blue) in primary microglia cells from qkI^{FL} and $qkI^{Cx3cr1-KO}$. Scale bar represents 10 µm.

F, Diameter of the zymosan particle engulfed by qkI^{FL} and $qkI^{Cx3cr1-KO}$ microglia were quantified. Data presented as mean ± SEM. *P* values were analyzed using a parametric unpaired t test (*** *p*<0.001). Data is representative of three independent experiments.

G, Freshly sorted microglia from qkI^{FL} mice treated with CPZ diet for 5 weeks were analyzed for active RhoA GTPase using G-LISA assay (absorbance at 490nm). At least two independent experiments were performed. Data presented as mean ± SEM. *P* values were analyzed using the Mann–Whitney U-statistical test (**p* < 0.05)

Table S1. MS patient samples information. Related to Figure 7.

Type	Age	Sex	Types of lesion analysed		
			Preactive	Chronic active	Remyelinated
SPMS	48	M	2	1	
PPMS	55	M		1	1
SPMS	60	F		1	1
SPMS	65	M	1	2	1
RRMS	26	M		1	1
Control	46	F			
Control	42	M			
Control	30	F			
Control	unknown	M			
Control	31	F			
Control	64	M			

Table S2. Sequences of primers use for q-PCR and RT-PCR. Related to Figure

	Forward (5'-3')	Reverse (5'-3')
Qki_exon2	ACGGAAAGACATGTACAATGACAC	GAACAATGGGTCCCACCGC
Myo9b	CCTGCCACTCGAAGTCACAT	TGTGCACTGATGCTAGGTGG
Diaph1	GGGACAAGAAGAAGGGTCGG	CAATGACTGAGCAGTGGGGT
Ocrl	ACCATCCTGAACTCCGGTGA	TCTTTGGGGACTTGAAGGGG
Arhgap32	AGAGGAGCAGATGTCCCTGA	TGCCAAACTCCACGTTCTCA
Clasp2	GTTTGCAGATCCTCATGGCA	CAGCAGCTGTGTCAGCAGAA
Arhgap17	GGTGGATGGTGGCCTTACAT	GCCAGGCACTTCTTTGCTTG
Cd81	AGGCTTCCTGGGGTGCTATG	TTGGCATTGTTGGCATCATCA
Bnip2	CTAGGCTGAGGATGGAAGGTG	GTCTGGGGCCATCAGTTTCTT
Ccl22	TCTGATGCAGGTCCCTATGGT	TTATGGAGTAGCTTCTTCAC
Il-6	GATGCTACCAAACTGGATATAATC	GGTCCTTAGCCACTCCTTCTGTG
Il-1b	TCCAGGATGAGGACATGAGCAC	GAACGTCACACACCAGCAGGTTA
Ccl5	CAGCAGCAAGTGCTCCAATCTT	TTCTTGAACCCACTTCTTCTCTGG
Trem2	GGAACCGTCACCATCACTCT	ATGCTGGCTGCAAGAAACTT
Apoe	TGTGGGCCGTGCTGTTGGTC	GCCTGCTCCCAGGGTTGGTTG
Spp1	CCATCTCAGAAGCAGAATCTCCTT	GGTCATGGCTTTCATTGGAATT
Ccl2	GCATCTGCCCTAAGGTCTTCA	TGCTTGAGGTGGTTGTGGAA
Fabp5	CCTGTCCAAAGTGATGATGG	CAGCATCAGGAGTGGGATG
Axl	TGAAGCCACCTTGAACAGTC	GCCAAATTCTCCTTCTCCCA
Cybb	GCCAGTGTGTCGAAATCTGC	AATTGTGTGGATGGCGGTGT
Gapdh	CATCACTGCCACCCAGAAGACTG	ATGCCAGTGAGCTTCCCGTTCAG
Hprt	GCCTAAGATGAGCGCAAGTTG	TACTSGGCAGATGGCCACAGG
Bactin	CTGTCCCTGTATGCCTCTG	ATGTCACGCACGATTTCC

CHAPTER 3: PRMT1 PROMOTES IFN-ASSOCIATED MICROGLIA AND AFFECTS THE REMYELINATION OF THE CENTRAL NERVOUS SYSTEM

Jeesan Lee[1], Oscar David Villarreal[1], Joey Heath[2], Yu Chang Wang[3], Jiannis Ragoussis[3], Alexandre Orthwein[2], David Gosselin[4] and Stéphane Richard[1*]

[1]Segal Cancer Center, Lady Davis Institute for Medical Research and Gerald Bronfman Department of Oncology and Departments of Biochemistry, Human Genetics, and Medicine, McGill University, Montreal, QC H3T1E2, Canada

[2]Segal Cancer Center, Lady Davis Institute for Medical Research and Gerald Bronfman Department of Experimental Medicine, McGill University, Montreal, QC H3T1E2, Canada

[3]Department for Human Genetics, McGill University Genome Centre, McGill University, Montréal, QC, Canada.

[4]Neuroscience laboratory, CHU de Quebec Research Center and Department of Molecular Medicine, Faculty of Medicine, Laval University, Quebec, QC G1V 4G2, Canada

Running title: *PRMT1 regulates IFN-associated microglia cluster during de/remyelination*

Keywords: PRMT1, PRMT5, microglia, type I interferon, remyelination, multiple sclerosis

3.1 Preface

In chapter 2, we identified QKI as a crucial regulator of microglia function by impacting global alternative splicing patterns. The protein arginine methyltransferases 1 (PRMT1), the major type I PRMT, methylates RBPs regulating their protein stability, cellular localization and RNA binding activity. Moreover, many studies report PRMTs as a major modulator of various immune cell functions, thereby impacting disease pathogenesis. How PRMT1 mediates microglia function in the basal and disease setting has not been investigated. Therefore, we utilized the CX3CR1-CreERT system to conditionally delete PRMT1 in microglia and investigated its role.

3.2 Abstract

Remyelination failure in multiple sclerosis (MS) leads to progressive demyelination and inflammation, resulting in neurodegeneration and a decline in patient quality of life. Microglia are innate immune cells that can acquire a regenerative phenotype to promote remyelination, yet little is known about the regulators controlling the activation of this cell type. Here, using a cuprizone (CPZ)-diet induced de- and remyelination mouse model, we identify PRMT1 as a driver of the expansion of an interferon (IFN)-associated microglia population that is required for remyelination in the central nervous system (CNS). The loss of PRMT1, but not PRMT5, specifically in microglia resulted in impairment of the remyelination process, with a reduction in oligoprogenitor cell number and prolonged microgliosis and astrogliosis. Using single-cell RNA sequencing, we found eight distinct microglial clusters in mice under the CPZ diet. Furthermore, we observed that PRMT1-depleted microglia were unable to form the IFN-associated cluster, characterized by the expression of MHCII+ and CD11c+. Additionally, PRMT1-deficient bone marrow-derived macrophages (BMDMs) challenged with a polyinosinic:polycytidylic acid (poly(I:C)), an analog

of viral dsRNA, were defective in their type I IFN responses. Mechanistically, we show that PRMT1-KO microglia have reduced H3K27ac peaks at the promoter regions of IFN-associated genes, and exhibited a further suppression of gene expression during the CPZ diet. Overall, our findings demonstrate that PRMT1 is a critical regulator of the IFN-microglia cluster, and therefore impacts remyelination in the CNS.

3.3 Introduction

Microglia are tissue-resident innate immune cells of the central nervous system (CNS), constituting 5–12% of the CNS (Wolf et al., 2017). Microglia constantly patrol the CNS to recognize homeostatic disturbances, and quickly change their transcriptional program, morphology, and electrophysical properties to perform a wide range of roles (Prinz et al., 2019; Wolf et al., 2017). For instance, microglia use unique cell surface-receptors to sense pathogens, apoptotic cells, and protein aggregates, and then rapidly switch to a phagocytic phenotype to eliminate these materials (Prinz et al., 2019). Furthermore, upon sensing any injuries to the CNS, microglia proliferate, migrate to the site of the damage, and secrete cytokines, chemokines, nitric oxide, and reactive oxygen species to modulate the injury-induced immune response (Li and Barres, 2018). Increasing studies using single-cell sequencing technology have unveiled the dynamic phenotypes of microglia during development and pathological conditions (Masuda et al., 2020). However, the molecular mechanisms leading to expansion of specific microglial subpopulations during CNS pathophysiology remains underexplored.

Cuprizone is a copper chelating agent that results in demyelination, a pathological hallmark of multiple sclerosis (MS) (Vega-Riquer et al., 2019). Administration of a 0.2% cuprizone diet (CPZ) in mice induces apoptosis of oligodendrocytes, with activation of microglia and astrocyte

116

populations (Lloyd and Miron, 2019; Vega-Riquer et al., 2019). Under these conditions, microglia recognize damaged oligodendrocytes and become the main phagocytic cell type to clear myelin debris, which allows the recruitment of oligoprogenitor cells (OPCs) at the demyelinating plaques (Lloyd and Miron, 2019). Additionally, microglia secrete various pro-regenerative factors to aid in OPC proliferation, migration, and differentiation (Lloyd and Miron, 2019). Emerging evidence implies that a transcriptionally distinct subset of microglia promotes the remyelination process; however, the molecular mechanisms regulating this subset are poorly understood (Lloyd and Miron, 2019; Masuda et al., 2020).

Post-translation modifications (PTMs) are instrumental in modifying protein stability, interactions, and localization, and thereby impact a diverse array of singaling pathways (Xu and Richard, 2021). Among these PTMs, arginine methylation is catalyzed by protein arginine methyltransferases (PRMTs), which utilize the co-substrate S-adenosyl-L-methionine (AdoMet, SAM) to transfer a methyl group to the guanidino nitrogen atoms of arginine residues (Bedford and Clarke, 2009). PRMTs are categorized according to the types of methylation they can catalyze (Bedford and Clarke, 2009). PRMT1 is the major type I enzyme responsible for catalyzing asymmetric dimethylarginine (ADMA), whereas PRMT5 is the major Type II enzyme and generates symmetric dimethylarginine (SDMA) (Rotshenker, 2009). The substrates of PRMTs include RNA binding proteins (RBPs), DNA damage repair proteins, transcription factors, signaling proteins and histones (Guccione and Richard, 2019; Xu and Richard, 2021). In recent years, PRMTs have been shown to play instrumental roles in immune cell differentiation, activation, and viral-mediated type I Interferon (IFN) responses by methylating proteins and histones (Sengupta et al., 2020; Xu and Richard, 2021). Nevertheless, the role of PRMTs in modulating microglia function during de/remyelination processes has never been investigated.

Here, using the CPZ mouse model, we report that PRMT1 is an epigenetic regulator of the IFN-associated MHCII+ and CD11c+ microglia cluster. Lack of this IFN-associated microglia cluster in $PRMT1^{Cx3cr1-KO}$ mice correlates with a failure to induce CNS remyelination in CPZ-fed mice.

3.4 Results

3.4.1 CNS remyelination defects and microgliosis in cuprizone induced demyelination in $PRMT1^{Cx3cr1-KO}$ mice

To investigate the role of arginine methylation in microglia, we generated mice with microglia deficient for PRMT1 or PRMT5 using the $Cx3cr1^{CreERT}$ driver (Supplementary Figure s1A). Microglia isolated from 4-hydroxytamoxifen (TAM) injected $PRMT1^{FL/FL;Cx3cr1-KO}$ ($PRMT1^{Cx3cr1-KO}$) and $PRMT5^{FL/FL;Cx3cr1-KO}$ ($PRMT5^{Cx3cr1-KO}$) exhibited the loss PRMT1 and PRMT5 with reduction in the histone marks, H4R3me2a and H4R3me2s, respectively (Supplementary Figure S1A). The impact of PRMT1 and PRMT5 ablation on microglia number and morphology was assessed using anti-Iba-1 antibody. During the resting state, $PRMT1^{Cx3cr1-KO}$ or $PRMT5^{Cx3cr1-KO}$ microglia did not show any differences in the cell number in the corpus callosum (CC), cortex, and hippocampus of the CNS compared to their respective controls, $PRMT1^{FL}$ and $PRMT5^{FL}$, (Figure 1A and Supplementary Figure S1B). However, distinct morphological changes were observed only in the $PRMT1^{Cx3cr1-KO}$ microglia (Figure 1B and Supplementary Figure S1C). The IMARIS based detail morphological analysis showed that $PRMT1^{Cx3cr1-KO}$ microglia had significantly longer total dendritic length with increased number of branches, segments, and terminals compared to control $PRMT1^{FL}$ (Figure 1B).

We examined the ability of the *PRMT1$^{Cx3cr1-KO}$* and *PRMT5$^{Cx3cr1-KO}$* mice to influence CNS demyelination and remyelination using the cuprizone mouse model of myelin lesion (Gudi et al., 2009). The mice were fed with 0.2% cuprizone (CPZ) diet for 5 weeks to instigate CNS demyelination followed by 1week of normal diet to induce remyelination (Gudi et al., 2014). We focused on the CC area to qualitatively visualize the demyelination and remyelination. At five weeks of CPZ diet, myelin was completely absent in the CC, and there were no significant differences in the extent of demyelination between the genotypes (Figure 1C, 1D and Supplementary Figure S1D, S1E). However, upon changing to a normal diet for 1-week, significant remyelination was visible in the *PRMT1^{FL}*, but not in the *PRMT1$^{Cx3cr1-KO}$* mice (Figure 1C, 1D). Conversely, the loss of PRMT5 in microglia did not impair the CNS remyelination (Supplementary Figure S1D, S1E). Microglia accumulate at the CC during the demyelination period and dissipate following the remyelination (Gudi et al., 2014). Consistent with this, microglia significantly increased during the CPZ diet (microgliosis; Iba1+) and subsequently decreased upon changing to a normal chow (+ 1week off) in CC of *PRMT1^{FL}* , *PRMT5^{FL}* and *PRMT5$^{Cx3cr1-KO}$* mice (Figure 1E, 1F and Supplementary Figure S1F, S1G). Nevertheless, in the *PRMT1$^{Cx3cr1-KO}$* mice, microglia (Iba1+) significantly increased during the CPZ diet and remained in the CC upon changing to a normal chow (+ 1week off)(Figure 1E, 1F). Thus, *PRMT1$^{Cx3cr1-KO}$* mice have defects in remyelination with prolonged microgliosis in the CPZ demyelination mouse model.

Figure_1
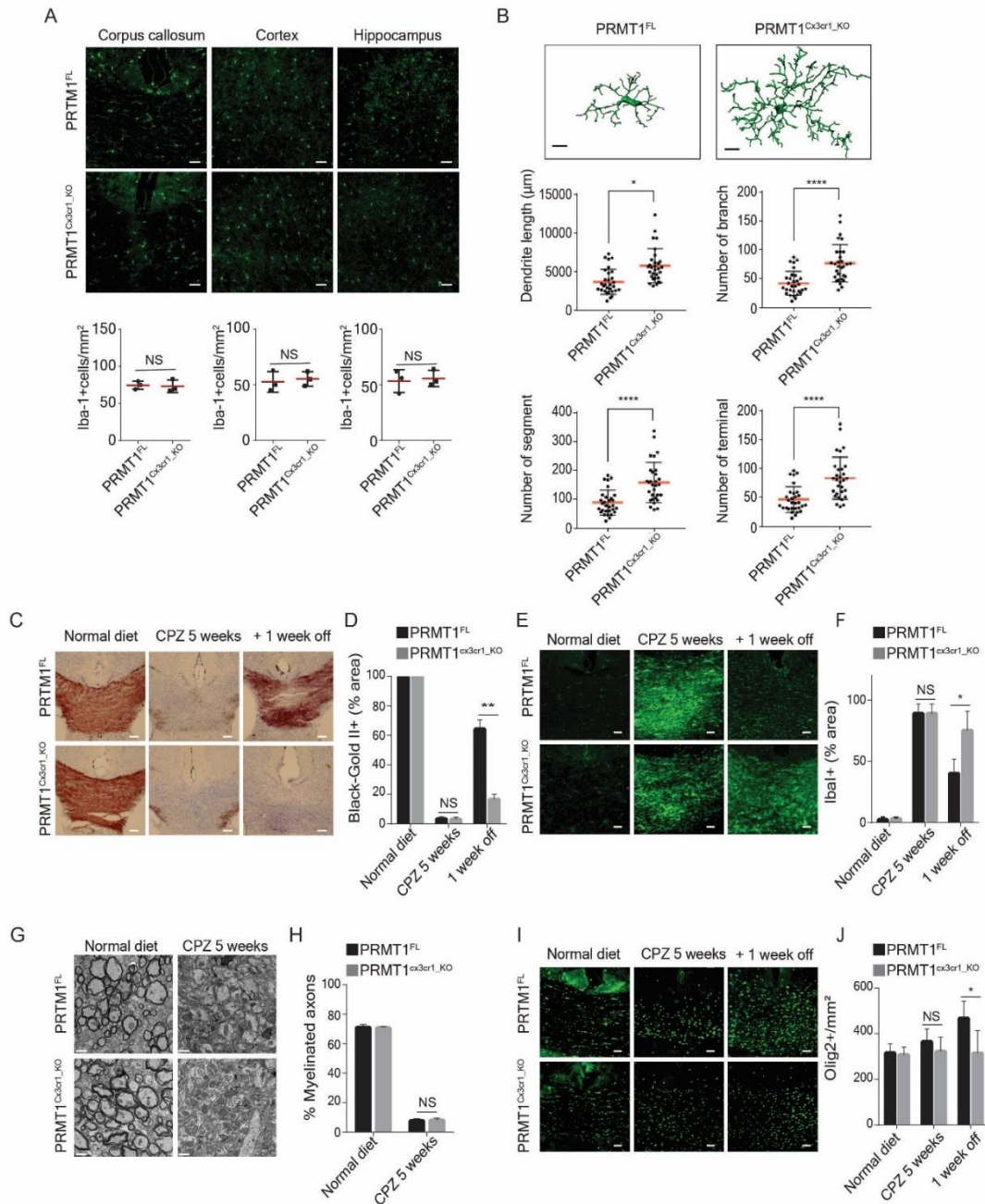
Figure 1 CNS remyelination defects in *PRMT1*-deficient mice

A, Iba-1(green) staining in cortex, hippocampus and corpus callosum (CC) of *PRMT1^FL^* (n=3), and *PRMT1^Cx3cr1-KO^* (n=3) CNS. Representative images are shown. Scale bars represent 50 μm. Data presented as mean ± SEM. *P* values were analyzed using Mann–Whitney U-statistical test (NS: Not significant).

B, IMARIS based morphological analysis of microglia from *PRMT1^FL^* (n=3), and *PRMT1^Cx3cr1-KO^* (n=3) CNS. Representative images are shown. 10 cells were analyzed for dendritic length, number of branches, number of segments and terminals and presented as a dot plot. Scale bars represent 10 μm. Data presented

120

as mean ± SEM. *P* values were analyzed using Mann–Whitney U-statistical test (* *p* < 0.05, **** *p* < 0.0001).

C, Mice fed with 0.2% cuprizone diet (CPZ) were sacrificed according to the following time points: Normal diet, CPZ diet 5 weeks (n=5) and CPZ diet 5weeks+ normal diet 1week (n=5). Black gold II staining (brown) was performed to visualize myelin and quantified at the CC of *PRMT1^{FL}* (n=5), and *PRMT1^{Cx3cr1-KO}* (n=5) CNS. Representative images are shown. Scale bars represent 50 µm.

D, Bar graph depicts average myelin staining in the CC. Data presented as mean ± SEM. *P* values were analyzed using Mann–Whitney U-statistical test (** *p*<0.01, NS: Not significant). Scale bars represent 50µm.

E-F, Anti-Iba-1 (green) was stained during the normal diet, CPZ diet 5 weeks and CPZ diet 5weeks+normal diet 1week in *PRMT1^{FL}* (n=5), and *PRMT1^{Cx3cr1-KO}* (n=5). Representative images are shown. Scale bars represent 50 µm. **F,** Iba-1 staining was quantified at the CC and illustrated as a bar graph. Data presented as mean ± SEM. *P* values were analyzed using Mann–Whitney U-statistical test (* *p*<0.05, NS: Not significant).

G- H, Representative transmission electron microscope image of myelinated axons from *PRMT1^{FL}* (n=3), and *PRMT1^{Cx3cr1-KO}* (n=3) at the indicated time points. **H,** Myelinated axons were quantified and displayed in a bar graph. Data presented as mean ± SEM. *P* values were analyzed using Mann–Whitney U-statistical test (NS: Not significant).

I- J, Anti-Olig2 (green) was stained during the normal diet, CPZ diet 5 weeks and CPZ diet 5weeks+ normal diet 1week in *PRMT1^{FL}* (n=3), and *PRMT1^{Cx3cr1-KO}* (n=3) CNS. Representative images are shown. Scale bars represent 50 µm. **J,** Olig2 staining was quantified at the CC and illustrated as a bar graph. Data presented as mean ± SEM. *P* values were analyzed using Mann–Whitney U-statistical test (* *p*<0.05, NS: Not significant).

3.4.2 PRMT1^{Cx3cr1-KO} mice have prolonged gliosis and reduced number of oligoprogenitor cells during the remyelination phase

One possible explanation for remyelination failure observed in the *PRMT1^{Cx3cr1-KO}* mice was the inability of the microglia to clear the myelin debris during the demyelination phase. Thus, we performed transmission electron microscope (TEM) analysis and measured the myelin lamellae during the normal and CPZ diet 5 weeks in cross-sections of the CC of *PRMT1^{FL}* and *PRMT1^{Cx3cr1-KO}* mice (Figure 1G, 1H). The TEM analysis showed a complete loss of the myelin layer during the CPZ diet in both *PRMT1^{FL}* and *PRMT1^{Cx3cr1-KO}* mice and no myelin debris was observed in both genotypes, suggesting that the phagocytosis activity of PRMT1-deficient microglia was not impaired (Figure 1G, 1H).

The remyelination process is normally preceded by the proliferation of oligoprogenitor cells (OPCs), which subsequently differentiate into myelinating oligodendrocytes (Matsushima

121

and Morell, 2001). Therefore, we first analyzed the number of OPCs by staining with anti-Olig2-antibody (Yokoo et al., 2004). In *PRMT1^{FL}* mice, Olig2+ cells increased at the CC after changing to a normal diet (+ 1week off), but this increase was impaired in the *PRMT1$^{Cx3cr1-KO}$* mice (Figure 1I, 1J).

We next asked whether extension of the normal chow for 3 weeks (+ 3 week off) would recover the remyelination defects observed in *PRMT1$^{Cx3cr1-KO}$* mice. We did not recover the remyelination phenotype, as we observed severe impairment of remyelination, reduction in the recruitment of Olig2+ cells at the site of demyelination, accumulation of Iba1+ microglia and GFAP+ astrocytes in *PRMT1$^{Cx3cr1-KO}$* CC compared to the *PRMT1^{FL}* (Supplementary Figure 2A-D). To see whether these accumulated microglia were activated, we stained for Mac2, a marker of highly phagocytic microglia (Rotshenker, 2009). The expression of Mac2+ cells was significantly increased in the *PRMT1$^{Cx3cr1-KO}$* mice compared to the *PRMT1^{FL}* control (Supplementary Figure S2E), suggesting the microglia from *PRMT1$^{Cx3cr1-KO}$* mice are continuously activated during the remyelination phase with increased gliosis and decreased OPC recruitment.

3.4.3 scRNA-seq reveal a lack of IFN-associated microglia population in PRMT1$^{Cx3cr1-KO}$ mice

To closely inspect the microglia heterogeneity during the CPZ diet in *PRMT1^{FL}* and *PRMT1$^{Cx3cr1-KO}$* mice, we performed single-cell RNA sequencing (scRNA-seq) using the 10X Genomics platform. Mouse brains were enzymatically dissociated into single-cell suspension and sorted for CD45$^+$ and CD11b$^+$ to isolate microglia and macrophages. A total of 10,000 sorted cells at CPZ diet 5 weeks were sequenced from two separate *PRMT1^{FL}* and *PRMT1$^{Cx3cr1-KO}$* mice. Using the Seurat software package, a total of 6,000 microglia per genotype passed the quality control. The Uniform Manifold Approximation and Projection (UMAP) analysis revealed nine transcriptionally

defined clusters (labelled A to I) with unique genesets in *PRMT1^{FL}* and *PRMT1^{Cx3cr1-KO}* microglia (Figure 2A).

Eight clusters were microglia populations and there was a minor cluster representing 2% of the cells that expressed monocyte markers (*Ccr2, Mrc1, Mgl2, F13a1*) (Figure 2B, 2C and Supplementary Figure S3A). Thus, brain infiltrating monocytes were minimally present during the CPZ-diet induced demyelination and remyelination process.

Notably, single-cell mapping showed altered microglia composition in *PRMT1^{Cx3cr1-KO}* microglia, with the loss of C1 (11%), C2 (3%) and D (3%) populations with gains of B1 (9%) and E (24%) populations (Figure 2A-C). Close inspection revealed that the B1 cluster expressed transcripts found in disease-associated microglia phenotype (*Spp1, Cybb, Apoe, Cd38*) (Figure 2C). The cluster E expressed mixtures of homeostatic microglia signature (*P2ry12, Sall1*) and genes associated with pro-inflammatory transcripts (*Tnfaip2, Nfkbia*) (Figure 2C). The transition of microglia during the CPZ diet is poorly defined. Therefore, we subsequently utilized the scVelo algorithm, which uses the ratio of spliced to unspliced transcripts to infer RNA velocity and predict the transition of the clusters (Bergen et al., 2020). In the *PRMT1^{FL}*, the scVelo analysis showed two divergent trajectories of microglia, A1 to A2 clusters and B2 to C1 to C2 to D clusters (Figure 3A). The cluster A1 exclusively expressed (*Birc5, Mki67, Cdk1, Ccnb2)* which are indicative of proliferating cells in addition to oxidative phosphorylation (OXPHOS) associated genes (Figure 2C, and Supplementary Figure S3A). Cluster A2 also expressed OXPHOS genes (*Rps26, Ndufa1, Cox6a2, Uqcc2*) and the cytoplasmic translation processing genes (*Rps26, Rpl41, Rps8*) (Figure 2C, and Supplementary Figure S3A). Therefore, we will now call these A1 and A2 clusters "proliferating population," and these subsets possibly emerge from the stress and inflammatory condition exerted by the CPZ diet.
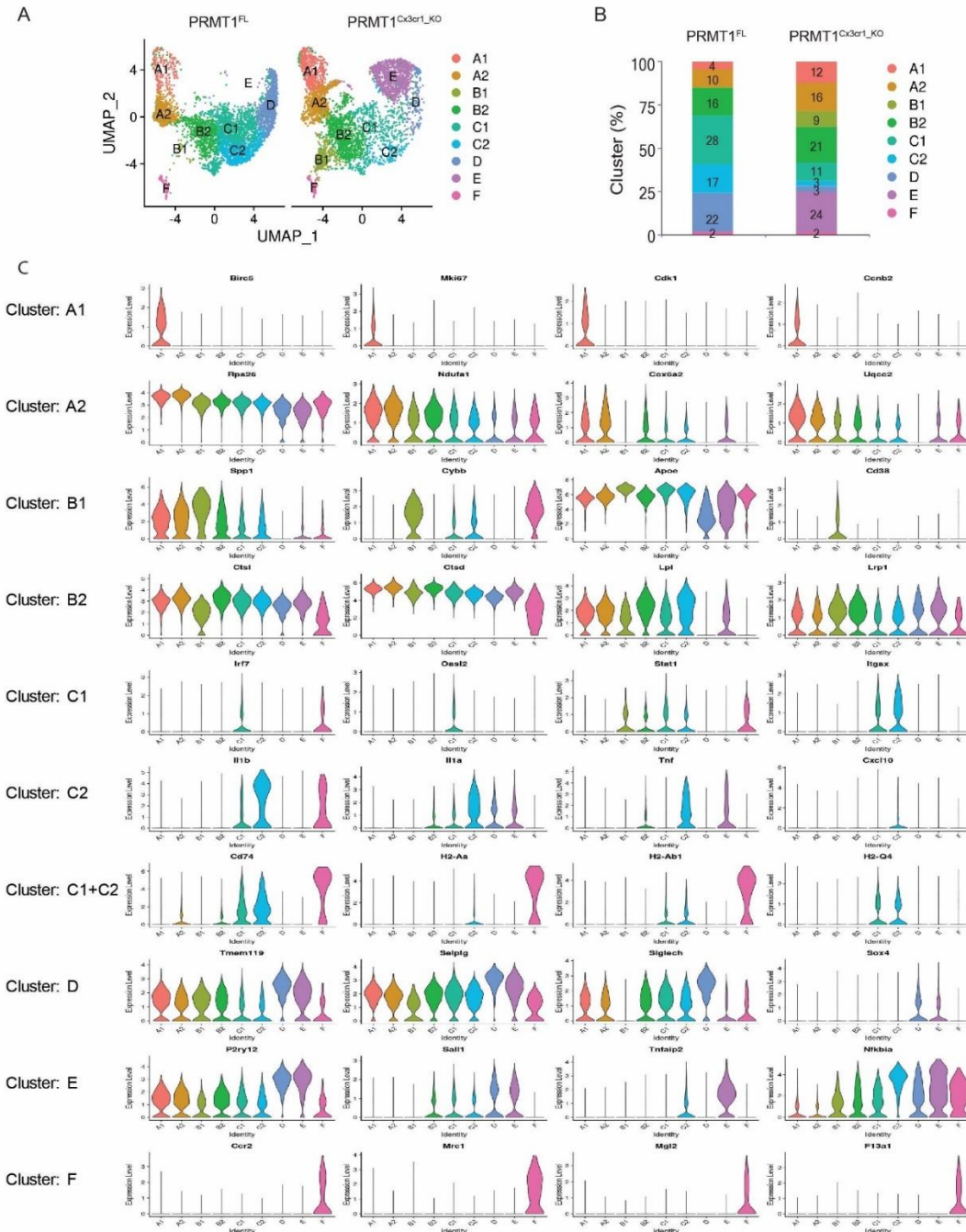
Figure 2 Single-cell RNA sequencing analysis on *PRMT1^FL* , and *PRMT1^{Cx3cr1-KO}* microglia during the CPZ diet 5 weeks

A, UMAP visualization of sc-RNA seq data showing 9 distinct cluster of microglia during the 5 weeks of CPZ diet in *PRMT1^FL* , and *PRMT1^{Cx3cr1-KO}*. Cells are coloured differentially according to the clusters.

B, Stacked bar chart representing percentage of each clusters.

C, Violin plot showing marker genes for individual clusters.

The B2 cluster was enriched for transcripts linked to lysosome (*Ctsl, Ctsd ,Cspg4, Gusb, Ctsb*) and lipid recycling (*Lpl, Lrp1*), signifying that the B2 cluster are phagocytic microglia likely involved in the demyelination from CPZ (Figure 2C, and Supplementary Figure S3A). B2 cluster transitioned to C1 to C2 clusters of which C1 and C2 express relatively high levels of IFN-associated transcripts (*Irf7, Oasl2, Stat1, Itgax*), pro-inflammatory cytokine and chemokine transcripts (*Il1b, Il1a, Tnf, Cxcl10, CCrl2*), and MHCI and II processing transcripts (*CD74, H2-Q4, H2-Ab1, H2-D1*) (Figure 2C, and Supplementary Figure S3A) compared to the remaining clusters. Therefore, we will call the B2 cluster the "phagocytic population" and C1 to C2 clusters the "IFN-associated population". Finally, the IFN-associated cluster transitioned to the D cluster, which expressed homeostatic microglia markers (*Tmem119, Seplg, Siglech, Sox4*) (Figure 2C). In stark contrast, the loss of PRMT1 dramatically reduced the transition from B2 to C1 cluster, thus abolishing the IFN-associated and homeostatic clusters (Figure 3A and 3B). To summarize, wild type microglia adopt two defined trajectories upon CPZ insult, proliferating microglia or phagocytic/IFN-associated/ homeostatic microglia, but the loss of PRMT1 impedes the transition from phagocytic to IFN-associated and ultimately to homeostatic microglia (Figure 3B).
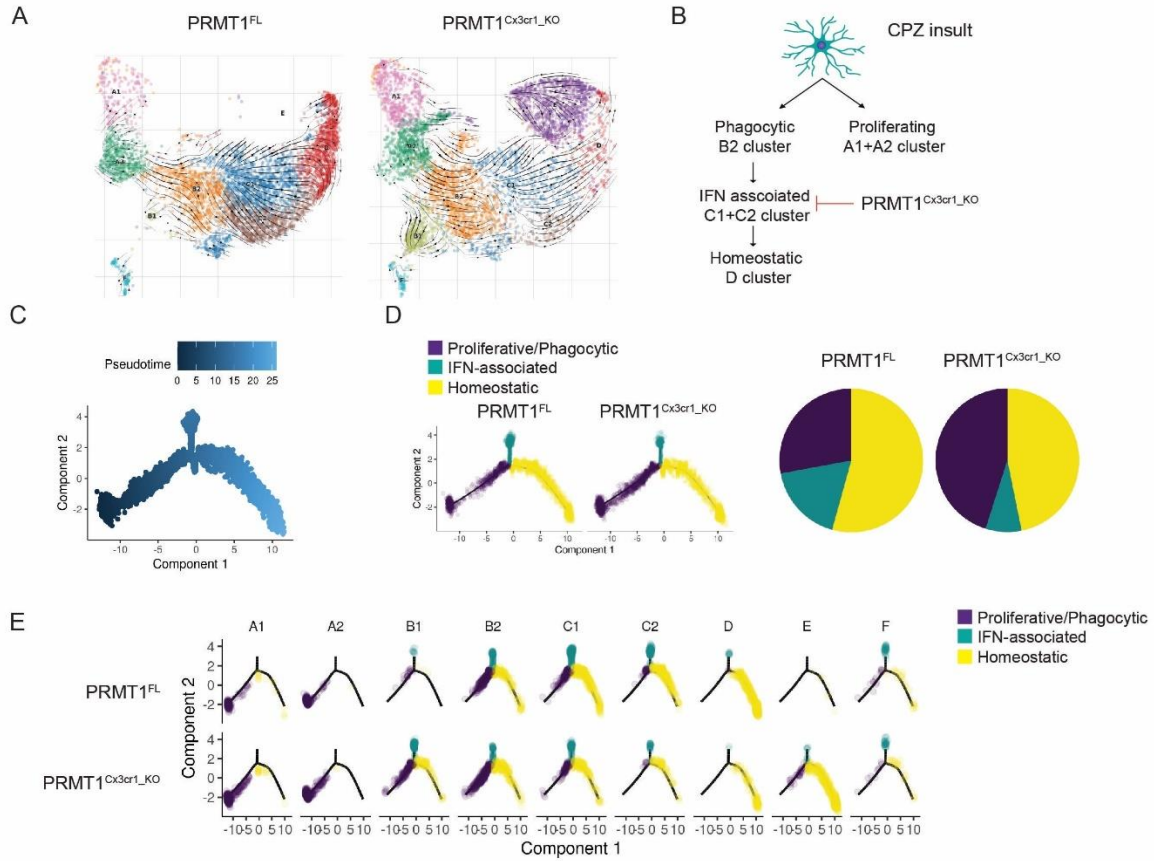
Figure 3 The IFN-associated cluster is lost with *PRMT1* deficiency
A, Trajectory of microglia were analyzed using scVelo algorithm and projected on the UMAP. Black arrow heads indicate the transition of microglia from one cluster to the other.
B, Schema illustrating the transition of clusters according to the scVelo analysis
C-E, Monocle pseudotime trajectory analysis using the sc-RNA seq data from *PRMT1^FL^*, and *PRMT1^Cx3cr1-KO^* microglia. Cells are labelled according to **C,** pseudotime **D,** 3 defined states and **E,** 9 clusters according to the 3 defined states.

We further performed monocle analysis, which aligns the cells in the pseudotime trajectory (Qiu et al., 2017b)(Figure 3C). In a similar fashion as scVelo analysis, *PRMT1^FL^* microglia begin with the proliferative state (A1 and A2 clusters), which then transition to phagocytic (B2 cluster), IFN-associated clusters (C1 and C2), and homeostatic state (Figure 3D). In *PRMT1^Cx3cr1-KO^* microglia, proliferating and phagocytic microglia are dominant populations that are hindered to transition to the IFN-associated and homeostatic populations (Figure 3D and 3E). We further confirmed the

single-cell analysis results by performing FACS on $PRMT1^{FL}$ and $PRMT1^{Cx3cr1-KO}$ microglia during the CPZ diet. We analyzed the CD11c+ and MHCII+ microglia for their presence of markers of the IFN-associated cluster. Consistently, during the CPZ diet, we found an increased number of MHCII+ (35.3%) and CD11c+ (37.7%) microglia cells in the $PRMT1^{FL}$ (Figure 4A-D). In contrast, $PRMT1^{Cx3cr1-KO}$ microglia did not increase the MHCII+(5.64%) and CD11c+ (9.15%) populations during the CPZ diet (Figure 4A-D). These data suggest that $PRMT1^{Cx3cr1-KO}$ mice are deficient in the IFN-associated microglia cluster expressing MHCII+ and CD11c+ during the CPZ diet.
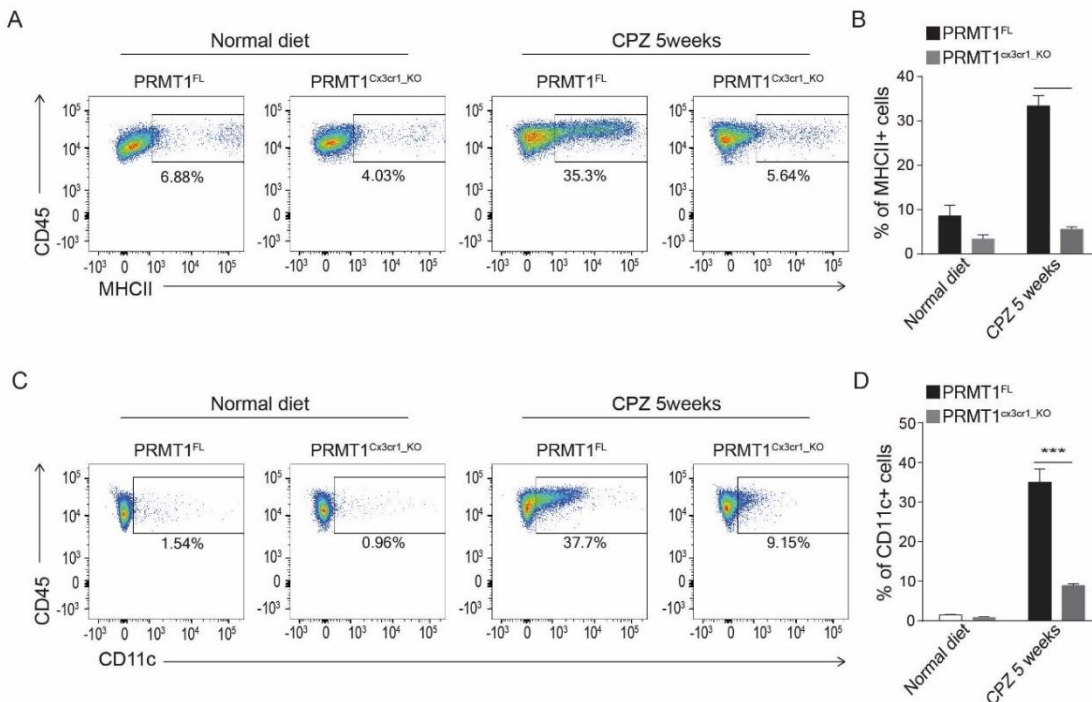
Figure 4 The IFN-associated cluster expresses MHCII and CD11c
A, Representative FACs analysis of MHCII+ microglia at the indicative time points in $PRMT1^{FL}$(n=3), and $PRMT1^{Cx3cr1-KO}$(n=3). **B**, Bar graph visualizing the percent positive of MHCII microglia. Data presented as mean ± SEM. *P* values were analyzed using Mann–Whitney U-statistical test (**** *p*<0.0001).
C, Representative FACs analysis of CD11c+ microglia during the normal and 5weeks of CPZ diet in $PRMT1^{FL}$(n=3) , and $PRMT1^{Cx3cr1-KO}$(n=3). **D**, Bar graph visualizing the percent positive of CD11c microglia. Data presented as mean ± SEM. *P* values were analyzed using Mann–Whitney U-statistical test (*** *p*<0.001).

3.4.4 *H3K27ac peaks of IFN-associated transcripts are lost in PRMT1-deficient microglia*

PRMT1 is known to asymmetrically dimethylates histone 4 arginine 3 (H4R3me2a)(Wang et al., 2001). The H4R3me2a activates transcription and acetylation of histones (Fatoba et al., 2020; Huang et al., 2005). Genome-wide H4R3me2a are notoriously impossible to perform as enrichment is not observed input for chromatin immunoprecipitation (ChIP) (Guccione and Richard, 2019). Further, due to a small yield of microglia cells per mouse, H4R3me2a ChIP was not feasible. As an alternative, we performed H3K27ac ChIP- and RNA-sequencing in *PRMT1^{FL} and PRMT1$^{Cx3cr1-KO}$* microglia during the normal and CPZ diet to decipher if PRMT1 could impact the transcriptional landscape of microglia (Figure 5A). Specifically, during the CPZ diet, we isolated *PRMT1^{FL}* microglia according to the CD11c+ and CD11c- populations (Figure 5A).

The heatmap and density plots show a striking increase of H3K27ac during the CPZ diet in both *PRMT1^{FL} and PRMT1$^{Cx3cr1-KO}$* microglia compared to the normal diet (Figure 5B, 5C). Interestingly, during the CPZ diet, the increase of H3K27ac peak and tag count densities was partially suppressed in the *PRMT1$^{Cx3cr1-KO}$* compared to the *PRMT1^{FL}*, indicating that PRMT1 is required for deposition H3K27ac at specific promoters (Figure 5C). Further analysis showed reduced H3K27ac peak at the gene's promoter region associated with IFN (Ikkbe, Gadd24b, Irf1, Csf1 and Cd11c) and MHCII (H2-ab1, H2-eb1, H2-aa) in *PRMT1$^{Cx3cr1-KO}$* compared to *PRMT1^{FL}* (Figure 5D). Likewise, the decrease in the H3K27ac at the IFN- and MHCII-associated genes reduced the total mRNA level (Figure 5E). Collectively, our data point to the role of PRMT1 in transcriptionally promoting H3K27ac in IFN-associated genes where it regulates IFN-associated microglia clusters.

Figure_5
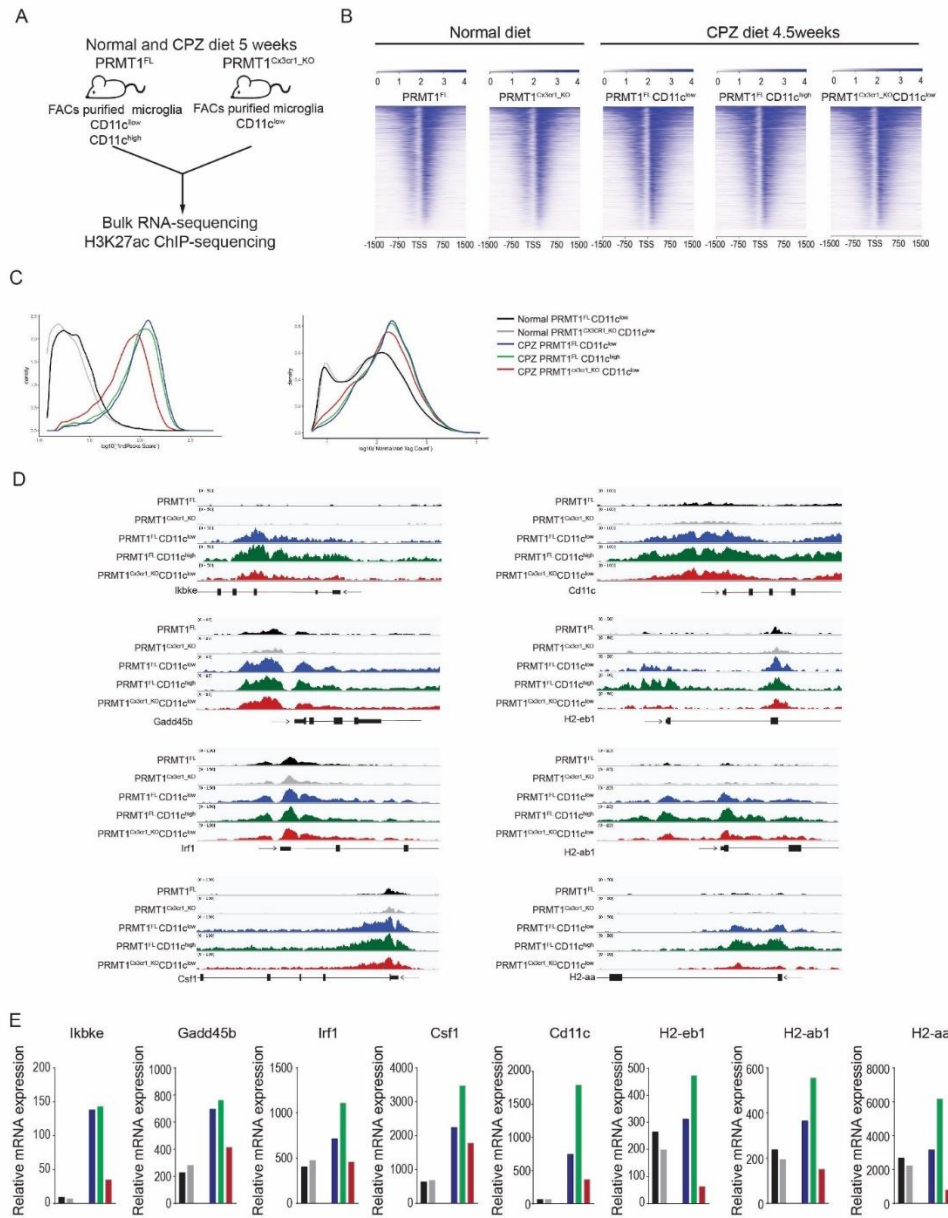
Figure 5 *PRMT1* **is required for the H3K27ac deposition at the promoters of the IFN-associated genes**

A, Schematic illustrating *PRMT1^{FL}*, and *PRMT1$^{Cx3cr1-KO}$* microglia ChIP- and RNA-sequencing during the normal and CPZ diet 5weeks.

B, H3K27ac enrichment at the transcriptional site (TSS) of genes in *PRMT1^{FL}*, *PRMT1$^{Cx3cr1-KO}$ PRMT1^{FL}* CD11c^{low}, *PRMT1^{FL}*CD11c^{high},and *PRMT1$^{Cx3cr1-KO}$*CD11c^{low} microglia

C, H3K27ac peaks and tag counts were illustrated according to the densities

D, A genome track of the IFN-associated locus displaying H3K27ac ChIP-seq in *PRMT1^{FL}*, *PRMT1$^{Cx3cr1-KO}$ PRMT1^{FL}* CD11c^{low}, *PRMT1^{FL}*CD11c^{high},and *PRMT1$^{Cx3cr1-KO}$*CD11c^{low} microglia **E**, mRNA-expression of IFN-associated genes in *PRMT1^{FL}*, *PRMT1$^{Cx3cr1-KO}$ PRMT1^{FL}* CD11c^{low}, *PRMT1^{FL}*CD11c^{high},and *PRMT1$^{Cx3cr1-KO}$*CD11c^{low} microglia

3.4.5 PRMT1 deficient bone-marrow-derived macrophages (BMDMs) exhibit IFN production defects

D*e novo* DNA motif analysis of the promoter regions genes from the IFN-associated clusters identified the Interferon Regulatory Factors (IRFs) transcription factors as being enriched (Supplemental Figure S4A). The IRFs are crucial transcription factors that regulate type I and type II IFN responses in the innate immune cells such as macrophages (McNab et al., 2015). We therefore questioned whether macrophages phenocopy the defective type I and II IFN responses observed in microglia. We utilized bone marrow-derived macrophages (BMDM) from $PRMT1^{Cx3cr1-KO}$ mice for this purpose, as they have similar function as microglia.

We collected bone marrow cells from $PRMT1^{Cx3cr1-KO}$ mouse and differentiated them into BMDM by supplementing them with the macrophage colony-stimulating factor (MCSF1)(Toda et al., 2021). Half the isolated $PRMT1^{Cx3cr1-KO}$ bone marrow cells were treated with 4-OHT to induce PRMT1 knockout (PRMT1-KO), while the other half was treated with vehicle for 7 days (WT). The PRMT1-KO and WT BMDMs were treated with type I (poly(I:C) or IFNβ) and type II (IFNγ) IFN agonists for 6 h (Figure 6A). The cells were subsequently analyzed for the activation of the IFN pathways by measuring IFN regulated pro-inflammatory transcripts including *Cxcl9, Cxcl10,* and *Il6* by RT-qPCR. We observed a defect in poly(I:C) induced *Cxcl9, Cxcl10,* and *Il6* expression in PRMT1-KO compared to WT BMDMs (Figure 6A). In contrast, no difference in *Cxcl9, Cxcl10,* and *Il6* expression was observed in the cultures treated with either IFNβ or IFNγ (Figure 6A). We further show that the poly(I:C) induction of two other IFN regulated genes *Ifnβ* and *Il12* were impaired in PRMT1-KO BMDMs (Figure 6B).

Because the loss of PRMT1inhibited the expression of IFNβ, we added recombinant IFNβ in combination with poly(I:C) to see if we could partially rescue the type I IFN responses in PRMT1-KO BMDMs. Indeed, the mRNA levels of *Cxcl9, Cxcl10,* and *Il6* were partially rescued

with the recombinant IFNβ treatment in PRMT1-KO BMDMs (Figure 6C). To further substantiate

the defective type I IFN phenotype, we performed FACS analysis for cell surface CD86, a marker

for pro-inflammatory M1 macrophages (Orecchioni et al., 2019). We observed a significant

increase in the CD86+ BMDMs in the WT with poly(I:C)(64.9%), but to a lesser extent in the

PRMT1-KO (24.3%)(Figure 6D, 4E). Moreover, the addition of IFNβ treatment in PRMT1-KO

BMDMs enhanced the CD86+ population from 38.2% to 67.%. Therefore these results indicate

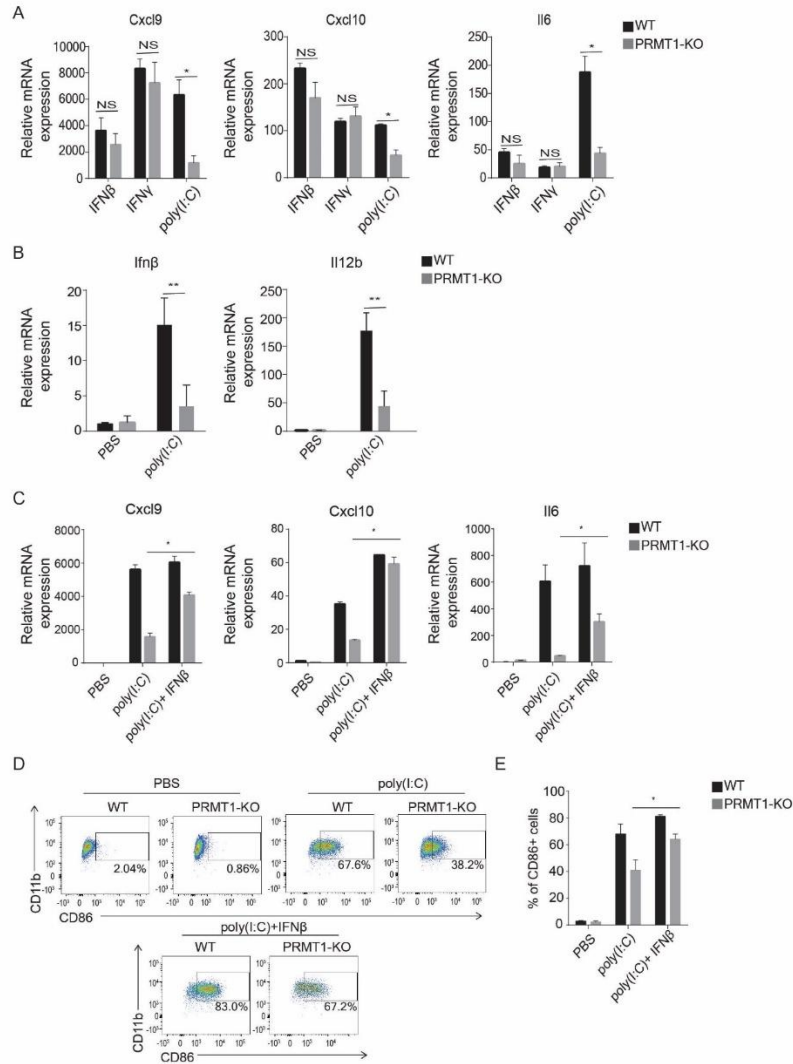that PRMT1 is required for the type I IFN response in the BMDMs.

Figure 6 The type I IFN signaling is perturbed with *PRMT1* deficiency in BMDMs
A, WT and PRMT1-KO BMDMs were treated with IFNβ (20ng/mL), IFNγ (20ng/mL), and Poly(I:C) (5mg/mL) respectively for 6 h and analyzed for pro-inflammatory molecules (*Cxcl9, Cxcl10* and *Il6*) using real-time PCR. Bar graph indicates the relative expressions of *Cxcl9, Cxcl10* and *Il6* normalized to GAPDH. Data presented as mean ± SEM. *P* values were analyzed using Mann–Whitney U-statistical test. (* *p*<0.05, NS: Not significant). **B,** Bar graph delineating expression levels of pro-inflammatory (*Ifnβ* and *Il12b*) molecules in PBS or poly(I:C) treated WT and KO BMDMs. Data presented as mean ± SEM. *P* values were analyzed using Mann–Whitney U-statistical test. (* *p*<0.05, ** *p*<0.01). **C,** WT and PRMT1-KO BMDMs were treated with PBS, Poly(I:C), and Poly(I:C)+IFNβ respectively for 6 h and analyzed for pro-inflammatory molecules (*Cxcl9, Cxcl10* and *Il6*) using real-time PCR. Bar graph indicates the relative expressions of *Cxcl9, Cxcl10* and *Il6* normalized to GAPDH. Data presented as mean ± SEM. *P* values were analyzed using Mann–Whitney U-statistical test. (* *p*<0.05) **D-E,** Representative FACs analysis of CD86+ BMDMs in WT and PRMT1-KO treated with PBS, Poly(I:C) and Poly(I:C)+IFNβ respectively for 24hrs. **E,** Bar graph visualizing percent positive of CD86 BMDMs. Data presented as mean ± SEM. *P* values were analyzed using Mann–Whitney U-statistical test. (* *p*<0.05)

3.5 Discussion

In this work, we show for the first time the role of PRMT1 in microglia during CPZ induced de/remyelination of the CNS. We found that PRMT1 but not PRMT5 is required to modify microglia phenotype to promote remyelination in the CNS. Inhibition of PRMT1 using Cx3cr1CreERT mice model completely blocked the remyelination process accompanied by prolonged microgliosis, astrogliosis with a reduction of total oligoprogenitor cells. Specifically, PRMT1 regulated IFN-associated microglia cluster expressing MHCII+ and CD11c+ during de/remyelination. Mechanistically, the loss of PRMT1 reduced the H3K27ac deposition at the promoters of the IFN-associated genes and reduced the expression of type I IFN-associated genes. Furthermore, PRMT1-KO BMDMs were defective in type I IFN response triggered with poly(I:C). Taken together, we identified a role for the PRMT1 in regulating the IFN-associated microglia population that is indispensable for remyelination in the CNS.

The loss of PRMT1 but not PRMT5 in microglia had significant ramifications in the CNS during the cuprizone diet. This finding was surprising since PRMT5 regulates a diverse spectrum of lymphocyte biology and is involved in pattern recognition receptors (PRR) sensing in BMDMs(Cui et al., 2020; Ma et al., 2021; Sengupta et al., 2020). However, since our study was limited to the cuprizone-diet model, we cannot rule out that PRMT5 might play a role during microglia development or in a different pathological context of the CNS. Thus, further studies are warranted to decipher the exact role of PRMT5 in microglia. Based on our RNA sequencing data, we did not observe any significant change in the gene expression between WT compared to PRMT-KO microglia during the basal condition. Nevertheless, upon CPZ-diet, the loss of PRMT1 had a profound impact on regulations of microglia subpopulations. This finding suggests that PRMT1 is required for microglia to become activated and transition to specific microglia subsets. Therefore,

further studies are needed to understand if PRMT1 could regulate the activation of different subtypes of microglia in a different pathological context.

We identified PRMT1 as a driver for IFN-associated microglia population that is required to regenerate myelin in the CNS, and this work extends the elegant work by Lloyd *et al*(Lloyd et al., 2019). They used myelin toxin lysophosphatidylcholine (LPC) to induce de/remyelination found type I IFN associated microglia populations during the remyelination. Further, inhibiting the IFN-signaling in microglia by using antibody against IFNAR2 impaired remyelination(Lloyd et al., 2019). Therefore, this result highlights the importance of the IFN-associated microglia cluster in promoting regeneration in the CNS. Given the substantial amount of research showing an IFN-associated microglia phenotype during neurodegenerative pathology and in brain injury, this suggests that different environmental factors can activate microglia and converge to IFN-signaling to protect or regenerate the CNS(Lloyd et al., 2019; Masuda et al., 2019; Mathys et al., 2017; Olah et al., 2020). Whether and how IFN-associated microglia arises are open areas of investigation. However, based on our data, we envision that, like most antigen-presenting cells, microglia use their PRR to detect the damaged cells, myelin debris, or aggregated proteins and activate the IFN response(Prinz et al., 2019).

Our results show that H3K27ac marks are lost at the promoter of the IFN-associated transcripts in microglia. The decrease in H3K27ac suggests that PRMT1 is required for the H3K27ac activity. However, how PRMT1 modulates the H3K27ac activity remains to be answered. One possible explanation could be that PRMT1-mediated methylation of H4R3me2a might promote H3K27ac at the promoter of the IFN-associated transcripts. Previous research showed H4R3me2a induces acetylation of H4 Lys8 and Lys12 and H3 Lys9(Huang et al., 2005; Wang et al., 2001). Therefore, if we can improve the method to ChIP H4R3me2a and align the

H4R3me2a ChIP-sequencing data with H3K27ac, it will give us a better idea if H4R3me2a acts as an activator to enhance the H3K27ac deposit.

Although identifying the driver for regenerative microglia is a critical step in gaining knowledge on microglia heterogeneity, much additional work is required in the future(Prinz et al., 2019; Wolf et al., 2017). For example, how PRMT1 mechanistically plays a role in driving an IFN-associated cluster will help elucidate a more defined signaling cascade and critical components leading to this cluster. Another essential aspect is understanding the functional role of IFN-associated clusters in augmenting the remyelination of the CNS. For example, does IFN-associated microglia directly impact remyelination by secreting regenerative factors to promote OPCs proliferation or differentiation? Or does it indirectly impact remyelination by communicating with other cells such as astrocytes? Future studies elucidating this conundrum could extend our finding to therapeutic application to induce remyelination in the CNS.

In sum, we report PRMT1 as a molecular driver of the IFN-associated microglia cluster. Therefore, enhancing PRMT1 expression might have therapeutic implications in promoting remyelination in the CNS.

3.6 Materials and methods

3.6.1 Mice

The *PRMT1^{FL}* (Yu et al, 2009) and *PRMT5^{FL}* (Calabreta et al) alleles were generated previously and maintained on the C57BL/6 background. These mice were bred with *Cx3cr1^{CreERT}* driver mice (Jackson lab # 021160). To induce the Cre recombinase activity, tamoxifen(T5648, Millipore-Sigma, Burlington, MA) dissolved in corn oil (C8267, Millipore-Sigma), and 100uL was intraperitoneally injected (1mg/mL) in 5–6-weeks-old mice for five consecutive days. For all mice

procedures, age- and sex-matched mice were used for the experiments. All animal works were carried out following the McGill University guidelines directed by the Canadian council of animal care.

3.6.2 Microglia isolation

To isolate microglia, adult mice were anesthetized by administrating isoflurane and perfused with ice-cold phosphate-buffered saline (PBS). The brain was isolated, chopped into fragments, and enzymatically dissociated using a neural tissue dissociation kit (Miltenyi Biotec Inc). To remove myelin debris, cells were spun down in 30% percoll gradient for 20 min at 600xg (accel 5, decel 1). The myelin layer was carefully discarded, and pellets were filtered through 70um strainer and washed two times with 1X Hank's Balanced Salt Solution (HBSS). Subsequently cells were stained in FACs buffer with targeted antibodies.

3.6.3 Flow cytometry

To isolate microglia, cells were first Fc-blocked with anti-CD16/32 (1:200, BD Biosciences). Cells were then stained with anti-CD11b APC (1:200, BioLegend), anti-CD45 BV786 (1:200, BD Biosciences), anti-CD11c PE (1:400, BioLegend), and anti-MHCII BUV737 (1:200, BD Biosciences) for 30 min at 4 C. Cells were washed with PBS and stained with LIVE/DEAD Fixable Aqua Dead Cell Stain (1:500, Invitrogen) for 20 min. CD11b+/CD45inter microglia were sorted utilizing a FACSAria Fusion (BD Bioscience). For BMDMs, cells were first blocked with anti-CD16/32 (1:200, BD Biosciences) and stained for anti-CD86 (), anti-F4/80 (), anti-CD11b() and anti-MHCII BUV737 (1:200, BD Biosciences). Cells were washed and stained for LIVE/DEAD Fixable far-red dead Cell Stain (1:500, Invitrogen) for 20 min and washed with PBS. Cells were analyzed on LSR Fortessa and FlowJo software (Tree Star).

3.6.4 Cuprizone diet

5-6 weeks old $PRMT1^{FL}$, $PRMT1^{Cx3cr1-KO}$, $PRMT5^{FL}$ and $PRMT5^{Cx3cr1-KO}$ mice were injected with tamoxifen and waited for 2weeks to start the cuprizone diet (CPZ). The 0.2% cuprizone (Millipore-Sigma) was mixed with the powdered standard diet (Envigo Teklad) and fed for five weeks. To induce remyelination, mice were fed with standard chow for 1 or 3 weeks.

3.6.5 Immunohistochemical analysis for in vivo brain section

Anesthetized mice were first perfused with PBS followed by 4% paraformaldehyde (PFA). Brains were isolated and incubated in 4% PFA for overnight and subsequently placed on graded sucrose (10%, 20%, 30%) for 24 h at 4C each. The brains were embedded with OCT compound and snap-frozen in a mixture of dry ice and isopentane. Next, 12µm of serial coronal section of the brain was sliced with a cryostat (Leitz Camera) and mounted immediately onto Superfrost (+) slides (Fisherbrand). Immunofluorescent staining was performed by blocking the sections with 5% bovine serum albumin (BSA) containing 0.3% Triton X-100 in PBS for 1hr. The following primary antibodies were incubated overnight at 4C: Iba-1 (1:200, WAKO), Iba-1 (1:200, Millipore), anti-GFAP (1:300, Abcam), anti-Olig2 (1:200, NovusBiologicals), and anti-Mac2 (1:200, Cedarlane) antibodies. Sections were washed three times with PBS and subsequently incubated for 1h with the following secondary conjugated antibodies at RT: Alexa Fluor 488 (1:200, Invitrogen) and Alexa Fluor 568 (1:200, Invitrogen). Counterstain was performed with DAPI for 30sec and mounted. For floating sections, 30µm of the coronal section was sliced and immersed in PBS and followed the procedure described above. The presence of myelin was observed using a Black-Gold II staining kit (TR-100-BG, Biosensis) according to the manufacture's instruction (Millipore, Temecula).

3.6.6 3D reconstruction of microglia

Free-floating 30μm of the coronal sections of brain were stained with anti-Iba-1 overnight at 4C, and secondary antibody was incubated for 2h at RT. Nuclei were stained with DAPI. Confocal images were taken at x40 oil immersion objective with 1um interval for 20μm depth using LSM880 Zeiss microscope. Microglia structure was rendered using IMARIS software.

3.6.7 Transmission electron microscope analysis

Mice were anesthetized and first perfused with 50mL of ice-cold PBS followed by 100mL of fixative solution (2.5% glutaraldehyde, 2.0% paraformaldehyde in 0.1M sodium cacodylate buffer at pH 7.4). Brains were isolated and incubated overnight in fixative solution at 4C. The corpus callosum were dissected out and postfixed in 1% aqueous OsO_4 (Mecalab) with 1.5% aqueous potassium ferrocyanide for 2 h. UltraCut E ultramicrotome (Reichert-Jung) was used to cut the tissues into 90–100 nm sections and placed in the 200 mesh copper grid (Electron Microscopy Sciences). Myelin layer was captured using an FEI Tecnai 12 120 kV transmission electron microscope equipped with an AMT XR80C 8 megapixel CCD camera (McGill University, Department of Anatomy and Cell Biology). At least 10 images are taken, and percentage of myelinated axons were quantified.

3.6.8 RNA isolation, cDNA synthesis, RT-qPCR analysis

As previously described, total RNA was extracted and purified using TRIzol (Invitrogen). Extracted RNA was quantified and cDNA synthesis was performed utilizing M-MLV reverse transcriptase (Promega). mRNA expression was measured using targeted primers with PowerUp SYBR Mastermix (Life Technologies), and applied on 7500 Fast Real-Time PCR System (Applied biosystem). All reactions were performed in duplicate and quantified using the "delta-delta Ct" method. The primers used in this study are listed in Supplementary Table 1.

138

3.6.9 Protein extraction and immunoblotting

Cells were lysed with RIPA buffer (50mM Tris pH 7.4, 150mM NaCl, 1mM DTT, 1% NP40, 0.1% SDS and 0.5% sodium deoxycholate) and placed on ice for 30min. Lysed extracts were centrifuged at 12,000 rpm for 10min in 4C. Protein concentration was quantified using Rapid Gold BCA Protein Assay Kit (PIA53227, Thermo Scientific). Equal amount of proteins were separated using SDS-PAGE and transferred to nitrocellulose membranes using an immunoblot TurboTransfer system (Bio-Rad). Membranes were blocked with 5% skim milk, and incubated with primary antibodies overnight at 4C (Supplementary Table 2). Appropriate HRP-conjugated secondary antibodies were applied for 1h at RT. Proteins were visualized by Western Lightning Plus ECL (PerkinElmer).

3.7.0 BMDM differentiation

Bone marrow cells were isolated from the 6–9-week-old $PRMT1^{FL}$ mouse. The tibia, femur, and spine were removed and crushed using mortar and pestle. Crushed lysates were passed through the 40µM strainer and washed with PBS. Lysates were spun down, and the supernatant was discarded. Cells were treated with red blood cell (RBC) lysis buffer for 30 seconds. Bone marrow cells were cultured in RPMI media containing 10% FBS, 1% penicillin-streptomycin, and 20% L929-conditioned media as a source of MCSF-1. To induce the KO of PRMT1, 2nM of 4-OHT or EtOH was treated for seven days. BMDMs were then polarized with either 20 ng/mL of IFNβ (R&D systems), 20 ng/mL of IFNγ (Peprotech), and 5ug/ml of poly (I:C) (Invivogen). Cells were then analyzed for real-time PCR, western blot and FACs analysis.

3.7.1 BV2 cell polarization

BV2 cells were purchased from IRCCS Ospedale Policlinico San Martino Genova. Cells were cultured in DMEM (Invitrogen) supplemented with 10% FBS and 1% penicillin-streptomycin.

Cells were treated with MS023(1μM) or DMSO for 48hrs and, treated with Poly(I:C) for 6hrs and harvested for protein and mRNA analysis.

3.7.2 ChIP and RNA sequencing analysis

Single-end reads of length 76 were first trimmed off the adapter sequence as well as the polyA tail and then mapped through the Bowtie2 short read aligner v2.4.1 to the hg19 reference genome from the University of California Santa Cruz (UCSC) (Lander et al., 2001; Langmead and Salzberg, 2012). Quality control checks on the raw sequence data were carried out through the FASTQC software v0.11.9. BAM files were sorted and indexed, and duplicate reads were removed through Samtools v0.1.19. Peak calling and motif enrichment for ChIP-seq experiments relative to the input was carried out by the Hypergeometric Optimization of Motif Enrichment (HOMER) software v4.11 in histone or super-enhancer mode using default parameters(Heinz et al., 2010). Average read coverage profiles across TSS, TTS or gene body regions and corresponding heatmaps were plotted with the NGS PLOT software (Shen et al., 2014). Density plots of reading coverage were made using the Integrative Genomics Viewer (IGV) software. Gene expression was quantified for RNA-seq experiments using HOMER, and the differential expression relative to the control was computed by DESeq2 (Love et al., 2014). Upregulated or downregulated genes were defined as having a false discovery rate (FDR) smaller than 0.05 and absolute log fold change larger than one.

3.7.3 Single-cell sequencing

Mice brains were harvested at five weeks of cuprizone diet and sorted according to CD11b+ and CD45+ by BD FACS Aria III (BD Biosciences). The single-cell library was prepared with the McGill Genome center using GemCode Single- Cell Instrument (10x Genomics, Pleasanton, CA, USA), and Single Cell 3' Library & Gel Bead Kit v2. The SPRIselect was used to purify the

libraries. Quality was assessed using the size distribution and yield(LabChip GX Perkin Elmer) was quantified by qPCR (KAPA Biosystems Library Quantification Kit for Illumina platforms P/N KK4824). Libraries were sequenced utilizing the Illumina NovaSeq6000 at IGM Genomics Center (UCSD, San Diego, CA). Paired-end reads of length 101 were aligned to the mm10 mouse genome using Cell Ranger v3.1.0 program (10X Genomics, https://support.10xgenomics.com/single-cell-gene-expression/software/pipelines/latest/what-is-cell-ranger). Afterwards, the Seurat v3.2.0 software was used to carry out quality control as well as for pre-processing analysis(Stuart et al., 2019). Cells containing less than 200 genes and more than 6000 genes were removed. Cells containing more than 10% of the mitochondria genes were filtered out. Reads counts were then normalized using the "LogNormalize" method. Next, we calculated highly variable features between cells, by applying the linear transformation. The dimensionality of the dataset was determined using an elbow plot. The cluster of the cells were visualized using a Uniform Manifold Approximation and Projection (UMAP). The scVelo v0.2.2 python module was used to perform RNA velocity analysis. Monocle 2 was used to analyze the single-cell pseudotime trajectories(Qiu et al., 2017a).

3.7.4 Quantification and Statistical analysis

All experiments were statistically tested using GraphPad Prism 6. All values were represented as means ± standard error of the mean (SEM). The specific tests used for analysis are indicated in the figure legends. The number of replicates and the animals are described in the figure legends. No blinding was performed during the animal experiments procedure and all the experiments were randomized. No outliers were excluded.

3.8 Acknowledgements

3.9 Supplemental information

Supplementary Figure 1
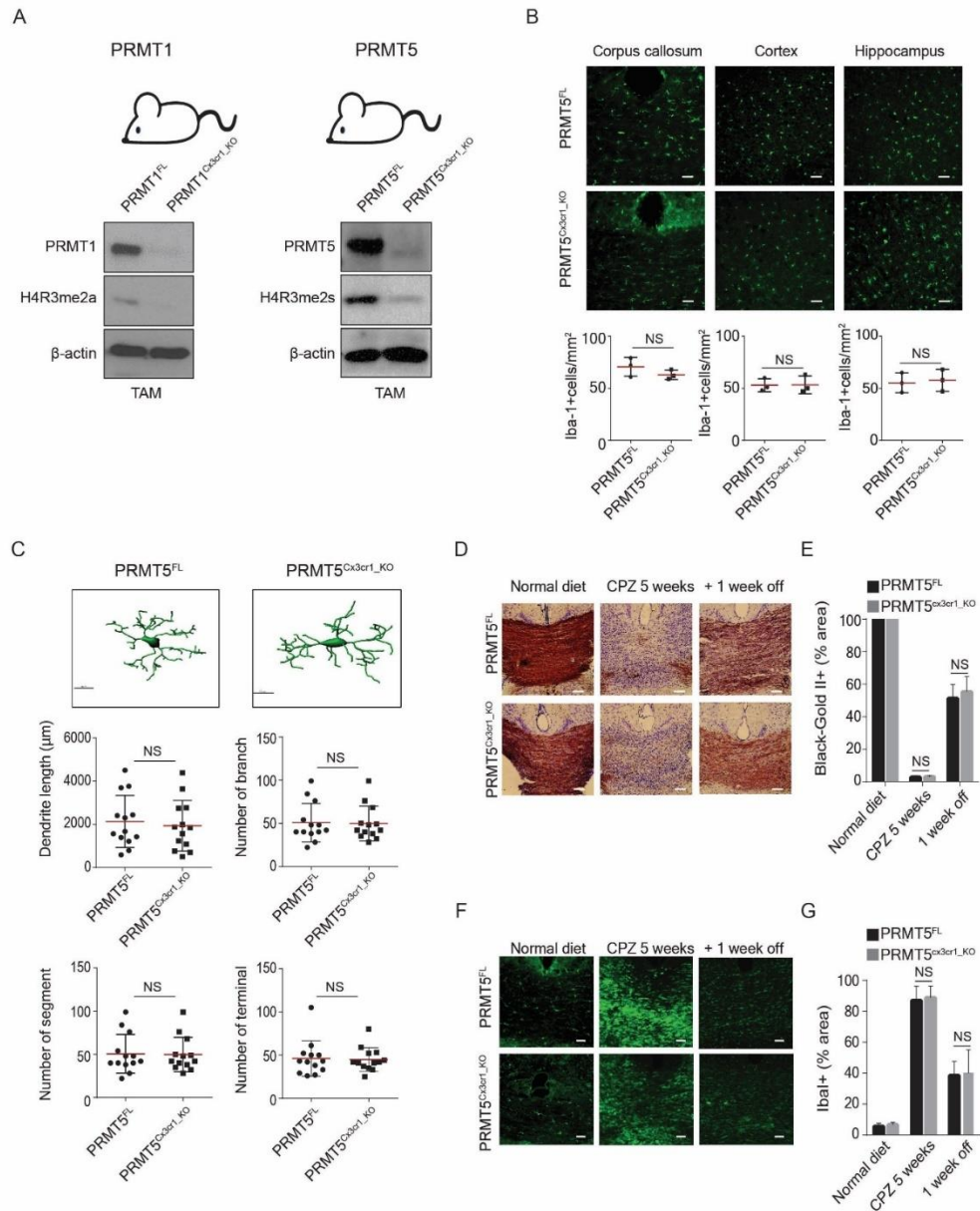
Supplementary Figure 1 *PRMT5* is dispensable for microglia function during the CPZ-induced demyelination and remyelination in the CNS

A, Scheme of the PRMT1 and PRMT5 mice models used in this study. Isolated microglia from *PRMT1^FL^*, and *PRMT1^Cx3cr1-KO^*, were blotted for PRMT1, H4R3me2a and β-actin. Isolated microglia from *PRMT5^FL^*, and *PRMT5^Cx3cr1-KO^* mice were blotted for PRMT5, H4R3me2s and β-actin.

B, Iba-1(green) staining in cortex, hippocampus and corpus callosum (CC) of *PRMT5^FL^* (n=3), and *PRMT5^Cx3cr1-KO^* (n=3) CNS. Representative images are shown. Scale bars represent 50 μm. Data presented as mean ± SEM. *P* values were analyzed using Mann–Whitney U-statistical test (NS: Not significant).

C, IMARIS based morphological analysis of microglia from $PRMT5^{FL}$ (n=3), and $PRMT5^{Cx3cr1-KO}$ (n=3) CNS. Representative images are shown. 10 cells were analyzed for dendritic length, number of branches, number of segments and terminals and presented as a dot plot. Scale bars represent 10 µm. Data presented as mean ± SEM. *P* values were analyzed using Mann–Whitney U-statistical test (NS: Not significant).

D, Mice fed with 0.2% cuprizone diet (CPZ) were sacrificed according to the following time points: Normal diet, CPZ diet 5 weeks (n=5) and CPZ diet 5weeks+ normal diet 1week (n=5). Black gold II staining (brown) was performed to visualize myelin and quantified at the CC of $PRMT5^{FL}$ (n=5), and $PRMT5^{Cx3cr1-KO}$ (n=5) CNS. Representative images are shown. Scale bars represent 50 µm.

E, Bar graph depicts average myelin staining in the CC. Data presented as mean ± SEM. *P* values were analyzed using Mann–Whitney U-statistical test (NS: Not significant). Scale bars represent 50µm.

F-G, Anti-Iba-1 (green) was stained during the normal diet, CPZ diet 5 weeks and CPZ diet 5weeks+normal diet 1week in $PRMT5^{FL}$ (n=5), and $PRMT5^{Cx3cr1-KO}$ (n=5). Representative images are shown. Scale bars represent 50 µm. **G,** Iba-1 staining was quantified at the CC and illustrated as a bar graph. Data presented as mean ± SEM. *P* values were analyzed using Mann–Whitney U-statistical test (NS: Not significant).
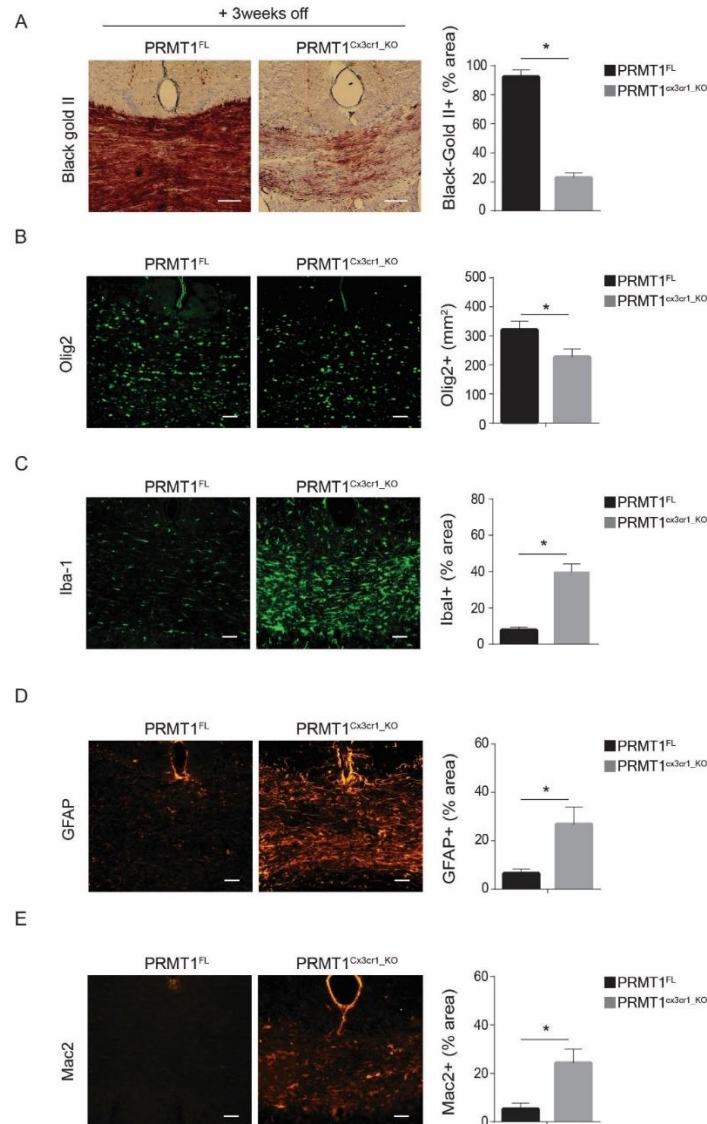
Supplementary Figure 2 CNS remyelination defects in *PRMT1*-deficient mice with 3 weeks of normal chow

Normal diet was extended for 3weeks and analyzed for the extent of remyelination, number of oligoprogenitor cells, microglia, astrocyte and activated microglia

A, Black gold II staining (brown) was performed to visualize myelin and quantified at the CC of $PRMT1^{FL}$ (n=4), and $PRMT1^{Cx3cr1-KO}$ (n=4) CNS. Representative images are shown. Scale bars represent 50 µm. Data presented as mean ± SEM. P values were analyzed using Mann–Whitney U-statistical test (* $p < 0.05$) .

B, Anti-Olig2 (green) was stained in $PRMT1^{FL}$ (n=4), and $PRMT1^{Cx3cr1-KO}$ (n=4) CNS. Representative images are shown. Scale bars represent 50 µm. Olig2 staining was quantified at the CC and illustrated as a bar graph. Data presented as mean ± SEM. P values were analyzed using Mann–Whitney U-statistical test (* $p<0.05$).

145

C, Anti-Iba-1 (green) was stained in *PRMT1^{FL}* (n=4), and *PRMT1$^{Cx3cr1-KO}$* (n=4) CNS. Representative images are shown. Scale bars represent 50 µm. Iba-1staining was quantified at the CC and illustrated as a bar graph. Data presented as mean ± SEM. *P* values were analyzed using Mann–Whitney U-statistical test (* *p*<0.05).

D, Anti-GFAP (orange) was stained in *PRMT1^{FL}* (n=4), and *PRMT1$^{Cx3cr1-KO}$* (n=4) CNS. Representative images are shown. Scale bars represent 50 µm. GFAP staining was quantified at the CC and illustrated as a bar graph. Data presented as mean ± SEM. *P* values were analyzed using Mann–Whitney U-statistical test (* *p*<0.05).

E, Anti-Mac2 (orange) was stained in *PRMT1^{FL}* (n=4), and *PRMT1$^{Cx3cr1-KO}$* (n=4) CNS. Representative images are shown. Scale bars represent 50 µm. Mac2 staining was quantified at the CC and illustrated as a bar graph. Data presented as mean ± SEM. *P* values were analyzed using Mann–Whitney U-statistical test (* *p*<0.05).

Supplementary Figure 3
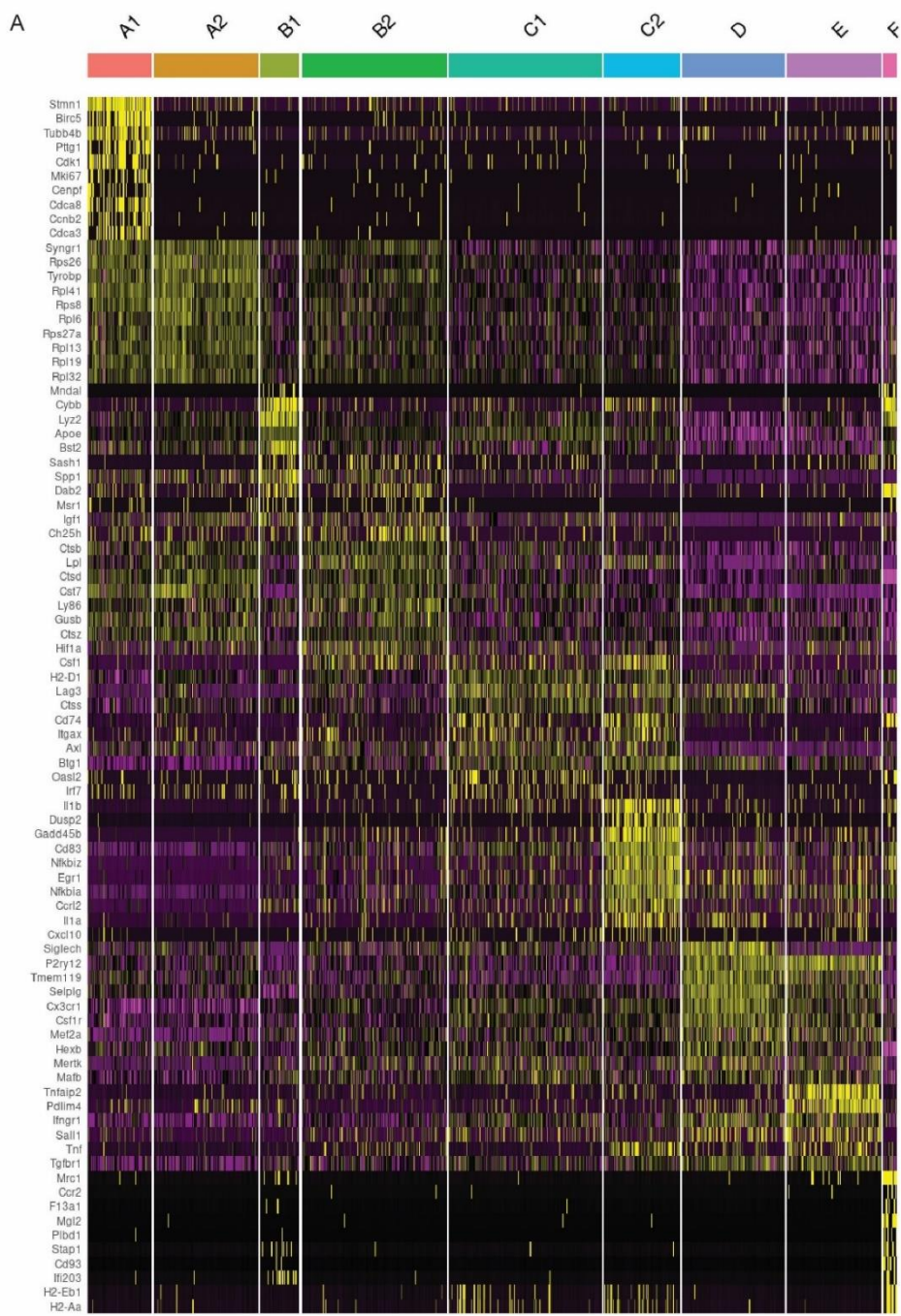
Supplementary Figure 3 A. Heat map of marker genes according to the microglial clusters.

Supplementary Figure 4

A

Motif enriched in IFN-associated cluster (C1)

Motif	Name	P-value	# Target Sequences with Motif
	IRF3	1e-10	17
	IRF2	1e-6	9
	IRF8	1e-6	10
	IRF1	1e-6	15
	FOXP1	1e-3	9
	Foxo3	1e-3	11

Motif enriched in IFN-associated cluster (C2)

Motif	Name	P-value	# Target Sequences with Motif
	NFkB-p65-Rel	1e-10	14
	TATABox	1e-5	46
	HOXB13	1e-4	29.0
	Atf1	1e-3	33.0
	PU.1:IRF8	1e-3	13.0
	ATF2	1e-3	23.0

Supplementary Figure 4 A. *De novo* **motif analysis for cluster C1 and C2**

References

Bedford, M.T., and Clarke, S.G. (2009). Protein arginine methylation in mammals: who, what, and why. Mol Cell *33*, 1-13.

Bergen, V., Lange, M., Peidli, S., Wolf, F.A., and Theis, F.J. (2020). Generalizing RNA velocity to transient cell states through dynamical modeling. Nat Biotechnol *38*, 1408-1414.

Cui, S., Yu, Q., Chu, L., Cui, Y., Ding, M., Wang, Q., Wang, H., Chen, Y., Liu, X., and Wang, C. (2020). Nuclear cGAS Functions Non-canonically to Enhance Antiviral Immunity via Recruiting Methyltransferase Prmt5. Cell Rep *33*, 108490.

Fatoba, O., Itokazu, T., and Yamashita, T. (2020). Microglia as therapeutic target in central nervous system disorders. J Pharmacol Sci *144*, 102-118.

Guccione, E., and Richard, S. (2019). The regulation, functions and clinical relevance of arginine methylation. Nat Rev Mol Cell Biol *20*, 642-657.

Gudi, V., Gingele, S., Skripuletz, T., and Stangel, M. (2014). Glial response during cuprizone-induced de- and remyelination in the CNS: lessons learned. Front Cell Neurosci *8*, 73.

Gudi, V., Moharregh-Khiabani, D., Skripuletz, T., Koutsoudaki, P.N., Kotsiari, A., Skuljec, J., Trebst, C., and Stangel, M. (2009). Regional differences between grey and white matter in cuprizone induced demyelination. Brain Res *1283*, 127-388.

Heinz, S., Benner, C., Spann, N., Bertolino, E., Lin, Y.C., Laslo, P., Cheng, J.X., Murre, C., Singh, H., and Glass, C.K. (2010). Simple combinations of lineage-determining transcription factors prime cis-regulatory elements required for macrophage and B cell identities. Mol Cell *38*, 576-589.

Huang, S., Litt, M., and Felsenfeld, G. (2005). Methylation of histone H4 by arginine methyltransferase PRMT1 is essential in vivo for many subsequent histone modifications. Genes Dev *19*, 1885-1893.

Lander, E.S., Linton, L.M., Birren, B., Nusbaum, C., Zody, M.C., Baldwin, J., Devon, K., Dewar, K., Doyle, M., FitzHugh, W.*, et al.* (2001). Initial sequencing and analysis of the human genome. Nature *409*, 860-921.

Langmead, B., and Salzberg, S.L. (2012). Fast gapped-read alignment with Bowtie 2. Nat Methods *9*, 357-359.

Li, Q., and Barres, B.A. (2018). Microglia and macrophages in brain homeostasis and disease. Nat Rev Immunol *18*, 225-242.

Lloyd, A.F., Davies, C.L., Holloway, R.K., Labrak, Y., Ireland, G., Carradori, D., Dillenburg, A., Borger, E., Soong, D., Richardson, J.C.*, et al.* (2019). Central nervous system regeneration is driven by microglia necroptosis and repopulation. Nat Neurosci *22*, 1046-1052.

Lloyd, A.F., and Miron, V.E. (2019). The pro-remyelination properties of microglia in the central nervous system. Nat Rev Neurol *15*, 447-458.

Love, M.I., Huber, W., and Anders, S. (2014). Moderated estimation of fold change and dispersion for RNA-seq data with DESeq2. Genome Biol *15*, 550.

Ma, D., Yang, M., Wang, Q., Sun, C., Shi, H., Jing, W., Bi, Y., Shen, X., Ma, X., Qin, Z.*, et al.* (2021). Arginine methyltransferase PRMT5 negatively regulates cGAS-mediated antiviral immune response. Sci Adv *7*.

Masuda, T., Sankowski, R., Staszewski, O., Bottcher, C., Amann, L., Sagar, Scheiwe, C., Nessler, S., Kunz, P., van Loo, G.*, et al.* (2019). Spatial and temporal heterogeneity of mouse and human microglia at single-cell resolution. Nature *566*, 388-392.

Masuda, T., Sankowski, R., Staszewski, O., and Prinz, M. (2020). Microglia Heterogeneity in the Single-Cell Era. Cell Rep *30*, 1271-1281.

Mathys, H., Adaikkan, C., Gao, F., Young, J.Z., Manet, E., Hemberg, M., De Jager, P.L., Ransohoff, R.M., Regev, A., and Tsai, L.H. (2017). Temporal Tracking of Microglia Activation in Neurodegeneration at Single-Cell Resolution. Cell Rep *21*, 366-380.

Matsushima, G.K., and Morell, P. (2001). The neurotoxicant, cuprizone, as a model to study demyelination and remyelination in the central nervous system. Brain Pathol *11*, 107-116.

McNab, F., Mayer-Barber, K., Sher, A., Wack, A., and O'Garra, A. (2015). Type I interferons in infectious disease. Nat Rev Immunol *15*, 87-103.

Olah, M., Menon, V., Habib, N., Taga, M.F., Ma, Y., Yung, C.J., Cimpean, M., Khairallah, A., Coronas-Samano, G., Sankowski, R.*, et al.* (2020). Single cell RNA sequencing of human microglia uncovers a subset associated with Alzheimer's disease. Nat Commun *11*, 6129.

Orecchioni, M., Ghosheh, Y., Pramod, A.B., and Ley, K. (2019). Macrophage Polarization: Different Gene Signatures in M1(LPS+) vs. Classically and M2(LPS-) vs. Alternatively Activated Macrophages. Front Immunol *10*, 1084.

Prinz, M., Jung, S., and Priller, J. (2019). Microglia Biology: One Century of Evolving Concepts. Cell *179*, 292-311.

Qiu, X., Hill, A., Packer, J., Lin, D., Ma, Y.A., and Trapnell, C. (2017a). Single-cell mRNA quantification and differential analysis with Census. Nat Methods *14*, 309-315.

Qiu, X., Mao, Q., Tang, Y., Wang, L., Chawla, R., Pliner, H.A., and Trapnell, C. (2017b). Reversed graph embedding resolves complex single-cell trajectories. Nat Methods *14*, 979-982.

Rotshenker, S. (2009). The role of Galectin-3/MAC-2 in the activation of the innate-immune function of phagocytosis in microglia in injury and disease. J Mol Neurosci *39*, 99-103.

Sengupta, S., Kennemer, A., Patrick, K., Tsichlis, P., and Guerau-de-Arellano, M. (2020). Protein Arginine Methyltransferase 5 in T Lymphocyte Biology. Trends Immunol *41*, 918-931.

Shen, L., Shao, N., Liu, X., and Nestler, E. (2014). ngs.plot: Quick mining and visualization of next-generation sequencing data by integrating genomic databases. BMC Genomics *15*, 284.

Stuart, T., Butler, A., Hoffman, P., Hafemeister, C., Papalexi, E., Mauck, W.M., 3rd, Hao, Y., Stoeckius, M., Smibert, P., and Satija, R. (2019). Comprehensive Integration of Single-Cell Data. Cell *177*, 1888-1902 e1821.

Toda, G., Yamauchi, T., Kadowaki, T., and Ueki, K. (2021). Preparation and culture of bone marrow-derived macrophages from mice for functional analysis. STAR Protoc *2*, 100246.

Vega-Riquer, J.M., Mendez-Victoriano, G., Morales-Luckie, R.A., and Gonzalez-Perez, O. (2019). Five Decades of Cuprizone, an Updated Model to Replicate Demyelinating Diseases. Curr Neuropharmacol *17*, 129-141.

Wang, H., Huang, Z.Q., Xia, L., Feng, Q., Erdjument-Bromage, H., Strahl, B.D., Briggs, S.D., Allis, C.D., Wong, J., Tempst, P.*, et al.* (2001). Methylation of histone H4 at arginine 3 facilitating transcriptional activation by nuclear hormone receptor. Science *293*, 853-857.

Wolf, S.A., Boddeke, H.W., and Kettenmann, H. (2017). Microglia in Physiology and Disease. Annu Rev Physiol *79*, 619-643.

Xu, J., and Richard, S. (2021). Cellular pathways influenced by protein arginine methylation: Implications for cancer. Mol Cell *81*, 4357-4368.

Yokoo, H., Nobusawa, S., Takebayashi, H., Ikenaka, K., Isoda, K., Kamiya, M., Sasaki, A., Hirato, J., and Nakazato, Y. (2004). Anti-human Olig2 antibody as a useful immunohistochemical marker of normal oligodendrocytes and gliomas. Am J Pathol *164*, 1717-1725

CHAPTER 4: GENERAL DISCUSSION

Multiple sclerosis (MS) is the most common neurological autoimmune disease of the CNS. MS affects an estimated 2 million people globally with no available cure (Hartung et al., 2019). Thus far, the main focus of disease-modifying therapies (DMTs) for MS has been suppressing the infiltration or activation of lymphocytes to the CNS (Hartung et al., 2019). However, even though DMTs have spectacularly reduced relapses and slowed disability, they are unable to fully cure or prevent MS. Along with lymphocytes, the MS environment consists of numerous other immune cell types, including microglia, which emerges as a crucial contributor to the MS pathogenesis (Guerrero and Sicotte, 2020). Likewise single-cell technologies have demonstrated that microglia exhibit considerable phenotypic heterogeneity and that their phenotypes can be damaging or beneficial for MS disease progression (Voet et al., 2019). For example, beneficial microglia express specific markers (CD11c, IGF1, CSF1) and promote remyelination by recruiting and expanding OPCs or triggering differentiation of OPCs (Lloyd and Miron, 2019; Voet et al., 2019). Conversely, detrimental microglia have impaired phagocytic ability and secrete proinflammatory molecules, ROS and nitric oxide that can exacerbate neurodegeneration (Lloyd and Miron, 2019; Voet et al., 2019). Still, many questions remain regarding the molecular mechanisms that drive the creation of beneficial or damaging microglia during MS progression. To tackle these questions, many studies are trying to identify the molecular drivers that can tweak the essential functions of microglia to potentially enhance the remyelination of the CNS.

In my Ph.D. study, I was interested in seemingly very different two proteins, QKI and PRMT1, in modulating the microglial phenotype. As mentioned in the introduction, QKI is an RBP that regulates the diverse RNA biogenesis. PRMT1 is a methyltransferase known to methylate proteins, including RBPs, thereby indirectly controlling mRNA biogenesis. Even with extensive ongoing research in the microglia field, how RBPs or RBP regulating proteins modulate the microglial functions have never been investigated. By utilizing the transgenic mouse model and CPZ-diet to induce de/remyelination, I have uncovered QKI and PRMT1 as drivers for regenerative microglia that are indispensable to promote remyelination of the CNS. My findings have therefore identified previously unknown molecular drivers of regenerative microglia and thus broadened our understanding in the field of microglia biology.

4.1 QKI-deficient microglia phenotype

Microglia are versatile immune cells with the ability to acquire distinctive morphological appearances and transcriptional signatures leading to the spectrum of phenotypes (Masuda et al., 2020b). The deletion of QKI in microglia triggered amoeboid morphology with increased DAM and pro-inflammatory transcriptional signatures and decreased phagocytosis. This phenotype mimics the aged microglia signature found in the Alzheimer's disease (AD), Parkinson's disease (PD), stroke and epilepsies (Candlish and Hefendehl, 2021). The aged microglia present amoeboid morphology and secrete pro-inflammatory molecules with impaired phagocytosis, further contributing to the neurodegeneration (Candlish and Hefendehl, 2021). During de/remyelination, both the QKI- and PRMT1-deficient microglia impaired the remyelination process in the CNS. However, the mechanism leading to the compromised remyelination capacity differs between the QKI- and PRMT1-deficient microglia. Unlike the PRMT1-deficiency, the loss of QKI did not lose

the CD11c+ subpopulation during the CPZ diet and therefore maintained the IFN-associated microglia cluster. As mentioned in Chapter 2 of the discussion, the impaired remyelination is possibly due to the defective phagocytosis of microglia. This could be due to the deregulated alternative splicing of endocytosis-associated transcripts. However, I did not perform RNA-seq based splicing analysis on QKI-deficient microglia during the CPZ diet. Thus, further research is required to understand the critical alternative splicing events mediated by QKI, during the CPZ induced de/remyelination.

As I saw a decrease in QKI expression in microglia of the MS patient samples, it would be interesting to know if the expression of QKI is lost in the microglia of age-related neurodegenerative diseases. If I see the decrease in QKI expression, finding the contributing factors for the QKI deregulation in microglia would be interesting to investigate. In various cancers, QKI expression is downregulated, which is induced by the different microRNAs (miRNAs) that bind to the 3'UTR of the QKI mRNA to repress the translation of QKI (Kim et al., 2019; Mukohyama et al., 2019). Therefore, similar to this mechanism, other cell types in the CNS might secrete exosomal miRNAs that can be taken up by microglia to reduce the expression of QKI (Xia et al., 2019).

4.2 QKI as an alternative splicing regulator

As mentioned previously, QKI binds to a specific mRNA sequence, termed QRE, located within introns (Galarneau and Richard, 2005b). These sequences can be half QREs (ACUAAY) or full QREs (ACUAAY(1–20nt) UAAY (Y; C/U)(Galarneau and Richard, 2005b). To my surprise, I found only 40% of QKI-regulates spliced genes contained a full QRE, and 70% of the transcripts contained a half QRE. Therefore I was intrigued to determine if the transcripts without a QRE

contained another specific motif to which QKI could bind. Unfortunately, I did not find any significant motifs within the introns or exons of these spliced transcripts. This then led me to question how QKI can impact the splicing of transcripts without QREs. One possibility is that QKI could form a complex with other RBPs and impact the splicing of these mRNAs indirectly. Another hypothesis is that QKI could modulate the alternative splicing, and stability, of various RBPs. This might then impact the splicing ability of RBP, and result in the alternative splicing of transcripts without QREs. To answer these questions, I could further perform mass-spec or bio-spec analysis to look for RBPs interacting with QKI. I could further look for the presence of alternative splicing events of RBPs in the QKI-KO splicing data sets. This would improve our understanding of how QKI regulates alternative splicing events for various transcripts, independent of the presence of a QRE.

4.3 Therapeutic perspective on QKI-regulated splicing in microglia

The role of QKI in microglia seems endless, and alternative splicing mediated by QKI may be crucial for microglia functions in multiple pathological contexts. One major hurdle in the alternative splicing field is that we still lack the technological tool to screen for the consequences of alternative splicing events. According to previous and our RNA-seq based splicing analysis, QKI regulates more than 200 splicing events in different cell types. However, we only know a handful of alternative splicing events that functionally mediate cellular physiology. Therefore, better screening systems are required to monitor how each of the mis-spliced transcripts leads to altered protein functions and cellular phenotype. One way to answer this question would be through designing a genome-wide screening tool using the CRISPR/Cas9 system to induce individual splicing events by incorporating antisense oligonucleotide (ASO) technology. ASO is

a short, single-stranded oligodeoxynucleotide that can alter transcript splicing by directly binding to the targeted mRNAs and sterically blocking the attachment of splicing factors (Rinaldi and Wood, 2018). Each ASO can be barcoded and manufactured to target the QRE sequence located in the proximal regions of specific exons. Ideally, the ASOs will inhibit the binding of QKI and generate the same splicing events observed in QKI-deficient microglia. Finally, the barcoded ASOs can be transfected into microglia cell lines that can then be screened for phagocytic and cytokine secretion abilities.

By utilizing this system, I can potentially identify the crucial splicing events and ASOs that could either enhance microglia's phagocytic, inflammatory or regenerative abilities. Finally, I can deliver ASOs either by using the right bioconjugates or lipid nanoparticles (LNPs) to precisely and effectively target microglia. ASO therapies appear promising as two of the ASO therapies have been approved by the FDA for spinal muscular atrophy (SMA), and Duchenne muscular dystrophy (DMD) (Rinaldi and Wood, 2018). In addition, several companies are putting a large number of resources into modifying the ASOs and developing a bioconjugates or LNPs to cross the blood-brain barrier (BBB) to treat diverse neurological diseases (Rinaldi and Wood, 2018)(Zhao et al., 2020). Improved understanding of QKI-mediated alternative splicing events and enhanced delivery method hold exciting potential for future clinical applications to treat neurological diseases.

4.4 IFN-associated cluster

I also found a complete loss of remyelination capacity in the PRMT1-deficient mouse model. Systematic single-cell transcriptomic analysis of WT and PRMT1-deficient microglia during the CPZ diet revealed that the PRMT1-deficient microglia lacked a microglial population that

expressed surface marker CD11c, which I termed it as IFN-associated microglia. The possible role of the IFN-associated microglia cluster in mediating remyelination is further discussed in Chapter 3 of the discussion. However, another burning question that I want to address is how does the IFN-associated microglia cluster arises in the context of de/remyelination?

In the presence of the β-amyloid fibrils, one of pathological hallmark of AD, microglia use the scavenger receptors (A1, CD36, CD47, CD14, and TLRs) to detect the β-amyloid fibrils, which can then activate pro-inflammatory signaling cascades (Zhang et al., 2021). Also, the accumulation of α-synuclein are ingested by microglia which is mediated by the TLR4-NFkb signaling axis (Choi et al., 2020). Previous studies have also revealed that the saturated fatty acids are sensed by liver macrophages in a TLR4 dependent manner and produce pro-inflammatory cytokine (Diehl et al., 2020). Therefore, the TLR4 could potentially act as a major sensor to detect myelin debris during the demyelination, which give rise to the IFN-associated microglia population.

4.5 Trajectory of microglia during de/remyelination

Transcriptional changes in microglia during de/remyelination processes has been previously defined; however, our study provides an improved sequencing resolution with cellular clusters defined by specific markers. In addition, using two independent trajectory analyses, I found specific transitional states of microglia. According to this analysis, microglia engulf damaged oligodendrocytes, turn on IFN signaling to present MHCII receptors on their surface, and secrete a diverse range of cytokines. This trajectory is reminiscent of the transitional state of phagocytic antigen-presenting cells (APCs) (Gaudino and Kumar, 2019). These APCs are primary phagocytes that can engulf foreign materials, degrade these materials by forming phagolysosomes, present part of the foreign antigens on the cell surface using MHCII, and secrete cytokines and chemokines

to recruit and activate adaptive immune cells (Gaudino and Kumar, 2019). As the main phagocytic cell type in the CNS, microglia embark on a similar trajectory to APCs. However, in the CNS, microglia are the only immune cells without any adaptive immune cell capabilities. It would therefore be interesting to uncover the functional role of APC-like microglia (Prinz et al., 2019). As increasing studies demonstrate the complex interplay between microglia and other cell types, including astrocytes, oligodendrocytes, and OPCs, in playing a significant role in disease pathogenesis(Liddelow et al., 2020; Szepesi et al., 2018). I can also observe the profound interaction between microglia and astrocyte during demyelination, as they localize extensively at the CC of the CNS. In addition, in the PRMT1-KO microglia mouse, change to the regular chow sustained the activation and accumulation of microglia, accompanied by the prolonged activation of astrocytes. Whether or not activated astrocytes contribute to the impaired remyelination is subjected to further studies. In addition, the signaling molecules or surface receptors responsible for the microglia-astrocyte interaction will be an exciting avenue for ongoing research.

4.6 The role of PRMT1 in IFN pathway

Another significant finding of our study was the identification of PRMT1 as a driver of the IFN-associated cluster, and type I IFN responses, in BMDMs. I used our cx3cr1-cre-ert2 system to delete PRMT1 in bone-marrow cells and differentiated these cells into macrophages. To our surprise, the loss of PRMT1 did not impact macrophage differentiation or cell number. Interestingly, treatment with IFNβ or IFNγ had no impact on type I and II IFN responses in PRMT1-KO BMDMs. However, treatment with poly(I:C) significantly suppressed the type I IFN response in the PRMT1-KO BMDMs, indicating that PRMT1 is involved in the anti-viral sensing pathway. Previously it was shown that the PRMT5 and PRMT7 methylate proteins involved in the

anti-viral sensing pathway and modulate type I IFN activity (Ma et al., 2021; Zhu et al., 2021). Therefore, it is plausible that PRMT1 mediates the methylation of a protein involved in anti-viral sensing and control the type I IFN pathway. Also, PRMT1 is known to methylate RBPs and control the alternative splicing of transcripts (Li et al., 2021; Zhang et al., 2015) ((Newman et al., 2016; Uchida et al., 2019). Therefore, PRMT1 might mediate methylation of RBPs and indirectly contribute to the IFN responses in microglia and macrophages.

4.7 Therapeutic potential of PRMT1 in microglia

According to previous and our studies, the IFN-associated microglia population might contribute to the remyelination process and ameliorate MS disease progression. Our genetic knock-out mouse model identified that the PRMT1 is the driver for IFN-associated microglia cluster. To extend this concept to the therapeutic avenue for MS, we can first check the expression of PRMT1 in microglia in the MS patient tissue samples. If the PRMT1 expression is lost, we can think of an option to restore the expression of PRMT1 in microglia. For example, we can utilize mRNA therapy where PRMT1 mRNA is administered to the patient to compensate for the loss of PRMT1 in microglia (Damase et al., 2021). Alternatively, we can deliver a combination of immunomodulators to the CNS to promote IFN-associated microglia populations by utilizing mRNA therapy (Damase et al., 2021). Similar work is ongoing with BioNTech in which mRNAs encoding different immune molecules are delivered to the tumor in order to activate a certain population of T cells (Damase et al., 2021). The crucial part of this therapy is to design an LNP that can cross the blood-brain barrier and specifically target microglia. Recent publication partially resolved this issue by designing BBB-permeable LNPs by utilizing neurotransmitter-derived lipidoids (NT-lipidoids)(Ma et al., 2020). Lastly, we can use human pluripotent stem cells (hPSCs) to generate

158

microglia that can be transplanted back to the patient (Xu et al., 2020). For example, we can Crispr edit the hPSCs-derived microglia to promote the IFN-associated microglia phenotype and transplant back to the MS patients.

4.8 Technical modifications for the future experiments

Lastly, I want to highlight experimental procedures that could be modified in the future to improve the microglia and MS research. First, I used Cx3cr1-cre based mouse model to conditionally delete targeted proteins in microglia. This mouse-model targets microglia, peripheral immune cells and CNS-associated macrophages (Wolf et al., 2013). To exclusively target microglia, I can utilize the Hexb-cre mouse model, which was elegantly demonstrated in 2020 to target only microglia (Masuda et al., 2020a). Secondly, transcriptional profile of microglia change during the *ex vivo* isolation from the mouse brain (Woolf et al., 2021). This can be partially avoided by using certain inhibitor cocktails that might reduce cell preparation artifacts (Woolf et al., 2021). Thirdly, I used the CPZ diet to analyze the function of QKI- and PRMT1- deficient microglia during de/myelination pathology of the CNS. This mouse model is great at focusing on microglia, astrocyte, or oligoprogenitor functions but does not accurately recapitulate the condition found in MS patients. The EAE mouse model better resembles the microenvironment of MS with infiltration of lymphocytes and peripheral myeloid cells to the CNS, therefore this model will be suitable for the future research(Constantinescu et al., 2011). Lastly, the phagocytosis assay, cytokine array, and immunofluorescent analysis of microglia were performed using *ex vivo* isolated microglia cultured *in vitro*. Unfortunately, culturing microglia *in vitro* changes the complete transcriptional and epigenetic profiles of microglia that we can almost consider as a different cell type (Gosselin et al., 2017). However, the current methodologies do not provide an

alternative method in culturing isolated microglia to maintain the microglia signature. Thus, future research is required to construct a 3D-brain-like tissue model to better recapitulate the CNS microenvironment that can maintain microglia signature *ex vivo* (Raimondi et al., 2020).

CHAPTER 5: A FINAL CONCLUSION AND THE SUMMARY

The thesis focused on defining the roles of QKI and PRMT1 in microglia during the CPZ-induced de/remyelination in the CNS. The major contribution to the original knowledge are summarized below.

1. QKI, PRMT1, and PRMT5 deficient microglia in vivo models were generated

2. QKI is microexon regulator in microglia

3. QKI regulated microexons were associated with Rho-GTPase pathway

4. The loss of QKI activates RhoA-GTP and Rock2 pathway

5. QKI-deficient microglia are pro-inflammatory and defective at phagocytosis function

6. The loss of QKI impairs remyelination process

7. QKI-5 expression is down-regulated in the MS patient samples

8. PRMT1 is required for the remyelination process

9. PRMT1 regulates IFN-associated microglia cluster

10. PRMT1 affects the H3K27ac deposition at the promoters of IFN-associated transcripts

11. PRMT1-KO BMDMs are defective in dsRNA induced type I IFN response

CHAPTER 6: REFERENCES

Aberg, K., Saetre, P., Lindholm, E., Ekholm, B., Pettersson, U., Adolfsson, R., and Jazin, E. (2006). Human QKI, a new candidate gene for schizophrenia involved in myelination. Am J Med Genet B Neuropsychiatr Genet *141B*, 84-90.

Aguzzi, A., Barres, B.A., and Bennett, M.L. (2013). Microglia: scapegoat, saboteur, or something else? Science *339*, 156-161.

Ahnert-Hilger, G., Holtje, M., Grosse, G., Pickert, G., Mucke, C., Nixdorf-Bergweiler, B., Boquet, P., Hofmann, F., and Just, I. (2004). Differential effects of Rho GTPases on axonal and dendritic development in hippocampal neurones. J Neurochem *90*, 9-18.

Ajami, B., Bennett, J.L., Krieger, C., Tetzlaff, W., and Rossi, F.M. (2007). Local self-renewal can sustain CNS microglia maintenance and function throughout adult life. Nat Neurosci *10*, 1538-1543.

Ajami, B., Samusik, N., Wieghofer, P., Ho, P.P., Crotti, A., Bjornson, Z., Prinz, M., Fantl, W.J., Nolan, G.P., and Steinman, L. (2018). Single-cell mass cytometry reveals distinct populations of brain myeloid cells in mouse neuroinflammation and neurodegeneration models. Nat Neurosci *21*, 541-551.

Almolda, B., Gonzalez, B., and Castellano, B. (2010). Activated microglial cells acquire an immature dendritic cell phenotype and may terminate the immune response in an acute model of EAE. J Neuroimmunol *223*, 39-54.

Alonso, A., and Hernan, M.A. (2008). Temporal trends in the incidence of multiple sclerosis: a systematic review. Neurology *71*, 129-135.

Anna, A., and Monika, G. (2018). Splicing mutations in human genetic disorders: examples, detection, and confirmation. J Appl Genet *59*, 253-268.

Antoine-Bertrand, J., Villemure, J.F., and Lamarche-Vane, N. (2011). Implication of rho GTPases in neurodegenerative diseases. Curr Drug Targets *12*, 1202-1215.

Auweter, S.D., Fasan, R., Reymond, L., Underwood, J.G., Black, D.L., Pitsch, S., and Allain, F.H. (2006). Molecular basis of RNA recognition by the human alternative splicing factor Fox-1. EMBO J *25*, 163-173.

Baralle, F.E., and Giudice, J. (2017). Alternative splicing as a regulator of development and tissue identity. Nat Rev Mol Cell Biol *18*, 437-451.

Baranzini, S.E., and Oksenberg, J.R. (2017). The Genetics of Multiple Sclerosis: From 0 to 200 in 50 Years. Trends Genet *33*, 960-970.

Beachy, P.A., Helfand, S.L., and Hogness, D.S. (1985). Segmental distribution of bithorax complex proteins during Drosophila development. Nature *313*, 545-551.

Bedford, M.T., and Clarke, S.G. (2009). Protein arginine methylation in mammals: who, what, and why. Mol Cell *33*, 1-13.

Begg, B.E., Jens, M., Wang, P.Y., Minor, C.M., and Burge, C.B. (2020). Concentration-dependent splicing is enabled by Rbfox motifs of intermediate affinity. Nat Struct Mol Biol *27*, 901-912.

Benedek, G., Chaudhary, P., Meza-Romero, R., Calkins, E., Kent, G., Offner, H., Bourdette, D., and Vandenbark, A.A. (2017). Sex-dependent treatment of chronic EAE with partial MHC class II constructs. J Neuroinflammation *14*, 100.

Bennett, F.C., Bennett, M.L., Yaqoob, F., Mulinyawe, S.B., Grant, G.A., Hayden Gephart, M., Plowey, E.D., and Barres, B.A. (2018). A Combination of Ontogeny and CNS Environment Establishes Microglial Identity. Neuron *98*, 1170-1183 e1178.

Beuck, C., Qu, S., Fagg, W.S., Ares, M., Jr., and Williamson, J.R. (2012). Structural analysis of the quaking homodimerization interface. J Mol Biol *423*, 766-781.

Biamonti, G., Amato, A., Belloni, E., Di Matteo, A., Infantino, L., Pradella, D., and Ghigna, C. (2019). Alternative splicing in Alzheimer's disease. Aging Clin Exp Res.

Bjornevik, K., Cortese, M., Healy, B.C., Kuhle, J., Mina, M.J., Leng, Y., Elledge, S.J., Niebuhr, D.W., Scher, A.I., Munger, K.L.*, et al.* (2022). Longitudinal analysis reveals high prevalence of Epstein-Barr virus associated with multiple sclerosis. Science *375*, 296-301.

Black, D.L. (1992). Activation of c-src neuron-specific splicing by an unusual RNA element in vivo and in vitro. Cell *69*, 795-807.

Boutz, P.L., Stoilov, P., Li, Q., Lin, C.H., Chawla, G., Ostrow, K., Shiue, L., Ares, M., Jr., and Black, D.L. (2007). A post-transcriptional regulatory switch in polypyrimidine tract-binding proteins reprograms alternative splicing in developing neurons. Genes Dev *21*, 1636-1652.

Buckanovich, R.J., Yang, Y.Y., and Darnell, R.B. (1996). The onconeural antigen Nova-1 is a neuron-specific RNA-binding protein, the activity of which is inhibited by paraneoplastic antibodies. J Neurosci *16*, 1114-1122.

Butovsky, O., Jedrychowski, M.P., Moore, C.S., Cialic, R., Lanser, A.J., Gabriely, G., Koeglsperger, T., Dake, B., Wu, P.M., Doykan, C.E.*, et al.* (2014). Identification of a unique TGF-beta-dependent molecular and functional signature in microglia. Nat Neurosci *17*, 131-143.

Candlish, M., and Hefendehl, J.K. (2021). Microglia Phenotypes Converge in Aging and Neurodegenerative Disease. Front Neurol *12*, 660720.

Carbonell, A.U., Freire-Cobo, C., Deyneko, I.V., Erdjument-Bromage, H., Clipperton-Allen, A.E., Rasmusson, R.L., Page, D.T., Neubert, T.A., and Jordan, B.A. (2021). Comparing synaptic proteomes across seven mouse models for autism reveals molecular subtypes and deficits in Rho GTPase signaling. bioRxiv, 2021.2002.2002.429412.

Carlo, T., Sierra, R., and Berget, S.M. (2000). A 5' splice site-proximal enhancer binds SF1 and activates exon bridging of a microexon. Mol Cell Biol *20*, 3988-3995.

Carlo, T., Sterner, D.A., and Berget, S.M. (1996). An intron splicing enhancer containing a G-rich repeat facilitates inclusion of a vertebrate micro-exon. RNA *2*, 342-353.

Cataldo, A.M., Peterhoff, C.M., Troncoso, J.C., Gomez-Isla, T., Hyman, B.T., and Nixon, R.A. (2000). Endocytic pathway abnormalities precede amyloid beta deposition in sporadic Alzheimer's disease and Down syndrome: differential effects of APOE genotype and presenilin mutations. Am J Pathol *157*, 277-286.

Chan, R.C., and Black, D.L. (1995). Conserved intron elements repress splicing of a neuron-specific c-src exon in vitro. Mol Cell Biol *15*, 6377-6385.

Chan, R.C., and Black, D.L. (1997). The polypyrimidine tract binding protein binds upstream of neural cell-specific c-src exon N1 to repress the splicing of the intron downstream. Mol Cell Biol *17*, 4667-4676.

Chen, E.Y., Tan, C.M., Kou, Y., Duan, Q., Wang, Z., Meirelles, G.V., Clark, N.R., and Ma'ayan, A. (2013). Enrichr: interactive and collaborative HTML5 gene list enrichment analysis tool. . BMC Bioinformatics *14*, 128.

Chen, H.R., Sun, Y.Y., Chen, C.W., Kuo, Y.M., Kuan, I.S., Tiger Li, Z.R., Short-Miller, J.C., Smucker, M.R., and Kuan, C.Y. (2020). Fate mapping via CCR2-CreER mice reveals monocyte-to-microglia transition in development and neonatal stroke. Sci Adv *6*, eabb2119.

Chen, T., and Richard, S. (1998). Structure-function analysis of Qk1: a lethal point mutation in mouse quaking prevents homodimerization. Mol Cell Biol *18*, 4863-4871.

Cherfils, J., and Zeghouf, M. (2013). Regulation of small GTPases by GEFs, GAPs, and GDIs. Physiol Rev *93*, 269-309.

Choi, I., Zhang, Y., Seegobin, S.P., Pruvost, M., Wang, Q., Purtell, K., Zhang, B., and Yue, Z. (2020). Microglia clear neuron-released alpha-synuclein via selective autophagy and prevent neurodegeneration. Nat Commun *11*, 1386.

Choudhury, R., Noakes, C.J., McKenzie, E., Kox, C., and Lowe, M. (2009). Differential clathrin binding and subcellular localization of OCRL1 splice isoforms. J Biol Chem *284*, 9965-9973.

Chu, Y., Jin, X., Parada, I., Pesic, A., Stevens, B., Barres, B., and Prince, D.A. (2010). Enhanced synaptic connectivity and epilepsy in C1q knockout mice. Proc Natl Acad Sci U S A *107*, 7975-7980.

Conboy, J.G. (2017). Developmental regulation of RNA processing by Rbfox proteins. Wiley Interdiscip Rev RNA *8*.

Conn, S.J., Pillman, K.A., Toubia, J., Conn, V.M., Salmanidis, M., Phillips, C.A., Roslan, S., Schreiber, A.W., Gregory, P.A., and Goodall, G.J. (2015). The RNA binding protein quaking regulates formation of circRNAs. Cell *160*, 1125-1134.

Constantinescu, C.S., Farooqi, N., O'Brien, K., and Gran, B. (2011). Experimental autoimmune encephalomyelitis (EAE) as a model for multiple sclerosis (MS). Br J Pharmacol *164*, 1079-1106.

Cooper, T.A., and Ordahl, C.P. (1985). A single cardiac troponin T gene generates embryonic and adult isoforms via developmentally regulated alternate splicing. J Biol Chem *260*, 11140-11148.

Cui, S., Yu, Q., Chu, L., Cui, Y., Ding, M., Wang, Q., Wang, H., Chen, Y., Liu, X., and Wang, C. (2020). Nuclear cGAS Functions Non-canonically to Enhance Antiviral Immunity via Recruiting Methyltransferase Prmt5. Cell Rep *33*, 108490.

Damase, T.R., Sukhovershin, R., Boada, C., Taraballi, F., Pettigrew, R.I., and Cooke, J.P. (2021). The Limitless Future of RNA Therapeutics. Front Bioeng Biotechnol *9*, 628137.

Danan-Gotthold, M., Golan-Gerstl, R., Eisenberg, E., Meir, K., Karni, R., and Levanon, E.Y. (2015). Identification of recurrent regulated alternative splicing events across human solid tumors. Nucleic Acids Res *43*, 5130-5144.

Darbelli, L., and Richard, S. (2016). Emerging functions of the Quaking RNA-binding proteins and link to human diseases. Wiley Interdiscip Rev RNA *7*, 399-412.

Darbelli, L., Vogel, G., Almazan, G., and Richard, S. (2016). Quaking Regulates Neurofascin 155 Expression for Myelin and Axoglial Junction Maintenance. J Neurosci *36*, 4106-4120.

de Bruin, R.G., Shiue, L., Prins, J., de Boer, H.C., Singh, A., Fagg, W.S., van Gils, J.M., Duijs, J.M., Katzman, S., Kraaijeveld, A.O.*, et al.* (2016). Quaking promotes monocyte differentiation into pro-atherogenic macrophages by controlling pre-mRNA splicing and gene expression. Nat Commun *7*, 10846.

de Bruin, R.G., Vogel, G., Prins, J., Duijs, J.M.J.G., Bijkerk, R., van der Zande, H.J.P., van Gils, J.M., de Boer, H.C., Rabelink, T.J., van Zonneveld, A.J.*, et al.* (2020). Targeting the RNA-Binding Protein QKI in Myeloid Cells Ameliorates Macrophage-Induced Renal Interstitial Fibrosis. Epigenomes *4*, 2.

de Hoon, M.J., Imoto, S., Nolan, J., and Miyano, S. (2004). Open Source Clustering Software. . Bioinformatics *20*, 1453-1454.

De Jager, P.L., Jia, X., Wang, J., de Bakker, P.I., Ottoboni, L., Aggarwal, N.T., Piccio, L., Raychaudhuri, S., Tran, D., Aubin, C*., et al.* (2009). Meta-analysis of genome scans and replication identify CD6, IRF8 and TNFRSF1A as new multiple sclerosis susceptibility loci. Nat Genet *41*, 776-782.

de la Torre-Ubieta, L., Won, H., Stein, J.L., and Geschwind, D.H. (2016). Advancing the understanding of autism disease mechanisms through genetics. Nat Med *22*, 345-361.

De, S., Van Deren, D., Peden, E., Hockin, M., Boulet, A., Titen, S., and Capecchi, M.R. (2018). Two distinct ontogenies confer heterogeneity to mouse brain microglia. Development *145*.

DeGeer, J., and Lamarche-Vane, N. (2013). Rho GTPases in neurodegeneration diseases. Exp Cell Res *319*, 2384-2394.

Dergai, M., Tsyba, L., Dergai, O., Zlatskii, I., Skrypkina, I., Kovalenko, V., and Rynditch, A. (2010). Microexon-based regulation of ITSN1 and Src SH3 domains specificity relies on introduction of charged amino acids into the interaction interface. Biochem Biophys Res Commun *399*, 307-312.

Dhaeze, T., Tremblay, L., Lachance, C., Peelen, E., Zandee, S., Grasmuck, C., Bourbonniere, L., Larouche, S., Ayrignac, X., Rebillard, R.M*., et al.* (2019). CD70 defines a subset of proinflammatory and CNS-pathogenic TH1/TH17 lymphocytes and is overexpressed in multiple sclerosis. Cell Mol Immunol *16*, 652-665.

Diehl, K.L., Vorac, J., Hofmann, K., Meiser, P., Unterweger, I., Kuerschner, L., Weighardt, H., Forster, I., and Thiele, C. (2020). Kupffer Cells Sense Free Fatty Acids and Regulate Hepatic Lipid Metabolism in High-Fat Diet and Inflammation. Cells *9*.

Ding, J., Li, Q.Y., Wang, X., Sun, C.H., Lu, C.Z., and Xiao, B.G. (2010). Fasudil protects hippocampal neurons against hypoxia-reoxygenation injury by suppressing microglial inflammatory responses in mice. J Neurochem *114*, 1619-1629.

Dissing-Olesen, L., LeDue, J.M., Rungta, R.L., Hefendehl, J.K., Choi, H.B., and MacVicar, B.A. (2014). Activation of neuronal NMDA receptors triggers transient ATP-mediated microglial process outgrowth. J Neurosci *34*, 10511-10527.

Dong, Y., and Yong, V.W. (2019). When encephalitogenic T cells collaborate with microglia in multiple sclerosis. Nat Rev Neurol *15*, 704-717.

Du, M., Jillette, N., Zhu, J.J., Li, S., and Cheng, A.W. (2020). CRISPR artificial splicing factors. Nat Commun *11*, 2973.

Dupraz, S., Hilton, B.J., Husch, A., Santos, T.E., Coles, C.H., Stern, S., Brakebusch, C., and Bradke, F. (2019). RhoA Controls Axon Extension Independent of Specification in the Developing Brain. Curr Biol *29*, 3874-3886 e3879.

Duquette, P.M., and Lamarche-Vane, N. (2014). Rho GTPases in embryonic development. Small GTPases *5*, 8.

Ebersole, T.A., Chen, Q., Justice, M.J., and Artzt, K. (1996). The quaking gene product necessary in embryogenesis and myelination combines features of RNA binding and signal transduction proteins. Nat Genet *12*, 260-265.

Elmore, M.R., Najafi, A.R., Koike, M.A., Dagher, N.N., Spangenberg, E.E., Rice, R.A., Kitazawa, M., Matusow, B., Nguyen, H., West, B.L*., et al.* (2014). Colony-stimulating factor 1 receptor signaling is necessary for microglia viability, unmasking a microglia progenitor cell in the adult brain. Neuron *82*, 380-397.

Erny, D., Hrabe de Angelis, A.L., Jaitin, D., Wieghofer, P., Staszewski, O., David, E., Keren-Shaul, H., Mahlakoiv, T., Jakobshagen, K., Buch, T*., et al.* (2015). Host microbiota

constantly control maturation and function of microglia in the CNS. Nat Neurosci *18*, 965-977.

Fagg, W.S., Liu, N., Braunschweig, U., Chen, X., Widen, S.G., Donohue, J.P., Fair, J.H., Weirauch, M.T., Blencowe, B.J., and Garcia-Blanco, M.A. (2020). Definition of germ cell lineage alternative splicing programs reveals a critical role for Quaking in specifying cardiac cell fate. bioRxiv, 2020.2012.2022.423880.

Fantin, A., Vieira, J.M., Gestri, G., Denti, L., Schwarz, Q., Prykhozhij, S., Peri, F., Wilson, S.W., and Ruhrberg, C. (2010). Tissue macrophages act as cellular chaperones for vascular anastomosis downstream of VEGF-mediated endothelial tip cell induction. Blood *116*, 829-840.

Fatoba, O., Itokazu, T., and Yamashita, T. (2020). Microglia as therapeutic target in central nervous system disorders. J Pharmacol Sci *144*, 102-118.

Filippi, M., Bar-Or, A., Piehl, F., Preziosa, P., Solari, A., Vukusic, S., and Rocca, M.A. (2018). Multiple sclerosis. Nat Rev Dis Primers *4*, 43.

Fourgeaud, L., Traves, P.G., Tufail, Y., Leal-Bailey, H., Lew, E.D., Burrola, P.G., Callaway, P., Zagorska, A., Rothlin, C.V., Nimmerjahn, A.*, et al.* (2016). TAM receptors regulate multiple features of microglial physiology. Nature *532*, 240-244.

Frankish, A., Diekhans, M., Ferreira, A.M., Johnson, R., Jungreis, I., and et al. (2019). GENCODE reference annotation for the human and mouse genomes. . Nucleic acids research *47*, D766-773.

Fu, Y.F., Zhu, Y.N., Ni, J., Zhong, X.G., Tang, W., Re, Y.D., Shi, L.P., Wan, J., Yang, Y.F., Yuan, C.*, et al.* (2006). A reversible S-adenosyl-L-homocysteine hydrolase inhibitor ameliorates experimental autoimmune encephalomyelitis by inhibiting T cell activation. J Pharmacol Exp Ther *319*, 799-808.

Galarneau, A., and Richard, S. (2005a). Target RNA motif and target mRNAs of the Quaking STAR protein. Nat Struct Mol Biol *12*, 691-698.

Galarneau, A., and Richard, S. (2005b). Target RNA motif and target mRNAs of the Quaking STAR protein. Nat Struct Mol Biol *12*, 691-698.

Gandal, M.J., Zhang, P., Hadjimichael, E., Walker, R.L., Chen, C., Liu, S., Won, H., van Bakel, H., Varghese, M., Wang, Y.*, et al.* (2018). Transcriptome-wide isoform-level dysregulation in ASD, schizophrenia, and bipolar disorder. Science *362*.

Gaudino, S.J., and Kumar, P. (2019). Cross-Talk Between Antigen Presenting Cells and T Cells Impacts Intestinal Homeostasis, Bacterial Infections, and Tumorigenesis. Front Immunol *10*, 360.

Geoghegan, V., Guo, A., Trudgian, D., Thomas, B., and Acuto, O. (2015). Comprehensive identification of arginine methylation in primary T cells reveals regulatory roles in cell signalling. Nat Commun *6*, 6758.

Gerth, F., Japel, M., Sticht, J., Kuropka, B., Schmitt, X.J., Driller, J.H., Loll, B., Wahl, M.C., Pagel, K., Haucke, V.*, et al.* (2019). Exon Inclusion Modulates Conformational Plasticity and Autoinhibition of the Intersectin 1 SH3A Domain. Structure *27*, 977-987 e975.

Gil, A., Sharp, P.A., Jamison, S.F., and Garcia-Blanco, M.A. (1991). Characterization of cDNAs encoding the polypyrimidine tract-binding protein. Genes Dev *5*, 1224-1236.

Ginhoux, F., Greter, M., Leboeuf, M., Nandi, S., See, P., Gokhan, S., Mehler, M.F., Conway, S.J., Ng, L.G., Stanley, E.R.*, et al.* (2010). Fate mapping analysis reveals that adult microglia derive from primitive macrophages. Science *330*, 841-845.

Ginhoux, F., and Guilliams, M. (2016). Tissue-Resident Macrophage Ontogeny and Homeostasis. Immunity *44*, 439-449.

Ginhoux, F., Lim, S., Hoeffel, G., Low, D., and Huber, T. (2013). Origin and differentiation of microglia. Front Cell Neurosci *7*, 45.

Gomez, A.M., Traunmuller, L., and Scheiffele, P. (2021). Neurexins: molecular codes for shaping neuronal synapses. Nat Rev Neurosci.

Gonatopoulos-Pournatzis, T., Niibori, R., Salter, E.W., Weatheritt, R.J., Tsang, B., Farhangmehr, S., Liang, X., Braunschweig, U., Roth, J., Zhang, S.*, et al.* (2020). Autism-Misregulated eIF4G Microexons Control Synaptic Translation and Higher Order Cognitive Functions. Mol Cell *77*, 1176-1192 e1116.

Gonatopoulos-Pournatzis, T., Wu, M., Braunschweig, U., Roth, J., Han, H., Best, A.J., Raj, B., Aregger, M., O'Hanlon, D., Ellis, J.D.*, et al.* (2018). Genome-wide CRISPR-Cas9 Interrogation of Splicing Networks Reveals a Mechanism for Recognition of Autism-Misregulated Neuronal Microexons. Mol Cell *72*, 510-524 e512.

Gosselin, D., Link, V.M., Romanoski, C.E., Fonseca, G.J., Eichenfield, D.Z., Spann, N.J., Stender, J.D., Chun, H.B., Garner, H., Geissmann, F.*, et al.* (2014). Environment drives selection and function of enhancers controlling tissue-specific macrophage identities. Cell *159*, 1327-1340.

Gosselin, D., Skola, D., Coufal, N.G., Holtman, I.R., Schlachetzki, J.C.M., Sajti, E., Jaeger, B.N., O'Connor, C., Fitzpatrick, C., Pasillas, M.P.*, et al.* (2017). An environment-dependent transcriptional network specifies human microglia identity. Science *356*.

Granqvist, M., Boremalm, M., Poorghobad, A., Svenningsson, A., Salzer, J., Frisell, T., and Piehl, F. (2018). Comparative Effectiveness of Rituximab and Other Initial Treatment Choices for Multiple Sclerosis. JAMA Neurol *75*, 320-327.

Greer, J.M., and McCombe, P.A. (2011). Role of gender in multiple sclerosis: clinical effects and potential molecular mechanisms. J Neuroimmunol *234*, 7-18.

Greter, M., Lelios, I., Pelczar, P., Hoeffel, G., Price, J., Leboeuf, M., Kundig, T.M., Frei, K., Ginhoux, F., Merad, M.*, et al.* (2012). Stroma-derived interleukin-34 controls the development and maintenance of langerhans cells and the maintenance of microglia. Immunity *37*, 1050-1060.

Grubman, A., Choo, X.Y., Chew, G., Ouyang, J.F., Sun, G., Croft, N.P., Rossello, F.J., Simmons, R., Buckberry, S., Landin, D.V.*, et al.* (2021). Transcriptional signature in microglia associated with Abeta plaque phagocytosis. Nat Commun *12*, 3015.

Gu, Z., Eils, R., and Schlesner, M. (2016). Complex heatmaps reveal patterns and correlations in multidimensional genomic data. Bioinformatics *18*, 2847-2849.

Guerrero, B.L., and Sicotte, N.L. (2020). Microglia in Multiple Sclerosis: Friend or Foe? Front Immunol *11*, 374.

Guneykaya, D., Ivanov, A., Hernandez, D.P., Haage, V., Wojtas, B., Meyer, N., Maricos, M., Jordan, P., Buonfiglioli, A., Gielniewski, B.*, et al.* (2018). Transcriptional and Translational Differences of Microglia from Male and Female Brains. Cell Rep *24*, 2773-2783 e2776.

Guo, D., Yang, X., and Shi, L. (2020). Rho GTPase Regulators and Effectors in Autism Spectrum Disorders: Animal Models and Insights for Therapeutics. Cells *9*.

Hafner, M., Landthaler, M., Burger, L., Khorshid, M., Hausser, J., Berninger, P., Rothballer, A., Ascano, M., Jr., Jungkamp, A.C., Munschauer, M.*, et al.* (2010). Transcriptome-wide

identification of RNA-binding protein and microRNA target sites by PAR-CLIP. Cell *141*, 129-141.

Halladay, A.K., Bishop, S., Constantino, J.N., Daniels, A.M., Koenig, K., Palmer, K., Messinger, D., Pelphrey, K., Sanders, S.J., Singer, A.T.*, et al.* (2015). Sex and gender differences in autism spectrum disorder: summarizing evidence gaps and identifying emerging areas of priority. Mol Autism *6*, 36.

Hammond, T.R., Dufort, C., Dissing-Olesen, L., Giera, S., Young, A., Wysoker, A., Walker, A.J., Gergits, F., Segel, M., Nemesh, J.*, et al.* (2019). Single-Cell RNA Sequencing of Microglia throughout the Mouse Lifespan and in the Injured Brain Reveals Complex Cell-State Changes. Immunity *50*, 253-271 e256.

Hanley, P.J., Xu, Y., Kronlage, M., Grobe, K., Schon, P., Song, J., Sorokin, L., Schwab, A., and Bahler, M. (2010). Motorized RhoGAP myosin IXb (Myo9b) controls cell shape and motility. Proc Natl Acad Sci U S A *107*, 12145-12150.

Hannigan, M.M., Zagore, L.L., and Licatalosi, D.D. (2017). Ptbp2 Controls an Alternative Splicing Network Required for Cell Communication during Spermatogenesis. Cell Rep *19*, 2598-2612.

Harirchian, M.H., Fatehi, F., Sarraf, P., Honarvar, N.M., and Bitarafan, S. (2018). Worldwide prevalence of familial multiple sclerosis: A systematic review and meta-analysis. Mult Scler Relat Disord *20*, 43-47.

Hartung, H.P., Graf, J., Aktas, O., Mares, J., and Barnett, M.H. (2019). Diagnosis of multiple sclerosis: revisions of the McDonald criteria 2017 - continuity and change. Curr Opin Neurol *32*, 327-337.

Hashimoto, D., Chow, A., Noizat, C., Teo, P., Beasley, M.B., Leboeuf, M., Becker, C.D., See, P., Price, J., Lucas, D.*, et al.* (2013). Tissue-resident macrophages self-maintain locally throughout adult life with minimal contribution from circulating monocytes. Immunity *38*, 792-804.

Hawker, K., O'Connor, P., Freedman, M.S., Calabresi, P.A., Antel, J., Simon, J., Hauser, S., Waubant, E., Vollmer, T., Panitch, H.*, et al.* (2009). Rituximab in patients with primary progressive multiple sclerosis: results of a randomized double-blind placebo-controlled multicenter trial. Ann Neurol *66*, 460-471.

Head, S.A., Hernandez-Alias, X., Yang, J.S., Ciampi, L., Beltran-Sastre, V., Torres-Mendez, A., Irimia, M., Schaefer, M.H., and Serrano, L. (2021). Silencing of SRRM4 suppresses microexon inclusion and promotes tumor growth across cancers. PLoS Biol *19*, e3001138.

Heinz, S., Benner, C., Spann, N., Bertolino, E., and al., e. (2010). Simple Combinations of Lineage-Determining Transcription Factors Prime cis-Regulatory Elements Required for Macrophage and B Cell Identities. . Mol Cell *38*, 576-589.

Hoeffel, G., Chen, J., Lavin, Y., Low, D., Almeida, F.F., See, P., Beaudin, A.E., Lum, J., Low, I., Forsberg, E.C.*, et al.* (2015). C-Myb(+) erythro-myeloid progenitor-derived fetal monocytes give rise to adult tissue-resident macrophages. Immunity *42*, 665-678.

Huang, D., Sherman, B., and Lempicki, R. (2009). Systematic and integrative analysis of large gene lists using DAVID bioinformatics resources. Nat Protoc *4*, 44-57.

Huang, G.H., Sun, Z.L., Li, H.J., and Feng, D.F. (2017). Rho GTPase-activating proteins: Regulators of Rho GTPase activity in neuronal development and CNS diseases. Mol Cell Neurosci *80*, 18-31.

IButovsky, O., Jedrychowski, M.P., Moore, C.S., Cialic, R., Lanser, A.J., and al., e. (2014). Identification of a unique TGF-β-dependent molecular and functional signature in microglia. Nat Neurosci *17*, 131-143.

Infantino, S., Benz, B., Waldmann, T., Jung, M., Schneider, R., and Reth, M. (2010). Arginine methylation of the B cell antigen receptor promotes differentiation. J Exp Med *207*, 711-719.

Infantino, S., Light, A., O'Donnell, K., Bryant, V., Avery, D.T., Elliott, M., Tangye, S.G., Belz, G., Mackay, F., Richard, S.*, et al.* (2017). Arginine methylation catalyzed by PRMT1 is required for B cell activation and differentiation. Nat Commun *8*, 891.

Inoue, M., Okamoto, K., Terashima, A., Nitta, T., Muro, R., Negishi-Koga, T., Kitamura, T., Nakashima, T., and Takayanagi, H. (2018). Arginine methylation controls the strength of gammac-family cytokine signaling in T cell maintenance. Nat Immunol *19*, 1265-1276.

International Multiple Sclerosis Genetics, C., Beecham, A.H., Patsopoulos, N.A., Xifara, D.K., Davis, M.F., Kemppinen, A., Cotsapas, C., Shah, T.S., Spencer, C., Booth, D.*, et al.* (2013). Analysis of immune-related loci identifies 48 new susceptibility variants for multiple sclerosis. Nat Genet *45*, 1353-1360.

Irimia, M., Weatheritt, R.J., Ellis, J.D., Parikshak, N.N., Gonatopoulos-Pournatzis, T., Babor, M., Quesnel-Vallieres, M., Tapial, J., Raj, B., O'Hanlon, D.*, et al.* (2014). A highly conserved program of neuronal microexons is misregulated in autistic brains. Cell *159*, 1511-1523.

Johnson, V., Junge, H.J., and Chen, Z. (2019). Temporal regulation of axonal repulsion by alternative splicing of a conserved microexon in mammalian Robo1 and Robo2. Elife *8*.

Kagoya, Y., Saijo, H., Matsunaga, Y., Guo, T., Saso, K., Anczurowski, M., Wang, C.H., Sugata, K., Murata, K., Butler, M.O.*, et al.* (2019). Arginine methylation of FOXP3 is crucial for the suppressive function of regulatory T cells. J Autoimmun *97*, 10-21.

Kana, V., Desland, F.A., Casanova-Acebes, M., Ayata, P., Badimon, A., Nabel, E., Yamamuro, K., Sneeboer, M., Tan, I.L., Flanigan, M.E.*, et al.* (2019). CSF-1 controls cerebellar microglia and is required for motor function and social interaction. J Exp Med *216*, 2265-2281.

Kapoor, R., Ho, P.R., Campbell, N., Chang, I., Deykin, A., Forrestal, F., Lucas, N., Yu, B., Arnold, D.L., Freedman, M.S.*, et al.* (2018). Effect of natalizumab on disease progression in secondary progressive multiple sclerosis (ASCEND): a phase 3, randomised, double-blind, placebo-controlled trial with an open-label extension. Lancet Neurol *17*, 405-415.

Keren-Shaul, H., Spinrad, A., Weiner, A., Matcovitch-Natan, O., Dvir-Szternfeld, R., Ulland, T.K., David, E., Baruch, K., Lara-Astaiso, D., Toth, B.*, et al.* (2017). A Unique Microglia Type Associated with Restricting Development of Alzheimer's Disease. Cell *169*, 1276-1290 e1217.

Kierdorf, K., Erny, D., Goldmann, T., Sander, V., Schulz, C., Perdiguero, E.G., Wieghofer, P., Heinrich, A., Riemke, P., Holscher, C.*, et al.* (2013). Microglia emerge from erythromyeloid precursors via Pu.1- and Irf8-dependent pathways. Nat Neurosci *16*, 273-280.

Kim, E.J., Kim, J.S., Lee, S., Lee, H., Yoon, J.S., Hong, J.H., Chun, S.H., Sun, S., Won, H.S., Hong, S.A.*, et al.* (2019). QKI, a miR-200 target gene, suppresses epithelial-to-mesenchymal transition and tumor growth. Int J Cancer *145*, 1585-1595.

Kim, H., Kim, H., Feng, Y., Li, Y., Tamiya, H., Tocci, S., and Ronai, Z.A. (2020). PRMT5 control of cGAS/STING and NLRC5 pathways defines melanoma response to antitumor immunity. Sci Transl Med *12*.

Kippert, A., Trajkovic, K., Rajendran, L., Ries, J., and Simons, M. (2007). Rho regulates membrane transport in the endocytic pathway to control plasma membrane specialization in oligodendroglial cells. J Neurosci *27*, 3560-3570.

Kocur, M., Schneider, R., Pulm, A.K., Bauer, J., Kropp, S., Gliem, M., Ingwersen, J., Goebels, N., Alferink, J., Prozorovski, T.*, et al.* (2015). IFNbeta secreted by microglia mediates clearance of myelin debris in CNS autoimmunity. Acta Neuropathol Commun *3*, 20.

Kostrub, C.F., al-Khodairy, F., Ghazizadeh, H., Carr, A.M., and Enoch, T. (1997). Molecular analysis of hus1+, a fission yeast gene required for S-M and DNA damage checkpoints. Mol Gen Genet *254*, 389-399.

Kuhlmann, T., Ludwin, S., Prat, A., Antel, J., Bruck, W., and Lassmann, H. (2017). An updated histological classification system for multiple sclerosis lesions. Acta Neuropathol *133*, 13-24.

Kuleshov, M.V., Jones, M.R., Rouillard, A.D., Fernandez, N.F., Duan, Q., and al., e. (2016). Enrichr: a comprehensive gene set enrichment analysis web server 2016 update. Nucleic acids research *44*, W90-97.

Kunkle, B.W., Vardarajan, B.N., Naj, A.C., Whitehead, P.L., Rolati, S., Slifer, S., Carney, R.M., Cuccaro, M.L., Vance, J.M., Gilbert, J.R.*, et al.* (2017). Early-Onset Alzheimer Disease and Candidate Risk Genes Involved in Endolysosomal Transport. JAMA Neurol *74*, 1113-1122.

Kuroyanagi, H. (2009). Fox-1 family of RNA-binding proteins. Cell Mol Life Sci *66*, 3895-3907.

Lahrtz, F., Horstkorte, R., Cremer, H., Schachner, M., and Montag, D. (1997). VASE-encoded peptide modifies NCAM- and L1-mediated neurite outgrowth. J Neurosci Res *50*, 62-68.

Lampron, A., Larochelle, A., Laflamme, N., Préfontaine, P., Plante, M.M., Sánchez, M.G., Yong, V.W., Stys, P.K., Tremblay, M.È., and Rivest, S. (2015). Inefficient clearance of myelin debris by microglia impairs remyelinating processes. J Exp Med *212*, 481-495.

Lee, J., Villarreal, O.D., Chen, X., Zandee, S., Young, Y.K., Torok, C., Lamarche-Vane, N., Prat, A., Rivest, S., Gosselin, D.*, et al.* (2020). QUAKING Regulates Microexon Alternative Splicing of the Rho GTPase Pathway and Controls Microglia Homeostasis. Cell Rep *33*, 108560.

Leone, D.P., Srinivasan, K., Brakebusch, C., and McConnell, S.K. (2010). The rho GTPase Rac1 is required for proliferation and survival of progenitors in the developing forebrain. Dev Neurobiol *70*, 659-678.

Levy, J.B., Dorai, T., Wang, L.H., and Brugge, J.S. (1987). The structurally distinct form of pp60c-src detected in neuronal cells is encoded by a unique c-src mRNA. Mol Cell Biol *7*, 4142-4145.

Lewis, N.D., Hill, J.D., Juchem, K.W., Stefanopoulos, D.E., and Modis, L.K. (2014). RNA sequencing of microglia and monocyte-derived macrophages from mice with experimental autoimmune encephalomyelitis illustrates a changing phenotype with disease course. J Neuroimmunol *277*, 26-38.

Li, J., Choi, P.S., Chaffer, C.L., Labella, K., Hwang, J.H., Giacomelli, A.O., Kim, J.W., Ilic, N., Doench, J.G., Ly, S.H.*, et al.* (2018). An alternative splicing switch in FLNB promotes the mesenchymal cell state in human breast cancer. Elife *7*.

Li, Q., and Barres, B.A. (2018). Microglia and macrophages in brain homeostasis and disease. Nat Rev Immunol *18*, 225-242.

Li, Q., Cheng, Z., Zhou, L., Darmanis, S., Neff, N.F., Okamoto, J., Gulati, G., Bennett, M.L., Sun, L.O., Clarke, L.E.*, et al.* (2019). Developmental Heterogeneity of Microglia and Brain Myeloid Cells Revealed by Deep Single-Cell RNA Sequencing. Neuron *101*, 207-223 e210.

Li, W.J., He, Y.H., Yang, J.J., Hu, G.S., Lin, Y.A., Ran, T., Peng, B.L., Xie, B.L., Huang, M.F., Gao, X.*, et al.* (2021). Profiling PRMT methylome reveals roles of hnRNPA1 arginine methylation in RNA splicing and cell growth. Nat Commun *12*, 1946.

Li, Y.I., Sanchez-Pulido, L., Haerty, W., and Ponting, C.P. (2015). RBFOX and PTBP1 proteins regulate the alternative splicing of micro-exons in human brain transcripts. Genome Res *25*, 1-13.

Liddelow, S.A., Marsh, S.E., and Stevens, B. (2020). Microglia and Astrocytes in Disease: Dynamic Duo or Partners in Crime? Trends Immunol *41*, 820-835.

Lim, K.H., Ferraris, L., Filloux, M.E., Raphael, B.J., and Fairbrother, W.G. (2011). Using positional distribution to identify splicing elements and predict pre-mRNA processing defects in human genes. Proc Natl Acad Sci U S A *108*, 11093-11098.

Lin, L., Zhang, M., Stoilov, P., Chen, L., and Zheng, S. (2020). Developmental Attenuation of Neuronal Apoptosis by Neural-Specific Splicing of Bak1 Microexon. Neuron *107*, 1180-1196 e1188.

Litzler, L.C., Zahn, A., Meli, A.P., Hebert, S., Patenaude, A.M., Methot, S.P., Sprumont, A., Bois, T., Kitamura, D., Costantino, S.*, et al.* (2019). PRMT5 is essential for B cell development and germinal center dynamics. Nat Commun *10*, 22.

Liu, F., Cheng, G., Hamard, P.J., Greenblatt, S., Wang, L., Man, N., Perna, F., Xu, H., Tadi, M., Luciani, L.*, et al.* (2015). Arginine methyltransferase PRMT5 is essential for sustaining normal adult hematopoiesis. J Clin Invest *125*, 3532-3544.

Lloyd, A.F., Davies, C.L., Holloway, R.K., Labrak, Y., Ireland, G., Carradori, D., Dillenburg, A., Borger, E., Soong, D., Richardson, J.C.*, et al.* (2019). Central nervous system regeneration is driven by microglia necroptosis and repopulation. Nat Neurosci *22*, 1046-1052.

Lloyd, A.F., and Miron, V.E. (2019). The pro-remyelination properties of microglia in the central nervous system. Nat Rev Neurol *15*, 447-458.

Love, J.E., Hayden, E.J., and Rohn, T.T. (2015). Alternative Splicing in Alzheimer's Disease. J Parkinsons Dis Alzheimers Dis *2*.

Love, M.I., Huber, W., and Anders, S. (2014). Moderated estimation of fold change and dispersion for RNA-seq data with DESeq2. Genome Biol *15*, 550.

Lukong, K.E., Chang, K.W., Khandjian, E.W., and Richard, S. (2008). RNA-binding proteins in human genetic disease. Trends Genet *24*, 416-425.

Ma, D., Yang, M., Wang, Q., Sun, C., Shi, H., Jing, W., Bi, Y., Shen, X., Ma, X., Qin, Z.*, et al.* (2021). Arginine methyltransferase PRMT5 negatively regulates cGAS-mediated antiviral immune response. Sci Adv *7*.

Ma, F., Yang, L., Sun, Z., Chen, J., Rui, X., Glass, Z., and Xu, Q. (2020). Neurotransmitter-derived lipidoids (NT-lipidoids) for enhanced brain delivery through intravenous injection. Sci Adv *6*, eabb4429.

Makeyev, E.V., Zhang, J., Carrasco, M.A., and Maniatis, T. (2007). The MicroRNA miR-124 promotes neuronal differentiation by triggering brain-specific alternative pre-mRNA splicing. Mol Cell *27*, 435-448.

Marin-Teva, J.L., Dusart, I., Colin, C., Gervais, A., van Rooijen, N., and Mallat, M. (2004). Microglia promote the death of developing Purkinje cells. Neuron *41*, 535-547.

Markovtsov, V., Nikolic, J.M., Goldman, J.A., Turck, C.W., Chou, M.Y., and Black, D.L. (2000). Cooperative assembly of an hnRNP complex induced by a tissue-specific homolog of polypyrimidine tract binding protein. Mol Cell Biol *20*, 7463-7479.

Masuda, T., Amann, L., Sankowski, R., Staszewski, O., Lenz, M., P, D.E., Snaidero, N., Costa Jordao, M.J., Bottcher, C., Kierdorf, K.*, et al.* (2020a). Novel Hexb-based tools for studying microglia in the CNS. Nat Immunol *21*, 802-815.

Masuda, T., Sankowski, R., Staszewski, O., Bottcher, C., Amann, L., Sagar, Scheiwe, C., Nessler, S., Kunz, P., van Loo, G.*, et al.* (2019). Spatial and temporal heterogeneity of mouse and human microglia at single-cell resolution. Nature *566*, 388-392.

Masuda, T., Sankowski, R., Staszewski, O., and Prinz, M. (2020b). Microglia Heterogeneity in the Single-Cell Era. Cell Rep *30*, 1271-1281.

Matcovitch-Natan, O., Winter, D.R., Giladi, A., Vargas Aguilar, S., Spinrad, A., Sarrazin, S., Ben-Yehuda, H., David, E., Zelada Gonzalez, F., Perrin, P.*, et al.* (2016). Microglia development follows a stepwise program to regulate brain homeostasis. Science *353*, aad8670.

Mathys, H., Adaikkan, C., Gao, F., Young, J.Z., Manet, E., Hemberg, M., De Jager, P.L., Ransohoff, R.M., Regev, A., and Tsai, L.H. (2017). Temporal Tracking of Microglia Activation in Neurodegeneration at Single-Cell Resolution. Cell Rep *21*, 366-380.

McAllister, L., Rehm, E.J., Goodman, G.S., and Zinn, K. (1992). Alternative splicing of micro-exons creates multiple forms of the insect cell adhesion molecule fasciclin I. J Neurosci *12*, 895-905.

Meldolesi, J. (2020). Alternative Splicing by NOVA Factors: From Gene Expression to Cell Physiology and Pathology. Int J Mol Sci *21*.

Min, H., Chan, R.C., and Black, D.L. (1995). The generally expressed hnRNP F is involved in a neural-specific pre-mRNA splicing event. Genes Dev *9*, 2659-2671.

Misra, C., Bangru, S., Lin, F., Lam, K., Koenig, S.N., Lubbers, E.R., Hedhli, J., Murphy, N.P., Parker, D.J., Dobrucki, L.W.*, et al.* (2020). Aberrant Expression of a Non-muscle RBFOX2 Isoform Triggers Cardiac Conduction Defects in Myotonic Dystrophy. Dev Cell *52*, 748-763 e746.

Montalban, X., Hauser, S.L., Kappos, L., Arnold, D.L., Bar-Or, A., Comi, G., de Seze, J., Giovannoni, G., Hartung, H.P., Hemmer, B.*, et al.* (2017). Ocrelizumab versus Placebo in Primary Progressive Multiple Sclerosis. N Engl J Med *376*, 209-220.

Moreno, B., Hevia, H., Santamaria, M., Sepulcre, J., Munoz, J., Garcia-Trevijano, E.R., Berasain, C., Corrales, F.J., Avila, M.A., and Villoslada, P. (2006). Methylthioadenosine reverses brain autoimmune disease. Ann Neurol *60*, 323-334.

Mrdjen, D., Pavlovic, A., Hartmann, F.J., Schreiner, B., Utz, S.G., Leung, B.P., Lelios, I., Heppner, F.L., Kipnis, J., Merkler, D.*, et al.* (2018). High-Dimensional Single-Cell

Mapping of Central Nervous System Immune Cells Reveals Distinct Myeloid Subsets in Health, Aging, and Disease. Immunity *48*, 380-395 e386.

Mukohyama, J., Isobe, T., Hu, Q., Hayashi, T., Watanabe, T., Maeda, M., Yanagi, H., Qian, X., Yamashita, K., Minami, H.*, et al.* (2019). miR-221 Targets QKI to Enhance the Tumorigenic Capacity of Human Colorectal Cancer Stem Cells. Cancer Res *79*, 5151-5158.

Nakahata, S., and Kawamoto, S. (2005). Tissue-dependent isoforms of mammalian Fox-1 homologs are associated with tissue-specific splicing activities. Nucleic Acids Res *33*, 2078-2089.

Naro, C., Cesari, E., and Sette, C. (2021). Splicing regulation in brain and testis: common themes for highly specialized organs. Cell Cycle *20*, 480-489.

Newman, R., McHugh, J., and Turner, M. (2016). RNA binding proteins as regulators of immune cell biology. Clin Exp Immunol *183*, 37-49.

Niftullayev, S., and Lamarche-Vane, N. (2019). Regulators of Rho GTPases in the Nervous System: Molecular Implication in Axon Guidance and Neurological Disorders. Int J Mol Sci *20*.

O'Rawe, J.A., Wu, Y., Dorfel, M.J., Rope, A.F., Au, P.Y., Parboosingh, J.S., Moon, S., Kousi, M., Kosma, K., Smith, C.S.*, et al.* (2015). TAF1 Variants Are Associated with Dysmorphic Features, Intellectual Disability, and Neurological Manifestations. Am J Hum Genet *97*, 922-932.

Ochocka, N., Segit, P., Walentynowicz, K.A., Wojnicki, K., Cyranowski, S., Swatler, J., Mieczkowski, J., and Kaminska, B. (2021). Single-cell RNA sequencing reveals functional heterogeneity of glioma-associated brain macrophages. Nat Commun *12*, 1151.

Olah, M., Menon, V., Habib, N., Taga, M.F., Ma, Y., Yung, C.J., Cimpean, M., Khairallah, A., Coronas-Samano, G., Sankowski, R.*, et al.* (2020). Single cell RNA sequencing of human microglia uncovers a subset associated with Alzheimer's disease. Nat Commun *11*, 6129.

Olofsson, B. (1999). Rho guanine dissociation inhibitors: pivotal molecules in cellular signalling. Cell Signal *11*, 545-554.

Pan, Q., Shai, O., Lee, L.J., Frey, B.J., and Blencowe, B.J. (2008). Deep surveying of alternative splicing complexity in the human transcriptome by high-throughput sequencing. Nat Genet *40*, 1413-1415.

Parada, G.E., Munita, R., Georgakopoulos-Soares, I., Fernandes, H.J.R., Kedlian, V.R., Metzakopian, E., Andres, M.E., Miska, E.A., and Hemberg, M. (2021). MicroExonator enables systematic discovery and quantification of microexons across mouse embryonic development. Genome Biol *22*, 43.

Pare, A., Mailhot, B., Levesque, S.A., and Lacroix, S. (2017). Involvement of the IL-1 system in experimental autoimmune encephalomyelitis and multiple sclerosis: Breaking the vicious cycle between IL-1beta and GM-CSF. Brain Behav Immun *62*, 1-8.

Parikshak, N.N., Swarup, V., Belgard, T.G., Irimia, M., Ramaswami, G., Gandal, M.J., Hartl, C., Leppa, V., Ubieta, L.T., Huang, J.*, et al.* (2016). Genome-wide changes in lncRNA, splicing, and regional gene expression patterns in autism. Nature *540*, 423-427.

Paronetto, M.P., Passacantilli, I., and Sette, C. (2016). Alternative splicing and cell survival: from tissue homeostasis to disease. Cell Death Differ *23*, 1919-1929.

Patton, J.G., Mayer, S.A., Tempst, P., and Nadal-Ginard, B. (1991). Characterization and molecular cloning of polypyrimidine tract-binding protein: a component of a complex necessary for pre-mRNA splicing. Genes Dev *5*, 1237-1251.

Perez-Martin, M., Cifuentes, M., Grondona, J.M., Lopez-Avalos, M.D., Gomez-Pinedo, U., Garcia-Verdugo, J.M., and Fernandez-Llebrez, P. (2010). IGF-I stimulates neurogenesis in the hypothalamus of adult rats. Eur J Neurosci *31*, 1533-1548.

Peri, F., and Nusslein-Volhard, C. (2008). Live imaging of neuronal degradation by microglia reveals a role for v0-ATPase a1 in phagosomal fusion in vivo. Cell *133*, 916-927.

Pluvinage, J.V., Haney, M.S., Smith, B.A.H., Sun, J., Iram, T., Bonanno, L., Li, L., Lee, D.P., Morgens, D.W., Yang, A.C.*, et al.* (2019). CD22 blockade restores homeostatic microglial phagocytosis in ageing brains. Nature *568*, 187-192.

Poliani, P.L., Wang, Y., Fontana, E., Robinette, M.L., Yamanishi, Y., Gilfillan, S., and Colonna, M. (2015). TREM2 sustains microglial expansion during aging and response to demyelination. J Clin Invest *125*, 2161-2170.

Polman, C.H., O'Connor, P.W., Havrdova, E., Hutchinson, M., Kappos, L., Miller, D.H., Phillips, J.T., Lublin, F.D., Giovannoni, G., Wajgt, A.*, et al.* (2006). A randomized, placebo-controlled trial of natalizumab for relapsing multiple sclerosis. N Engl J Med *354*, 899-910.

Polman, C.H., Reingold, S.C., Banwell, B., Clanet, M., Cohen, J.A., Filippi, M., Fujihara, K., Havrdova, E., Hutchinson, M., Kappos, L.*, et al.* (2011). Diagnostic criteria for multiple sclerosis: 2010 revisions to the McDonald criteria. Ann Neurol *69*, 292-302.

Ponomarev, E.D., Maresz, K., Tan, Y., and Dittel, B.N. (2007). CNS-derived interleukin-4 is essential for the regulation of autoimmune inflammation and induces a state of alternative activation in microglial cells. J Neurosci *27*, 10714-10721.

Priller, J., and Prinz, M. (2019). Targeting microglia in brain disorders. Science *365*, 32-33.

Prinz, M., Jung, S., and Priller, J. (2019). Microglia Biology: One Century of Evolving Concepts. Cell *179*, 292-311.

Quesnel-Vallieres, M., Dargaei, Z., Irimia, M., Gonatopoulos-Pournatzis, T., Ip, J.Y., Wu, M., Sterne-Weiler, T., Nakagawa, S., Woodin, M.A., Blencowe, B.J.*, et al.* (2016). Misregulation of an Activity-Dependent Splicing Network as a Common Mechanism Underlying Autism Spectrum Disorders. Mol Cell *64*, 1023-1034.

Quesnel-Vallieres, M., Irimia, M., Cordes, S.P., and Blencowe, B.J. (2015). Essential roles for the splicing regulator nSR100/SRRM4 during nervous system development. Genes Dev *29*, 746-759.

Quesnel-Vallieres, M., Weatheritt, R.J., Cordes, S.P., and Blencowe, B.J. (2019). Autism spectrum disorder: insights into convergent mechanisms from transcriptomics. Nat Rev Genet *20*, 51-63.

Raimondi, I., Tunesi, M., Forloni, G., Albani, D., and Giordano, C. (2020). 3D brain tissue physiological model with co-cultured primary neurons and glial cells in hydrogels. J Tissue Eng *11*, 2041731420963981.

Raj, T., Li, Y.I., Wong, G., Humphrey, J., Wang, M., Ramdhani, S., Wang, Y.C., Ng, B., Gupta, I., Haroutunian, V.*, et al.* (2018). Integrative transcriptome analyses of the aging brain implicate altered splicing in Alzheimer's disease susceptibility. Nat Genet *50*, 1584-1592.

Rajasekharan, S., Bin, J.M., Antel, J.P., and Kennedy, T.E. (2010). A central role for RhoA during oligodendroglial maturation in the switch from netrin-1-mediated chemorepulsion to process elaboration. J Neurochem *113*, 1589-1597.

Ratcliffe, C.D.H., Siddiqui, N., Coelho, P.P., Laterreur, N., Cookey, T.N., Sonenberg, N., and Park, M. (2019). HGF-induced migration depends on the PI(3,4,5)P3-binding microexon-spliced variant of the Arf6 exchange factor cytohesin-1. J Cell Biol *218*, 285-298.

Reiner, D.J., and Lundquist, E.A. (2018). Small GTPases. WormBook *2018*, 1-65.

Ren, J., Dai, C., Zhou, X., Barnes, J.A., Chen, X., Wang, Y., Yuan, L., Shingu, T., Heimberger, A.B., Chen, Y.*, et al.* (2021). Qki is an essential regulator of microglial phagocytosis in demyelination. J Exp Med *218*.

Rosati, G. (2001). The prevalence of multiple sclerosis in the world: an update. Neurol Sci *22*, 117-139.

Roser, A.E., Tonges, L., and Lingor, P. (2017). Modulation of Microglial Activity by Rho-Kinase (ROCK) Inhibition as Therapeutic Strategy in Parkinson's Disease and Amyotrophic Lateral Sclerosis. Front Aging Neurosci *9*, 94.

Ryder, S.P., Frater, L.A., Abramovitz, D.L., Goodwin, E.B., and Williamson, J.R. (2004). RNA target specificity of the STAR/GSG domain post-transcriptional regulatory protein GLD-1. Nat Struct Mol Biol *11*, 20-28.

Safaiyan, S., Kannaiyan, N., Snaidero, N., Brioschi, S., Biber, K., Yona, S., Edinger, A.L., Jung, S., Rossner, M.J., and Simons, M. (2016). Age-related myelin degradation burdens the clearance function of microglia during aging. Nat Neurosci *19*, 995-998.

Saldanha, A.J. (2004). Java Treeview—extensible visualization of microarray data. . Bioinformatics *20*, 3246-3248.

Schafer, D.P., Lehrman, E.K., Kautzman, A.G., Koyama, R., Mardinly, A.R., Yamasaki, R., Ransohoff, R.M., Greenberg, M.E., Barres, B.A., and Stevens, B. (2012). Microglia sculpt postnatal neural circuits in an activity and complement-dependent manner. Neuron *74*, 691-705.

Schulz, C., Gomez Perdiguero, E., Chorro, L., Szabo-Rogers, H., Cagnard, N., Kierdorf, K., Prinz, M., Wu, B., Jacobsen, S.E., Pollard, J.W.*, et al.* (2012). A lineage of myeloid cells independent of Myb and hematopoietic stem cells. Science *336*, 86-90.

Schulze, U., Hepp, B., Ong, C.S., and Ratsch, G. (2007). PALMA: mRNA to genome alignments using large margin algorithms. Bioinformatics *23*, 1892-1900.

Schwabenland, M., Salie, H., Tanevski, J., Killmer, S., Lago, M.S., Schlaak, A.E., Mayer, L., Matschke, J., Puschel, K., Fitzek, A.*, et al.* (2021). Deep spatial profiling of human COVID-19 brains reveals neuroinflammation with distinct microanatomical microglia-T-cell interactions. Immunity *54*, 1594-1610 e1511.

Scotti, M.M., and Swanson, M.S. (2016). RNA mis-splicing in disease. Nat Rev Genet *17*, 19-32.

Sedel, F., Bechade, C., Vyas, S., and Triller, A. (2004). Macrophage-derived tumor necrosis factor alpha, an early developmental signal for motoneuron death. J Neurosci *24*, 2236-2246.

Sekiguchi, M., Sobue, A., Kushima, I., Wang, C., Arioka, Y., Kato, H., Kodama, A., Kubo, H., Ito, N., Sawahata, M.*, et al.* (2020). ARHGAP10, which encodes Rho GTPase-activating protein 10, is a novel gene for schizophrenia risk. Transl Psychiatry *10*, 247.

Sen, S., He, Z., Ghosh, S., Dery, K.J., Yang, L., Zhang, J., and Sun, Z. (2018). PRMT1 Plays a Critical Role in Th17 Differentiation by Regulating Reciprocal Recruitment of STAT3 and STAT5. J Immunol *201*, 440-450.

Sengupta, S., Kennemer, A., Patrick, K., Tsichlis, P., and Guerau-de-Arellano, M. (2020). Protein Arginine Methyltransferase 5 in T Lymphocyte Biology. Trends Immunol *41*, 918-931.

Sharma, S., Kohlstaedt, L.A., Damianov, A., Rio, D.C., and Black, D.L. (2008). Polypyrimidine tract binding protein controls the transition from exon definition to an intron defined spliceosome. Nat Struct Mol Biol *15*, 183-191.

Shemer, A., Grozovski, J., Tay, T.L., Tao, J., Volaski, A., Suss, P., Ardura-Fabregat, A., Gross-Vered, M., Kim, J.S., David, E.*, et al.* (2018). Engrafted parenchymal brain macrophages differ from microglia in transcriptome, chromatin landscape and response to challenge. Nat Commun *9*, 5206.

Shen, K., Sidik, H., and Talbot, W.S. (2016). The Rag-Ragulator Complex Regulates Lysosome Function and Phagocytic Flux in Microglia. Cell Rep *14*, 547-559.

Shen, S., Park, J.W., Lu, Z.X., Lin, L., Henry, M.D., Wu, Y.N., Zhou, Q., and Xing, Y. (2014). rMATS: robust and flexible detection of differential alternative splicing from replicate RNA-Seq data. Proceedings of the National Academy of Sciences of the United States of America *111*, E5593-5601.

Singh, R.K., Xia, Z., Bland, C.S., Kalsotra, A., Scavuzzo, M.A., Curk, T., Ule, J., Li, W., and Cooper, T.A. (2014). Rbfox2-coordinated alternative splicing of Mef2d and Rock2 controls myoblast fusion during myogenesis. Mol Cell *55*, 592-603.

Sipe, G.O., Lowery, R.L., Tremblay, M.E., Kelly, E.A., Lamantia, C.E., and Majewska, A.K. (2016). Microglial P2Y12 is necessary for synaptic plasticity in mouse visual cortex. Nat Commun *7*, 10905.

Small, S.J., and Akeson, R. (1990). Expression of the unique NCAM VASE exon is independently regulated in distinct tissues during development. J Cell Biol *111*, 2089-2096.

Small, S.J., Haines, S.L., and Akeson, R.A. (1988). Polypeptide variation in an N-CAM extracellular immunoglobulin-like fold is developmentally regulated through alternative splicing. Neuron *1*, 1007-1017.

Socodato, R., Portugal, C.C., Canedo, T., Rodrigues, A., Almeida, T.O., Henriques, J.F., Vaz, S.H., Magalhaes, J., Silva, C.M., Baptista, F.I.*, et al.* (2020). Microglia Dysfunction Caused by the Loss of Rhoa Disrupts Neuronal Physiology and Leads to Neurodegeneration. Cell Rep *31*, 107796.

Spellman, R., Llorian, M., and Smith, C.W. (2007). Crossregulation and functional redundancy between the splicing regulator PTB and its paralogs nPTB and ROD1. Mol Cell *27*, 420-434.

Stephan, A.H., Barres, B.A., and Stevens, B. (2012). The complement system: an unexpected role in synaptic pruning during development and disease. Annu Rev Neurosci *35*, 369-389.

Sterner, D.A., and Berget, S.M. (1993). In vivo recognition of a vertebrate mini-exon as an exon-intron-exon unit. Mol Cell Biol *13*, 2677-2687.

Szepesi, Z., Manouchehrian, O., Bachiller, S., and Deierborg, T. (2018). Bidirectional Microglia-Neuron Communication in Health and Disease. Front Cell Neurosci *12*, 323.

Tahirovic, S., Hellal, F., Neukirchen, D., Hindges, R., Garvalov, B.K., Flynn, K.C., Stradal, T.E., Chrostek-Grashoff, A., Brakebusch, C., and Bradke, F. (2010). Rac1 regulates neuronal polarization through the WAVE complex. J Neurosci *30*, 6930-6943.

Tatsumi, E., Yamanaka, H., Kobayashi, K., Yagi, H., Sakagami, M., and Noguchi, K. (2015). RhoA/ROCK pathway mediates p38 MAPK activation and morphological changes downstream of P2Y12/13 receptors in spinal microglia in neuropathic pain. Glia *63*, 216-228.

Teplova, M., Hafner, M., Teplov, D., Essig, K., Tuschl, T., and Patel, D.J. (2013). Structure-function studies of STAR family Quaking proteins bound to their in vivo RNA target sites. Genes Dev *27*, 928-940.

Thion, M.S., Ginhoux, F., and Garel, S. (2018a). Microglia and early brain development: An intimate journey. Science *362*, 185-189.

Thion, M.S., Low, D., Silvin, A., Chen, J., Grisel, P., Schulte-Schrepping, J., Blecher, R., Ulas, T., Squarzoni, P., Hoeffel, G.*, et al.* (2018b). Microbiome Influences Prenatal and Adult Microglia in a Sex-Specific Manner. Cell *172*, 500-516 e516.

Tikhanovich, I., Zhao, J., Olson, J., Adams, A., Taylor, R., Bridges, B., Marshall, L., Roberts, B., and Weinman, S.A. (2017). Protein arginine methyltransferase 1 modulates innate immune responses through regulation of peroxisome proliferator-activated receptor gamma-dependent macrophage differentiation. J Biol Chem *292*, 6882-6894.

Torres-Mendez, A., Bonnal, S., Marquez, Y., Roth, J., Iglesias, M., Permanyer, J., Almudi, I., O'Hanlon, D., Guitart, T., Soller, M.*, et al.* (2019). A novel protein domain in an ancestral splicing factor drove the evolution of neural microexons. Nat Ecol Evol *3*, 691-701.

Tsyba, L., Gryaznova, T., Dergai, O., Dergai, M., Skrypkina, I., Kropyvko, S., Boldyryev, O., Nikolaienko, O., Novokhatska, O., and Rynditch, A. (2008). Alternative splicing affecting the SH3A domain controls the binding properties of intersectin 1 in neurons. Biochem Biophys Res Commun *372*, 929-934.

Uchida, Y., Chiba, T., Kurimoto, R., and Asahara, H. (2019). Post-transcriptional regulation of inflammation by RNA-binding proteins via cis-elements of mRNAs. J Biochem *166*, 375-382.

Ule, J., and Blencowe, B.J. (2019). Alternative Splicing Regulatory Networks: Functions, Mechanisms, and Evolution. Mol Cell *76*, 329-345.

Ulland, T.K., and Colonna, M. (2018). TREM2 - a key player in microglial biology and Alzheimer disease. Nat Rev Neurol *14*, 667-675.

Vainchtein, I.D., Chin, G., Cho, F.S., Kelley, K.W., Miller, J.G., Chien, E.C., Liddelow, S.A., Nguyen, P.T., Nakao-Inoue, H., Dorman, L.C.*, et al.* (2018). Astrocyte-derived interleukin-33 promotes microglial synapse engulfment and neural circuit development. Science *359*, 1269-1273.

Van Hove, H., Martens, L., Scheyltjens, I., De Vlaminck, K., Pombo Antunes, A.R., De Prijck, S., Vandamme, N., De Schepper, S., Van Isterdael, G., Scott, C.L.*, et al.* (2019). A single-cell atlas of mouse brain macrophages reveals unique transcriptional identities shaped by ontogeny and tissue environment. Nat Neurosci *22*, 1021-1035.

Van Nostrand, E.L., Freese, P., Pratt, G.A., Wang, X., Wei, X., Xiao, R., Blue, S.M., Chen, J.Y., Cody, N.A.L., Dominguez, D.*, et al.* (2020). A large-scale binding and functional map of human RNA-binding proteins. Nature *583*, 711-719.

Vaquero-Garcia, J., Barrera, A., Gazzara, M.R., González-Vallinas, J., Lahens, N.F., Hogenesch, J.B., Lynch, K.W., and Barash, Y. (2016). A new view of transcriptome complexity and regulation through the lens of local splicing variations. Elife *5*, e11752.

Vecellio Reane, D., Vallese, F., Checchetto, V., Acquasaliente, L., Butera, G., De Filippis, V., Szabo, I., Zanotti, G., Rizzuto, R., and Raffaello, A. (2016). A MICU1 Splice Variant Confers High Sensitivity to the Mitochondrial Ca(2+) Uptake Machinery of Skeletal Muscle. Mol Cell *64*, 760-773.

Voet, S., Prinz, M., and van Loo, G. (2019). Microglia in Central Nervous System Inflammation and Multiple Sclerosis Pathology. Trends Mol Med *25*, 112-123.

Volfovsky, N., Haas, B.J., and Salzberg, S.L. (2003). Computational discovery of internal micro-exons. Genome Res *13*, 1216-1221.

Wang, G.S., and Cooper, T.A. (2007). Splicing in disease: disruption of the splicing code and the decoding machinery. Nat Rev Genet *8*, 749-761.

Wang, Y., Szretter, K.J., Vermi, W., Gilfillan, S., Rossini, C., Cella, M., Barrow, A.D., Diamond, M.S., and Colonna, M. (2012). IL-34 is a tissue-restricted ligand of CSF1R required for the development of Langerhans cells and microglia. Nat Immunol *13*, 753-760.

Webb, L.M., Amici, S.A., Jablonski, K.A., Savardekar, H., Panfil, A.R., Li, L., Zhou, W., Peine, K., Karkhanis, V., Bachelder, E.M.*, et al.* (2017). PRMT5-Selective Inhibitors Suppress Inflammatory T Cell Responses and Experimental Autoimmune Encephalomyelitis. J Immunol *198*, 1439-1451.

Webb, L.M., Sengupta, S., Edell, C., Piedra-Quintero, Z.L., Amici, S.A., Miranda, J.N., Bevins, M., Kennemer, A., Laliotis, G., Tsichlis, P.N.*, et al.* (2020). Protein arginine methyltransferase 5 promotes cholesterol biosynthesis-mediated Th17 responses and autoimmunity. J Clin Invest *130*, 1683-1698.

Weyn-Vanhentenryck, S.M., Mele, A., Yan, Q., Sun, S., Farny, N., Zhang, Z., Xue, C., Herre, M., Silver, P.A., Zhang, M.Q.*, et al.* (2014). HITS-CLIP and integrative modeling define the Rbfox splicing-regulatory network linked to brain development and autism. Cell Rep *6*, 1139-1152.

Wlodarczyk, A., Holtman, I.R., Krueger, M., Yogev, N., Bruttger, J., Khorooshi, R., Benmamar-Badel, A., de Boer-Bergsma, J.J., Martin, N.A., Karram, K.*, et al.* (2017). A novel microglial subset plays a key role in myelinogenesis in developing brain. EMBO J *36*, 3292-3308.

Wolf, Y., Shemer, A., Levy-Efrati, L., Gross, M., Kim, J.S., Engel, A., David, E., Chappell-Maor, L., Grozovski, J., Rotkopf, R.*, et al.* (2018). Microglial MHC class II is dispensable for experimental autoimmune encephalomyelitis and cuprizone-induced demyelination. Eur J Immunol *48*, 1308-1318.

Wolf, Y., Yona, S., Kim, K.W., and Jung, S. (2013). Microglia, seen from the CX3CR1 angle. Front Cell Neurosci *7*, 26.

Woodbury-Smith, M., and Scherer, S.W. (2018). Progress in the genetics of autism spectrum disorder. Dev Med Child Neurol *60*, 445-451.

Woolf, Z., Stevenson, T.J., Lee, K., Jung, Y., Park, T.I.H., Curtis, M.A., Montgomery, J.M., and Dragunow, M. (2021). Isolation of adult mouse microglia using their in vitro adherent properties. STAR Protoc *2*, 100518.

Wu, J., Anczukow, O., Krainer, A.R., Zhang, M.Q., and Zhang, C. (2013). OLego: fast and sensitive mapping of spliced mRNA-Seq reads using small seeds. Nucleic Acids Res *41*, 5149-5163.

Xia, X., Wang, Y., Huang, Y., Zhang, H., Lu, H., and Zheng, J.C. (2019). Exosomal miRNAs in central nervous system diseases: biomarkers, pathological mediators, protective factors and therapeutic agents. Prog Neurobiol *183*, 101694.

Xu, J., and Richard, S. (2021). Cellular pathways influenced by protein arginine methylation: Implications for cancer. Mol Cell *81*, 4357-4368.

Xu, R., Li, X., Boreland, A.J., Posyton, A., Kwan, K., Hart, R.P., and Jiang, P. (2020). Human iPSC-derived mature microglia retain their identity and functionally integrate in the chimeric mouse brain. Nat Commun *11*, 1577.

Yan, Z., Wu, H., Liu, H., Zhao, G., Zhang, H., Zhuang, W., Liu, F., Zheng, Y., Liu, B., Zhang, L.*, et al.* (2021). The protein arginine methyltransferase PRMT1 promotes TBK1 activation through asymmetric arginine methylation. Cell Rep *36*, 109731.

Yang, A.C., Kern, F., Losada, P.M., Agam, M.R., Maat, C.A., Schmartz, G.P., Fehlmann, T., Stein, J.A., Schaum, N., Lee, D.P.*, et al.* (2021). Dysregulation of brain and choroid plexus cell types in severe COVID-19. Nature *595*, 565-571.

Yang, M.L., Gee, A.J., Gee, R.J., Zurita-Lopez, C.I., Khare, S., Clarke, S.G., and Mamula, M.J. (2013). Lupus autoimmunity altered by cellular methylation metabolism. Autoimmunity *46*, 21-31.

Yang, Y.Y., Yin, G.L., and Darnell, R.B. (1998). The neuronal RNA-binding protein Nova-2 is implicated as the autoantigen targeted in POMA patients with dementia. Proc Natl Acad Sci U S A *95*, 13254-13259.

Yuan, J., Ma, Y., Huang, T., Chen, Y., Peng, Y., Li, B., Li, J., Zhang, Y., Song, B., Sun, X.*, et al.* (2018). Genetic Modulation of RNA Splicing with a CRISPR-Guided Cytidine Deaminase. Mol Cell *72*, 380-394 e387.

Zeug, A., Muller, F.E., Anders, S., Herde, M.K., Minge, D., Ponimaskin, E., and Henneberger, C. (2018). Control of astrocyte morphology by Rho GTPases. Brain Res Bull *136*, 44-53.

Zhang, G., Wang, Z., Hu, H., Zhao, M., and Sun, L. (2021). Microglia in Alzheimer's Disease: A Target for Therapeutic Intervention. Front Cell Neurosci *15*, 749587.

Zhang, L., Tran, N.T., Su, H., Wang, R., Lu, Y., Tang, H., Aoyagi, S., Guo, A., Khodadadi-Jamayran, A., Zhou, D.*, et al.* (2015). Cross-talk between PRMT1-mediated methylation and ubiquitylation on RBM15 controls RNA splicing. Elife *4*.

Zhang, X., Huang, T.Y., Yancey, J., Luo, H., and Zhang, Y.W. (2019). Role of Rab GTPases in Alzheimer's Disease. ACS Chem Neurosci *10*, 828-838.

Zhao, N., Francis, N.L., Calvelli, H.R., and Moghe, P.V. (2020). Microglia-targeting nanotherapeutics for neurodegenerative diseases. APL Bioeng *4*, 030902.

Zheng, J., Ru, W., Adolacion, J.R., Spurgat, M.S., Liu, X., Yuan, S., Liang, R.X., Dong, J., Potter, A.S., Potter, S.S.*, et al.* (2021). Single-cell RNA-seq analysis reveals compartment-specific heterogeneity and plasticity of microglia. iScience *24*, 102186.

Zheng, S. (2020). Alternative splicing programming of axon formation. Wiley Interdiscip Rev RNA *11*, e1585.

Zheng, S., and Black, D.L. (2013). Alternative pre-mRNA splicing in neurons: growing up and extending its reach. Trends Genet *29*, 442-448.

Zhu, J., Li, X., Cai, X., Zha, H., Zhou, Z., Sun, X., Rong, F., Tang, J., Zhu, C., Liu, X.*, et al.* (2021). Arginine monomethylation by PRMT7 controls MAVS-mediated antiviral innate immunity. Mol Cell *81*, 3171-3186 e3178.

Zrzavy, T., Hametner, S., Wimmer, I., Butovsky, O., Weiner, H.L., and Lassmann, H. (2017). Loss of 'homeostatic' microglia and patterns of their activation in active multiple sclerosis. Brain *140*, 1900-1913.